Development, Optimisation and Applications of Screen-Printed Electrochemical Sensors

By

Giuseppina (Giusy) Matzeu (M.Sc.)

Thesis submitted in partial fulfilment of the requirements for the degree of **Doctor of Philosophy**

Dublin City University

Supervisor:

Prof. Dermot Diamond

Co-Supervisor:

Dr. Aoife Morrin

National Centre for Sensor Research/ School of Chemical Sciences

September 2015

Declaration

I hereby certify that this material, which I now submit for assessment on the programme of study leading to the award of Doctor of Philosophy is entirely my own work, and that I have exercised reasonable care to ensure that the work is original, and does not to the best of my knowledge breach any law of copyright, and has not been taken from the work of others save and to the extent that such work has been cited and acknowledged within the text of my work.

Signed: _____

Giuseppina (Giusy) Matzeu

ID No: 11100095

Date: 20/08/2015

Quotes

I love life in spite of all that mars it. I love friendship, jokes and laughter.

Tahar Ben Jelloun

Dum loquimur, fugerit invida aetas: carpe diem, quam minimum credula postero.

Horace

Occorre invece violentemente attirare l'attenzione nel presente cosí com'é, se si vuole trasformarlo. Pessimismo dell'intelligenza, ottimismo della volontà.

Antonio Gramsci

Sarda Sarda, troglodita di lusso, dimessa e pure diffidente e distante, con memoria d'elefante e vellutino e oggettivamente piccola di statura, ma ben fatta, sarda sarda.

Marcello Fois

Dedication

To my grandparents Mariuccio and Virginia

Ai miei nonni Mariuccio e Virginia

Acknowledgments

I have always thought that life is a journey, and the time spent here at Dublin City University was part of a new and amazing experience that I had the opportunity to enjoy.

This was possible thanks to Prof. Dermot Diamond and the opportunity that he gave me for pursuing a Ph. D. within his research group. His vision, his acumen (the one of a wise wolf scientist), and his creativity made my experience in the Adaptive Sensors Group (ASG) challenging and amazing.

I would like to give thanks to Dr. Aoife Morrin for being my secondary supervisor.

Special thanks also goes to Dr. Claudio Zuliani as I had the opportunity to work with him in my first two years. Claudio, you introduced me to the world of electrochemistry that was unknown and scary to me, especially due to the fact that my background was completely different.

In these acknowledgments, there is somebody that cannot be forgotten, the one that was a mentor and is still a friend, Dr. Fabio Di Francesco.

Now it is time to acknowledge the big crowd that makes the place I worked in for 4 years (N205) amazing, an environment where you can actually work but especially enjoy having great chats and laughs. Thanks to my Mediterranean Buddies Isa and Aymen Ben Azouz, I don't think our laughing out loud and noisy discussions will be missed once we leave ;). Thanks to one of the most crazed person that I have ever met, the devil Cormac (Macchi) Fay. Thanks to K. J. Fraser for all his help during the last 4 years and especially for the "Spritz and Narghilé sessions". I will never forget "Mad Mags" from Limerick, Deirdre whom I shared the Ph. D. journey with, Eoghan, Fiachra, Conor, Tom, Patrick (aka Patricheddu), Dave, Kevin, Larisa, Shirley, Simon Coleman and Nigel. A special thank also goes to all the guys based in SG07, to all the past members of the ASG (Bartosz, Michele, Vincenzo, Simon Gallagher and Monika) and to the NCSR and Insight Staff. You have all been really helpful along the years, amazing people such as Margaret and Ruth.

But living in Dublin was not just related to work, it was also strictly bound to countless funny moments outside DCU. I had the great opportunity to meet people from all over

the world and a special thanks goes to Monika, Declan, Dirk, Marco, Antonios, Eva and Alex. Zeliha, you are the sister that I have never had, I can simply say thanks for everything and for being as crazy as I am.

There were vast distances separating us, but I know that you were always there for me. I love you all Alessandra, Elisa, Francesca, Alessio, Ste Lai, Virgilio, Letizia, Ylenia and Silvia.

To my mum Giuliana, for her unconditional love, for always reminding me that no matter what happens we are all people that deserve the same chance despite where we are from and the way we grew up. The world in which we live improves due to our diversities.

A mia mamma Giuliana, per il suo amore incondizionato, per ricordarmi in ogni momento che qualunque cosa accada siamo tutte persone che meritano le stesse opportunità, a prescindere dal luogo e dal modo in cui si è cresciuti. Il mondo intorno a noi può migliorare solo grazie alle nostre differenze.

Thanks to my big happy family for their constant support. You are all fantastic starting from grand dad and grand mum, uncles, aunties and cousins.

Grazie alla mia grande gioiosa famiglia per il supporto costante. Siete tutti fantastici a cominciare da nonno e nonna, zii, zie e cugini.

A special thanks goes to Auntie Lucia and Uncle Francesco, Rosanna and Alberto, Antonio, Luigi and Maria Luisa. You all grew me up and you are my second family.

Un ringraziamento speciale va a Zia Lucia e Zio Francesco, Rosanna e Alberto, Antonio, Luigi e Maria Luisa. Mi avete cresciuto e siete la mia seconda famiglia.

Last but not least, there you are Paolo. It was tough but thrilling, sometimes sad but exciting, sometimes we were angry with each other but then sweet again. Being divided by an ocean was an experience that has been nice and has been part of our growing up together since we first met. However, I hope that soon our road will be the same again. I love you!

Publications

Peer-Reviewed Journal Articles

1. **G. Matzeu**, C. O'Quigley, E. McNamara, C. Zuliani, C. Fay, T. Glennon and D. Diamond, *An Integrated Sensing and Wireless Communications Platform for Sensing Sodium in Sweat*, submitted to Analyst.
2. **G. Matzeu**[1] and C. Fay[1], A. Vaillant, S. Coyle and D. Diamond, *A Wearable Sensing Device: Monitoring Sweat Rates via Image Analysis*, submitted to IEEE Transactions on Biomedical Engineering.
3. **G. Matzeu**[1] and C. Zuliani[1], D. Diamond, *Solid-Contact Ion-Selective Electrodes (ISEs) based on Ligand Functionalised Gold Nanoparticles,* Electrochimica Acta (159) 2015: 158-165.
4. **G. Matzeu,** L. Florea and D. Diamond, *Advances in Wearable Chemical Sensor Design for Monitoring Biological Fluids*, Sensors and Actuators B (211) 2015: 403-418.
5. C. Zuliani, **G. Matzeu** and D. Diamond, *A Liquid-Junction-Free Reference Electrode based on a PEDOT Solid-Contact and Ionogel Capping Membrane*, Talanta (125) 2014: 58-64.
6. C. Zuliani[1] and **G. Matzeu**[1], D. Diamond, *A Potentiometric Disposable Sensor Strip for Measuring pH in Saliva*, Electrochimica Acta (132) 2014: 292-296.
7. S. Anastasova, A. Radu, **G. Matzeu**, C. Zuliani, U. Mattinen, J. Bobacka and D. Diamond, *Disposable Solid-Contact Ion-Selective Electrodes for Environmental Monitoring of Lead with ppb Limit-of-Detection*, Electrochimica Acta (73) 2012: 93-97.

[1] Authors contributed equally to this work

[3.a] BDDA (characterised by a -$(CH_2)_4$- chain) produced membranes with almost identical behaviour than the ones obtained using HDDA (with a -$(CH_2)_6$- chain) (results not shown).

Book Chapter

1. C. Zuliani, V. F. Curto, **G. Matzeu**, K. J. Fraser and D. Diamond, *Properties and Customization of Sensor Materials for Biomedical Applications*, Comprehensive Materials Processing 13 (2014): 221-243.

Conference Contributions

Conference Proceedings

1. **G. Matzeu,** C. Fay, C. O'Quigley, D. Orpen, S. Coleman, A. Kavanagh and D. Diamond, *On-Body Chemo/Bio-Sensing - Opportunities and Challenges*, Advances in Science and Technology, 96 (2014): 78-88.
2. **G. Matzeu,** C. Zuliani and D. Diamond, *Recent Progress in Disposable Ion-Selective Sensors for Environmental Applications*, Advances in Science and Technology 77 (2013): 65-70.

Oral Presentations

1. **G. Matzeu,** N. E. O'Connor, K. Moran, C. Fay, C. O'Quigley, S. Coyle, L. Florea and D. Diamond, *Wearable Fluidics – The Key to Bringing Chemistry and Biology into On-Body Measurements,* In: 2015Flex, 23-26 February 2015, Monterey, California, USA.
2. **G. Matzeu,** C. O'Quigley, E. McNamara, C. Fay, C. Zuliani and D. Diamond, *Non-Invasive Detection of Biological Fluids: a New Perspective in Monitoring pH in Saliva and Sodium in Sweat*, In: 66th Irish Universities Chemistry Research Colloquium, 19 June 2014, NUIG, Galway, Ireland.
3. **G. Matzeu,** C. Zuliani and D. Diamond, *Recent Progress in Disposable Ion-Selective Sensors for Environmental Applications*, In: CIMTEC 2012, 10-14 June 2012, Montecatini Terme, Italy.
4. C. Zuliani, **G. Matzeu** and D. Diamond, *Towards Wearable Sensors for Wireless pH Monitoring in Sweat*, In: PITTCON 2012, 10-15 March 2012, Orlando, Florida, USA.

Poster Presentations

1. **G. Matzeu,** C. O'Quigley, E. McNamara, C. Fay and D. Diamond, *Non Invasive Detection of Biological Fluids*, In: Insight Student Conference 2014, 12 September 2014, Dublin, Ireland.

2. J. Deignan, **G. Matzeu,** S. Coyle, C. O'Quigley, C. Zuliani, P. Fitzpatrick, G. Warrington and D. Diamond, *Wearable Chemical Sensing: Sensor Design and Sampling Techniques for Real-Time Sweat Analysis*, In: CIMTEC- 6th Forum on New Materials, 15-19 June 2014, Montecatini Terme, Italy.
3. **G. Matzeu,** C. O'Quigley, E. McNamara, C. Fay and D. Diamond, *Screen-Printed Electrochemical Sensors for Real-Time Sodium Monitoring in Sweat*, In: 3D Bioprinting Symposium 2014, 14-15 May 2014, Dublin, Ireland.
4. M. Marinho Muraro, C. Zuliani, E. Nesterenko, S. Coyle, P. Fitzpatrick, G. Warrington, **G. Matzeu**, E. J. X. Costa and D. Diamond, *Impact of Sport Drinks on Sweat Composition*, In: 13th Analitica Latin America, 24-26 September 2013, Sao Paulo, Brazil.
5. **G. Matzeu,** C. Zuliani and D. Diamond, *Disposable Potentiometric Strips: a Versatile Tool for Low-Cost Sensing*, In: AAMG Sensors 2013, 19 June 2013, London, United Kingdom.
6. **G. Matzeu,** C. Zuliani V. F. Curto, S. Coyle, C. Fay, E. Mc Namara, J. Torres-Sanchez, B. O'Flynn, J. Barton, C. O'Mathuna and D. Diamond, *Wearable Devices: a New Wave for Sweat and Saliva Detection*, In: Workshop for wearable sensors and health, 5 March 2013, Dublin, Ireland.
7. **G. Matzeu,** C. Zuliani and D. Diamond, *Ion-Selective Electrodes for Sodium Detection*, In: Clarity Open Day, 21 November 2012, Dublin, Ireland
8. **G. Matzeu,** C. Zuliani and D. Diamond, *A New Generation of Disposable Ion-Selective Electrodes for Low Cost Environmental Chemical Sensing*, In: Clarity Site Review, 25 April 2012, Dublin, Ireland.
9. **G. Matzeu,** C. Zuliani, K. T. Lau and D. Diamond, *A New Generation of Disposable Ion-Selective Electrodes for Low Cost Environmental Chemical Sensing*, In: Printed Functional Materials, 12 September 2011, Dublin, Ireland.

Aims of the Thesis

The development of reliable, low-cost, miniaturised potentiometric sensors (based on screen-printed substrates) was the aim of this thesis. The miniaturised sensing devices consist of a new Solid-Contact Reference Electrode (SC-RE) (based on the use of ionogels) coupled to an Ion-Selective Electrode (ISE) specifically tailored according to the application of interest. They were designed and implemented for future integration on miniaturised wireless electronic platforms, aiming at realisation of smart-devices for heavy metals detection in water or wearable sensing approaches for continuous monitoring of physiological parameters such as pH in saliva and Na^+ in sweat. For instance, continuous monitoring of pH in saliva would allow a better clinical management of pathologies that alter acid contents within the mouth. Similarly, the real-time tracking of sodium levels in sweat can assist clinicians in the diagnosis and treatment of Cystic Fibrosis. Furthermore, athletes could reap many benefits from an optimal strategy for personalised rehydration, which might be informed by continuously measuring the amount of minerals lost in sweat.

The technological advancements presented here exemplify the realisation of more flexible designs of miniaturised sensors together with their integration into devices allowing for remote monitoring. More work still needs to be done but this thesis underlines the pivotal steps and advantages of realising different kinds of sensors such as ISEs integrated into fabrics for personal health monitoring, and autonomous sensors to be deployed in rivers and lakes for monitoring water quality.

List of Publications and Author Contribution to Chapters

The work presented in this thesis was carried out by the candidate under the supervision of Prof. Dermot Diamond at Dublin City University, within the Insight Centre for Data Analytics, a research centre part of the National Centre for Sensor Research. Parts of the chapters have already been published in peer-reviewed journals and the others have been submitted for revision. Chapter 2 is a peer-reviewed paper (review) on the main challenges behind the development of wearable applications for non-invasive monitoring of different biological fluids. The candidate conceived the design and organisation of the paper and wrote the manuscript.

Chapter 3 is a peer-reviewed paper that describes the development of solid-contact reference electrodes. The candidate is the second author and contributed in conceiving, designing and performing some of the experiments. She also contributed in analysing the data and writing the manuscript.

Chapter 4 is a peer-reviewed paper on the implementation of solid-contact Ion-Selective Electrodes (ISEs) to monitor pH in saliva. The candidate is a co-author and conceived, designed and performed the experiments. She analysed the data and wrote the manuscript.

Chapter 5 is a peer-reviewed paper that describes the use of ligand functionalised gold nanoparticles as solid-contact for developing Ion-Selective Electrodes. The candidate is a co-author and conceived, designed and performed the experiments. She analysed the data and wrote the manuscript.

Chapter 6 is an original paper, submitted for revision. It is focused on the realisation of an all integrated wearable platform (sensors, microfluidics, electronics) to monitor Na^+ variations in sweat. The candidate is the primary author and conceived, designed and performed the experiments. She analysed the data and wrote the manuscript. This work highlights the collaboration between the engineers and the team of chemists within the Adaptive Sensors Group.

Chapter 7 is an original paper submitted for revision. It is focused on the use of a wearable device that after image analysis allows estimating sweat rates. The candidate conceived, designed and performed the experiments in collaboration with the co-author. She analysed the data and wrote the manuscript.

Paper	Chapter	Title	Publication Status*
1	2	Advances in Wearable Chemical Sensor Design for Monitoring Biological Fluids	10.1016/j.snb.2015.01.077
2	3	A Liquid-Junction-Free Reference Electrode Based on a PEDOT Solid-Contact and Ionogel Capping Membrane	10.1016/j.talanta.2014.02.018
3	4	A Potentiometric Disposable Sensor Strip for Measuring pH in Saliva	10.1016/j.electacta.2014.03.140
4	5	Solid-Contact Ion-Selective Electrodes (ISEs) Based on Ligand Functionalised Gold Nanoparticles	10.1016/j.electacta.2015.01.143
5	6	An Integrated Sensing and Wireless Communications Platform for Sensing Sodium in Sweat	Submitted to Analyst
6	7	A Wearable Device for Monitoring Sweat Rates for Image Analysis	Submitted to IEEE Transactions on Biomedical Engineering

* I have renumbered sections of submitted or published papers in order to generate a consistent presentation within the Thesis.

Signed: _____ Date: 20/08/2015_____

Giuseppina (Giusy) Matzeu

Signed: _____ Date: 20/08/2015_____

Prof. Dermot Diamond

Signed:  Date:_20/08/2015_____

Dr. Claudio Zuliani

Thesis Outline

An overview summary of each chapter is given below.

Chapter 1 introduces the challenges that characterise the field of chemical sensors, associated to their development and use in daily lives. Particular attention is devoted to the description of potentiometric sensors, the theoretical background that describes their behaviour and all the possible configurations allowed by the diversity of materials used for their implementation. Furthermore, the trends that will revolutionise the realisation of ISEs are discussed. An important role will be played by mass production technologies allowing for miniaturisation and integration of potentiometric sensors on paper based microfluidic systems or on smart garments for non-invasive monitoring via wearable applications.

Chapter 2 is a more detailed summary on the advances in wearable chemical sensor design for monitoring biological fluids (e.g. interstitial fluids, breath, sweat, saliva and tears). Particular attention is devoted to interstistial fluid monitoring, especially on minimally and non-invasive detection of glucose. Breath also represents a good alternative where humidity, NO, O_2, ammonia and acetone are the markers successfully quantified to date. Sweat monitoring is of great interest to monitor analytes that can help improving sports performances or non-invasively quantify biological markers for cystic fibrosis treatment. Tears are under the spotlight since they are going to be the fluid of choice for non-invasive glucose monitoring via integration of sensors (electrochemical or optical) on the surface of contact lenses.

Chapter 3 describes the different approaches used to realise reliable miniaturised reference electrodes. This research was mainly focused on the careful embedding of the membrane components (e.g. choice of the IL used in the ionogel capping layer, the use of different polymers), able to tailor the features of novel solid-contact reference electrodes. The effect of the material used as solid-contact was also analysed, specifically how the media (i.e. type of IL) and electrochemical techniques used for electrodeposition can affect the SC-RE behaviour.

Chapter 4 focuses on the optimisation (e.g. choice of materials, fabrication procedure, etc.) of screen-printed electrodes tuned to realise pH potentiometric strips. After on-

bench calibration, the monitoring of real saliva samples was accomplished via all solid state, low-cost, flexible potentiometric strips.

Chapter 5 introduces the importance played by the material used as solid-contact in the implementation of ISEs, especially the opportunities behind the use of nanostructures. Gold nanoparticles decorated with different ligands were indeed synthesised, characterised and tested as solid-contact material while realising Pb^{2+} or Na^{+} ISEs. There were striking differences in the performances of both types of sensors, mainly dictated by the different functional group decorating the gold nanoparticle surface.

Chapter 6 describes the development of potentiometric strips to monitor Na^{+} levels in sweat and their integration into microfluidic chips, used to harvest the fluid of interest. They were first tested on the bench and then connected to a miniaturised, wireless electronic platform verified during real-time cycling sessions.

Chapter 7 proposes a wearable sensing device used to monitor sweat rates via image analysis. Sweat Rates are usually estimated via methods that imply the use of cumbersome protocols. It was proposed a localised approach of analytical consistency based on the use of Macroducts®, devices commonly employed in the clinical practice as sweat collectors. Using reverse engineering, it was possible to develop a technique to estimate sweat rates by examination of camera images taken or videos frames recorded during cycling trials.

Chapter 8 gives an overview on the impact that this thesis can have on the development of miniaturised, low-cost electrochemical sensors. Additionally, some ideas will be proposed as progressive developments that will take place in the near future. For example, different configurations will be tested aiming at the development and spreading of wearable chemical sensors in the world wide community.

Table of Contents

Table of Contents

Abstract

The sustainability of healthcare delivery depends on the adoption of new low-cost devices to support the transition of services from centralised generic models to home and community-based care models, through which the patient status can be monitored remotely. Easily accessible body fluids (like saliva, sweat and interstitial fluids) represent alternative sampling media to blood that in principle can be conveniently analysed through wearable sensors. For instance, continuous monitoring of pH in saliva would allow a better clinical management of pathologies that alter acid contents within the mouth. Similarly, the real-time tracking of sodium levels in sweat and other body fluids can assist clinicians in the diagnosis and treatment of Cystic Fibrosis. Furthermore, athletes could reap many benefits from an optimal strategy for personalised rehydration, which might be informed by continuously measuring the amount of minerals lost in sweat.

Electrochemical sensors based on the combination of screen-printed working and solid-contact reference electrodes are versatile and low-cost tools that are effective in facing many of the challenges in current sensing technology. They can be readily adapted for the detection of several ionic species, and in this thesis, as an example, two electrochemical platforms to monitor pH in saliva and sodium in sweat are going to be presented. The final devices are minimally-invasive and wearable, with a compact format due to the integration of miniaturised solid state ion-selective and reference electrodes. The technological advancements developed for their realisation are significant contributions for the more flexible design of novel miniaturised sensors for remote monitoring in general. Future developments of this technology could be pivotal for realising devices for applications as diverse as sensors integrated into fabrics for personal health monitoring, or autonomous sensors deployed in rivers and lakes for monitoring water quality.

Chapter 1.

Ion-Selective Electrodes: Past, Present and Future.

1.1 Introduction

Sensors detect variations of physical or chemical parameters (e.g. temperature, pressure, light, concentration), and convert them into signals that can be quantified [1]. Although we are often unaware of it, our lives are already pervasively connected to hundreds of sensors [2]. The demand for pervasive acquisition of information from multiple sources spread throughout our surrounding environment is indeed rising rapidly in our technology-savvy society. This serves as a significant stimulus for the development of new sensing devices at the core of wireless appliances for environmental or biological monitoring [3]. Healthcare represents one of the main markets for novel sensors. For example, portable electrochemical sensors help diabetic patients to control their glucose levels (see Figure 1.1 (a)) [4, 5], allowing for the implementation of personalised health management strategies. Similarly, other commercially available sensors enable the monitoring of vital signs such as breathing and heart rates [6], while motion sensors are employed in orthopaedics and sports science to analyse and correct body postures and movement executions (see Figure 1.1 (b)) [3].

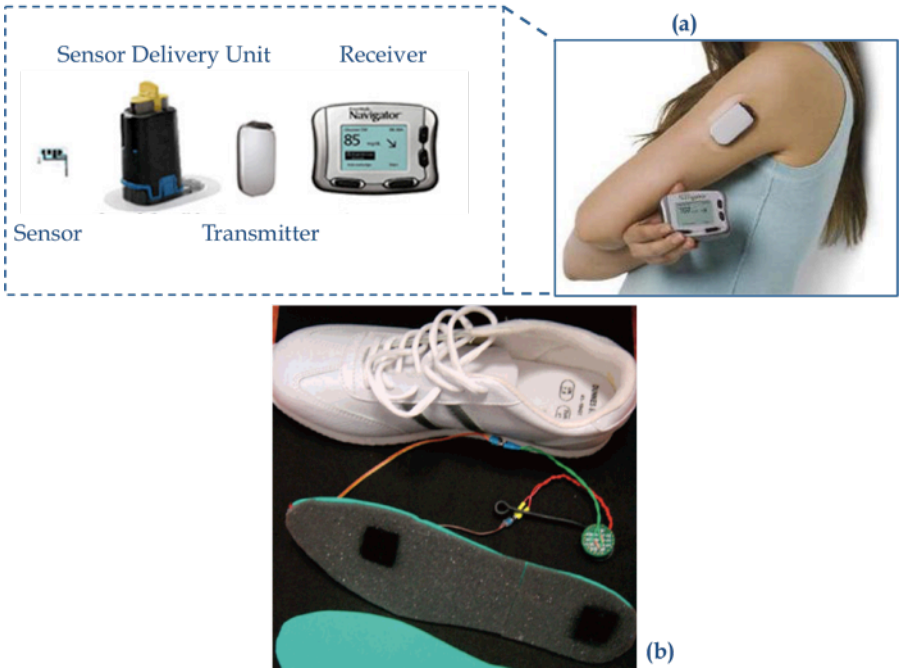

Figure 1. 1: (a) Components of the FreeStyle Navigator® (Abbott Inc.) allowing for minimal invasive monitoring of glucose in interstitial fluids. The device can be worn on different locations such as the upper arm (image adapted from [5]). (b) Wearable pressure sensors integrated on the insole of shoes for gait analysis purposes (image adapted from [3]).

The success of sensing technologies depends on their cost, accuracy, reliability, and on their robustness against noise. Fabrication via mass production techniques using inexpensive materials is necessary to access the market. Commercial thermistors, LEDs, gyroscopes and strain gauges already meet most of these features. Moreover, they can be miniaturised enough to be integrated onto hand-held or wireless systems. They are also currently used in demanding applications where they work unattended in inconvenient (if not even otherwise inaccessible) locations, and with constrained resources [3, 7].

In contrast, generally speaking, equivalent cheap and reliable chemical sensing platforms are not currently available on the market. There are a number of reasons for this, such as their need for frequent re-calibration. Additionally, the fact that they have to be in direct contact with the sample of interest to permit its monitoring makes them naturally fragile and hampers their development and commercialisation [3]. Such limitations can be overcome thanks to strategies allowing integration of miniaturised sensors within microfluidic sampling units and their connection to wireless electronic platforms (e.g. based on Bluetooth [8], Radio Frequency Identification (RFID) [9], etc.).

During the last four years, attention was focused on the development of low-cost, miniaturised screen-printed potentiometric strips (see Figure 1.2). These sensors can be easily tuned according to the application of interest and their solid state nature facilitates the implementation of different configurations. Additionally, after connection with wireless electronic platforms, their deployment in different scenarios is possible, allowing for environmental (detection of heavy metals such as lead) or non-invasive monitoring of biological fluids like saliva and sweat. The latter are the core of this thesis.

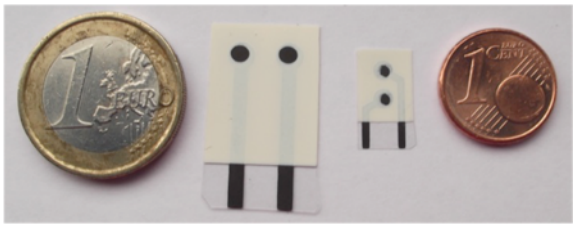

Figure 1. 2: Screen-printed electrodes realised using the same materials (i.e. carbon ink and ceramic dielectric) but different design.

1.2 Ion-Selective Electrodes (ISEs)

Recently, some publications have pointed out a sort of revival that is characterising research into the Ion-Selective Electrodes (ISEs) field. It is not uncommon to find

expressions like "new wave" to describe recent trends behind the development of new configurations embedding potentiometric sensors [10].

It must be underlined, however, that this technology dates back to the beginning of the 20th century, when Cremer illustrated changes in the behaviour of glass while varying pH [11, 12]. This discovery was followed by the realisation of the first glass electrode by Beckman in 1932 [13]. In the sixties, the first liquid membrane based on an ion exchanger [14] was introduced. Further improvements were made possible by advances in host-guest chemistry [15] and by the integration of ionophores in polyvinyl chloride (PVC) membranes [16]. These key advances led to the realisation of ISEs specific to more than 50 ions [17, 18]. Their first deployment took place in clinical environments to estimate electrolytes in whole blood (in particular Na^+, Ca^{2+}, Cl^- and K^+, avoiding matrix effects or sample pre-treatments) [19, 20] and environmental monitoring (Pb^{2+}, Cu^{2+}, NO_3^-) [11]. In the 90s, after a period of relative stagnation, some ground breaking work significantly helped to improve the Limits of Detection (LODs) [21, 22] and the selectivity [23] of ISEs. Furthermore, new designs that include reliable solid-contact electrodes [24] paved the way for their miniaturisation [25].

The beginning of the 21st century witnessed the introduction of significantly miniaturised sensors based on new solid-contact configurations able to reach low LODs (for example, 10^{-9} in Pb^{2+} monitoring [26, 27]). Moreover, the reduced dimensions allowed the integration of solid-contact ISEs (SC-ISEs) in wireless platforms [9, 28, 29] with enormous potential benefits in environmental and wearable sensing applications [18] mainly based on tattoo [30] and patch like designs [31].

1.2.1 Working Mechanism of ISEs

Conventional ISEs are membrane based sensors with a liquid-contact, in which an inner reference wire (usually Ag(s)/AgCl(s)/Cl^-) is immersed in a buffered internal solution of a salt of the primary ion that needs to be detected [32]. The membrane, which is sensitive to the variations in activity of the analyte of interest, is positioned between the inner solution and the sample [33]. The target dictates the difference in potential at the interface membrane/sample solution, which can be measured connecting the ISE to a reference electrode. The latter is usually a double junction Ag(s)/AgCl(s)/Cl^-, insensitive to any variation in the analysed system. Traditionally, the ISE and reference electrode are connected in a closed circuit to a potentiometer with high input impedance (10^{13} Ω or higher) [13]. In an ideal situation, no external

electrical current flows between the reference electrode and the ISE [34]. The setup employed to carry out this type of measurements is shown in Figure 1.3.

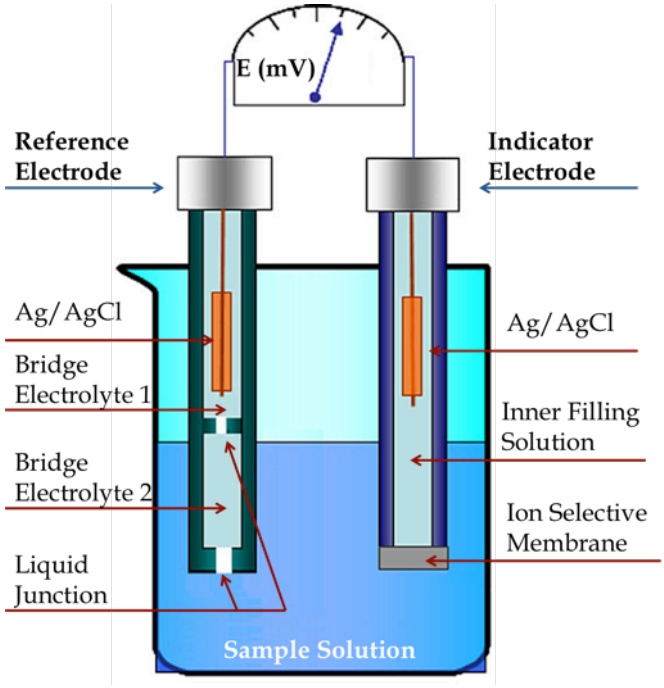

Figure 1. 3: Experimental set-up for a potentiometric measurement realised using a liquid-contact ISE and double junction reference electrode (adapted from reference [35]).

Different theoretical models have been developed to describe the behaviour of ISEs. Non-Equilibrium Responses are taken into account by various models such as the Nernst-Planck-Poisson. The Nernst-Planck equation describes the transport of ions due to diffusion and migration phenomena while the Poisson equation governs the electrical interactions within the membrane. They form a system of non-linear partial differential equations that can be numerically solved via the finite element method providing valuable information on the behaviour over time before reaching equilibrium [36]. The phase boundary model is preferred, however, to describe the behaviour of potentiometric sensors under steady-state/equilibrium conditions. This model assumes electroneutrality of the bulk phases, chemical equilibrium at the selective membrane/aqueous interface and avoids time dependent effects. Furthermore, the diffusion potential is ignored [34]. The sensor response is dictated by the charge separation that occurs at the interface membrane/sample, which generates a difference of potential as described by a Nernstian-like Equation [13]

$$E_{EMF} = E_i^0 + \frac{RT}{z_i F} \ln a_{i,sol} \quad (1.1)$$

where E_i^0 includes all constant terms represented by the activity of the ion/ionophore complex within the membrane and the potential contributions at the various interfaces characterising the system; z_i represents the charge of the ion; R is the universal gas constant (8.314 J/(mol K)); F is the Faraday constant (9.65×10^4 C/mol); T is the absolute temperature; and $a_{i,sol}$ represents the activity of the target ion in solution, which also takes into account the interactions with other ions in the solution [13]. Activities can be related to concentrations via [37]

$$a_i = \gamma_i C_i \quad (1.2)$$

where γ_i is the activity coefficient and C_i is the ion concentration.

In turn, γ_i can be estimated via the Debye-Hückel equation [37] as

$$log\gamma_{\pm} = \frac{A\|z_+ z_-\|\sqrt{I}}{1+Bd_{\pm}\sqrt{I}} + CI \quad (1.3)$$

where A and B are tabulated for every solution and depend on density, electrical permittivity, and temperature of the solvent; z_+ and z_- are the charge of the cation and anion of the electrolyte of interest; $d_{\pm}$ is the effective ion radius; C is usually extrapolated from experimental data obtained while changing the ionic strength of a solution containing the ion of interest (usually corresponding to ~0.1 for ionic strengths higher than 0.3 M); I represents the ionic strength of the sample solution [37]

$$I = \frac{1}{2}\sum_i C_i z_i^2 \quad (1.4)$$

Common parameters used to evaluate the performance of ISEs are derived from the Nernstian-like equation (see equation 1.1). The sensor sensitivity is the slope of the line ($\frac{RT}{z_i F}$ V/dec) that best fits the linear range of the calibration curve. Experimentally, (sub- or super-) deviations from the Nernstian trend are often observed due to interfering ions in solution, leaching phenomena, and trans-membrane fluxes [33, 38]. The LOD, i.e., the lowest activity of the target ion that can be reliably measured [39], is defined as the intersection between the two linear fittings describing the sensitive and insensitive range at low activities. An ISE is also characterised by an upper LOD that indicates the saturation of the recognition layer [39]. This is calculated as the intersection between the two linear fittings describing the sensitive and insensitive ranges at high activities, respectively. The lowest and highest limits of detection define the dynamic range of the sensor.

1.2.2 Composition of the Ion-Selective Membrane.

Different materials have been used to produce the sensitive layer of ISEs, but polymeric membranes containing homogeneously dispersed ionophores and ion-exchangers have given the best results so far [17, 33]. The ionophores are the molecules within the polymer matrix that interact with the target analytes and confer selectivity to the ISE [17]. More than 100 types are available on the market and through these, a wide range of ions is detectable [40]. To avoid interference from the counter ion, an ion-exchanger must always be present in this mixture to minimise co-extraction into the membrane (in a suitable molar ratio with the ionophore). Ion-exchangers are composed of a hydrophobic ion and a hydrophilic counterion, selected so that the former of these has an opposite charge to that of the target ion [17, 40]. To confer flexibility to the membrane, it is usually necessary to use a highly hydrophobic polymer having a glass transition temperature (T_g) lower than room temperature [41]. Silicone rubbers [42, 43], polyacrylic polymers [44, 45] and especially PVC [17] are among the preferred materials for the ISE membranes.

However, in the last 5 years, many studies were focused on the development of more hydrophobic polymeric cocktails that are able to decrease water uptake and allow for faster response times (when the concentration of the analyte in solution is changing), with reduced drift and improved selectivity. Membranes based on perfluoro polymers indeed represent a new alternative, thanks to their low polarity and anti-biofouling features and additional features that allow for good surface functionalisation [46, 47]. Another option is represented by the employment of layered polyacrylate membranes, where each stratum is characterised by ion-diffusion coefficients that gradually change. These membranes show better selectivity and stability over time, since they hamper the accumulation of primary ions in the most external layer [48]. This configuration is at an early developmental stage and deep insights are still needed to describe their working mechanism in detail.

1.3 Solid-Contact ISEs

As already briefly introduced in Section 1.2, in the last 20 years, there has been the tendency to replace the inner filling solution with solid materials mainly due to their compatibility with microfabrication technologies [10, 49-52], and their suitability for miniaturised design and mass production of sensors.

However, in order to obtain SC-ISEs with a stable electrode potential, it is necessary to design the solid state to have sufficiently fast and reversible ion to electron transduction, without any contribution from parasitic side reactions.

In a first attempt to replace liquid-contacts (see Figure 1.4 (a)), coated wire electrodes [53] (see Figure 1.4 (b)) employed a sensitive membrane attached to a conductive layer (usually a gold, platinum or Ag/AgCl wire) [54]. These sensors were characterised by acceptable sensitivity, good selectivity, and fast response times, but their behaviour was affected by irreproducibility and instability over time [52]. These phenomena were often associated with the formation of a water layer at the interface between membrane and conductive layer [55], and to the absence of a reversible fast ion to electron transduction mechanism at the solid-contact level [52].

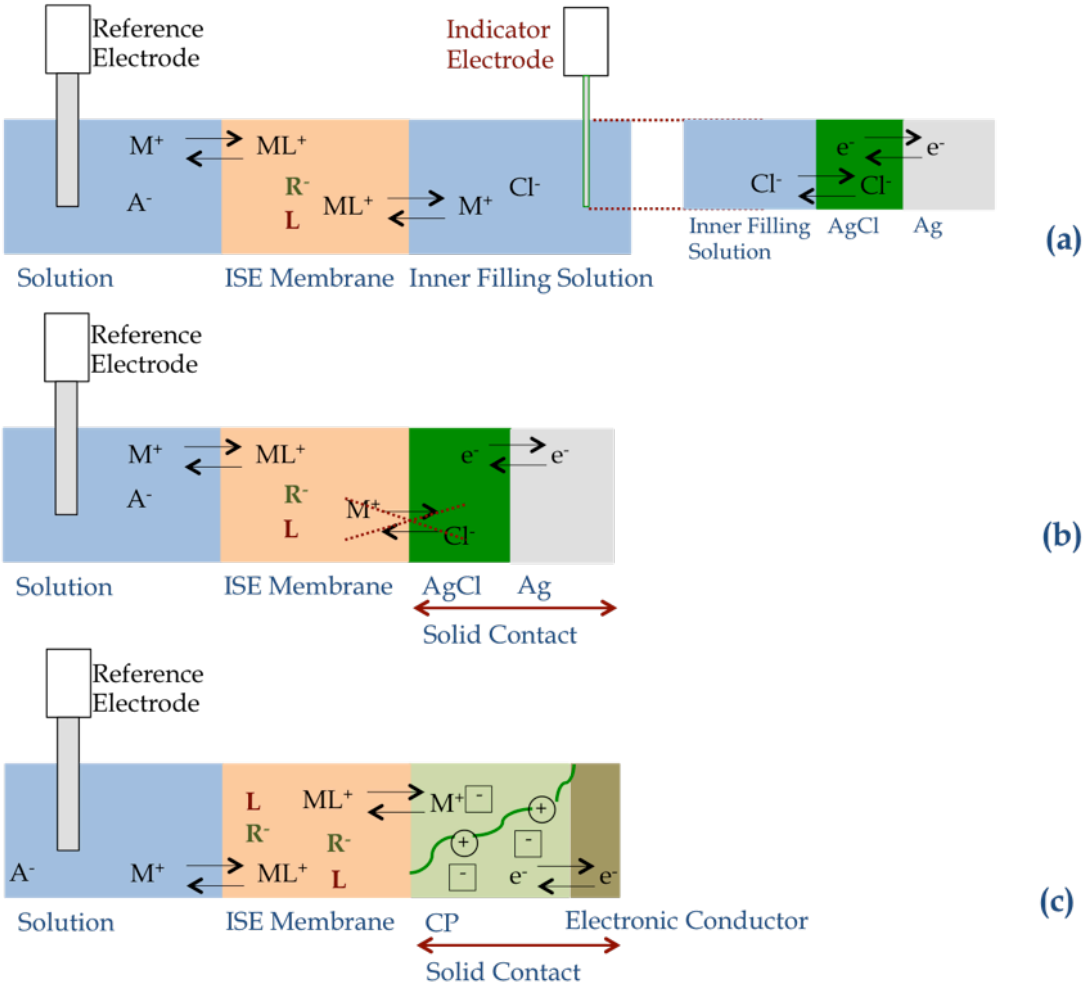

Figure 1. 4: Configuration adopted for the realisation of potentiomeric measurements: (a) displays a conventional symmetrical cell with liquid-contact electrodes on both sides of the sensitive membrane (i.e. reference electrode and indicator electrode); (b) shows the configuration of a coated wire electrode, with the sensitive membrane on top of the conductive layer represented in this case by an Ag/AgCl wire; (c) represents a solid-contact ISE, with an electroactive material (e.g. a conducting polymer (CP)) between the membrane and the conductive layer. M^+ is the analyte of interest. In the sensitive membrane, L is the ionophore, ML^+ is the complex ion-ionophore and R^- represents the anionic sites. e^- represents an electron. In the CP layer, + (i.e. within circles) characterise the oxidised conducting polymer moiety while – (i.e. within squares) are the doping ions.

Subsequent attempts employed electroactive materials as transducers deposited between the sensitive membrane and the conducting layer. Among the most recently analysed we can list conducting polymers [56], carbon nanotubes [57], graphene [58], and nanocomposites [59] with large double-layer capacitances.

1.3.1 Conducting Polymers (CPs)

Conducting Polymers (CPs) have recently emerged as materials of choice to accomplish ion to electron transduction duties since they can enhance SC-ISE longevity, improve stability over time, and enhance the LOD [13, 50, 52, 56, 60, 61]. They can also be optimally selected depending on the application [61]. A general feature of CPs is that their conductivity or optical properties change according to the doping state. Much of the research related to ISE characterised by the use of CPs as solid-contact focuses on their intrinsically mixed electronic and ionic conductivity. This means that they can transduce an ionic signal into an electronic one at the solid-contact level [56] (see Figure 1.4 (c)). However, there are some drawbacks related to the use of CPs as solid-contact mainly dictated by impaired thermal, chemical and mechanical properties over time [62, 63].

Recently, significant effort has been devoted to the use of primary derivatives of polypyrrole (PPy), polythiophene, polyaniline (PANI), and poly(3,4-ethylenedioxythiophene) (PEDOT) [64] (see Figure 1.5). PPy is known for its good mechanical properties, even though it is penalised by low ion accessibility due to its dense films, relatively low conductivity (10–50 S/cm), and chemical instability (e.g. due to oxygen) [65]. Compared to PPy, PEDOT has 10 times greater conductivity (300–500 S/cm), greater chemical and thermal stability, and higher optical transparency [64]. It became one of the most studied and appealing materials as a result of commercial inks such as PEDOT:PSS allowing for the development of low-cost printed devices. For example, an ethylene glycol/tetraoctylammonium bromide (TOAB) modified PEDOT:PSS ink was drop-cast on top of glassy carbon electrodes and employed during Pb^{2+} monitoring [66].

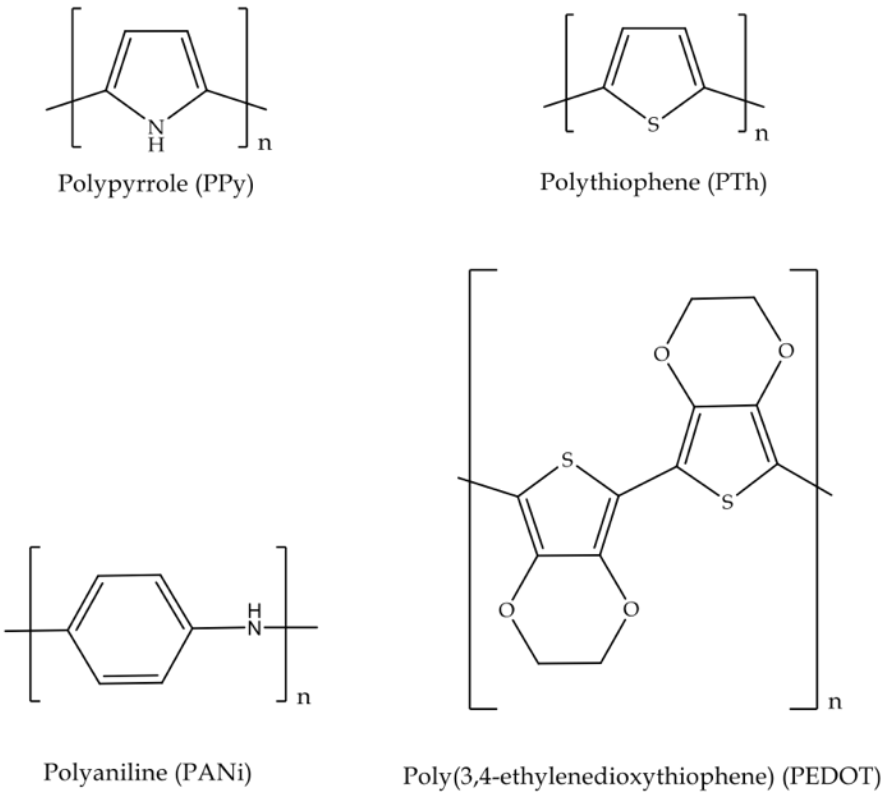

Figure 1. 5: The most common conducting polymers in the undoped form including polypyrrole, polythiophene, polyaniline, and poly(3,4-ethylenedioxythiophene) (EDOT).

The green emeraldine salt form of PANI has conductivity in the range 1–10 S/cm and it has the ability to form a broad range of nanostructures without the use of a template, via chemical synthesis or electrochemical deposition [67]. PANI was used previously as the SC layer in K^+ ISEs, to detect potassium in artificial serum, with a linear range between 10^{-5} M and 10^{-1} M, without pH interference under physiological conditions [68]. Poly(3-octylthiophene) (POT) has been used as a solid-contact due to its hydrophobicity, improved membrane adhesion and limited water uptake [25]. Its working mechanism has been recently clarified. It is characterised by a surface-confined spontaneous oxidation, with an oxidised overlayer of CP on top of unoxidised CP (independent on thicknesses). This establishes a stable interfacial potential characterised by surface confined transfer of ions (e.g. when it involves bulky anions such as $TFPB^-$) and oxidation of POT at the interface between the CP and the sensitive membrane [69].

While PANI, PPy, and PEDOT have been extensively investigated for the possible improvement of SC-ISE performances, the use of other CPs, or the effect of nanostructuring CPs seems to be relatively unexplored [70]. For instance, polypyrrole

microcapsules have previously been employed as solid-contact in Ca^{2+} ISEs [71, 72]. The authors claim that through this, they can control the electrolyte composition of the microcapsules, thus providing a means to fine-tune the LOD [71, 72]. The use of CPs doped with selected ionophores as a sensing layer is another interesting approach. However, thus far, such sensors suffer from poor sensitivity and high limits of detection [70, 73]. Recently, metal complexing agents were introduced on the CP backbone, without modification of their oxidation state. They can directly sense different cationic groups (e.g. alkaline earth cations, copper, cadmium, lead and zinc) although this approach is still at early stages [74].

Recent research suggests that the electrochemical growth of CPs in new media like Ionic Liquids (ILs) might offer some improvements in their physico-chemical properties (mechanical, physical, and chemical) [75-77]. For instance, control of the water content during electropolymerisation seems to affect the conductivity of the CP layers. This was observed during the electropolymerisation of thiophene in an aqueous electrolyte, and it resulted in the formation of a non-conducting polymer film [78]. In addition, the choice of IL cation/anion is important since it affects the stabilisation of the radical produced during IL electrochemical oxidation. It also regulates the degree of electrostatic interaction between the anion and the polymer backbone [79]. Finally, the IL ions may also affect chemical doping, thickness and morphology of the conductive polymer film [79]. The possibilities of tuning CP properties thanks to the versatility of ILs (due to the very wide range of cations and anions available) suggest that they could be used as a convenient solid-contact material in the realisation of different types of ISEs and reference electrodes (see Chapters 3, 4 and 6).

One of the major limitations associated to the use of CP is related to the difficulties in obtaining stable and reproducible intra- and inter-batch standard electrode potentials (E^0), which is fundamental when aiming to create calibration-free sensors. Last year, it was shown that this problem can be overcome with electrode tuning via electrochemical techniques [80]. The potential of a solid-contact ISE was kept at zero versus a standard reference electrode. In a first attempt, they were connected in a 3 electrodes configuration to a standard potentiometer [81]. Secondly, the ISE and the RE were short circuited via a wire [82], and always kept in a solution containing the primary ion. Electrical current flows influencing the redox state and ionic content of the conducting polymer [81] and a new overall open circuit potential is established. This novel approach might help in solving problems like potential instability. It also gives the opportunity to monitor high concentrations (thanks to its accuracy after small

variations) and to test the performances of new materials employed as solid-contact [82]. The variations in the electrochemical redox properties that are usually considered deleterious are exploited here to instrumentally improve the performances of ISEs.

1.3.2 Carbon Materials: from 3D Ordered Macroporous Carbon to Carbon Nanotubes (CNTs) and Graphene

During the last ten years, much attention was focused on the use of different carbon materials to overcome the difficulties characterising solid-contact ISEs based on conducting polymers. Three dimensionally ordered macroporous (3DOM) carbon layers were realised after colloidal crystal templating. This synthetic step creates a skeleton of glassy carbon that surrounds a periodic array of uniform spherical pores (with diameters of few hundreds nanometers) interconnected in 3 dimensions (with skeletal walls on the order of tens nanometers thick). A Nickel mesh used as conductive connection was coated (in a specific area) with 3DOM carbon then covered by a PVC K^+ selective membrane. This electrode showed a Nernstian response, characterised by the absence of a water layer (the 3DOM structures are strongly hydrophobic), without interference from O_2 and light and a drift of 11.7 μV/h (over a month). The interconnected wall structure provides a continuous pathway for electron conduction (around 0.2-0.3 S/cm) while the ion conductivity is afforded by the pores filled by the ion-selective membrane [83]. This configuration was compared with untemplated carbon layers (causing a water layer, drifts of 1530 μV/h over 70 h) and proved that pores are essential for excellent electrode performances [84].

3DOM carbon structures are however characterised by some disadvantages. First, the monolithic nature hampers mass production and the presence of redox-active surface functional groups affects reproducibility. These drawbacks were overcome after the synthesis of colloid imprinted mesoporous carbon (CIM) (uniform mesopores around 24 nm). They are characterised by decreased functional groups (0.43 wt%) when compared to 3DOM carbon (1.7 wt%), which contribute to the absence of side reactions such as the formation of a water layer and interference from O_2, CO_2 and light. An additional advantage is the easy processability of the material, which is available in a powder form that can be easily deposited employing different approaches [85].

Another carbon material that might offer advantages in the realisation of solid-contact electrodes is porous carbon cloth. Its working mechanism is based on double layer capacitive charging effects, however lacking in terms of standard potential reproducibility [86]. The use of this material is still at an early stage but given its

mechanical flexibility it has potential for future implementation of built-in fabric electrodes.

Nanomaterials such as Carbon Nanotubes (CNTs) offer additional appealing properties that recently started to be exploited while realising solid-contact ISEs. CNTs exist mainly in two forms, single and multiwall, termed SWCNTs and MWCNTs, respectively. SWCNTs can be considered as a long, wrapped graphene sheet consisting of two separate regions (side and end cap) (see Figure 1.6 (a)) with very different physical and chemical properties [87, 88]. For instance, certain studies imply that the tips of CNTs are more reactive than the cylindrical parts [87]. MWCNTs consist of concentric SWCNTs of different diameter (see Figure 1.6 (b)), in which the shells of carbon are closely separated [87]. The lengths of CNTs play an important role in determining the electrical, optical, and mechanical properties [88].

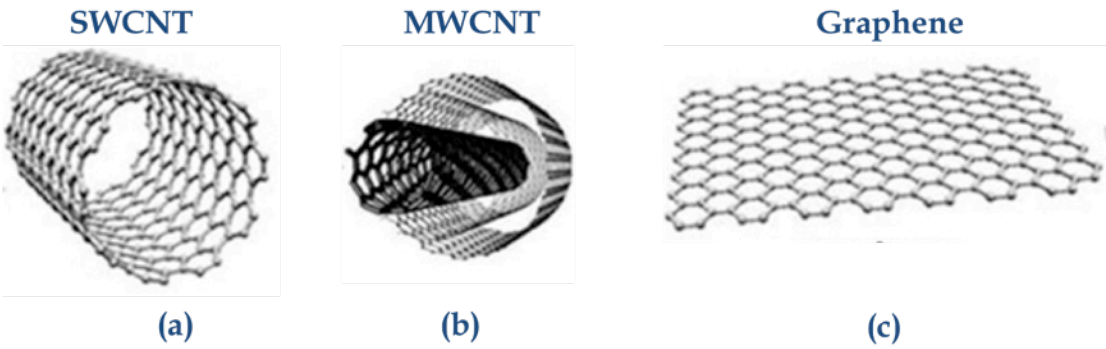

Figure 1. 6: Configuration of a Single Walled Carbon Nanotube (SWCNT) (a), a Multi Walled Carbon Nanotubes (MWCNT) (b) and a graphene layer (c).

Crespo et al. [57] underlined the non-Faradic nature of the transduction principle of SWCNTs (deposited on a glassy carbon electrode and used as solid-contact), whose configuration is that of an asymmetric capacitor. One interface is represented by the solution (or ion-selective membrane) and the other is represented by the CNTs, characterised by a very large surface to volume ratio. They feature a fast and reversible ion to electron transduction (due to the high capacitance of the double layer), without any contribution from parasitic side reactions thanks to their high hydrophobicity, insensitivity to light and absence of redox behaviours. These materials are easily processed and transferred on top of screen-printed electrodes via drop casting. This approach was used to build disposable potentiometric strips able to monitor K^+ in drinks and diluted saliva samples after one point calibration. They were suitable for use after 8 months of dry storage [89]. A CNT based ink [90] was also used as electrical

connector and transducer in spray-coated pH potentiometric sensors (based on a spray-coated PVC sensitive membrane) [90].

The immobilisation of sensitive elements on the surface of CNTs, concentrating both recognition and transduction properties on the same substrate creates hybrid nanomaterials. The Pb^{2+} ionophore benzo-18-crown-6 (B18C6) was covalently grafted to MWCNTs [91] using different approaches [92], then added to a poly(ethylene-co-acrylic acid) (PEAA) cocktail (used as dispersant) [91]. The recorded signal was really stable, characterised by good selectivity, reproducibility and stability, without interference from light and water [91, 92]. However, the covalent functionalisation affects the linear range: it causes co-extraction of the counter-ion from the solution in the membrane, pH interferences and ion exchanger properties because of the charged groups on the backbone of MWCNTs. An immobilisation strategy based on π-π interactions between the pyrene group and MWCNTs was implemented and it was able to increase loading without affecting properties and structures of the CNTs [93]. This approach is still at a development stage and quite demanding from a synthetic point of view, and so far did not really improve the performance of ISEs.

Graphene is another material that is under the spotlight thanks to its unique properties. In graphene, carbon atoms are arranged in a regular hexagonal pattern similar to graphite, but in a one-atom thick sheet (see Figure 1.6 (c)) [94]. It is a zero band gap semiconductor having conductivity akin to metals, which accounts for materials with exceptional electrocatalytic abilities [94]. Large-scale patterned growth of graphene is still problematic [95] and electrolytic exfoliation is particularly promising for producing graphene nanosheets in aqueous environments at low-cost [96].

Carboxy functionalised graphene (CFG) water suspensions were used for the first time as solid-contact while realising K^+ ISEs based on PVC sensitive membranes. Their characteristics were compared to ISEs whose solid-contact was made of conducting polymers (PEDOT:PSS and POT). The performance was similar in terms of stability but CFG based sensors were characterised by the lowest LOD ($10^{-7.1}$ M) [97]. This preliminary study just showed the potential of graphene, whose working mechanism was better clarified by Hernandez et al. [58]. They tested reduced graphene layers in SC-ISEs after drop casting on glassy carbon electrodes. As per CNTs, graphene layers behaved as an asymmetric capacitor, with double-layer capacities increasing with the thickness of the film. When employed as solid-contact in Ca^{2+} ISEs, reproducibility and

drift over time were both outstanding thanks to the absence of metallic impurities and any side reaction (e.g. redox phenomena) [58].

Surfactant free dispersions of CNTs and graphene were drop-cast on plastic substrates and used as connector lead and solid-contact while realising all solid state disposable configurations for K^+ monitoring. Both types of ISEs were characterised by similar performance although CNTs were featured by better conductivity and reduced interference from H^+ [98].

1.3.3 Gold Nanoparticles (Au-NPs)

In recent years, Nanoparticles (NPs) have been the centre of multiple research efforts. In a seminal work, Brust et al. [99] developed an easy pathway for their chemical synthesis and stabilisation. Chemical synthesis is still one of the best approaches for their preparation, although other methods such as evaporation under vacuum or laser ablation [100] have also proven effective. NPs have been prepared using different metals such as gold, silver, platinum, and palladium, with each metal imparting specific catalytic and optical properties [101, 102]. In NP chemical synthesis, the choice of ligands, the metal to reducing agent ratio, time, and temperature all play an important role in determining the morphological aspects and properties of the resulting NPs [100].

Synthetic methods to functionalise NPs have achieved a great level of control and sophistication. NPs can indeed be prepared with a number of different ligands and coatings, therefore offering opportunities to tailor specific properties for sensing applications. They might have a significant role to play in solving most of the problems (previously listed) characterising solid-contact ISEs. This might be possible thanks to their chemical stability and tunable properties, for example, through control of the ligands and the core materials used in their fabrication [103].

Jaworska et al. [103] compared ISEs whose SC was realised using Au-NPs functionalised with aliphatic thiols (butyl and octane thiol chains) or POT. The authors showed that K^+ ISEs incorporating these Au-NPs demonstrated better stability over time, without affecting performance characteristics such as the LOD (when compared to POT). Similarly, Woznica et al. [104] employed dithizone modified Au-NPs as a solid-contact in Cu^{2+} ISEs. When the NP ligand was changed from butanethiol to dithizone, which is known to bind Cu^{2+} selectively, the response of electrodes shifted from Nernstian to super-Nernstian. However, when dithizone functionalised Au-NPs were loaded with copper ions (by conditioning for 15 minutes in 10^{-5} M $CuSO_4$

solution, before the deposition of the Cu^{2+} selective membrane), the calibration slope became Nernstian and was characterised by a lower LOD ($10^{-7.5}$ M) than that obtained using butanethiol (10^{-6} M). This showed clearly that the choice of the ligand bound to the NPs influences the ion fluxes at the membrane/solid-contact interface.

Our group compared two solid-contact films prepared from Lipoic Amide (LAm) and Lipoic Acid (LAc) Au-NPs. In particular, we investigated the impact of the differing physico-chemical properties of the so-functionalised NPs and of their concentration on the sensitivity and dynamic range of the sensors. Electrochemical Impedance Spectroscopy (EIS) allowed explanation of the mechanism of ion transport through the membrane and how this is modulated by Au-NPs. This study highlights the importance of matching the functionalising group of Au-NPs to the target ion, with particular attention on the role played by the solid-contact in the development of low-cost solid state ISEs compatible with high volume production fabrication technologies [105] (as described realising Pb^{2+} and Na^{+} ISEs).

Jágerski et al. [106] showed that it is possible to decorate NPs with ionophores. The spontaneous self-assembly of Ag^{+} selective thiacalixarene derivatives with dithiolate groups took place on the surface of gold nanoparticles, characterised by a space filling thiol (1-dodecanethiol) that confers hydrophobicity to the Au-NPs conjugate. These ionophore gold nanoparticles were mixed to an optimal PVC:2-nitropheyl octyl ether (o-NPOE) (1:3) mixture, able to prevent their segregation. A very low LOD (9 nM) was reached and this configuration might also be advantageous for long-term use, hampering the leaching of the ionophore, characterised by low mobility ($5x10^{-12}$ cm^2/s) within the polymer network [106].

1.4 Reference Electrodes

The reference is the other electrode completing the galvanic cell in potentiometric measurements. One of the most common ones is the double junction silver/silver chloride electrode, which is able to maintain a stable potential under a wide range of conditions (e.g. changing the concentration of an analyte from 10^{-10} M to 1M). Although there have been some attempts to improve the performance and configuration of commercially available reference electrodes [107, 108], the scheme has remained unchanged from the original concepts introduced more than fifty years ago [107, 109]. Only minor variations of the salt bridge or junction design have been practically implemented, and they commonly suffer from drying and leaching [110, 111].

One of the first examples of solid-contact reference electrode, still quite bulky but with the ability to reduce the cost of reference electrodes, was developed by Mousavi et al. [109]. They embedded an Ag/AgCl wire (acting as reference element) into a polyvinyl acetate (PVAc)/KCl composite. These electrodes were used to monitor Pb^{2+} and Cl^- variations, and showed optimal potential stability (±0.5 mV). Their salt leaching was less than that measured with standard liquid-contact reference electrodes [109]. These all solid state reference electrodes turned out to be compatible with thin and thick film technologies since they can be realised via injection moulding. They maintained astonishing performances throughout 4 months, particularly when stored in a constant 3 M KCl solution or humid environment [112]. They were integrated in all solid state potentiometric platforms and used to test river water samples when associated to a Cl^- working electrode [113].

To allow their integration in miniaturised devices, reference electrodes should ideally be fabricated with techniques suitable for mass production (e.g. planar type design) such as screen printing [110]. A reference electrode was implemented via a photocured poly(n-butylacrilate) membrane (containing Ag, AgCl and KCl salts) on top of a drop-cast layer of SWCNT octadecylamine (ODA), on screen-printed substrates. Despite their insensitivity towards various ionic compounds and different molecules (slope inferior than 2 mV/dec), they were constantly subjected to a one point calibration (due to the variability in E^0), strict storing conditions (i.e. dark and dry environment) and previous conditioning before testing in 10^{-3} M KCl for 12 h [114]. These last constraints suggest that the former could be employed as a disposable, single use reference electrode.

A significant challenge remains in the production of devices capable of continuous use over longer periods of time [110, 111, 115]. There is a need for all solid state reference electrodes of analytical quality that can retain the performance of a classical reference electrode while offering additional advantages such as maintenance-free use [109]. Two different approaches seem to overcome these issues. For example, Kisiel et al. [116] reduced salt leaching and obtained stable responses over 3 weeks of testing and storage (change of 5 mV in the potential values recorded) of poly(n-butyl acrylate) microspheres loaded with solid KCl partially converted to AgCl [116]. Outstanding results were also obtained by Guinovart et al. [117]. They developed a solid-contact reference electrode based on a polyvinyl butyral (PVB) cocktail containing dispersed Ag, Ag/Cl and NaCl, drop-cast on top of glassy carbon electrodes. The couple Ag/AgCl covers the surface of the glassy carbon, creating a precise phase boundary

potential, while nanopores localised at the surface of the PVB layer dictate the flow of NaCl towards the solution. These reference electrodes must be subjected to 12 h conditioning in 3 M KCl solution and consequently stored dry, requiring a short pre-conditioning step (from 10 to 30 minutes) before use (constantly employed for 3 months). They are additionally characterised by stability towards variations in the monitoring solution, insensitive to light, pH and redox potential, with reproducible baselines [117].

Mi et al. [118] introduced a novel concept for the preparation of a pseudo-reference using hydrophobic anion-exchanger membranes loaded with the polyanion heparin. Because heparin passively diffuses at a low rate from the ion-exchanger membranes into the sample, the potential drop across the solution/membrane interface is almost sample-independent and well defined [107, 118]. Following this advance, water-immiscible Ionic Liquids, or hydrophobic polymeric membranes doped with Ionic Liquids were employed to overcome some of the typical reference electrode limitations described above [107, 119]. For instance, Kakiuchi et al. [120] introduced ionogels based on the bis(trifluoromethylsulfonyl)imide [NTf_2] Ionic Liquid family as a novel salt-bridge material for reference electrodes. Following this investigation, ionogels based on [NTf_2] ILs [107, 121] were employed as capping membranes in order to prepare disposable Solid-Contact Ionogels Reference Electrodes (SCI-REs). Since the hydrophobic polymeric membrane contains an Ionic Liquid that is sparingly soluble in water, its partition between the two phases creates a local equilibrium distribution thus establishing a potential defined by the phase boundary model [121, 122].

The use of ionogels to prepare reference electrodes can be seen as an improvement of the lipophilic salt approach introduced by Mattinen et al. [26, 122], since no solvent is required. However, Cicmil et al. [121] showed that electrodes prepared by drop casting [NTf_2]/PVC ionogels onto a poly(3-octylthiophene-2,5-diyl) (POT) solid-contact layer exhibited changes in potential of up to 20-25 mV and 15-20 mV when the concentration of bathing solutions of KCl and NaCl was increased from 1 to 10 mM, respectively. In addition, Zhang et al. [107] showed that protonation of [NTf_2] within the ionogel phase at pH<4.5 caused trans-membrane fluxes that generated significant changes in the electrode potential. A similar approach was followed when realising a PVC based reference membrane containing the Ionic Liquid 1-methyl-3-octylimidazolium bis(trifluoromethylsulfonyl)imide ([C_8min^+]-[$C_1C_1N^-$]). Partitioning in solution defines the potential at the reference membrane/sample interface. The presence of a hydrophobic redox buffer within the same membrane (cobalt(II) and cobalt(III) tris(4,4-

dinonyl-2,2-bipyridyl) ($[Co(C_9,C_9\text{-bipy})_3]^{2+/3+}$) fixes the potential at the CIM (used as solid-contact/reference membrane interface). Its behaviour was satisfactory and the reference electrodes were transferred onto paper substrates, representing the other half cell of a potentiometric strip used to monitor Cl^- (e.g. intra-batch E^0 variation of 2.8 mV, Nernstian behaviour in the range 10^{-1}-$10^{-3.5}$ M) [123].

1.5 Trends in Ion-Selective Electrodes: looking at the Future

The revival in ISEs is very substantial, especially when considering the different approaches, materials and configurations that have been explored in the last 5 years to overcome their most common drawbacks.

For example, the need for non-invasive monitoring of biological fluids mainly relies on the availability of accurate chemical sensors. One of the main issues that so far hampered their exploitation is related to the inaccuracies in the analytical quantification of the targets of interest, mainly due to the small amount of sample collected (i.e. as per all chemical sensors).

For instance, potentiometric platforms based on a flat miniaturised multielectrode probe were developed to perform measurements on one drop of sample (i.e. serum) positioned on a microscope glass slide (able to minimise fluid evaporation) [124]. A similar configuration was employed to monitor simultaneously K^+, Cl^-, Na^+ and pH on both sides of an epithelial layer of human bronchial cells grown on a porous support. The cells were sandwiched (via two O-rings) between two electrodes [125]. However, these two examples are not easily miniaturised and cannot be employed outside a laboratory environment.

The use of low-cost technologies (such as screen printing [126], inkjet printing [95], spray coating [90] , etc. [127]) will allow implementation of reliable mass produced potentiometric sensors on flexible substrates, such as plastic, fabric and paper, that can be connected to miniaturised wireless electronic platforms [9]. Although built for environmental monitoring purposes, a study by Rius-Ruiz [128] allowed monitoring of NO_3^-, K^+, Ca^{2+} and Cl^- in a liquid circulating hydroponic system. The analytical device was based on a computer operated liquid handling system using commercial solid-contact CNTs based ISEs. This feasibility study accomplished the optimisation of all experimental conditions (i.e. when and how calibrate the sensors) and liquid handling. It was indeed possible to estimate the amount of nutrients that should be provided to the system during different growing stages of tomatoes [128].

1.5.1 Functionalisation of Polymer Sensitive Layers

Much research attention has been focused on the sensitive layer, the one exposed to the environment that needs to be monitored. Biofouling affects the time-based behaviour of sensors in direct contact with environmental or biological samples, especially if continuous monitoring is required for weeks or months. Furthermore, biocompatibility must be satisfied for in-vivo measurements to avoid inflammation (e.g. due to the leaching of the plasticiser from PVC membranes) and failure of the device.

Commercially available carboxylate PVC can be easily modified after nucleophilic substitution of chlorine atoms with azide groups via Click Chemistry reactions, carried out on the surface of the sensitive membrane under mild conditions (aqueous solutions and room temperature). It was indeed possible to increase the biocompatibility after modification with tetraethylene glycol (TEG) [129] or endow the polymer skeleton with redox properties thanks to the attachment of ferrocene groups [130]. A Poly(ethylene glycol)-biotin strepatividin with a high affinity for the antibody Palivizumab was also covalently attached to the surface of a PVC membrane via Click Chemistry. It allowed for label-free monitoring of the syncytial virus via ISEs, using a potentiometric transduction method that indirectly accounts for immune-binding (antibody antigen interactions) [131] (see Figure 1.7).

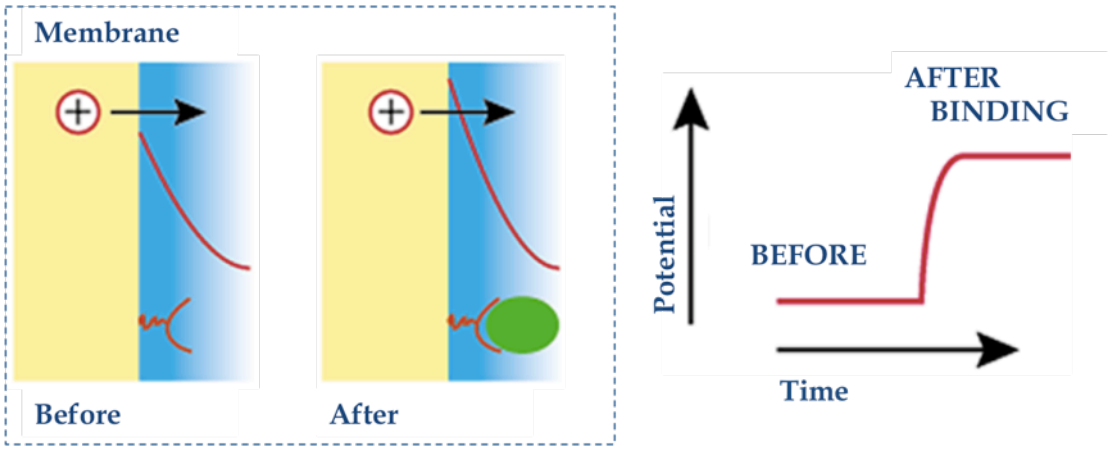

Figure 1. 7: Functionalised PVC membrane used to indirectly monitor immune-binding via potential variation. A quaternary ammonium ion is used as marker and constantly released by the membrane. Its concentration at the interface increases (causing an augmented potential reading over time) after interaction between respiratory syncytial virus and the Palivizumab on the PVC surface (image adapted from reference [131]).

The use of polymers that differ from PVC might offer even better opportunities, when tuning the hydrophilicity/hydrophobicity of their surfaces according to the application of interest. Poly(ethylene glycol) (PEG), phosphorylcholine and cellulose triacetate seem ideal candidates. Their surfaces can be functionalised (e.g. grafting biomolecules to increase the hydrophilicity of the exposed membrane) to improve the biocompatibility of the system [132].

1.5.2 Paper Based Sensitive Systems

The use of paper as a sampling unit (with embedded filtering actions and pump-free capillary flow) and as a sample container allows the development of robust, cost efficient, miniaturised analytical tools. In some cases, low-cost potentiometric devices have been employed as the detector module in these devices. One of the first examples is represented by the estimation of Ag^+ ions generated from a bioaffinity assay, proportional to the amount of human immunoglobulin E (IgE) contained in the sample [133] and directly quantified on paper (pore size of 0.2 μm).

Preliminary studies on how various types of commercial filter paper dictate the analytical performance of a potentiometric cell (solid-contact reference and working electrodes used to monitor K^+) were recently carried out. The pore size indeed affects the ionic equilibrium at the electrode/sample interface, influencing the transport of primary ions and causing an increased LOD (i.e. the best performances were obtained with pore sizes in the range of 12-25 μm) [134]. Additionally, the shape [134] and positioning of the paper layer affects the transport distance of the liquid inside the paper, and are really important when testing volumes as small as 200 μL [135]. The role played by the different functional groups localised on paper substrate and how they can impact on sensitivity, linear range and LOD is still not completely understood.

Paper sampling is however advantageous when analysing real samples (e.g. drinks such as coffee, milk, fruit juice, alcohol etc., and environmental water) because it behaves as anti-biofouling layer. It has a filtering action that might avoid the development of demanding sample treatment protocols [135], allowing for easier, accurate analytical quantifications.

Although there are many constraints that must be taken into account, the use of paper for delocalised analytical measurements can revolutionise many standard quantification approaches, considering the additional opportunity behind paper functionalisation and its use as substrate for the realisation of electrodes. A CNT-based ink was indeed employed to functionalise paper layers, conferring them an augmented

storage capacity thanks to the stabilisation of the cellulose fibers, and creation of three-dimensional structures that also improved mechanical properties. CNTs were used as ion-to-electron transducers and electrical conductors to realise K^+, NH_4^+ and pH ISEs with good performance when compared to the same configuration built on glassy carbon electrodes [136]. A Li^+ paper electrode was realised exploiting the same design and associated to a paper based reference electrode. They were combined together to create a potentiometric cell that can contain 50 μL of sample (see Figure 1.8 (a)) and successfully monitor Li^+ variations in blood, covering the range of analytical interest ($5x10^{-4}$-$1.5x10^{-3}$ M) [137].

Reproducibility is however one of the main issues that still needs to be addressed [136]. A possible solution could be avoiding any manual handling, using mass production techniques such as inkjet printing. An ink based on gold nanoparticles was applied as working and counter electrode, while its silver counterpart was used to make the reference electrode (covered by an Ag/AgCl layer electrochemically grown) on a paper substrate. The sensitive area was realised after printing a hydrophobic PDMS ink, as shown in Figure 1.8 (b). A polyaniline layer was electrochemically grown and used against the pseudo reference to successfully monitor pH. Although disposable, these paper-based sensors were able to work for over 5 hours. The system still needs to be improved but it represents one of the first examples of an all paper integrated sensing system useful for one-shot measurements [138].

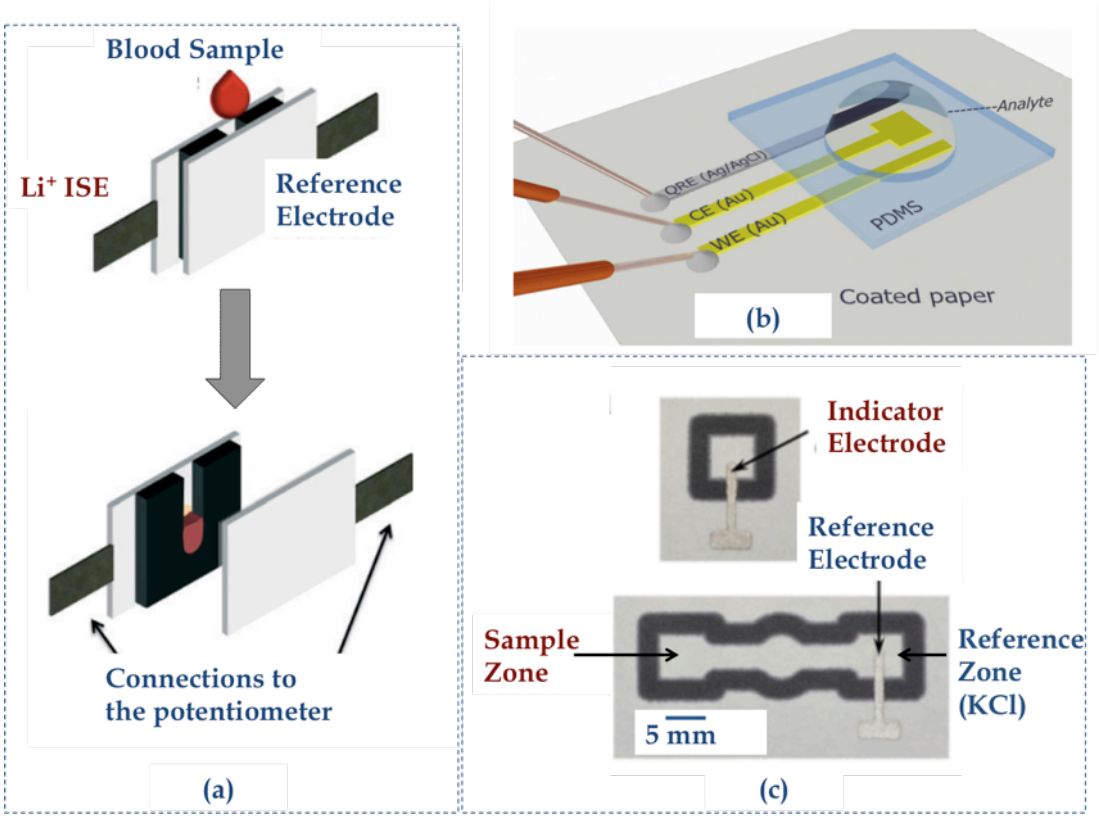

Figure 1. 8: Examples of paper based potentiometric sensors with different configurations. (a) Potentiometric cell implemented to monitor Li^+ in blood (adapted from reference [137]) or (b) pH (adapted from reference [138]). (c) All integrated potentiometric platforms (electrodes and sampling units built on the same substrate) (adapted from reference [139]).

The real breakthrough was represented by the work carried out by the Whitesides's Group, associated to the integration of wax designed microfluidic channels and electrochemical devices on the same paper substrate [140]. They were able to monitor different analytes, spanning from biological markers (cholesterol, glucose [141], etc. in urine and blood) to ionic compounds. In 2014, the first electrochemical paper-based analytical devices (EPADs) based on a potentiometric approach were developed. The platform consisted of chromatographic paper patterned with a hydrophobic wax used to localise the area integrating an Ag/AgCl (reference electrode) and a PVC based ISE (see Figure 1.8 (c)). The system was reliable and able to monitor Cl^-, K^+, Na^+ and Ca^{2+}, and it could potentially be adapted to quantify other ionic compounds, using roll to roll techniques for realisation. This design is however still quite complicated and although sample evaporation is hampered via a bulky experimental set up, a simplified configuration that will allow for their deployment outside of a lab environment is necessary [139].

1.5.3 Fabric and Tattoo Technology

One of the most popular trends of the last ten years is related to the design of chemical sensors for wearable applications to non-invasively monitor different biological fluids [142]. Different approaches were investigated to integrate many different configurations of potentiometric sensors. One of the pioneering works was based on ISEs for the real-time monitoring of Na^+ during exercise. The system was positioned at the lower back and the sweat harvested via a fabric pump (see Figure 1.9 (a)). The sensors were connected to a portable multimeter to measure variations in Na^+ levels and further verification was provided through Atomic Absorption Spectroscopy (AAS) performed on collected samples [143].

This design was quite bulky and many improvements were needed to implement pad-like configurations (applied on the skin to monitor biological markers [31] in sweat) (see Figure 1.9 (c)) or "smart bandages" to estimate pH in wounds (see Figure 1.9 (c)) [144]. Both designs were characterised by the use of screen-printed electrodes as sensitive element directly integrated onto the substrate. K^+ ISEs and reference electrodes (based on a polyvinyl butyral resin) were built on rubber using a CNT ink as solid-contact, finally integrated in a bracelet like configuration. They were tested on artificial sweat solutions, responding to variations in K^+ concentration [145].

However, a pivotal step was accomplished with the realisation of knitted electrodes directly integrated on garments. For example, ISEs were immobilised onto cotton yarns and made conductive through repeated immersions in carbon nanotube inks. Sensing capabilities for pH, K^+, and NH_4^+ were also added through partial coating with an ion-selective membrane [146].

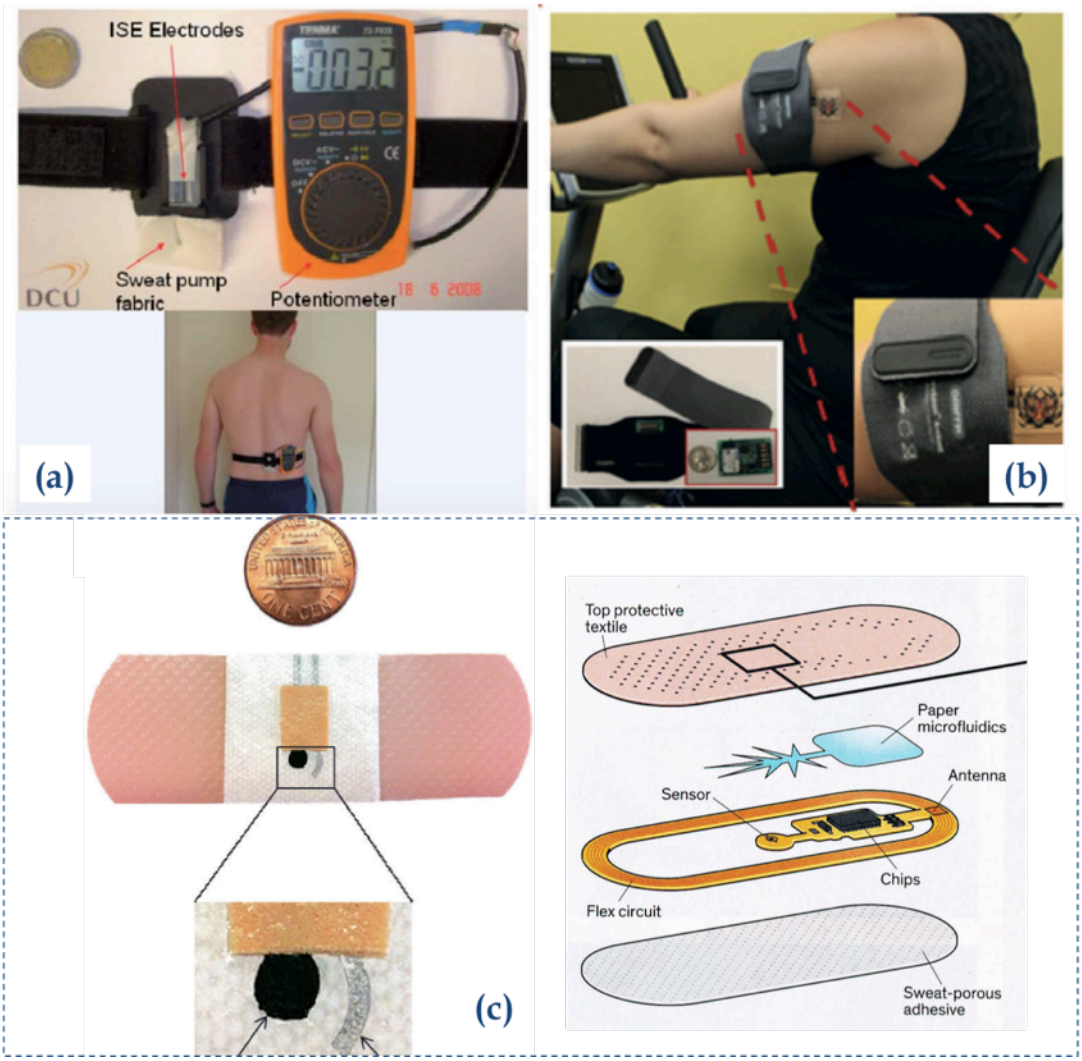

Figure 1. 9: Examples of wearable devices for sweat monitoring. (a) represents the first approach based on liquid-contact ISEs to monitor Na^+ in sweat (adapted from reference [143]) whereas (b) gives an example of a wireless tattoo configuration (adapted from reference [30]). (c) shows two different patch designs representing a pH (left, adapted from reference [145]) and Na^+ monitoring wireless device (right, adapted from reference [31]).

Even more promising is the development of skin-printable sensors following the pioneering work on skin-printable electronics of Rogers Research Group at the University of Illinois at Urbana-Champaign. A natural evolution of the lab's electronic tattoos [147] is the implementation of tattoo printed electrochemical sensors [148]. So far, ammonium [149], pH [150] and Na^+ [151] have been measured using tattoo-like potentiometric sensors. Tattoo sensors were able to withstand mechanical tests (stretching and bending) when applied on a Goretex substrate, simulating stress conditions for on-skin measurements. They were also employed during real-time tests on volunteers (see Figure 1.9 (b)). It must be emphasised that the tattoo sensors were

always connected to standard miniaturised electrochemical commercial potentiometers, except in the case of the Na^+ sensor, which was linked to a Bluetooth wireless wearable transceiver [151].

1.6 Conclusions

Despite Ion-Selective Electrodes technology dates back to the beginning of the 20th century, it is still an active and promising field in the area of chemical sensors and electroanalysis. This Chapter was mainly devoted to the introduction of potentiometric electrochemical sensors, focussing on their historical background, state of the art and future applications. Moreover, the theoretical mechanisms and the materials used for the realisation of ISEs were presented to make the reader familiar with the topic. The following chapters are focused on the development of solid state, low-cost, screen-printed electrodes used as substrate of potentiometric platforms suitable for different purposes (e.g. monitoring of pH in saliva, real-time detection of Na^+ in sweat). The work presented within this thesis and carried out during the last four years spans from theoretical to applied electrochemistry.

1.7 References

[1] J. Fraden, Chemical sensors, Handbook of Modern Sensors, Springer2010, pp. 569-606.

[2] D. Estrin, D. Culler, K. Pister, G. Sukhatme, Connecting the physical world with pervasive networks, Pervasive Computing, IEEE, 1(2002) 59-69.

[3] D. Diamond, S. Coyle, S. Scarmagnani, J. Hayes, Wireless sensor networks and chemo-biosensing, Chemical Reviews, 108(2008) 652-79.

[4] M.J. Tierney, J.A. Tamada, R.O. Potts, L. Jovanovic, S. Garg, C.R. Team, Clinical evaluation of the GlucoWatch® biographer: a continual, non-invasive glucose monitor for patients with diabetes, Biosensors and Bioelectronics, 16(2001) 621-9.

[5]http://www.fda.gov/MedicalDevices/ProductsandMedicalProcedures/DeviceApprovalsandClearances/Recently-ApprovedDevices/ucm074293.htm, Accessed on: 28 April 2015

[6] S. Brady, L.E. Dunne, A. Lynch, B. Smyth, D. Diamond, Wearable Sensors? What is there to sense?, Studies in Health Technology and Informatics, 117(2005) 80-8.

[7] D. Diamond, Internet-Scale Sensing, Analytical Chemistry, 76(2004) 278 A-86 A.

[8] A.J. Bandodkar, D. Molinnus, O. Mirza, T. Guinovart, J.R. Windmiller, G. Valdés-Ramírez, et al., Epidermal tattoo potentiometric sodium sensors with wireless signal transduction for continuous non-invasive sweat monitoring, Biosensors and Bioelectronics, 54(2014) 603-9.

[9] M. Novell, T. Guinovart, I.M. Steinberg, M. Steinberg, F.X. Rius, F.J. Andrade, A novel miniaturized radiofrequency potentiometer tag using ion-selective electrodes for wireless ion sensing, Analyst, 138(2013) 5250-7.

[10] E. Bakker, E. Pretsch, The new wave of ion-selective electrodes, Analytical Chemistry, 74(2002) 420 A-6 A.

[11] R.P. Buck, E. Lindner, Tracing the history of selective ion sensors, Analytical Chemistry, 73(2001) 88 A-97 A.

[12] M. Cremer, Z Biol, 47(1906) 562.

[13] A. Radu, D. Diamond, Ion-selective electrodes in trace level analysis of heavy metals: Potentiometry for the XXI century, in: S. Alegret, A. Merkoçi (Eds.), Electrochemical Sensor Analysis, Elsevier, 2007 2007, pp. 25-7.

[14] J.W. Ross, Calcium-selective electrode with liquid ion exchanger, Science, 156(1967) 1378-9.

[15] C.J. Pedersen, Cyclic polyethers and their complexes with metal salts, Journal of the American Chemical Society, 89(1967) 2495-6.

[16] R. Bloch, A. Shatkay, H. Saroff, Fabrication and evaluation of membranes as specific electrodes for calcium ions, Biophysical Journal, 7(1967) 865-77.

[17] P. Bühlmann, E. Pretsch, E. Bakker, Carrier-based ion-selective electrodes and bulk optodes. 2. Ionophores for potentiometric and optical sensors, Chemical Reviews, 98(1998) 1593-688.

[18] E. Pretsch, The new wave of ion-selective electrodes, TrAC Trends in Analytical Chemistry, 26(2007) 46-51.

[19] U. Oesch, D. Ammann, W. Simon, Ion-selective membrane electrodes for clinical use, Clinical Chemistry, 32(1986) 1448-59.

[20] A. Lewenstam, Routines and Challenges in Clinical Application of Electrochemical Ion-Sensors, Electroanalysis, 26(2014) 1171-81.

[21] T. Sokalski, A. Ceresa, M. Fibbioli, T. Zwickl, E. Bakker, E. Pretsch, Lowering the detection limit of solvent polymeric ion-selective membrane electrodes. 2. Influence of composition of sample and internal electrolyte solution, Analytical Chemistry, 71(1999) 1210-4.

[22] T. Sokalski, A. Ceresa, T. Zwickl, E. Pretsch, Large improvement of the lower detection limit of ion-selective polymer membrane electrodes, Journal of the American Chemical Society, 119(1997) 11347-8.

[23] E. Bakker, E. Pretsch, P. Bühlmann, Selectivity of potentiometric ion sensors, Analytical Chemistry, 72(2000) 1127-33.

[24] A. Cadogan, Z. Gao, A. Lewenstam, A. Ivaska, D. Diamond, All-solid-state sodium-selective electrode based on a calixarene ionophore in a poly(vinyl chloride) membrane with a polypyrrole solid contact, Analytical Chemistry, 64(1992) 2496-501.

[25] K.Y. Chumbimuni-Torres, N. Rubinova, A. Radu, L.T. Kubota, E. Bakker, Solid contact potentiometric sensors for trace level measurements, Analytical Chemistry, 78(2006) 1318-22.

[26] S. Anastasova, A. Radu, G. Matzeu, C. Zuliani, U. Mattinen, J. Bobacka, et al., Disposable solid-contact ion-selective electrodes for environmental monitoring of lead with ppb limit-of-detection, Electrochimica Acta, 73(2012) 93-7.

[27] M. Guziński, G. Lisak, T. Sokalski, J. Bobacka, A. Ivaska, M. Bocheńska, et al., Solid-contact ion-selective electrodes with highly selective thioamide derivatives of p-tert-butylcalix[4]arene for the determination of lead(II) in environmental samples, Analytical Chemistry, 85(2013) 1555-61.

[28] C. Fay, S. Anastasova, C. Slater, S.T. Buda, R. Shepherd, B. Corcoran, et al., Wireless ion-selective electrode autonomous sensing system, Sensors Journal, IEEE, 11(2011) 2374-82.

[29] A. Lynch, D. Diamond, M. Leader, Point-of-need diagnosis of cystic fibrosis using a potentiometric ion-selective electrode array, Analyst, 125(2000) 2264-7.

[30] A.J. Bandodkar, W. Jia, J. Wang, Tattoo-based wearable electrochemical devices: a review, Electroanalysis, 27(2015) 562-72.

[31] J. Heikenfeld, Let them see you sweat, Spectrum, IEEE, 51(2014) 46-63.

[32] J. Wang, Potentiometry, Analytical Electrochemistry, Wiley2000, pp. 140-69.

[33] E. Bakker, P. Bühlmann, E. Pretsch, Carrier-based ion-selective electrodes and bulk optodes. 1. General characteristics, Chemical Reviews, 97(1997) 3083-132.

[34] E. Bakker, P. Bühlmann, E. Pretsch, The phase-boundary potential model, Talanta, 63(2004) 3-20.

[35] E. Lindner, B.D. Pendley, A tutorial on the application of ion-selective electrode potentiometry: an analytical method with unique qualities, unexplored opportunities and potential pitfalls; tutorial, Analytica Chimica Acta, 762(2013) 1-13.

[36] A. Lewenstam, Non-equilibrium potentiometry—the very essence, Journal of Solid State Electrochemistry, 15(2011) 15-22.

[37] V.S. Bagotsky, Aqueous Electrolyte Solutions, Fundamentals of Electrochemistry, Wiley2005, pp. 112-22.

[38] T. Sokalski, T. Zwickl, E. Bakker, E. Pretsch, Lowering the detection limit of solvent polymeric ion-selective electrodes. 1. Modeling the influence of steady-state ion fluxes, Analytical Chemistry, 71(1999) 1204-9.

[39] R.P. Buck, E. Lindner, Recommendations for nomenclature of ionselective electrodes (IUPAC Recommendations 1994), Pure and Applied Chemistry, 66(1994) 2527-36.

[40] P. Bühlmann, L.D. Chen, Ion-selective electrodes with ionophore-doped sensing membranes, Supramolecular Chemistry: From Molecules to Nanomaterials, (2012).

[41] G. Moody, B. Saad, J. Thomas, Glass transition temperatures of poly(vinyl chloride) and polyacrylate materials and calcium ion-selective electrode properties, Analyst, 112(1987) 1143-7.

[42] T. Lindfors, J. Szücs, F. Sundfors, R.E. Gyurcsányi, Polyaniline nanoparticle-based solid-contact silicone rubber ion-selective electrodes for ultratrace measurements, Analytical Chemistry, 82(2010) 9425-32.

[43] Y. Tsujimura, M. Yokoyama, K. Kimura, Practical applicability of silicone rubber membrane sodium-selective electrode based on oligosiloxane-modified calix[4]arene neutral carrier, Analytical Chemistry, 67(1995) 2401-4.

[44] L.Y. Heng, E.A. Hall, Assessing a photocured self-plasticised acrylic membrane recipe for Na^+ and K^+ ion selective electrodes, Analytica Chimica Acta, 443(2001) 25-40.

[45] L.Y. Heng, K. Toth, E.A. Hall, Ion-transport and diffusion coefficients of non-plasticised methacrylic–acrylic ion-selective membranes, Talanta, 63(2004) 73-87.

[46] C.-Z. Lai, S.S. Koseoglu, E.C. Lugert, P.G. Boswell, J. Rábai, T.P. Lodge, et al., Fluorous polymeric membranes for ionophore-based ion-selective potentiometry: how inert is teflon AF?, Journal of the American Chemical Society, 131(2009) 1598-606.

[47] L.D. Chen, C.-Z. Lai, L.P. Granda, M.A. Fierke, D. Mandal, A. Stein, et al., Fluorous membrane ion-selective electrodes for perfluorinated surfactants: trace-level detection and in situ monitoring of adsorption, Analytical Chemistry, 85(2013) 7471-7.

[48] A. Kisiel, E. Woźnica, M. Wojciechowski, E. Bulska, K. Maksymiuk, A. Michalska, Potentiometric layered membranes, Sensors and Actuators B: Chemical, 207, Part B(2015) 995-1003.

[49] C. Zuliani, D. Diamond, Opportunities and challenges of using ion-selective electrodes in environmental monitoring and wearable sensors, Electrochimica Acta, 84(2012) 29-34.

[50] E. Lindner, R.E. Gyurcsányi, Quality control criteria for solid-contact, solvent polymeric membrane ion-selective electrodes, Journal of Solid State Electrochemistry, 13(2009) 51-68.

[51] E. Bakker, D. Diamond, A. Lewenstam, E. Pretsch, Ion sensors: current limits and new trends, Analytica Chimica Acta, 393(1999) 11-8.

[52] J. Bobacka, A. Ivaska, A. Lewenstam, Potentiometric ion sensors, Chemical Reviews, 108(2008) 329-51.

[53] R. Cattrall, H. Freiser, Coated wire ion-selective electrodes, Analytical Chemistry, 43(1971) 1905-6.

[54] P.W. Alexander, T. Dimitrakopoulos, D.B. Hibbert, A six sensor array of coated-wire electrodes for use in a portable flow injection analyzer, Electroanalysis, 10(1998) 707-12.

[55] M. Fibbioli, W.E. Morf, M. Badertscher, N.F. de Rooij, E. Pretsch, Potential drifts of solid‐contacted ion‐selective electrodes due to zero‐current ion fluxes through the sensor membrane, Electroanalysis, 12(2000) 1286-92.

[56] J. Bobacka, Conducting polymer‐based solid‐state ion‐selective electrodes, Electroanalysis, 18(2006) 7-18.

[57] G.A. Crespo, S. Macho, J. Bobacka, F.X. Rius, Transduction mechanism of carbon nanotubes in solid-contact ion-selective electrodes, Analytical Chemistry, 81(2009) 676-81.

[58] R. Hernandez, J. Riu, J. Bobacka, C. Valles, P. Jimenez, A.M. Benito, et al., Reduced graphene oxide films as solid transducers in potentiometric all-solid-state ion-selective electrodes, The Journal of Physical Chemistry C, 116(2012) 22570-8.

[59] A. Düzgün, G.A. Zelada-Guillén, G.A. Crespo, S. Macho, J. Riu, F.X. Rius, Nanostructured materials in potentiometry, Analytical and Bioanalytical Chemistry, 399(2011) 171-81.

[60] J. Bobacka, A. Ivaska, Ion sensors with conducting polymers as ion-to-electron transducers, in: S. Alegret, A. Merkoçi (Eds.), Electrochemical Sensor Analysis, Elsevier 2007, pp. 72-81.

[61] A. Michalska, M. Wojciechowski, E. Bulska, K. Maksymiuk, Experimental study on stability of different solid contact arrangements of ion-selective electrodes, Talanta, 82(2010) 151-7.

[62] A. Guiseppi-Elie, Electroconductive hydrogels: synthesis, characterization and biomedical applications, Biomaterials, 31(2010) 2701-16.

[63] S. Nambiar, J.T.W. Yeow, Conductive polymer-based sensors for biomedical applications, Biosensors and Bioelectronics, 26(2011) 1825-32.

[64] N. Rozlosnik, New directions in medical biosensors employing poly(3,4-ethylenedioxy thiophene) derivative-based electrodes, Analytical and Bioanalytical Chemistry, 395(2009) 637-45.

[65] J. Bobacka, Potential stability of all-solid-state ion-selective electrodes using conducting polymers as ion-to-electron transducers, Analytical Chemistry, 71(1999) 4932-7.

[66] M. Wagner, G. Lisak, A. Ivaska, J. Bobacka, Durable PEDOT:PSS films obtained from modified water-based inks for electrochemical sensors, Sensors and Actuators B: Chemical, 181(2013) 694-701.

[67] G.C. Marjanovic, Polyaniline nanostructures, in: A. Eftekhari (Ed.) Nanostructured Conductive Polymers, Wiley2011, pp. 19-98.

[68] W.-S. Han, Y.-H. Lee, K.-J. Jung, S.-Y. Ly, T.-K. Hong, M.-H. Kim, Potassium ion-selective polyaniline solid-contact electrodes based on 4′,4″(5 ″)-di-tert-butyldibenzo-18-crown-6-ether ionophore, Journal of Analytical Chemistry, 63(2008) 987-93.

[69] J. P. Veder, R. De Marco, K. Patel, P. Si, E. Grygolowicz-Pawlak, M. James, et al., Evidence for a surface confined ion-to-electron transduction reaction in solid-contact ion-selective electrodes based on poly(3-octylthiophene), Analytical Chemistry, 85(2013) 10495-502.

[70] G. Lisak , M. Wagner , C. Kvarnström, J. Bobacka, A. Ivaska, A. Lewenstam, Electrochemical behaviour of poly(benzopyrene) films doped with eriochrome black T as a Pb^{2+}-sensitive sensors, Electroanalysis, 22(2010) 2794-800.

[71] K. Kijewska, G.J. Blanchard, J. Szlachetko , J. Stolarski, A. Kisiel, A. Michalska, et al., Photopolymerized polypyrrole microvessels, Chemistry–A European Journal, 18(2012) 310-20.

[72] A. Kisiel, M. Mazur, S. Kuśnieruk, K. Kijewska, P. Krysiński, A. Michalska, Polypyrrole microcapsules as a transducer for ion-selective electrodes, Electrochemistry Communications, 12(2010) 1568-71.

[73] M. Vázquez, J. Bobacka, M. Luostarinen, K. Rissanen, A. Lewenstam, A. Ivaska, Potentiometric sensors based on poly (3, 4-ethylenedioxythiophene)(PEDOT) doped with sulfonated calix[4]arene and calix[4]resorcarenes, Journal of Solid State Electrochemistry, 9(2005) 312-9.

[74] J. Migdalski, T. Błaż, A. Lewenstam, Conducting polymers-mechanisms of cationic sensitivity and the methods of inducing thereof, Electrochimica Acta, 133(2014) 316-24.

[75] M.C. Buzzeo, R.G. Evans, R.G. Compton, Non‐haloaluminate room‐temperature ionic liquids in electrochemistry—A review, ChemPhysChem, 5(2004) 1106-20.

[76] W. Lu, A.G. Fadeev, B. Qi, E. Smela, B.R. Mattes, J. Ding, et al., Use of ionic liquids for π-conjugated polymer electrochemical devices, Science, 297(2002) 983-7.

[77] N. Winterton, Solubilization of polymers by ionic liquids, Journal of Materials Chemistry, 16(2006) 4281-93.

[78] S. Ahmad, J.-H. Yum, Z. Xianxi, M. Grätzel, H.-J. Butt, M.K. Nazeeruddin, Dye-sensitized solar cells based on poly(3, 4-ethylenedioxythiophene) counter electrode derived from ionic liquids, Journal of Materials Chemistry, 20(2010) 1654-8.

[79] P. Hapiot, C. Lagrost, Electrochemical reactivity in room-temperature ionic liquids, Chemical Reviews, 108(2008) 2238-64.

[80] U. Vanamo, J. Bobacka, Electrochemical control of the standard potential of solid-contact ion-selective electrodes having a conducting polymer as ion-to-electron transducer, Electrochimica Acta, 122(2014) 316-21.

[81] E. Hupa, U. Vanamo, J. Bobacka, Novel ion-to-electron transduction principle for solid-contact ISEs, Electroanalysis, 27(2015) 591-4.

[82] U. Vanamo, J. Bobacka, Instrument-free control of the standard potential of potentiometric solid-Contact ion-selective electrodes by short-circuiting with a conventional reference electrode, Analytical Chemistry, 86(2014) 10540-5.

[83] C.-Z. Lai, M.A. Fierke, A. Stein, P. Bühlmann, Ion-selective electrodes with three-dimensionally ordered macroporous carbon as the solid contact, Analytical Chemistry, 79(2007) 4621-6.

[84] M.A. Fierke, C.-Z. Lai, P. Bühlmann, A. Stein, Effects of architecture and surface chemistry of three-dimensionally ordered macroporous carbon solid contacts on performance of ion-selective electrodes, Analytical Chemistry, 82(2010) 680-8.

[85] J. Hu, X.U. Zou, A. Stein, P. Bühlmann, Ion-selective electrodes with colloid-imprinted mesoporous carbon as solid contact, Analytical Chemistry, 86(2014) 7111-8.

[86] U. Mattinen, S. Rabiej, A. Lewenstam, J. Bobacka, Impedance study of the ion-to-electron transduction process for carbon cloth as solid-contact material in potentiometric ion sensors, Electrochimica Acta, 56(2011) 10683-7.

[87] M. Feng, H. Han, J. Zhang, H. Tachikawa, Electrochemical sensors based on carbon Nanotubes, in: X. Zhang, H. Ju, J. Wang (Eds.), Electrochemical Sensors, Biosensors and Their Biomedical Applications, Academic Press 2007, pp. 459–500.

[88] Q. Cao, J.A. Rogers, Ultrathin films of single‐walled carbon nanotubes for electronics and sensors: a review of fundamental and applied aspects, Advanced Materials, 21(2009) 29-53.

[89] F.X. Rius-Ruiz, G.A. Crespo, D. Bejarano-Nosas, P. Blondeau, J. Riu, F.X. Rius, Potentiometric strip cell based on carbon nanotubes as transducer layer: toward low-cost decentralized measurements, Analytical Chemistry, 83(2011) 8810-5.

[90] E. Jaworska, M. Schmidt, G. Scarpa, K. Maksymiuk, A. Michalska, Spray-coated all-solid-state potentiometric sensors, Analyst, 139(2014) 6010-5.

[91] E.J. Parra, P. Blondeau, G.A. Crespo, F.X. Rius, An effective nanostructured assembly for ion-selective electrodes. An ionophore covalently linked to carbon nanotubes for Pb^{2+} determination, Chemical Communications, 47(2011) 2438-40.

[92] G. Kerric, E.J. Parra, G.A. Crespo, F. Xavier Rius, P. Blondeau, Nanostructured assemblies for ion-sensors: functionalization of multi-wall carbon nanotubes with benzo-18-crown-6 for Pb^{2+} determination, Journal of Materials Chemistry, 22(2012) 16611-7.

[93] E.J. Parra, F.X. Rius, P. Blondeau, A potassium sensor based on non-covalent functionalization of multi-walled carbon nanotubes, Analyst, 138(2013) 2698-703.

[94] K.E. Toghill, R.G. Compton, Electrochemical non-enzymatic glucose sensors: a perspective and an evaluation, International Journal of Electrochemical Science, 5(2010) 1246-301.

[95] K.S. Kim, Y. Zhao, H. Jang, S.Y. Lee, J.M. Kim, K.S. Kim, et al., Large-scale pattern growth of graphene films for stretchable transparent electrodes, Nature, 457(2009) 706-10.

[96] C. Sriprachuabwong, C. Karuwan, A. Wisitsorrat, D. Phokharatkul, T. Lomas, P. Sritongkham, et al., Inkjet-printed graphene-PEDOT: PSS modified screen printed carbon electrode for biochemical sensing, Journal of Materials Chemistry, 22(2012) 5478-85.

[97] E. Jaworska, W. Lewandowski, J. Mieczkowski, K. Maksymiuk, A. Michalska, Critical assessment of graphene as ion-to-electron transducer for all-solid-state potentiometric sensors, Talanta, 97(2012) 414-9.

[98] E. Jaworska, W. Lewandowski, J. Mieczkowski, K. Maksymiuk, A. Michalska, Simple and disposable potentiometric sensors based on graphene or multi-walled carbon nanotubes - carbon-plastic potentiometric sensors, Analyst, 138(2013) 2363-71.

[99] M. Brust, M. Walker, D. Bethell, D.J. Schiffrin, R. Whyman, Synthesis of thiol-derivatised gold nanoparticles in a two-phase liquid–liquid system, Journal of the Chemical Society, Chemical Communications, (1994) 801-2.

[100] C.R. Rao, G.U. Kulkarni, P.J. Thomas, P.P. Edwards, Metal nanoparticles and their assemblies, Chemical Society Reviews, 29(2000) 27-35.

[101] C.-J. Jia, F. Schüth, Colloidal metal nanoparticles as a component of designed catalyst, Physical Chemistry Chemical Physics, 13(2011) 2457-87.

[102] A.J. Haes, S. Zou, G.C. Schatz, R.P. Van Duyne, A nanoscale optical biosensor: the long range distance dependence of the localized surface plasmon resonance of noble metal nanoparticles, The Journal of Physical Chemistry B, 108(2004) 109-16.

[103] E. Jaworska, M. Wójcik, A. Kisiel, J. Mieczkowski, A. Michalska, Gold nanoparticles solid contact for ion-selective electrodes of highly stable potential readings, Talanta, 85(2011) 1986-9.

[104] E. Woźnica, M.M. Wójcik, J. Mieczkowski, K. Maksymiuk, A. Michalska, Dithizone modified gold nanoparticles films as solid contact for Cu^{2+} ion‐selective electrodes, Electroanalysis, 25(2013) 141-6.

[105] G. Matzeu, C. Zuliani, D. Diamond, Solid-contact ion-selective electrodes (ISEs) based on ligand functionalised gold nanoparticles, Electrochimica Acta, 159(2015) 158-65.

[106] G. Jagerszki, A. Grun, I. Bitter, K. Toth, R.E. Gyurcsanyi, Ionophore-gold nanoparticle conjugates for Ag^{+}-selective sensors with nanomolar detection limit, Chemical Communications, 46(2010) 607-9.

[107] T. Zhang, C.-Z. Lai, M.A. Fierke, A. Stein, P. Bühlmann, Advantages and limitations of reference electrodes with an ionic liquid junction and three-dimensionally ordered macroporous carbon as solid contact, Analytical Chemistry, 84(2012) 7771-8.

[108] R.E. Dohner, D. Wegmann, W.E. Morf, W. Simon, Reference electrode with free-flowing free-diffusion liquid junction, Analytical Chemistry, 58(1986) 2585-9.

[109] Z. Mousavi, K. Granholm, T. Sokalski, A. Lewenstam, An analytical quality solid-state composite reference electrode, Analyst, 138(2013) 5216-20.

[110] A. Michalska, All‐solid‐state ion selective and all‐solid‐state reference electrodes, Electroanalysis, 24(2012) 1253-65.

[111] U. Guth, F. Gerlach, M. Decker, W. Oelßner, W. Vonau, Solid-state reference electrodes for potentiometric sensors, Journal of Solid State Electrochemistry, 13(2009) 27-39.

[112] K. Granholm, Z. Mousavi, T. Sokalski, A. Lewenstam, Analytical quality solid-state composite reference electrode manufactured by injection moulding, Journal of Solid State Electrochemistry, 18(2014) 607-12.

[113] Z. Mousavi, K. Granholm, T. Sokalski, A. Lewenstam, All-solid-state electrochemical platform for potentiometric measurements, Sensors and Actuators B: Chemical, 207, Part B(2015) 895-9.

[114] F.X. Rius-Ruiz, D. Bejarano-Nosas, P. Blondeau, J. Riu, F.X. Rius, Disposable Planar Reference Electrode Based on Carbon Nanotubes and Polyacrylate Membrane, Analytical Chemistry, 83(2011) 5783-8.

[115] C. Zuliani, D. Diamond, Opportunities and challenges of using ion-selective electrodes in environmental monitoring and wearable sensors, Electrochimica Acta, 84(2012) 29-34.

[116] A. Kisiel, M. Donten, J. Mieczkowski, F.X. Rius-Ruiz, K. Maksymiuk, A. Michalska, Polyacrylate microspheres composite for all-solid-state reference electrodes, Analyst, 135(2010) 2420-5.

[117] T. Guinovart, G.A. Crespo, F.X. Rius, F.J. Andrade, A reference electrode based on polyvinyl butyral (PVB) polymer for decentralized chemical measurements, Analytica Chimica Acta, 821(2014) 72-80.

[118] Y. Mi, S. Mathison, E. Bakker, Polyion sensors as liquid junction‐free reference electrodes, Electrochemical and Solid-State Letters, 2(1999) 198-200.

[119] R. Mamińska, A. Dybko, W. Wróblewski, All-solid-state miniaturised planar reference electrodes based on ionic liquids, Sensors and Actuators B: Chemical, 115(2006) 552-7.

[120] T. Kakiuchi, T. Yoshimatsu, N. Nishi, New class of Ag/AgCl electrodes based on hydrophobic ionic liquid saturated with AgCl, Analytical Chemistry, 79(2007) 7187-91.

[121] D. Cicmil, S. Anastasova, A. Kavanagh, D. Diamond, U. Mattinen, J. Bobacka, et al., Ionic liquid‐based, liquid‐junction‐free reference electrode, Electroanalysis, 23(2011) 1881-90.

[122] U. Mattinen, J. Bobacka, A. Lewenstam, Solid‐contact reference electrodes based on lipophilic salts, Electroanalysis, 21(2009) 1955-60.

[123] J. Hu, K.T. Ho, X.U. Zou, W.H. Smyrl, A. Stein, P. Bühlmann, All-solid-state reference electrodes based on colloid-imprinted mesoporous carbon and their application in disposable paper-based potentiometric sensing devices, Analytical Chemistry, 87(2015) 2981-7.

[124] T. Blaz, B. Baś, J. Kupis, J. Migdalski, A. Lewenstam, Multielectrode potentiometry in a one-drop sample, Electrochemistry Communications, 34(2013) 181-4.

[125] R. Toczyłowska-Mamińska, A. Lewenstam, K. Dołowy, Multielectrode bisensor system for time-resolved monitoring of ion transport across an epithelial cell layer, Analytical Chemistry, 86(2014) 390-4.

[126] C. Zuliani, G. Matzeu, D. Diamond, A potentiometric disposable sensor strip for measuring pH in saliva, Electrochimica Acta, 132(2014) 292-6.

[127] L. Gonzalez-Macia, A. Morrin, M.R. Smyth, A.J. Killard, Advanced printing and deposition methodologies for the fabrication of biosensors and biodevices, Analyst, 135(2010) 845-67.

[128] F.X. Rius-Ruiz, F.J. Andrade, J. Riu, F.X. Rius, Computer-operated analytical platform for the determination of nutrients in hydroponic systems, Food Chemistry, 147(2014) 92-7.

[129] M. Pawlak, G. Mistlberger, E. Bakker, In situ surface functionalization of plasticized poly(vinyl chloride) membranes by 'click chemistry', Journal of Materials Chemistry, 22(2012) 12796-801.

[130] Z. Jarolímová, G.A. Crespo, M.G. Afshar, M. Pawlak, E. Bakker, All solid state chronopotentiometric ion-selective electrodes based on ferrocene functionalized PVC, Journal of Electroanalytical Chemistry, 709(2013) 118-25.

[131] M.S. Ozdemir, M. Marczak, H. Bohets, K. Bonroy, D. Roymans, L. Stuyver, et al., A label-free potentiometric sensor principle for the detection of antibody–antigen interactions, Analytical Chemistry, 85(2013) 4770-6.

[132] M. Pawlak, E. Bakker, Chemical modification of polymer ion-selective membrane electrode surfaces, Electroanalysis, 26(2014) 1121-31.

[133] J. Szűcs, R.E. Gyurcsányi, Towards protein assays on paper platforms with potentiometric detection, Electroanalysis, 24(2012) 146-52.

[134] J. Cui, G. Lisak, S. Strzalkowska, J. Bobacka, Potentiometric sensing utilizing paper-based microfluidic sampling, Analyst, 139(2014) 2133-6.

[135] G. Lisak, J. Cui, J. Bobacka, Paper-based microfluidic sampling for potentiometric determination of ions, Sensors and Actuators B: Chemical, 207, Part B(2015) 933-9.

[136] M. Novell, M. Parrilla, G.A. Crespo, F.X. Rius, F.J. Andrade, Paper-based ion-selective potentiometric sensors, Analytical Chemistry, 84(2012) 4695-702.

[137] M. Novell, T. Guinovart, P. Blondeau, F.X. Rius, F.J. Andrade, A paper-based potentiometric cell for decentralized monitoring of Li levels in whole blood, Lab on a Chip, 14(2014) 1308-14.

[138] A. Määttänen, U. Vanamo, P. Ihalainen, P. Pulkkinen, H. Tenhu, J. Bobacka, et al., A low-cost paper-based inkjet-printed platform for electrochemical analyses, Sensors and Actuators B: Chemical, 177(2013) 153-62.

[139] W.-J. Lan, X.U. Zou, M.M. Hamedi, J. Hu, C. Parolo, E.J. Maxwell, et al., Paper-based potentiometric ion sensing, Analytical Chemistry, 86(2014) 9548-53.

[140] Z. Nie, C.A. Nijhuis, J. Gong, X. Chen, A. Kumachev, A.W. Martinez, et al., Electrochemical sensing in paper-based microfluidic devices, Lab on a Chip, 10(2010) 477-83.

[141] Z. Nie, F. Deiss, X. Liu, O. Akbulut, G.M. Whitesides, Integration of paper-based microfluidic devices with commercial electrochemical readers, Lab on a Chip, 10(2010) 3163-9.

[142] G. Matzeu, L. Florea, D. Diamond, Advances in wearable chemical sensor design for monitoring biological fluids, Sensors and Actuators B: Chemical, 211(2015) 403-18.

[143] B. Schazmann, D. Morris, C. Slater, S. Beirne, C. Fay, R. Reuveny, et al., A wearable electrochemical sensor for the real-time measurement of sweat sodium concentration, Analytical Methods, 2(2010) 342-8.

[144] T. Guinovart, G. Valdés-Ramírez, J.R. Windmiller, F.J. Andrade, J. Wang, Bandage-based wearable potentiometric sensor for monitoring wound pH, Electroanalysis, 26(2014) 1345-53.

[145] M. Cuartero, J.S. del Río, P. Blondeau, J.A. Ortuño, F.X. Rius, F.J. Andrade, Rubber-based substrates modified with carbon nanotubes inks to build flexible electrochemical sensors, Analytica Chimica Acta, 827(2014) 95-102.

[146] T. Guinovart, M. Parrilla, G.A. Crespo, F.X. Rius, F.J. Andrade, Potentiometric sensors using cotton yarns, carbon nanotubes and polymeric membranes, Analyst, 138(2013) 5208-15.

[147] D.-H. Kim, N. Lu, R. Ma, Y.-S. Kim, R.-H. Kim, S. Wang, et al., Epidermal electronics, Science, 333(2011) 838-43.

[148] J.R. Windmiller, J. Wang, Wearable electrochemical sensors and biosensors: a review, Electroanalysis, 25(2013) 29-46.

[149] T. Guinovart, A.J. Bandodkar, J.R. Windmiller, F.J. Andrade, J. Wang, A potentiometric tattoo sensor for monitoring ammonium in sweat, Analyst, 138(2013) 7031-8.

[150] A.J. Bandodkar, V.W. Hung, W. Jia, G. Valdés-Ramírez, J.R. Windmiller, A.G. Martinez, et al., Tattoo-based potentiometric ion-selective sensors for epidermal pH monitoring, Analyst, 138(2013) 123-8.

[151] A.J. Bandodkar, D. Molinnus, O. Mirza, T. Guinovart, J.R. Windmiller, G. Valdés-Ramírez, et al., Epidermal tattoo potentiometric sodium sensors with wireless signal transduction for continuous non-invasive sweat monitoring, Biosensors and Bioelectronics, 54(2014) 603-9.

Chapter 2.

Advances in Wearable Chemical Sensor Design for Monitoring Biological Fluids

Giusy Matzeu[a], Larisa Florea*[a] and Dermot Diamond[a]

URL: http://www.sciencedirect.com/science/article/pii/S0925400515001033

ISSN and DOI: 10.1016/j.snb.2015.01.077

Sensors and Actuators B: Chemical 211 (2015): 403-418.

*Corresponding author

[a]Insight Centre for Data Analytics, Dublin City University, Dublin 9, Ireland.

Aims and Objectives

Chapter 2 gives an overview of the latest advances in the field of chemical sensors integrated on wearable applications. The attention was focused on the non-invasive monitoring of biological fluids such as interstitial fluid, breath, saliva, sweat and tears.

Contributions

- Design, conception and writing up of the manuscript.

Abstract

The state of the art and future challenges related to wearable chemical sensors are addressed within this review. Our attention is focused on the monitoring of biological fluids such as interstitial fluids, breath, sweat, saliva and tears, while aiming at the realisation of miniaturised, non-invasive and low-cost point of care systems. The development of such sensing devices is influenced by many factors and is usually addressed through the use of smart-materials such as graphene, carbon nanotubes, poly Ionic Liquids, etc. These are seen as the pivotal steps towards the integration of chemical sensors within pervasive applications for personal health care.

Keywords

Non-Invasive Monitoring, Biological Fluids, Chemical Sensors, Wearable, Smart-Materials, Personal Health.

2.1 Introduction

The pronounced increase in incidence of aging related pathologies observed in the recent years has greatly emphasised the need for a novel class of personalised point of care systems that could be extensively and effortlessly integrated into the daily life of a patient in the form of wireless body sensor networks (WBANs) [1]. So far, most research efforts in this direction have been focused on the adaptation of miniaturised wearable designs based on relatively mature technologies such as motion tracking [2], bio-electrical signals analysis [3] and temperature detection [4]. On the other hand, the biochemical analytes contained in biological fluids have been often overlooked as possible sensor targets despite the valuable information they convey about the state of health of an individual. Urine and blood are routinely analysed through standard analytical techniques such as Atomic Absorption Spectroscopy, Ion Chromatography and Gas Chromatography, but these methodologies are relatively expensive and can inevitably provide only discontinuous "one shot" measurements of the concentration of an analyte of interest, since they are currently not suitable for miniaturisation. While blood is by far the most understood sample for diagnostic measurements, other biological fluids such as sweat, saliva, interstitial fluids, tears and breath are more readily accessible and thus are attractive targets for non/minimally-invasive wearable sensor platforms, as recently described by Bandodkar et al. [5].

The multiple challenges faced by chemo/bio-sensors during their normal use have been described in detail in a recent review by Diamond et al. [6]. For instance, due to their continuous exposure to the fluid of interest and to wear and tear, portable sensors targeting biological fluid analytes need frequent recalibration to correct for signal drift over time, and in some cases have relatively high energy demands. Recent advances in materials science and microfluidic fabrication techniques [7-9] are opening routes towards enhanced miniaturisation and more efficient handling of the liquid substrates, and the more general availability of low-cost, reliable, and wearable "lab on a chip" systems. At the same time, the availability of novel smart-materials for the realisation of both protective and active layers for sensor production promises to greatly increase the performance of sensing devices, and are currently the object of intense research [6]. Finally, the integration of sensors within textiles could provide a much-needed improvement in robustness and mechanical durability of sensors thanks to a better protection of the sensing area. Materials that are currently employed for the embedding of electrochemical sensor are flexible polymers such as Kapton and Mylar,

which have excellent thermal properties and stability, and GoreTex, which combines hydrophobic character with water permeable behaviour [10].

Perhaps most striking is the recent dramatic movement by multinational IT companies into the wearable sensor space, including the first signs of attempts to integrate chemo/bio-sensors. For example, Google Glass [11] is a wearable spectacle-based electronics platform that can be used to harvest body sensor data. Google have announced a novel project to integrate a glucose sensor into a contact lens which, due to the close proximity to the spectacles, could be powered inductively to enable glucose measurements and short-range communications [12]. Similarly, Apple announced iWatch [13], which can be conveniently worn on the wrist and is rumoured to integrate a glucose sensing capability, while IBM [14] and Intel [15] have sponsored several initiatives aimed at promoting the design of novel wearable systems.

In this review, we will provide an overview of some of the advances occurring in the past decade and summarise on-going research activities aimed at integrating chemical sensors into wearable platforms for non/minimally-invasive monitoring of analytes in biological fluids. Particular attention will also be paid to the most promising trends observed in the development of new materials for the enhancement of the performance of wearable chemical sensors.

2.2 Interstitial Fluid Monitoring

Except for large molecules (e.g. lipids), the composition of the interstitial fluid is very similar to that of blood in terms of salt, protein, glucose, and ethanol contents. Preliminary studies were carried out on the employment of needle type biosensors to detect cholesterol [16]. However, a better minimally-invasive approach was based on the use of micro-needle arrays that allow for the realisation of miniaturised, wireless devices with a patch-like configuration. In preliminary studies H_2O_2 [17], pH, glucose [18] and lactate variations [17, 18] were monitored using hollow needles filled with carbon paste sensitive materials tested on bench. Validation through animal models and ad hoc miniaturised electronic platforms are still missing. Nevertheless, most of minimally-invasive devices already on the market are devoted to glucose monitoring. The correlation with blood glucose levels makes interstitial fluid a convenient target for continuous monitoring of patients affected by diabetes [19, 20]. The measurements obtained via subcutaneously implanted devices can then be corrected to take into

account the time lag between variations in blood and interstitial glucose levels via validated compartmental models [21].

2.2.1 Minimally-Invasive Devices for Glucose Monitoring

Several devices for glucose monitoring are already on the market, and enable continuous detection with no need for repeated finger pricking. All devices employ electrochemical sensors, while different approaches were taken for sampling within the subcutaneous adipose tissue. Some designs rely on a direct implantation through a needle (e.g. Guardian RT by Medtronic) [20] while others employ a microdialysis harvesting approach (e.g. GlucoDay by Menarini [20, 22]) correlated with external monitoring of the collected sample [20].

The most popular system is probably the Glucose Free Style Navigator by Abbott, which consists of a disposable sensor delivery unit, a radio frequency transmitter directly connected to the sensor, and a hand held receiver that shows the glucose levels. Abnormal conditions (e.g. hypoglycemia <70 mg/dL and hyperglycemia >240 mg/dL) are signalled by an acoustic alarm with high accuracy (96% and 99.7% of cases respectively for hypoglycemia and hyperglycemia) [23]. The minimally-invasive nature of such devices could be further enhanced by totally implantable devices inserted at the adipose levels, provided that a battery with sufficient durability and biocompatibility is available. In a 2006 review, Heller [24] described several possible battery configurations where the interstitial fluid is used as the electrolyte between cathode and anode. In particular, the adoption of wired bilirubin oxidase as cathode (where O_2 is electroreduced to water) and glucose oxidase as anode would provide the best biocompatibility for long-term implanted glucose sensors [24]. This approach seems revolutionary, and we expect that several investigations will be driven in this direction in the next coming years and additional solutions might be offered by the implementation of implantable biofuel cells [25].

Several improvements are still needed also in terms of sensor technology in order to enhance durability (currently available sensors must be replaced every 3 to 7 days) and sensitivity (especially in hypoglycemic and hyperglycemic conditions) [20]. Among the various devices that have been proposed in the last ten years, one of the most original and innovative relied on the integration of the sensor into a polymeric housing endowed with a microperfusion channel for sample collection. A cavity contained the Pt working electrode made of a Glucose Oxidase (GOx)/agarose/glutaraldehyde sensitive layer covered by a silicon pore membrane (105 pores with 50 μm diameter on

an area of 2650 μm²) that controlled glucose diffusion. At the same time, the membrane protected the sensor from fouling and improved its accuracy and reliability over time. Bench tests showed fast responses to glucose variations (30 s, flow rate of 0.5 μL/min) within the range of interest (0.05-20 mM) and stability over time (1 week). The sensor was also tested in a clinical environment showing promising results for its potential application for open flow microinfusion techniques [26]. Other approaches have involved integrating sensors within microfluidic chips, in order to reduce the overall size of the system. This was possible through optimisation of the length (1.0 cm) of a microdialysis membrane connected to an enzymatic microreactor endowed with a chaotic mixing channel, which was bonded to a glass chip providing the Pt working electrode. An overoxidised polypyrrole (PPy) layer was employed to avoid Faradaic interferences from other analytes present in the interstitial fluid (such as ascorbic acid, uric acid, acetaminophen) and an Ag/AgCl layer was used as a reference electrode. A constant supply of GOx was provided to the chamber at a flow rate of 1.5 μL/min. In the chamber, the GOx mixed with the interstitial fluid where it reacted with glucose, generating a linear signal within the range 2.1-20.6 mM (lag time of 18 minutes). The device was then implanted in the abdominal area of rats and successfully tested after bolus injection and under controlled insulin infusion. Before testing in humans, several improvements were recommended to increase sensor durability from hours (test on rats lasted four hours) to several days [27].

Despite these advances, it must be appreciated that there are still serious limitations to the in-vivo electrochemical sensing of glucose. These include glucose consumption at the electrode surface, suboptimal performance at low glucose levels, loss of electrode materials, degradation of enzymes, interference from other sample components, oxygen deficiency at the electrode, impact of biofilm formation, need for frequent recalibration, and short durability of the sensing strip. Nonetheless, various aspects of the sensor design and materials employed can bring many benefits in terms of sensor performance. For instance, the use of affinity materials can be advantageous to reduce biofouling through modification of the binding time of the molecule of interest. A differential affinity glucose sensor was developed for dielectric and viscometric detection, with the former showing the best performances [28]. This Microelectromechanical System (MEMS) consisted of two connected microchambers, one containing a glucose-sensitive (boronic acid containing the co-polymer poly(N-hydroxyethylacrylamide-*ran*-3-acrylamidophenylboronic acid) (PHEAA-*ran*-PAABA)) and the other a glucose-insensitive (poly(acrylamide) (PAA)) material. Two parallel electrodes were also integrated into the system, the lower one being realised on a glass

substrate while the upper one made on a perforated parylene diaphragm (sustained by stiff posts to prevent its collapse) that allowed analyte diffusion. In-vitro tests of the frequency responses to the electric field were conducted at 32 kHz and showed response (4.9 min) and recovery times (7.8 min) comparable with standard systems used for glucose monitoring within the sensitive range 0-500 mg/dL, with an accuracy of 1.74 mg/dL [28, 29]. Sensors implanted into the scapular area of mice provided a stable signal for ca. 8 minutes, as shown through comparison with capillary blood glucose levels measured at the tail region. The recorded time behaviour was similar (after bolus or insulin injection) to that of blood, with a delay of approximately 5 to 15 minutes. The results showed good correlation (r^2=0.962) and Clarke Error Grid analysis suggested the approach would be suitable for clinical tests (83.6% of the samples in zone A) [29].

New solutions might also be offered by optical systems, but they are still at their infancy. The use of Surface Enhanced Raman Spectroscopy (SERS) and more recently Spatially Offset Raman Spectroscopy (SORS) could indeed revolutionise the approaches for continuous glucose monitoring in interstitial fluids [30]. Raman Spectroscopy can detect the unique vibrational signature of molecules whose signal can be enhanced using surfaces covered by a film of silver nanospheres functionalised with a self-assembled monolayer of decanethiol (DT)/6-mercato-1-hexanol (MH) that is able to create a 'dynamic pocket' with the approximate size of a glucose molecule. The tip of an optical fibre was covered with this film, implanted in the abdominal area of rats, and was found to be able to successfully track low glucose levels (31-79 mg/dL) over a period of 17 days [31].

2.2.2 Non-Invasive Devices for Glucose Monitoring

Completely non-invasive designs for wearable interstitial fluid sensors aim at removing the need for subcutaneous implantation, to find a balance between the need to access a representative sample, and the need for more comfortable wearability and an effective usage model. With the GlucoWatch, realised by Tierney et al. [32], the solution adopted was to bring interstitial fluid through the skin to the external analytical platform using iontophoresis. Although it has been withdrawn from the market due to induced irritation problems in patients [32], the GlucoWatch stimulated intense research and follow up studies. Dachao et al. [33] developed a system that includes SonoPrep, a device that delivers ultrasonic energy at the skin level (frequency 55 kHz on an area of 0.8 cm^2). This also stimulates the release of interstitial fluid, which can be collected in an external glass chamber using a vacuum for up to 15 minutes.

Glucose in the fluid is monitored using a commercial biosensor. The system was validated after administering glucose to healthy subjects and sampling the fluid every 20 minutes. Glucose variations in the interstitial fluid followed those in blood, and a mathematical model was developed and validated to provide a predictive capability. However, this system was not miniaturised enough to be considered wearable [33].

The GlucoTrack was designed to be positioned at the tip of the earlobe of a user. Three sensors simultaneously monitored physical variations in electric and acoustic impedance and heat transfer for 1 minute. The combined measurement allowed the estimation of glucose levels indirectly and with increased accuracy with respect to the single measurements (Clarke Error Grid with a mean absolute relative difference (ARD) value of 15.8%). The system was first calibrated on each user to adjust the correlation parameters, and then measurements were taken at regular intervals (every 30 minutes) while subjects were carrying out standard daily activities. Clarke Error Grid data showed that the readings (96%) were within the clinically acceptable ranges [34].

Another non-invasive system was based on resonance-enhanced pulsed photoacoustic spectroscopy with a windowless resonator cell positioned on the skin of the fingertip. This open stainless-steel resonator cell was characterised by two perpendicularly connected absorption and resonance cylindrical cavities. The laser beam entered the system irradiating the sample on the far side (energy below 1 mW/mm, laser pulse width kept at 500 ns), inducing the photoacoustic effect in the absorption cavity. In response to the stimulus, the sample produced an acoustic wave that was detected by an ultrasound detector (i.e. a microphone), positioned at the end of the resonance cavity. This magnified the signals, which were then filtered via a lock-in amplifier. Experiments using a glassy carbon layer showed that the best resonance peak (best Q factor and the highest signal-to-noise ratio) was obtained at 51.7 kHz [35]. Principal component analysis of the IR spectra (obtained from the skin) showed that glucose was the first principal component [36]. Improvements in the configuration of the cell and its connection to a real, miniaturised portable instrument are still necessary [35].

2.2.3 Non-Invasive Monitoring of Ethanol

Glucose is not the only analyte of interest that can be detected and continuously monitored in the interstitial fluid samples. For instance, ethanol can be monitored via poration of the stratum corneum of the skin. This sampling technique is painless and consists of positioning a handheld porator that is able to create micropores roughly of

the diameter of a human hair (<100 μm in diameter, open for 3 days). An interstitial liquid harvesting system is positioned at the skin location wherein the pores have been generated. An electromechanical pump (6 to 9 inches of mercury) allows the fluid collection (10 μL/h) in the harvesting unit, which also contains an electrochemical sensor with an alcohol oxidase working electrode catalysing the reaction between ethanol and O_2, producing H_2O_2 which is then reduced to H^+ (see Equation 2.1 and 2.2)

$$\text{Ethanol} + O_2 \rightarrow \text{acetaldehyde} + H_2O_2 \quad (2.1)$$

$$H_2O_2 \rightarrow 2H^+ + O_2 + 2e^- \quad (2.2)$$

The sensor linear range was within 0-0.2% of ethanol content, with a resolution approaching 0.01%. The typical response delay was 8-12 minutes from the point of ethanol consumption. The system was shown to be insensitive to common interferents such as uric acid, ascorbic acid and glucose. The main drawbacks of this device were the long time (1-2 hours) needed to stabilise the baseline reading during tests and the use of a porator based on a laser source, which can cause burns, scars and facilitate bacterial growth, limiting the access over time to the underlying interstitial fluid for monitoring. A solution might be represented by the use of microneedles integrated on a patch, able to collect, drive and sense the analyte of interest within the sample. However, a really good outcome is represented by the connection of the harvesting/sensing chip to a wireless radio frequency (RF) platform allowing for the realisation of a portable, real-time wearable device [37].

2.3 Breath Monitoring

Monitoring of breath vapours allows for completely non-invasive detection of several analytes of interest in clinical diagnosis and therapy [38, 39].

Breath monitoring poses challenges across all aspects of the measurement procedure, spanning from the choice of an opportune target bio-marker, to the implementation of the measurement technique [38]. Efficient sampling is also complicated, and because of these difficulties the overall accuracy of breath-based measurements is generally not as good as one would like. Nonetheless, the convenience in accessing breath vapours has promoted the deployment of several successful sensing devices which are in common use, the most notable examples probably being the portable alcohol analysers (based on an electrochemical fuel cell) that are used by police officers to estimate (indirectly) ethanol concentration in blood [40]. In the following sections, we provide other

examples of devices that have successfully exploited breath to provide an indication on the content of analytes such as nitric oxide and oxygen, ammonia and acetone in the body. However, humidity is a common and serious interferent in breath-based sensing, as it is with most gas-phase measurements.

2.3.1 Humidity Monitoring in Breath

Pronounced variations in humidity occur naturally in the expirate of patients and this can affect sensor response. Regardless of the target analyte, most breath sensing devices need thus to be coupled with miniaturised fast-response humidity sensors to enable opportune bias corrections. Corres et al. [41] exploited the electrostatic self-assembly of super-hydrophilic SiO_2 nanoparticles to build a humidity sensor integrated into an optical fibre. The novel sensor showed good reproducibility and low hysteresis even when exposed to 3 consecutive human breathing cycles (inspiration and expiration times of 100 ms and 150 ms, respectively) [41]. Even better performances were obtained by exploiting humidity-induced variations in the metachromasy properties of methylene blue (MB). The dye was dip-coated on the tip of an optical fibre connected to a red light emitting diode (λ=660 nm). Increases in relative humidity reduced light absorbance due to MB dimerisation within working ranges of 8-98%, with fast response (0.5 s) and low hysteresis. This sensor was tested during a breathing trial, and was shown to be capable of detecting the characteristic respiration patterns of hyperventilation [42].

Despite their good performances, both these devices could not be categorised as wearable due to the sizes of each system. On the other hand, a humidity sensor based on a hydrophilic polytetrafluoroethylene membrane (80 μm thick), covered on both sides by a gold layer, appears to offer significant improvements in this regard. The sensitive area was insulated with a biocompatible cyanoacrylate adhesive that was also used to fix the electrode. The sensor was then connected to a miniaturised Inductance, Capacitance and Resistance (LCR) meter able to monitor changes in resistance with humidity levels. Overall the device was soft, flexible, tear resistant, chemically stable, and able to work within a 30-85% humidity range at room temperature (25 °C). Real-time tests on healthy subjects allowed the respiration rate to be tracked with the sensor positioned on the upper part of the mouth or on the fingertip for simultaneous, real-time sweat monitoring [43].

Graphene oxide (GO) is a promising material for use in humidity sensors thanks to the interactions between the exposed functional oxygen groups and water. Good results

were obtained with 15 nm GO layers deposited by spray coating on top of Ag screen-printed interdigitated electrodes. These sensors were able to follow changes in humidity over the range 10-90%, with fast response (20-30 ms) and recovery (30 ms) times. The fast response behaviour was mainly dictated by the 2D GO flake structures that created a porous layer with randomly connected bi-dimensional domains. The GO based sensing devices were able to not only track breathing, but also to classify different voices, by analysis of whistles tones through principal component analysis [44]. These results are really promising for eventual integration into smart fabrics, but they lack essential features for continuous measurements, and results showing the long-term stability of these patterns (for hours or days).

2.3.2 NO and O_2 Monitoring in Breath

The detection of NO levels or its related products (NO_2^- and NO_3^-) is important for understanding many biological processes and health conditions. For example, in asthmatic patients, events are signalled by release of NO from inflammatory cells. NO in breath ranges between low ppb to around 100 ppb. Most NO sensors are based on electrochemical techniques, and while these can cover the range of interest [45-47], in general they are not yet integrated into point of care systems for breath analysis. However, a portable hand-held breath analyser featuring a miniaturised spectrometer was recently realised. It was based on a mouth piece, a pressure meter endowed with 3 LEDs that helped the person to maintain constant exhalation flow, a fluoroplastic tube, and a Teflon piece with a hole characterised by different diameters (allowing different flow rates, keeping the mouth pressure at 10 mbar) connected to a Mylar balloon for sample collection. The sensing part was based on a wavelength modulation spectroscopy NO sensor coupled with a quantum cascade laser used as the source. Sensor performance was assessed through comparison with a Loccioni breath sampler, showing a correlation coefficient of r^2=0.993 and a slope of 0.986, with a limit of detection in the range 0-100 ppbv, a response time of 1 s and insensitivity to changes in flow rate [48].

Optical fibers also represent another inexpensive, real-time monitoring tool that can be exploited to realise portable or wearable devices. For example, this technology was used to realise an O_2 breath analyser, using sensors based on Organically Modified SILicate (ORMOSIL) sol-gel with embedded ruthenium O_2 sensitive luminophores [Ru(III)-tris(4,7-diphenyl-1,10-phenanthroline] ($[Ru(ddp)_3]^{2+}$) [49] or the cyclometalated iridium complexes bis(1-phenylisoquinoline)(acetylacetonate)iridium(III) ($[Ir(piq)_2(acac)]$) O_2 sensitive fluorophores, with the latter reporting the best

performances [50]. The fluorophore doped ORMOSILs (composed of alkyl ORMOSIL n-propyltrimethoxysilane (n-propyl-TriMOS) and perfluoroalkyl ORMOSIL 3,3,3 trifluoropropyltrimethoxysilane (TFP-TriMOS)) was dip coated on an uncladded optical fibre and subsequently inserted in a glass capillary to form a microchannel acting as a flow cell. An evanescent wave from a blue 475 nm LED was used to excite the fluorophore to produce a fluorescence emission which was quenched after interacting with O_2, decreasing the amplitude of the signal (as recorded by a photodiode). The different parameters were optimised (for a sample volume of 20 μL), and under these conditions, there was minimal influence from temperature changes (within the range 25-45 °C). The device was used to monitor real breath samples, with good response times (typically around 1 s), and agreement with standard analytical techniques (relative error of ca. 1.5%)) [50].

2.3.3 Ammonia Monitoring in Breath

Ammonia detection in breath can be used as a diagnostic tool for helicobacter pylori stomach infection, in which excess urea is converted to ammonia and bicarbonate within the acidic stomach environment. Knowledge of ammonia levels can also be helpful during hemodialysis, asthma assessment, diagnosis of hepatic encephalography, and analysis of halitosis. The ammonia diffuses out of the blood into the lungs, thus enabling non-invasive breath monitoring [39]. In addition, ammonia levels can be elevated during exercise, in the order of 0.1-10 ppm. The main features required for ammonia breath-sensing devices are a working range of 50-2000 ppb and response times of less than 1 minute, within the temperature range of 20-40°C [51].

Most recent research has been devoted to the development of electrochemical sensors with conducting polymers as the sensitive layer [51]. For example, a sensing system was reported based on a chamber in which sensors can be tested. It consisted of a respiratory air pump (to simulate human ventilation) bringing the air into a humidification chamber, in which the temperature was monitored and varied over the range 35-45 °C. The ammonia level in the humidified air could be varied using flow controller regulators [52]. A disposable, screen-printed interdigitated electrode on a polyethylene terephthalate (PET) substrate covered within the sensitive area by inkjet PANI nanoparticles was employed. An impedimetric approach was employed using as experimental conditions 962 Hz, 5 mV rms, under which the conductive polymer layer displayed a purely resistive behaviour. The best performance was obtained using a flow rate of 110.8±0.7 L/min as this prevented humidity accumulation within the system while also facilitating effective ammonia mass transfer at the sensor interface.

The sensor was sensitive within the range 40-2993 ppbv (e.g. covering the physiological range 50-2000 ppbv), allowing for 8 sequential breath measurements in 5 minutes without significant drift over time (2% during 3 weeks when continuously operated) [53]. This setup was interfaced with a laptop and programmed through a LabVIEW interface [52]. The system was evaluated using breath samples from healthy people, and the results compared to a reference photoacustic laser spectroscopic gas analyser (PALS) (slope of 0.93, r^2=0.9705, n=11). Other trials involved patients undergoing dialysis treatment, checking ammonia levels before and after treatment. The values ranged from an average of 930 ppbv down to 227 ppbv, which was in agreement with typical values previously reported in the literature [53]. However, this system was quite bulky and considerable further development would need to happen to convert it into a portable device.

2.3.4 Acetone Monitoring in Breath

Elevated acetone levels in breath are an indication of systemic ketosis, which can occur due to the conversion of fat to ketones. This is associated with people suffering from Alzheimer Disease and children undergoing seizure control treatment. In addition, abnormal acetone levels can also signal hypoglycaemia in diabetic patients, suggesting a possible future non-invasive monitoring approach to track this condition. Acetone was monitored in the breath of diabetic patients via a Pt electrode, with Cr-WO_3 nanopowder deposited on top of a commercial heater. ε-WO_3 is a ferroelectric material with a dielectric moment that is affected by polar acetone molecules, leading to a decrease in resistance. The sensor was integrated within a portable electronic device, insulated by a Teflon casing into which air was conveyed using a mouth-piece. When acetone reached levels of 1.8 ppm or higher (threshold value for diabetes), the resistance dropped from 20 MΩ to 3.5 MΩ activating a warning LED. The device was reported to be insensitive to the main interferents (up to 10 ppm) that are typically found in human breathing (NO, NH_3, CO), except for ethanol and methanol (at 3 ppm) [54]. A similar system was developed using a sensor made of 10 % mol Si-doped WO_3 nanoparticles synthesised and deposited by flame spray pyrolysis on a back heated alumina substrate incorporating Pt interdigitated electrodes. Under constant temperature monitoring, the breath sample was conveyed to a heated Teflon line (40°C) connected to a mask by a flow valve within a T-shaped chamber (see Figure 2.1 (a)). The sensor was connected to a multimeter that transmitted information to a computer. The sensor was able to discriminate between acetone and ethanol at varying temperature (best results obtained at 365°C). The sensor response was constant for

flow rates larger than 0.2 L/min, reaction-limited at the sensitive surface, and almost independent of the relative humidity present in the system. Real-time tests were carried out using breath samples from people at rest and under physical activity, showing no changes in the acetone levels. The concentration profiles measured with the sensor and with the standard proton transfer reaction-mass spectrometer (PTR-MS) showed good correlation, with response times around 27 s and a limit of detection of 20 ppb (see Figure 2.1 (b)) [55].

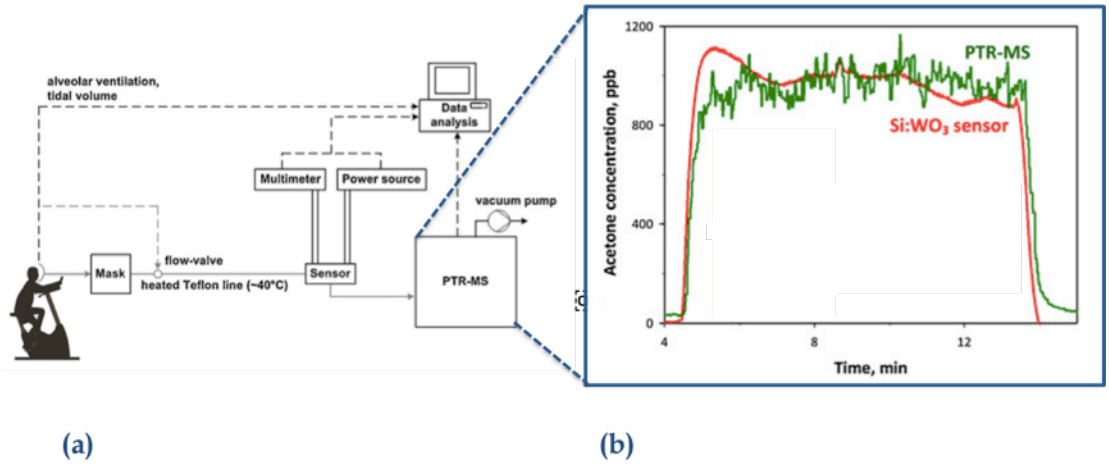

Figure 2. 1: (a): Experimental setup used to monitor acetone within breath samples. The grey lines represent the breath flow while the dashed lines show the data collected by the computer (adapted from reference [55]). (b): Comparison of the acetone variations measured by the Si:WO_3 oxide sensor (red line) and the one monitored by PTR-MS (green line) [55].

This system was not used to monitor diabetic patients, although it was potentially suitable for this application, despite its relatively large dimensions [54, 55]. In addition, the need to constantly keep the sensors at high working temperatures prevented their use in wearable, miniaturised platforms.

These difficulties were overcome using an array of chemo-resistive interdigitated µ-electrodes coated with 11-mercaptoundecanoic acid functionalised gold nanoparticles (MUA-Au_{2nm}). The electrodes were located within a chamber incorporating 6 channels, each associated with a separate electrode, connected to a computer controlled flow meter or a manual pump used to simulate real breath conditions. The sensor chamber was also interfaced to an electronic circuit for collecting and conditioning the sensor signals. Detection of pure air, acetone in air, human breath and acetone-spiked human breath samples was demonstrated using pattern recognition algorithms, allowing healthy subjects and simulated unhealthy breathing to be discriminated. This new non-

invasive device could change the current clinical management of diabetes while, at the same time, differently decorated Au-NPs would allow the monitoring of other analytes [56].

2.4 Sweat Monitoring

There has been a significant increase in sweat analysis in recent years due to its potential for non-invasive monitoring of fluid and electrolyte loss by elite athletes during sporting events (rehydration optimisation) [57] and also for improved clinical management of certain pathologies (e. g. Cystic Fibrosis (CF)) [58], where pH, Cl^- and Na^+ concentration monitoring can provide valuable information. Furthermore, changes in NH_4^+ concentrations can indicate switching from aerobic to anaerobic conditions, which can be linked to the breakdown of proteins related to dietary conditions or to hepatic dysfunctions [51].

As per breath monitoring (see Section 2.3), humidity can be an issue and the wearability of the system needs to be considered. An early example by Chang et al. [59] was a conductometric sensor based on poly-(2-acrylamido-2-methylpropane sulfonate) spin coated on a commercial interdigitated electrode, connected to a miniaturised home-made impedance meter, which was used to continuously monitor human perspiration. The device was integrated into a polystyrene mini-chamber and positioned on top of the palm of people tested. The sweat emerging from the skin was absorbed by the polymer leading to an increase in conductivity. The sensor had a time constant of 38 s and activity was recovered after drying [59]. This quite bulky device was characterised by an undefined response time for the entire system, mainly related to all the difficulties associated with accurate sampling. For this reason, it was necessary to replace it with flexible, wearable sensors based on poly-tetrafluoroethylene developed by Miyoshi et al. [43] (see Section 2.2 and Figure 2.2 (a)).

Sweat may also have a role in diabetes management through glucose monitoring, although few examples can be found in the literature. The work done by Caduff et al. [60] was based on the dielectrical and optical characterisation of the skin. Glucose variations were monitored through a multi-device characterised by 3 fringing field sensors, allowing the penetration of the magnetic field at three different depths (deep, mid and upper). Changes were mainly dictated by the mid and deep depths, while the data coming from the upper region were used to correct for common-mode variations not caused by glucose. The sensors were connected to a Li-Ion Battery (power of 1800

mAh) integrated in an arm-band (see Figure 2.2 (b)). Clinical trials were carried out but accuracy and stability evaluations still need to be performed [61].

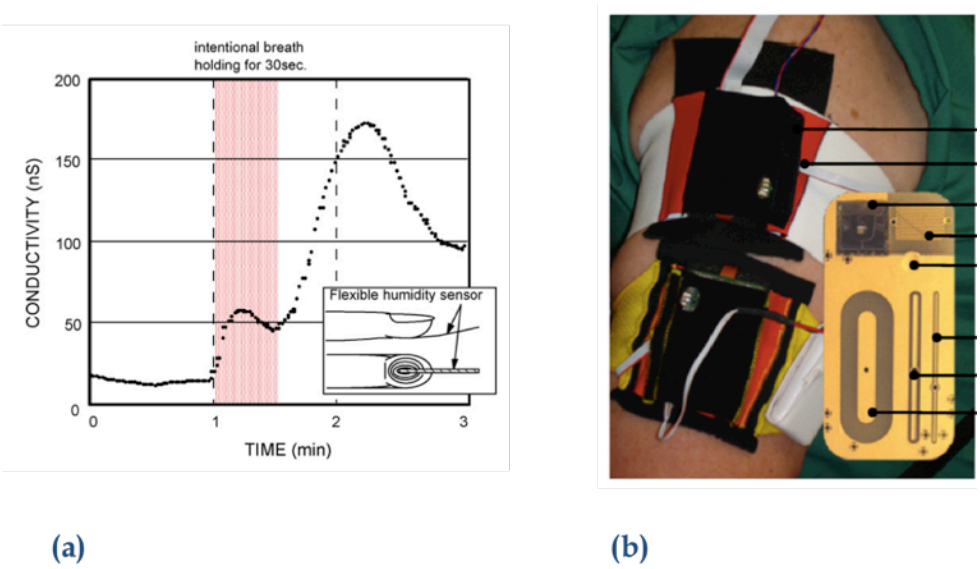

Figure 2. 2: (a): Changes into sweat rate measured at a finger tip using a wearable miniaturised flexible humidity sensor (adapted from reference [43]). (b): A completely wearable system used to monitor glucose in sweat (adapted from reference [61]).

Recently, sweat was also investigated as a medium to monitor ethanol using a device based on an amperometric biosensor characterised by a graphite electrode with embedded alcohol oxidase, horseradish peroxidase and ferrocene, in the presence of a working solution (0.05 M, pH 7.4), separated by a PTFE membrane from the contacting skin. It was connected to a miniaturised potentiostat and a microprocessor that translated the obtained signal into variation of ethanol concentration in sweat. Sweating was stimulated by pilocarpine iontophoresis and it was claimed that this allowed the concentration of ethanol in blood to be tracked continuously in real-time. The sensors showed high reproducibility (RSD value of 10.5%, n=10), repeatability (RSD value of 9.1%), with a shelf-life of at least 2 months. The linear range (0.0005-0.6 g/L) covered the legislation limits (0.002-0.03 g/L) with reduced false results compared to breath analysers. The system was able to detect and monitor ethanol variations 5 minutes after ingestion [62].

2.4.1 Monitoring Analytes for Sports Science Applications

Measuring biochemical parameters can be useful when monitoring athletes under effort, as this can help to improve their performance. One of these parameters is lactate, as this indicates the switch from aerobic to anaerobic metabolic conditions [63]. For

this, an electrogenerated chemiluminescence (ECL) biosensor was realised using a luminol hydrogen peroxide sensitive compound, lactate dehydrogenase and pyruvate oxidase (as catalyst), adsorbed onto a layer of carbon nanotubes. The maximum ECL signal was obtained at pH 8, at a temperature of 30 °C, covering the linear range $8.9x10^{-12}$-$8.9x10^{-6}$ mol/L (standard deviation of 4.13% in 6 parallel measurements) and a recovery ability of 101.3% after exposure to lactate. As the device was too bulky to be worn, sweat samples were collected from volunteers and brought to the system, which increased the risk of sample contamination [64]. Clearly, the ability to perform such measurements at point-of-need would be more attractive, as this would allow real-time tests, faster access to critical data, and reduced potential for sample contamination.

A wearable platform for monitoring pH was recently reported. It employed a textile-based fluid handling system made of a moisture wicking material (mixture of polyester (92%) and lycra (8%)), and an optical pH sensor based on bromocresol purple (see Figure 2.3 (a)), with the optical detection system shown in Figure 2.3 (b). The sensor worked over the pH range 4-7, suitable for monitoring pH in sweat, and was characterised by good repeatability (within 2%, n=2), without dye leaching during the experiments. The sensor was positioned on the body at the lower back, and held in place by a waist band. The pH values recorded with the fabric sensor were compared to parallel values obtained with a miniaturised pH electrode, sited on-body close to the textile based sensing platform [65].

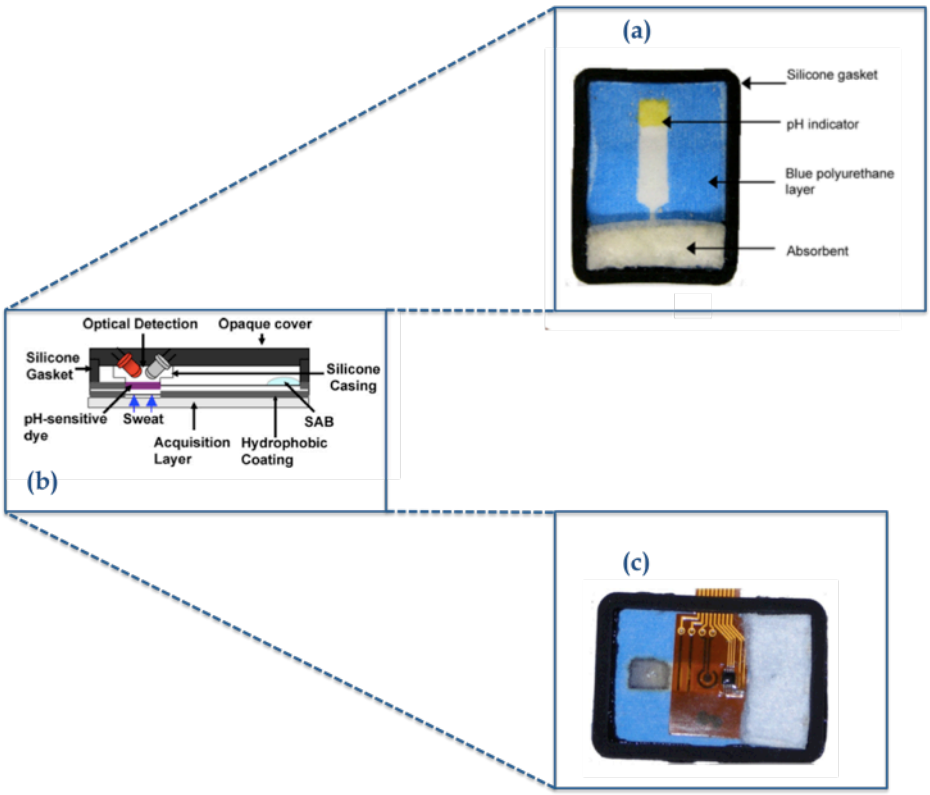

Figure 2. 3: (a) Top view of a textile-based passive pump with an embedded pH optical sensor. (b) Side view of the sensing area and detection system used (adapted from reference [65]). (c) Integration of a multi-sensor strip consisting of a pH indicator, conductivity, sodium and temperature sensors in contact with the fluidic handling system (adapted from reference [66]).

The same device incorporated sensors for monitoring sodium concentration (first tested connecting the Ion-Selective Electrodes (ISEs) to a portable multimeter [67]) and conductivity (shown in Figure 2.3 (c)), with the data collected and recorded on a SD card enclosed into the wearable electronic control unit. The time needed to collect the minimal amount of fluid for an accurate analysis was about 35 minutes [66], due to the delay in onset of sweat generation during exercise, and to the dead volume of the platform.

In an attempt to overcome such issues, Curto et al. [68] realised an integrated microfluidic device with a small sensitive area (5 mm in diameter) containing an absorbent material impregnated with the pH sensitive dye bromocresol purple (see Figure 2.4 (a)). The detection system was characterised by a surface-mount LED and light detector working in transmission mode, which responded to colorimetric changes of the pH indicator (see Figure 2.4 (b)). Real-time tests were conducted on samples collected directly from the lower back region of athletes during training. The results

were found to be in broad agreement with reference values obtained from a flat pH electrode [68].

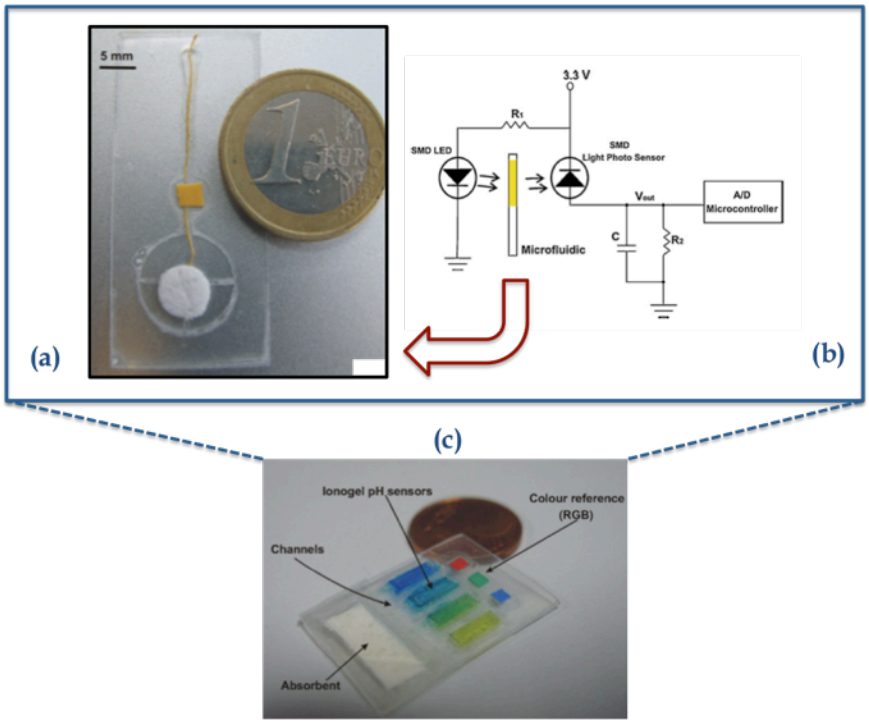

Figure 2. 4: (a) Microfluidic chip with an integrated pH optical sensor. (b): Electronic circuitry used as the detection system (adapted from reference [68]). (c): Microfluidic platform with 4 reservoirs containing a poly-IL, incorporating 4 different dyes used as pH indicators (adapted from reference [69]).

A further reduction of the device dimensions was deemed necessary to allow for more convenient wearable applications. Improvements were needed in terms of fluidic transportation, better positioning of the components, and shielding of the detectors from external lighting effects. Improvements in performance were offered by a patch worn during exercise (Figure 2.4 (c)). The device was based on cross-linked polymer gels (N-Isopropylacrylamide and N,N-Methylene-bis(acrylamide)) incorporating an Ionic Liquid (trihexyltetradecylphosphonium dicyanoamide) integrated within 4 reservoirs, each of which also contained a different pH dye (methyl red, bromocresol green, bromocresol purple and bromothymol blue) to cover the pH range 4-8, i.e. to overlap the range that can be physiologically found in sweat. Fluid movement through the device was induced by a wicking effect driven by a highly absorbent material, which allowed a continuous stream of fresh sweat to be in contact with the sensitive area, and an operational life-time of approximately 135 minutes. During an exercise period, images of the sensor array were captured at 10 minutes intervals, and

processed to extract the analytical information. The difference in measurements by this method, with respect to a glass pH meter, was found to be less or equal to 0.49 of a pH unit [69].

2.4.2 Fabric and Tattoos Technologies for Sweat Monitoring

The implementation of wearable chemical sensors would be greatly advanced by the realisation of sensing elements embedded in cotton yarns. A recent paper on this topic reported the use of potentiometric fibres, made conductive after repeated immersions in carbon nanotube ink (until a resistance of 500 Ω for a length of 1 cm was reached), partially coated with an ion-selective membrane (from 4 to 5 dips into a modified PVC solution) for pH, K^+ and NH_4^+. The sensors were able to function within the required physiological range (pH 3-11, NH_4^+ 10^{-6}-10^{-2} M, K^+ 10^{-5}-10^{-1} M) and were insensitive to mechanical stresses such as bending or stretching, thus preserving the cotton properties (softness, texture, etc.). They were then integrated into a garment, in a configuration that did not affect their performance, and tested using simulated sweat solutions. The concentration of the ion of interest was varied by changing the fluid that contacted the electrodes (through a cellulose acetate layer covering the sensitive area). It is hoped that such strategies will pave the way for mass produced wearable chemical sensors [70].

The pioneering work carried out by the Rogers research group at the University of Illinois at Urbana-Campaign on "epidermal electronic systems" was based on standard lithographic techniques to monitor physical parameters [71-73]. A natural evolution of this approach brought to the adaptation of electronic tattoos to the detection of chemical analytes. Screen-printed technology was used to realise electrodes that could be transferred onto the skin via a tattoo process [10]. So far, potentiometric sensors for ammonium (10^{-4}-10^{-1} M) [74], pH (3-7) [75] and Na^+ (0.1-100 mM) [76] and an amperometric sensor for lactate (1-20 mM) have been reported based on this approach [77]. The tattoo sensors were able to withstand mechanical tests (stretching and bending) when applied on a Goretex substrate, simulating stress conditions for on-skin measurements. They were also employed during real-time tests on volunteers. However, the tattoo sensors were normally connected to standard miniaturised electrochemical commercial potentiostats, except in the case of the Na^+ sensor, which was linked to a Bluetooth wireless wearable transceiver [76], (see Figure 2.5).

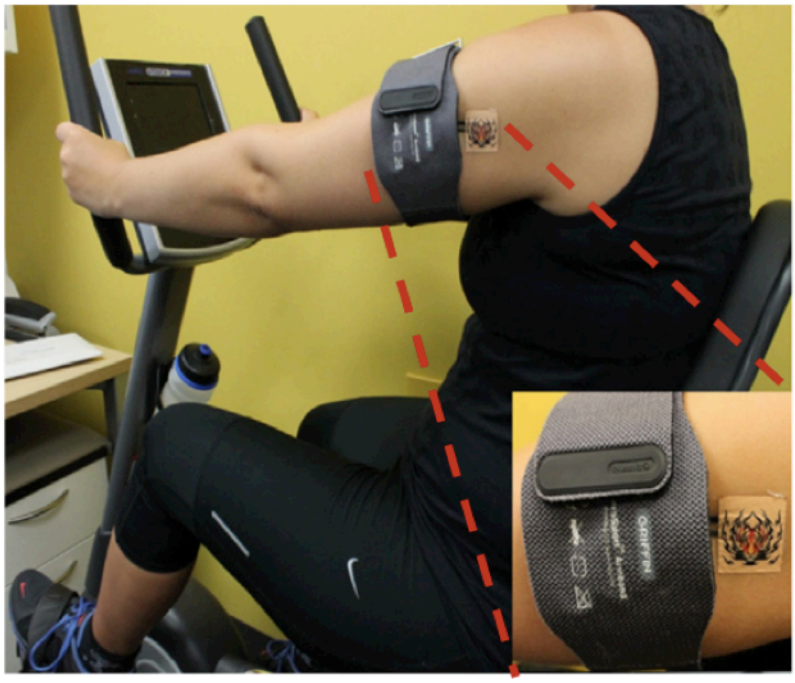

Figure 2. 5: Example of a wearable sensor for sweat monitoring: skin tattoo connected to a bluetooth electronic platform for sodium monitoring (adapted from reference [76]).

2. 5 Saliva Monitoring

Saliva is another valuable source of biochemical information accessible in a non-invasive fashion. While sweat production is primarily an inductive process, saliva is more readily available and therefore possesses advantages for patients suffering from conditions that inhibit sweat production. Saliva is even more readily available and real-time monitoring within the mouth can be extremely beneficial for detecting the presence of drugs [78], monitoring healthy mouth conditions [79], and detecting Gastroesophageal Reflux Disease (GERD) events [80].

A number of reports have described the development of SERS biosensor assays. The attention has been mainly focused on the detection of a good indicator for stress such as cortisol [81] and the hormone testosterone [82]. In a study on cortisol, the biosensor was characterised by a limit of detection of 49 pg/mL within undiluted saliva samples, and found to be highly correlated with radio-immunoassay measurements [81]. In contrast, for testosterone monitoring, saliva samples were stripped (i.e. treated with activated charcoal, then centrifuged to remove the charcoal) because of its lower concentration when compared to other analytes. The system was characterised by a limit of detection of 23 pg/mL, with a suitable sensitivity (range 25-250 pg/mL) for a

good resolution in the range of interest. In both cases the measurements were completed in nearly 10 minutes, allowing for an almost real-time monitoring system [82]. However, in this case, a benchtop instrument was used, and the approach was not suitable for home-based and wearable monitoring devices where additionally biocompatibility requirements for all the employed reagents must be taken into account.

The need for miniaturised devices is therefore driving attention towards the employment of other techniques such as the development of chemical sensors based on novel fluorescent materials. For example, a new polyfluorene derivative, poly(9,9-bis(6′-benzimidazole)hexyl) fluorene-*alt*-1,4-phenylene (PBP), was developed to detect Fe^{3+} and inorganic phosphate, based on the metal binding (Fe^{3+}) benzimidazole group which is capable of inducing large fluorescence quenching (97%) of the compound. Inorganic phosphate ($H_2PO_4^{2-}$:$H_2PO_4^{-1}$) was able to dequench the Fe^{3+}/PBP complex due to the ability of phosphate to displace the attached Fe^{3+}, showing a recovery of 106%. This assay was used to monitor phosphate in saliva with a dequenching ability of 94% and a limit of detection of 1.44 mmol/L. Absorbance (280 nm) and fluorescence (340 nm) peaks obtained in saliva did not overlap those of the PBP [83]. This is just one example of a new class of optical sensors that may well gain more popularity in the coming years.

Up to now, however, electrochemical sensors have been more popular than optical approaches. In the work presented by Kwan et al., phosphate levels were detected through the use of an amperometric screen-printed biosensor based on pyruvate oxidase (PyOD) immobilised within a Nafion matrix and covered by a poly(carbamoyl) sulfonate hydrogel as the working electrode. The increase in anodic current at 420 mV versus Ag/AgCl (reference electrode) was caused by the oxidation of H_2O_2 (generated by PyOD in the enzyme layer), which was proportional to the phosphate concentration. The process was diffusion controlled and the sensor was characterised by a sensitive range of 7.5-625 μM (limit of detection 3.6 μM), a fast response time (2 s), but slow recovery time (2 minutes). Efficient functioning was maintained for 12 hours. When testing 50 saliva samples, good correlation coefficients were obtained between the biosensors and a commercial kit [84]. Advances in terms of miniaturisation were obtained realising a microflow-injection system housing a disposable screen-printed biosensor based on the reactivation (in 15 minutes) of the enzyme cholinesterase (AchE) (inhibited after exposure to organophosphate) using pralidoximer iodide. A 3-fold dilution of saliva samples showed a reproducible response (less than 4% of

average relative standard deviation) demonstrating (through its low-cost, simplicity and sensitivity) the opportunity to assess subclinical organophosphate exposure [85]. A similar configuration was also used to monitor amylase, in which the sensitive element was based on an amperometric biosensor containing glucose oxidase and peroxidase. This device was characterised by a linear range of 0-190 kU/L, using a sample volume of 50 µL (injected at a flow rate of 0.79 mL/min), with no significant degradation of the enzymatic activity during continuous use over a period of 48 hours [86].

Glucose and pH are potential targets of great interest for minimally-invasive systems. While knowledge of glucose levels could assist improvements in terms of diabetes management, pH is very important in GERD monitoring, which relies otherwise on very invasive esophageal manometry over a period of 24 hours. Monitoring of glucose levels in saliva was reported using pyrene-1-boronic acid functionalised carbon nanotubes transistors realised via standard photo-litographic techniques. It was found that with increasing glucose concentration, the drain current was lower because of the increased carrier scattering due to the presence of boronate anions, which decreased the mobility in the transistor. The sensor response was estimated to be 1.3 s, with quite long recovery times (1 hour). They showed insensitivity to interferents such as lactose (for levels lower than 1 mM), with a limit of detection of 300 nM, suggesting potential future use as an integrated device able to detect glucose variations in saliva [87]. Similarly, dual screen-printed pH ISE/reference combination electrodes were used to realise a fully operational and disposable pH device. This system was able to work within the pH range 4-8, and the data were highly correlated with results obtained using a bench top pH meter [88].

A more radical strategy to improve wearability of devices employed direct integration of the sensing device within the mouth of a patient. Different biosensors were successfully developed, for example, to detect lactate variations in saliva [89, 90] but only Wang et al. [91] proposed a full integration into a mouth guard platform. In this work, a 3 screen-printed electrodes configuration of a printable Prussian Blue layer was covered by a poly-orthophenylenediamine layer that entrapped the lactate oxidase (avoiding potential interferences) as working, an Ag/AgCl layer as reference and a Prussian Blue graphite ink as counter electrode. It was suitable for monitoring lactate levels over the physiological range 0.1-0.5 mM, enabling the estimation of the lactate via a standard addition method [91]. However, the system evaluation was restricted to bench measurements, and no in-mouth real-time measurements were reported.

Another application was devoted to monitoring different bacteria through the use of nanosensors printed as a graphene layer on a water-soluble silk thin film and contacted by gold interdigitated electrodes connected to an inductive coiled antenna (see Figure 2.6 (a)). The nanosensors were then transferred onto suitable substrates (such as tooth enamel or tissue) while the water-soluble silk layer was completely dissolved, allowing the attachment of the Au-Graphene nanosensor to the substrate of interest (see Figure 2.6 (b)). The graphene layer was functionalised with a dodecapeptide graphene binding peptide, a triglycine linker and the naturally occurring antimicrobial peptide odorranin-HP, working as a biorecognition element. The resulting sensor showed activity towards Escherichia Coli, helicobacter pylori and straphylococcus aureus.

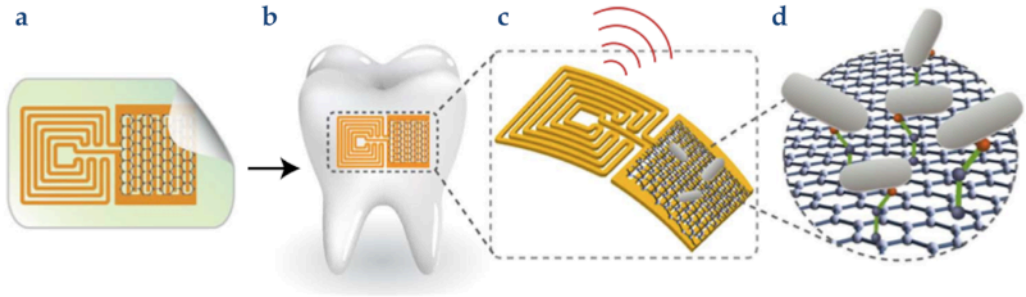

Figure 2. 6: (a) Tattoo based wireless nanosensor for bacteria monitoring within the mouth. (b) Sensor positioned on a tooth. (c) and (d) Wireless transmission of the signal during analyte interaction with the graphene sensitive sensor layer (adapted from reference [92]).

Detection of a single bacterium was claimed, due to the highly sensitive change in the electrical conductivity of the graphene layer, modulated and wireless monitored through an inductively coupled RF reader device. Detection of helicobacter pylori cells within saliva samples with a limit of detection of ~100 cells was also reported [92].

2.6 Tear Fluid Monitoring

The opportunity to integrate glucose sensors within contact lenses represents a high impact challenge for diabetes monitoring. It is then fundamental to find a better correlation between blood glucose levels and corresponding concentrations in tears [93]. To do so a better understanding of the mechanisms behind tear secretion is needed. For example the mechanical stimulation of tears induces higher glucose levels [94]. Moreover, it is known that diabetes mellitus can affect the production of tears, their composition, the anterior ocular environment [95] and the structure and function

of the tissues that contribute to their production [93]. Therefore the future implementation of sensor technologies within a contact lenses platform may lead to new continuous, non-invasive solutions for monitoring glucose and other important analytes [95, 96].

2.6.1 Electrochemical Sensors for Monitoring Tear-Fluid

Most research aimed at improving glucose monitoring in tears has relied on electrochemical approaches. The first attempts to detect glucose levels in the lacrimal duct fluid were based on a device inserted directly in the canaliculus due to the development of flexible, thick-film, miniaturised electrodes. The working electrode was based on a carbon ink containing glucose oxidase (10000 U GOx/gm) while the reference was an Ag/AgCl layer, both characterised by etched copper leads connected to insulated wires. An insulating layer was then applied on almost all the electrode area and then rolled in a tubular configuration (0.7 mm) suitable for insertion into polyethylene tubing that functioned as the electrode body. The measurements were carried out at a potential of +0.7 V and the linear range was reported as 20-200 μM, with a detection limit of 8 μM [97]. This configuration did not have the expected degree of uptake in the market, mainly due to its quite invasive nature. However, other research groups followed this trend through an amperometric enzymatic needle type glucose sensor, with improved performance, such as a working range of 1.5-800 μM and minimal interferences from the most common molecules found in tears (e. g. %RE for ascorbic acid=7.56, uric acid=11.16 and acetaminophen=4.85). Glucose levels recorded in tears and blood every thirty minutes showed intra-subject consistency but poorer performances when considering the whole sample population. The development of a general model that would allow correlation of blood and tear glucose concentrations is thus not a straightforward task and requires further investigation [98]. Further improvements were obtained by using a coulometric rather than amperometric approach, thanks to coulometric enzyme based biosensor characterised by a lower limit of detection of 0.38±0.13 μM (dynamic range 10-800 μM). Tear and blood samples were collected every 30 minutes within 7 hours. However, inter-subject variability was still manifested when glucose levels in blood were compared with tear fluid in the right and left eyes of the same subjects. A possible solution might involve the pre-calibration of the system before each measurement using tear and blood samples in order to obtain the exact ratio between blood and tear glucose concentrations [99]. A similar configuration based on flexible Teflon tubing integrating a 3 working electrodes system allowed variations in dopamine, ascorbate and glucose

to be tracked in tear fluid. Thanks to its flexibility, this device represents one of the best examples of minimally-invasive point of care systems [100].

Another approach is to integrate electrochemical sensors within contact lenses. This solution dates back to 2007 when an amperometric biosensor was realised on a flexible polymeric substrate through Soft-MEMS layer by layer techniques. It was based on GOx immobilised on a polypropylene gas permeable membrane placed on a film-type oxygen electrode located on a Pt working electrode. The sensor was able to cover the relevant normal range of glucose in tear fluid (0.025-1.475 mmol/L) while located on the pupil of a rabbit and kept in position with fixing tape. Upon obtaining a stable baseline signal, changes in the signal were used to monitor the effect of oral administration of glucose. Blood glucose concentration was monitored simultaneously, and this was characterised by an almost immediate response after bolus injection. In contrast, equivalent events tracked in tears were delayed by 10-20 minutes [101]. The same sensor was employed to measure kinetics of tear secretion by glucose instillation (20 μL) within the eye (5 mmol/L, 10 mmol/L). The current was stable at 0.5 μA and then increased after glucose instillation up to values of 0.61 μA (5 mmol/L) and 0.73 μA (10 mmol/L) after 45 s [102]. While this approach is exciting, the low biocompatibility of the employed materials was a significant issue [101].

This problem was overcome by integrating the GOx within a polytetrafluoroethylene membrane, using the phospholipid based polymer 2-methacryloxyloxyethyl phosphorylcholine (HPC) copolymerised with 2-ethylexylmethacrylate (EHMA:PMEH). The same design was implemented with the only difference being the use of a PDMS substrate. The flexible, wearable electrode worked within the range 0.05-1.00 mmol/L (the reported range of glucose in tears is 0.14-0.23 mmol/L), with an average response time of 41.6 s and sensitivity of 0.95 μA/mM [103]. The glucose basal concentration was extrapolated from the calibration curve obtained before the positioning of the sensor within the eye (0.11 mM) [104]. The real-time response was also monitored after glucose addition within the eye, which was characterised by an increase in the current signal, immediately followed by a dropping back towards the baseline levels, indicating dilution due to secretion of new tear fluid corresponding to 29.6%±8.42 min^{-1} [105]. Inflammation effects were absent within the trials but the fact that the system employed physical wire inter-connects to the potentiostat was a drawback [104].

These difficulties were resolved through the development of a wearable, wireless contact lens based on a PET substrate integrating an amperometric concentric 3

electrodes design (see Figure 2.7 (a)). The GOx solution was immobilised in a titania sol-gel membrane covered by a Nafion layer. The pads for the potentiostat connection were placed at the border of the contact lens, to allow unobstructed vision for the wearer (see Figure 2.7 (b)) [106]. This design was improved using a differential sensing arrangement based on an activated glucose oxidase (working electrode) and de-activated glucose oxidase ("control" electrode) employed in differential mode. They were integrated with a printed Au antenna and readout/telecommunication circuitry realised via microelectromechanical techniques. Tests showed that the differential approach enabled the signal component arising from the main interferent species at the concentrations normally found within tears (ascorbic acid 50 µM, lactate 10 mM and urea 10 mM) to be subtracted from the activated glucose oxidase electrode signal. The combined system was characterised by a linear range of 0-2 mM. However, while a stable signal was obtained for ca. 12 hours (97.4% of initial activity), performance deteriorated over time, and by day 4 it had declined to 54% of the initial signal. The effect of protein fouling was significant, causing a decrease to 49.9% of the signal recorded. Nevertheless, these results are promising, and they suggest that a use model based on daily replacement may be possible.

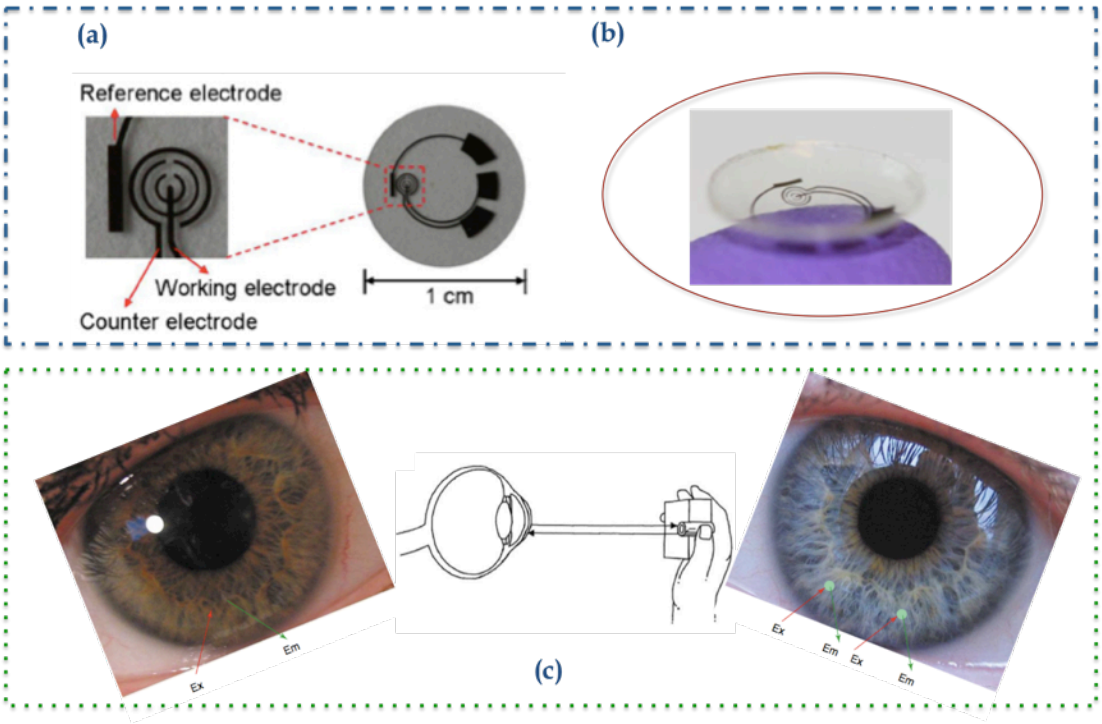

Figure 2. 7: Examples of devices used to monitor glucose in tears. (a) and (b) show the integration of a wireless electrochemical sensor within a contact lens (adapted from reference [106]). (c) Glucose sensitive contact lenses doped with a boronic acid glucose receptor together with the schematic of a possible glucose monitoring device for measuring the emission intensity of the system (adapted from reference [107]).

Because of its reasonable stability, and its wearable and wireless nature, this system could potentially represent a significant first step towards the realisation of a smart-contact lens [108] that could revolutionise glucose management in diabetic patients.

The same configuration was also examined for monitoring lactate levels, using a smaller working electrode (area 0.19 mm^2) based on lactate oxidase immobilised in a film based on bovine serum albumin (BSA) covalently and cross-linked glutaraldehyde, and a "control" electrode (same composition as the working electrode but without the enzyme). These electrodes were once again used in a differential configuration to enable common mode signal components arising from interferents to be automatically compensated to some extent. The entire system was covered with a medical grade polyurethane layer to reduce enzyme leaching, and a final Nafion outer layer. The sensors had a linear range 0-1 mM (limit of detection 50 μM, ca. 20 times below the minimum concentration of lactate in tears), and a response time of 25 s. Moreover, while the response was not linear within the range 1-5 mM, there was sufficient resolution and accuracy to enable this part of the analytical signal to be employed for clinical measurements. The system was reported to function satisfactorily for 24 hours [109].

2.6.2 Optical Sensors for Tears Monitoring

As described in Section 2.6.1, commercial contact lenses represent a good substrate for immobilising transduction elements. Because of its high affinity for different types of sugars, fluorophore labelled boronic acid derivatives (BAFs) represent one of the most studied optically responsive materials for glucose monitoring because of their ability to chelate different monosaccharides. Research specifically related to their application within commercial contact lenses has been mainly carried out by Badugu et al. [110] commencing around 2004 [111]. This group examined a number of derivatives in order to identify the ones with particularly high glucose binding affinity [107]. The dynamic range of the water-soluble BAFs was found to be reduced when solution experiments were compared to equivalent measurements with BAF immobilised within the contact lenses [111]. The best performance was obtained using 6-methylquindinium, used as the fluorescent indicator along with the ortho isomeric form of N-(boronobenzyl)-6-methoxyquinolinium bromide (o-BMOQBA). It was found that the pK_a of the probe was also reduced (which is an advantage because of the slightly acidic environment of the contact lens), and the boronate diester formed after the sugar complexation was stabilised. The addition of glucose and its subsequent binding to the boronic acid receptor caused a decrease in the fluorescence intensity (for example, the decrease is ca.

13% for glucose concentrations lower than 1 mM) [111]. The response range was reported as 50-500 μM [112]. Initially, this new fluorescent boronic acid probe was photo-physically characterised versus control probes that did not contain the boronic acid functional group. Subsequently, the contact lenses were functionalised with the sensitive compound and subjected to leaching, interference, pH and shelf-life stability tests [110]. It was found that the modified lenses changed colour in response to changes in glucose concentration, with a response time of 10 minutes [107]. A significant disadvantage of this approach is the need to excite the fluorophore by passing light into the eye in order to collect the emission spectra, as shown in Figure 2.7 (c) [110].

A different technique based on the use of optical near infrared spectroscopy and new glucose responsive materials based on polymer crystalline colloidal arrays was also applied to detect glucose in tears. The materials were based on poly(styrene-co-acrylamide-co-3-acryloamido)phenyl boronic acid embedded within a slightly positive hydrogel of poly(acrylamide-co-2-(dimethylamino)ethylacetate). This material showed spectral responses in the near infrared region (around 1722 nm) when binding glucose, which were detected with a UV-VIS-NIR spectrophotometer. The limit of detection was reported as 6.1 μg/dL, with almost no response to the main interferents such as lactate, albumin, and ions (K^+, Na^+, Ca^{2+}, Mg^{2+}, Ba^{2+}) (maximum relative error of ±3.3%). The effective temperature range was 15-43 °C, and the response time 22.1 s at a glucose concentration of 7.5 mg/dL. If integrated within a contact lens, this polycrystalline material may provide a route to non-invasive, continuous optical monitoring of glucose in tears [113]. In the future, photonic crystals capable of glucose-selective light diffraction behaviour should also be considered. When this effect coincides with the visible region, colour changes occur without the need for a dye label, and this effect could be used to determine the glucose concentration in the surrounding fluid through the use of a colour chart or a simple optical sensor. A significant disadvantage is the pH dependence of the binding behaviour of boronic acid receptors [114]. Therefore, significant attention is now focused on materials such as hydrogels based on (3-acrylamidopropyl)trimethylammonium chloride (ATMA) co-polymerised with 2-acrylamidophenylboronic acid (2-APB). These are reported to be sensitive to glucose within the pH range 6.5-7.8, with negligible interference from the biological medium [115].

2.7 Conclusions and Emerging Trends

Real-time monitoring of biochemical analytes within biological fluids requires research that crosses disciplines, spanning from electrical engineering and physics to materials science, chemistry and biology. In order to become commercially available for continuous health monitoring, wearable chemical and bio-chemical sensors must overcome significant challenges related to wearability, comfort, device and material biocompatibility, efficient energy usage, acceptable analytical performance and a practical usage model. Despite the wave of optimism that manifested related to implantation of biosensors within the body some 30 years ago [116], in reality, sensor technology is still far from delivering on this early promise of long-term use. Perhaps the most significant obstacle is biofouling, as it rapidly and profoundly affects sensor sensitivity and durability by altering the sensor-body fluid interface, leading to sensor malfunction [117]. Since the sensor is implanted, the body perceives it as a foreign object and, as a result, biological material builds up on the sensitive sensing surface. In contrast, implants that do not possess these very sensitive surfaces are used successfully in very large numbers. For example, cardiac pacemakers are implanted in 600,000 people per year [118] as part of a standard procedure. However, advances in biosensor performance continue to be reported, such as a glucose sensor (based on an enzyme-immobilised and amperometric detection) that has been implanted fully subcutaneously for extended periods (1-2 years) in pigs. Accurate glucose measurements were obtained over this duration after an initial stabilisation period (2-3 weeks after implantation) [119]. In contrast, needle-type glucose sensors implanted percutaneously cause infections and require frequent sensor calibration due to response drift [120]. Understanding and controlling in-vivo surface effects constitute one of the greatest challenges for biosensor research. Strategies investigated include improved enzyme stabilisation through entrapment in conductive polymer matrices [121] and Ionic Liquid membranes [122], coating of the sensor with biocompatible polymers [123], and the use of drug-release strategies for enhanced tissue integration [124-127].

On the other hand, wearable sensors placed in close contact with the body are easily accessible and do not suffer to the same extent from biofouling. Perhaps even more importantly, they are amenable to short-term use models (hours, days compared to many years for implants). Despite this, as already discussed in the previous sections, the number of effective wearable biochemical sensing devices reported in the literature is limited. Enhancing comfort while minimising size and maximising efficiency will increase the likelihood of their adoption by users. Recent advances in materials science

are starting to revolutionise this area thanks to flexible and stretchable fibers based on carbon nanotubes (CNTs) and graphene. At the same time, organic electronics is also demonstrating beneficial impact on wearable sensors [71]. Other flexible and stretchable electrolytes based on Ionic Liquids and Polyionic Liquids may also have a role to play in the development of wearable electro-chemical and biochemical sensors [69, 122, 128]. Ionic Liquids have shown potential as effective solvent media for many enzymatic reactions, and under certain conditions, several have demonstrated enhanced biocatalyst activity, thermal stability, and reusability [128, 129].

Moreover, suitable power sources (including power scavenging approaches) must be considered for practical applications of wearable devices. For example, portable, flexible batteries [130-132] or energy harvesting approaches can be integrated into the wearable platforms and used to power wearable devices.

Other components like antennas, fabricated by printing or etching metal patterns on rigid substrates, can be made flexible and stretchable, using new electronic materials and/or new device configurations. Recently, they have been realised using CNT sheets and polymer substrates [133] or silver nanowires embedded in an elastomeric substrate [134]. These antennas are thus well suited for applications like wireless strain sensing and could be implemented in smart textiles.

The newly developed electronic "tattoo" technology probably constitutes the state-of-the-art in wearable sensors and has been demonstrated for epidermal pH monitoring [75], real-time lactate sensing in human perspiration [77], and detection of bacteria in saliva [92]. These devices are easily fabricated using well established printing technologies and have the advantage of being non-invasive, and mechanically stable when directly applied on the skin [135] or teeth [92]. Although at present there are only few examples demonstrated, the potential of this technology is tremendous [136].

Recent advances in analytical chemistry, materials science, microfluidics and electric engineering are indeed deeply influencing technological approaches to fully integrate biochemical sensors into wearable devices. Physical sensors directly embedded into garments are already present on the market, often as the result of close interactions between universities and international companies. Checklight by Reebok, LifeShirt by Vivonoetics, and other smart-garments (including socks, t-shirts, and bras) by Sensoria are just few examples of commercially available items. Similar collaborations are now advancing research activities aimed at the development of low-cost wearable biochemical sensors. Several small companies (like OrSense) and spin offs (such as

Electrozym) that exploit low-cost technologies to realise non-invasive tools for biochemical sensing have recently made some impact in the global market. Simultaneously, larger companies are increasingly interested in the potential applications of wearable biochemical sensors. For example, Google recently filed a patent [137] and announced a project to further develop the electrochemical glucose sensors integrated into contact lenses [138], probably with the idea of eventually linking these sensors with the Google Glass instrumented spectacle platform. This has the advantage of enabling the sensorised contact lens to be inductively powered from the Google Glass platform due to the short distance involved, which greatly simplifies the lens requirements, as no integrated power source is required. Simultaneously, rumours abound on the possible integration of a glucose monitoring function integrated into the forthcoming Apple i-Watch [139], which will further integrate into the Apple 'HealthKit' health information software environment [140]. However, the most likely scenario will be an informatics platform level integration of biochemical information generated with existing technologies, rather than full integration of biochemical sensors into the iWatch platform, unless this can be achieved with a use model based on a replaceable sensing module (maximum use perhaps up to one week, more likely daily), as envisaged with the contact lens platform described above.

These are just a few examples of "a new wave" of innovation in the design and fabrication of devices for non-invasive monitoring of biological fluids that has just started, and involves exciting collaborations between university research teams, clinical groups, community health service providers, small companies emerging with specific technology offerings, and huge global corporations keen to leverage their existing technologies into new market offerings. It is clear that wearable biochemical sensors will be a central part of these offerings, which will provide patients and clinicians with extensive information for optimal management of a range of chronic conditions, enabling home-based therapeutic strategies and healthcare provision, which will generate substantial improvements in terms of quality of life and life expectancies of people.

2.8 References

[1] Y. Hao, R. Foster, Wireless body sensor networks for health-monitoring applications, Physiological Measurement, 29(2008) R27.

[2] F. Carpi, D. De Rossi, Electroactive polymer-based devices for e-textiles in biomedicine, Information Technology in Biomedicine, IEEE Transactions on, 9(2005) 295-318.

[3] S. Patel, H. Park, P. Bonato, L. Chan, M. Rodgers, A review of wearable sensors and systems with application in rehabilitation, Journal of Neuroengineering and Rehabilitation, 9(2012) 21.

[4] B. Latré, B. Braem, I. Moerman, C. Blondia, P. Demeester, A survey on wireless body area networks, Wireless Networks, 17(2011) 1-18.

[5] A.J. Bandodkar, J. Wang, Non-invasive wearable electrochemical sensors: a review, Trends in Biotechnology, 32(2014) 363-371.

[6] D. Diamond, S. Coyle, S. Scarmagnani, J. Hayes, Wireless sensor networks and chemo-/biosensing, Chemical Reviews, 108(2008) 652-79.

[7] J.-H. Lee, H.-I. Jung, Biochip technology for monitoring posttraumatic stress disorder (PTSD), BioChip Journal, 7(2013) 195-200.

[8] S. Sahoo, S. Parveen, J. Panda, The present and future of nanotechnology in human health care, Nanomedicine: Nanotechnology, Biology and Medicine, 3(2007) 20-31.

[9] R. Byrne, F. Benito-Lopez, D. Diamond, Materials science and the sensor revolution, Materials Today, 13(2010) 16-23.

[10] J.R. Windmiller, J. Wang, Wearable electrochemical sensors and biosensors: a review, Electroanalysis, 25(2013) 29-46.

[11] http://www.google.com/glass/start/, Accessed on: 28 April 2015

[12] http://www.diabetesmine.com/2014/01/newsflash-google-is-developing-glucose-sensing-contact-lenses.html, Accessed on: 28 April 2015

[13] http://medcitynews.com/2014/06/apple-worked-mayo-clinic-epic-build-heathkit-platform/#ixzz33WAJiDYV, Accessed on: 28 April 2015

[14] http://www.ibm.com/developerworks/library/wi-wear.html#1, Accessed on: 28 April 2015

[15] https://makeit.intel.com, Accessed on: 28 April 2015

[16] N.F. Chiu, J.M. Wang, C.W. Liao, C.H. Chen, H.C. Chen, L.J. Yang, et al., An implantable multifunctional needle type biosensor with integrated RF capability, Engineering in Medicine and Biology Society, 2005 IEEE-EMBS 2005 27th Annual International Conference of the, IEEE2006, pp. 1933-6.

[17] J.R. Windmiller, N. Zhou, M.-C. Chuang, G. Valdes-Ramirez, P. Santhosh, P.R. Miller, et al., Microneedle array-based carbon paste amperometric sensors and biosensors, Analyst, 136(2011) 1846-51.

[18] P.R. Miller, S.A. Skoog, T.L. Edwards, D.M. Lopez, D.R. Wheeler, D.C. Arango, et al., Multiplexed microneedle-based biosensor array for characterization of metabolic acidosis, Talanta, 88(2012) 739-42.

[19] J.K. Nielsen, C.B. Djurhuus, C.H. Gravholt, A.C. Carus, J. Granild-Jensen, H. Ørskov, et al., Continuous glucose monitoring in interstitial subcutaneous adipose tissue and skeletal muscle reflects excursions in cerebral cortex, Diabetes, 54(2005) 1635-9.

[20] J. Mader, H. Weinhandl, G. Köhler, J. Plank, G. Bock, S. Korsatko, et al., Assessment of different techniques for subcutaneous glucose monitoring in Type 1 diabetic patients during 'real-life'glucose excursions, Diabetic Medicine, 27(2010) 332-8.

[21] D.B. Keenan, J.J. Mastrototaro, G. Voskanyan, G.M. Steil, Delays in minimally invasive continuous glucose monitoring devices: a review of current technology, Journal of Diabetes Science and Technology, 3(2009) 1207-14.

[22] F. Ricci, D. Moscone, G. Palleschi, Ex vivo continuous glucose monitoring with microdialysis technique: the example of GlucoDay, Sensors Journal, IEEE, 8(2008) 63-70.

[23] R.L. Weinstein, S.L. Schwartz, R.L. Brazg, J.R. Bugler, T.A. Peyser, G.V. McGarraugh, Accuracy of the 5-day freestyle navigator continuous glucose monitoring system comparison with frequent laboratory reference measurements, Diabetes Care, 30(2007) 1125-30.

[24] A. Heller, Potentially implantable miniature batteries, Analytical and Bioanalytical Chemistry, 385(2006) 469-73.

[25] M. Falk, C.W. Narváez Villarrubia, S. Babanova, P. Atanassov, S. Shleev, Biofuel cells for biomedical applications: colonizing the animal kingdom, ChemPhysChem, 14(2013) 2045-58.

[26] G. Piechotta, J. Albers, R. Hintsche, Novel micromachined silicon sensor for continuous glucose monitoring, Biosensors and Bioelectronics, 21(2005) 802-8.

[27] B.-U. Moon, M.G. de Vries, C.A. Cordeiro, B.H. Westerink, E. Verpoorte, Microdialysis-coupled enzymatic microreactor for in vivo glucose monitoring in rats, Analytical Chemistry, 85(2013) 10949-55.

[28] X. Huang, C. Leduc, Y. Ravussin, S. Li, E. Davis, B. Song, et al., Continuous monitoring of glucose in subcutaneous tissue using microfabricated differential affinity sensors, Journal of Diabetes Science and Technology, 6(2012) 1436-44.

[29] X. Huang, C. Leduc, Y. Ravussin, S. Li, E. Davis, B. Song, et al., A differential dielectric affinity glucose sensor, Lab on a Chip, 14(2013) 294-301.

[30] J.M. Yuen, N.C. Shah, J.T. Walsh Jr, M.R. Glucksberg, R.P. Van Duyne, Transcutaneous glucose sensing by surface-enhanced spatially offset Raman spectroscopy in a rat model, Analytical Chemistry, 82(2010) 8382-5.

[31] K. Ma, J.M. Yuen, N.C. Shah, J.T. Walsh Jr, M.R. Glucksberg, R.P. Van Duyne, In vivo, transcutaneous glucose sensing using surface-enhanced spatially offset Raman spectroscopy: multiple rats, improved hypoglycemic accuracy, low incident power, and continuous monitoring for greater than 17 days, Analytical Chemistry, 83(2011) 9146-52.

[32] M.J. Tierney, J.A. Tamada, R.O. Potts, L. Jovanovic, S. Garg, Clinical evaluation of the GlucoWatch® biographer: a continual, non-invasive glucose monitor for patients with diabetes, Biosensors and Bioelectronics, 16(2001) 621-9.

[33] L. Dachao, Y. Haixia, H. Xian, H. Fuxiang, H. Xiaotang, X. Kexin, Prediction of blood glucose using interstitial fluid extracted by ultrasound and vacuum, Proc of SPIE Vol2007, pp. 64450I-1.

[34] I. Harman-Boehm, A. Gal, A.M. Raykhman, E. Naidis, Y. Mayzel, Noninvasive glucose monitoring: increasing accuracy by combination of multi-technology and multi-sensors, Journal of Diabetes Science and Technology, 4(2010) 583-95.

[35] M.A. Pleitez, T. Lieblein, A. Bauer, O. Hertzberg, H. von Lilienfeld-Toal, W. Mäntele, Windowless ultrasound photoacoustic cell for in vivo mid-IR spectroscopy of human epidermis: Low interference by changes of air pressure, temperature, and humidity caused by skin contact opens the possibility for a non-invasive monitoring of glucose in the interstitial fluid, Review of Scientific Instruments, 84(2013) 084901.

[36] M.A. Pleitez, T. Lieblein, A. Bauer, O. Hertzberg, H. von Lilienfeld-Toal, W. Mäntele, In vivo noninvasive monitoring of glucose concentration in human epidermis by mid-infrared pulsed photoacoustic spectroscopy, Analytical Chemistry, 85(2012) 1013-20.

[37] M. Venugopal, K.E. Feuvrel, D. Mongin, S. Bambot, M. Faupel, A. Panangadan, et al., Clinical evaluation of a novel interstitial fluid sensor system for remote continuous alcohol monitoring, Sensors Journal, IEEE, 8(2008) 71-80.

[38] T.H. Risby, S. Solga, Current status of clinical breath analysis, Applied Physics B, 85(2006) 421-6.

[39] T. Hibbard, A.J. Killard, Breath ammonia analysis: Clinical application and measurement, Critical Reviews in Analytical Chemistry, 41(2011) 21-35.

[40] T.R. Paixão, M. Bertotti, Development of a breath alcohol sensor using a copper electrode in an alkaline medium, Journal of Electroanalytical Chemistry, 571(2004) 101-9.

[41] J.M. Corres, I.R. Matias, M. Hernaez, J. Bravo, F.J. Arregui, Optical fiber humidity sensors using nanostructured coatings of SiO nanoparticles, Sensors Journal, IEEE, 8(2008) 281-5.

[42] E. Horvath, P.R. Ribic, F. Hashemi, L. Forro, A. Magrez, Dye metachromasy on titanate nanowires: sensing humidity with reversible molecular dimerization, Journal of Materials Chemistry, 22(2012) 8778-84.

[43] Y. Miyoshi, K. Miyajima, H. Saito, H. Kudo, T. Takeuchi, I. Karube, et al., Flexible humidity sensor in a sandwich configuration with a hydrophilic porous membrane, Sensors and Actuators B: Chemical, 142(2009) 28-32.

[44] S. Borini, R. White, D. Wei, M. Astley, S. Haque, E. Spigone, et al., Ultrafast graphene oxide humidity sensors, ACS Nano, 7(2013) 11166-73.

[45] A. Haynes, P. Gouma, Electrospun conducting polymer-based sensors for advanced pathogen detection, Sensors Journal, IEEE, 8(2008) 701-5.

[46] G. Hunter, J. Xu, A. Biaggi-Labiosa, D. Laskowski, P. Dutta, S. Mondal, et al., Smart sensor systems for human health breath monitoring applications, Journal of Breath Research, 5(2011) 037111.

[47] S. Pantalei, E. Zampetti, A. Bearzotti, F. De Cesare, A. Macagnano, Improving sensing features of a nanocomposite PEDOT: PSS sensor for NO breath monitoring, Sensors and Actuators B: Chemical, 179(2013) 87-94.

[48] S. Cristescu, D. Marchenko, J. Mandon, K. Hebelstrup, G. Griffith, L. Mur, et al., Spectroscopic monitoring of NO traces in plants and human breath: applications and perspectives, Applied Physics B, 110(2013) 203-11.

[49] C. Higgins, D. Wencel, C.S. Burke, B.D. MacCraith, C. McDonagh, Novel hybrid optical sensor materials for in-breath O_2 analysis, Analyst, 133(2008) 241-7.

[50] Y. Xiong, Z. Ye, J. Xu, Y. Zhu, C. Chen, Y. Guan, An integrated micro-volume fiber-optic sensor for oxygen determination in exhaled breath based on iridium (III) complexes immobilized in fluorinated xerogels, Analyst, 138(2013) 1819-27.

[51] B. Timmer, W. Olthuis, A.v.d. Berg, Ammonia sensors and their applications—a review, Sensors and Actuators B: Chemical, 107(2005) 666-77.

[52] T. Hibbard, K. Crowley, Z. Shahbazian, A.J. Killard, A system for the continuous generation of simulated human breath supplemented with trace gases, Analytical Methods, 4(2012) 2172-6.

[53] T. Hibbard, K. Crowley, F. Kelly, F. Ward, J. Holian, A. Watson, et al., Point of care monitoring of hemodialysis patients with a breath ammonia measurement device based on printed polyaniline nanoparticle sensors, Analytical Chemistry, 85(2013) 12158-65.

[54] L. Wang, K. Kalyanasundaram, M. Stanacevic, P. Gouma, Nanosensor device for breath acetone detection, Sensor Letters, 8(2010) 709-12.

[55] M. Righettoni, A. Tricoli, S. Gass, A. Schmid, A. Amann, S.E. Pratsinis, Breath acetone monitoring by portable Si:WO_3 gas sensors, Analytica Chimica Acta, 738(2012) 69-75.

[56] J. Luo, J. Luo, L. Wang, X. Shi, J. Yin, E. Crew, et al., Nanoparticle-structured thin film sensor arrays for breath sensing, Sensors and Actuators B: Chemical, 161(2012) 845-54.

[57] R. Morgan, M. Patterson, M. Nimmo, Acute effects of dehydration on sweat composition in men during prolonged exercise in the heat, Acta Physiologica Scandinavica, 182(2004) 37-43.

[58] B.J. Rosenstein, G.R. Cutting, The diagnosis of cystic fibrosis: A consensus statement, The Journal of Pediatrics, 132(1998) 589-95.

[59] B.-W. Chang, S.-J. Yeh, P.-P. Tsai, H.-C. Chang, Monitoring perspiration from palms of hypohidrosis patients with a stopped-flow conductometric mini-system, Clinica Chimica Acta, 348(2004) 107-11.

[60] M.S. Talary, F. Dewarrat, D. Huber, A. Caduff, In vivo life sign application of dielectric spectroscopy and non-invasive glucose monitoring, Journal of Non-Crystalline Solids, 353(2007) 4515-7.

[61] A. Caduff, M.S. Talary, M. Mueller, F. Dewarrat, J. Klisic, M. Donath, et al., Non-invasive glucose monitoring in patients with Type 1 diabetes: a multisensor system combining sensors for dielectric and optical characterisation of skin, Biosensors and Bioelectronics, 24(2009) 2778-84.

[62] M. Gamella, S. Campuzano, J. Manso, G. Rivera, F. López-Colino, A. Reviejo, et al., A novel non-invasive electrochemical biosensing device for in situ determination of the alcohol content in blood by monitoring ethanol in sweat, Analytica Chimica Acta, 806(2014) 1-7.

[63] D. Sakharov, M. Shkurnikov, M.Y. Vagin, E. Yashina, A. Karyakin, A. Tonevitsky, Relationship between lactate concentrations in active muscle sweat and whole blood, Bulletin of Experimental Biology and Medicine, 150(2010) 83-5.

[64] X. Cai, J. Yan, H. Chu, M. Wu, Y. Tu, An exercise degree monitoring biosensor based on electrochemiluminescent detection of lactate in sweat, Sensors and Actuators B: Chemical, 143(2010) 655-9.

[65] D. Morris, S. Coyle, Y. Wu, K.T. Lau, G. Wallace, D. Diamond, Bio-sensing textile based patch with integrated optical detection system for sweat monitoring, Sensors and Actuators B: Chemical, 139(2009) 231-6.

[66] S. Coyle, K.-T. Lau, N. Moyna, D. O'Gorman, D. Diamond, F. Di Francesco, et al., BIOTEX—Biosensing textiles for personalised healthcare management, Information Technology in Biomedicine, IEEE Transactions on, 14(2010) 364-70.

[67] B. Schazmann, D. Morris, C. Slater, S. Beirne, C. Fay, R. Reuveny, et al., A wearable electrochemical sensor for the real-time measurement of sweat sodium concentration, Analytical Methods, 2(2010) 342-8.

[68] V.F. Curto, S. Coyle, R. Byrne, N. Angelov, D. Diamond, F. Benito-Lopez, Concept and development of an autonomous wearable micro-fluidic platform for real time pH sweat analysis, Sensors and Actuators B: Chemical, 175(2012) 263-70.

[69] V.F. Curto, C. Fay, S. Coyle, R. Byrne, C. O'Toole, C. Barry, et al., Real-time sweat pH monitoring based on a wearable chemical barcode micro-fluidic platform incorporating ionic liquids, Sensors and Actuators B: Chemical, 171(2012) 1327-34.

[70] T. Guinovart, M. Parrilla, G.A. Crespo, F.X. Rius, F.J. Andrade, Potentiometric sensors using cotton yarns, carbon nanotubes and polymeric membranes, Analyst, 138(2013) 5208-15.

[71] D.-H. Kim, N. Lu, R. Ma, Y.-S. Kim, R.-H. Kim, S. Wang, et al., Epidermal electronics, Science, 333(2011) 838-43.

[72] X. Huang, Y. Liu, H. Cheng, W.J. Shin, J.A. Fan, Z. Liu, et al., Materials and designs for wireless epidermal sensors of hydration and strain, Advanced Functional Materials, 24(2014) 3846-3854.

[73] X. Huang, Y. Liu, K. Chen, W.J. Shin, C.J. Lu, G.W. Kong, et al., Stretchable, wireless sensors and functional substrates for epidermal characterization of sweat, Small, 10(2014) 3083-3090.

[74] T. Guinovart, A.J. Bandodkar, J.R. Windmiller, F.J. Andrade, J. Wang, A potentiometric tattoo sensor for monitoring ammonium in sweat, Analyst, 138(2013) 7031-8.

[75] A.J. Bandodkar, V.W. Hung, W. Jia, G. Valdés-Ramírez, J.R. Windmiller, A.G. Martinez, et al., Tattoo-based potentiometric ion-selective sensors for epidermal pH monitoring, Analyst, 138(2013) 123-8.

[76] A.J. Bandodkar, D. Molinnus, O. Mirza, T. Guinovart, J.R. Windmiller, G. Valdés-Ramírez, et al., Epidermal tattoo potentiometric sodium sensors with wireless signal transduction for continuous non-invasive sweat monitoring, Biosensors and Bioelectronics, 54(2014) 603-9.

[77] W. Jia, A.J. Bandodkar, G. Valdes-Ramirez, J.R. Windmiller, Z. Yang, J. Ramirez, et al., Electrochemical tattoo biosensors for real-time noninvasive lactate monitoring in human perspiration, Analytical Chemistry, 85(2013) 6553-60.

[78] S. Ghimenti, T. Lomonaco, M. Onor, L. Murgia, A. Paolicchi, R. Fuoco, et al., Measurement of warfarin in the oral fluid of patients undergoing anticoagulant oral therapy, PloS one, 6(2011) e28182.

[79] A. Millward, L. Shaw, E. Harrington, A.J. Smith, Continuous monitoring of salivary flow rate and pH at the surface of the dentition following consumption of acidic beverages, Caries Research, 31(1997) 44-9.

[80] M. Bouchoucha, F. Callais, P. Renard, O.G. Ekindjian, P.H. Cugnenc, J.P. Barbier, Relationship between acid neutralization capacity of saliva and gastro-oesophageal reflux, Archives of Physiology and Biochemistry, 105(1997) 19-26.

[81] J.S. Mitchell, T.E. Lowe, J.R. Ingram, Rapid ultrasensitive measurement of salivary cortisol using nano-linker chemistry coupled with surface plasmon resonance detection, Analyst, 134(2009) 380-6.

[82] J.S. Mitchell, T.E. Lowe, Ultrasensitive detection of testosterone using conjugate linker technology in a nanoparticle-enhanced surface plasmon resonance biosensor, Biosensors and Bioelectronics, 24(2009) 2177-83.

[83] G. Saikia, P.K. Iyer, A remarkable superquenching and superdequenching sensor for the selective and noninvasive detection of inorganic phosphates in saliva, Macromolecules, 44(2011) 3753-8.

[84] R.C. Kwan, H. Leung, P.Y. Hon, H.C. Cheung, K. Hirota, R. Renneberg, Amperometric biosensor for determining human salivary phosphate, Analytical Biochemistry, 343(2005) 263-7.

[85] D. Du, J. Wang, J.N. Smith, C. Timchalk, Y. Lin, Biomonitoring of organophosphorus agent exposure by reactivation of cholinesterase enzyme based on carbon nanotube-enhanced flow-injection amperometric detection, Analytical Chemistry, 81(2009) 9314-20.

[86] M. Yamaguchi, M. Deguchi, J. Wakasugi, Flat-chip microanalytical enzyme sensor for salivary amylase activity, Biomedical Microdevices, 7(2005) 295-300.

[87] M.B. Lerner, N. Kybert, R. Mendoza, R. Villechenon, M.A.B. Lopez, A.C. Johnson, Scalable, non-invasive glucose sensor based on boronic acid functionalized carbon nanotube transistors, Applied Physics Letters, 102(2013) 183113.

[88] C. Zuliani, G. Matzeu, D. Diamond, A potentiometric disposable sensor strip for measuring pH in saliva, Electrochimica Acta, 132(2014) 292-6.

[89] C. Schabmueller, D. Loppow, G. Piechotta, B. Schütze, J. Albers, R. Hintsche, Micromachined sensor for lactate monitoring in saliva, Biosensors and Bioelectronics, 21(2006) 1770-6.

[90] A.M. Spehar‐Délèze, S. Anastasova, P. Vadgama, Electropolymerised phenolic films as internal barriers for oxidase enzyme biosensors, Electroanalysis, (2013).

[91] J. Wang, J. Kim, P. Mercier, A. Badodkar, J. Ramirez, A.G. Martinez, et al., Non-invasive mouthguard biosensor for continuous salivary monitoring of metabolites, Analyst, (2014).

[92] M.S. Mannoor, H. Tao, J.D. Clayton, A. Sengupta, D.L. Kaplan, R.R. Naik, et al., Graphene-based wireless bacteria detection on tooth enamel, Nature Communications, 3(2012) 763.

[93] J.T. Baca, D.N. Finegold, S.A. Asher, Tear glucose analysis for the noninvasive detection and monitoring of diabetes mellitus, The Ocular Surface, 5(2007) 280-93.

[94] J.T. Baca, C.R. Taormina, E. Feingold, D.N. Finegold, J.J. Grabowski, S.A. Asher, Mass spectral determination of fasting tear glucose concentrations in nondiabetic volunteers, Clinical Chemistry, 53(2007) 1370-2.

[95] C. O'Donnell, N. Efron, Diabetes and contact lens wear, Clinical and Experimental Optometry, 95(2012) 328-37.

[96] J. Zhang, W. Hodge, C. Hutnick, X. Wang, Noninvasive diagnostic devices for diabetes through measuring tear glucose, Journal of Diabetes Science and Technology, 5(2011) 166-72.

[97] A. Kagie, D.K. Bishop, J. Burdick, J.T. La Belle, R. Dymond, R. Felder, et al., Flexible rolled thick-film miniaturized flow-cell for minimally invasive amperometric sensing, Electroanalysis, 20(2008) 1610-4.

[98] Q. Yan, B. Peng, G. Su, B.E. Cohan, T.C. Major, M.E. Meyerhoff, Measurement of tear glucose levels with amperometric glucose biosensor/capillary tube configuration, Analytical Chemistry, 83(2011) 8341-6.

[99] B. Peng, J. Lu, A.S. Balijepalli, T.C. Major, B.E. Cohan, M.E. Meyerhoff, Evaluation of enzyme-based tear glucose electrochemical sensors over a wide range of blood glucose concentrations, Biosensors and Bioelectronics, 49(2013) 204-9.

[100] V. Andoralov, S. Shleev, T. Arnebrant, T. Ruzgas, Flexible micro (bio) sensors for quantitative analysis of bioanalytes in a nanovolume of human lachrymal liquid, Analytical and Bioanalytical Chemistry, 405(2013) 3871-9.

[101] S. Iguchi, H. Kudo, T. Saito, M. Ogawa, H. Saito, K. Otsuka, et al., A flexible and wearable biosensor for tear glucose measurement, Biomedical Microdevices, 9(2007) 603-9.

[102] H. Kudo, S. Iguchi, K. Miyajima, H. Saito, K. Mitsubayashi, A flexible and wearable biosensor for continuous glucose monitoring on eye site, ECS Transactions, 16(2008) 99-104.

[103] M. Chu, H. Kudo, T. Shirai, K. Miyajima, H. Saito, N. Morimoto, et al., A soft and flexible biosensor using a phospholipid polymer for continuous glucose monitoring, Biomedical Microdevices, 11(2009) 837-42.

[104] M.X. Chu, K. Miyajima, D. Takahashi, T. Arakawa, K. Sano, S.-i. Sawada, et al., Soft contact lens biosensor for in situ monitoring of tear glucose as non-invasive blood sugar assessment, Talanta, 83(2011) 960-5.

[105] M. Chu, T. Shirai, D. Takahashi, T. Arakawa, H. Kudo, K. Sano, et al., Biomedical soft contact-lens sensor for in situ ocular biomonitoring of tear contents, Biomedical Microdevices, 13(2011) 603-11.

[106] H. Yao, A.J. Shum, M. Cowan, I. Lähdesmäki, B.A. Parviz, A contact lens with embedded sensor for monitoring tear glucose level, Biosensors and Bioelectronics, 26(2011) 3290-6.

[107] R. Badugu, J.R. Lakowicz, C.D. Geddes, A glucose-sensing contact lens: from bench top to patient, Current Opinion in Biotechnology, 16(2005) 100-7.

[108] H. Yao, Y. Liao, A. Lingley, A. Afanasiev, I. Lähdesmäki, B. Otis, et al., A contact lens with integrated telecommunication circuit and sensors for wireless and continuous tear glucose monitoring, Journal of Micromechanics and Microengineering, 22(2012) 075007.

[109] N. Thomas, I. Lähdesmäki, B.A. Parviz, A contact lens with an integrated lactate sensor, Sensors and Actuators B: Chemical, 162(2012) 128-34.

[110] R. Badugu, J.R. Lakowicz, C.D. Geddes, Ophthalmic glucose monitoring using disposable contact lenses—a review, Journal of Fluorescence, 14(2004) 617-33.

[111] R. Badugu, J.R. Lakowicz, C.D. Geddes, Noninvasive continuous monitoring of physiological glucose using a monosaccharide-sensing contact lens, Analytical Chemistry, 76(2004) 610-8.

[112] R. Badugu, J.R. Lakowicz, C.D. Geddes, Ophthalmic glucose sensing: a novel monosaccharide sensing disposable and colorless contact lens, Analyst, 129(2004) 516-21.

[113] Y. Hu, X. Jiang, L. Zhang, J. Fan, W. Wu, Construction of near-infrared photonic crystal glucose-sensing materials for ratiometric sensing of glucose in tears, Biosensors and Bioelectronics, 48(2013) 94-9.

[114] V.L. Alexeev, S. Das, D.N. Finegold, S.A. Asher, Photonic crystal glucose-sensing material for noninvasive monitoring of glucose in tear fluid, Clinical Chemistry, 50(2004) 2353-60.

[115] X. Yang, X. Pan, J. Blyth, C.R. Lowe, Towards the real-time monitoring of glucose in tear fluid: Holographic glucose sensors with reduced interference from lactate and pH, Biosensors and Bioelectronics, 23(2008) 899-905.

[116] L.B. Wingard, E.E. Spaeth, Implantable glucose sensor expected soon, Nature Biotechnology, 7(1989) 116.

[117] M.C. Frost, M.E. Meyerhoff, Implantable chemical sensors for real-time clinical monitoring: progress and challenges, Current Opinion in Chemical Biology, 6(2002) 633-41.

[118] M.A. Wood, K.A. Ellenbogen, Cardiac pacemakers from the patient's perspective, Circulation, 105(2002) 2136-8.

[119] D.A. Gough, L.S. Kumosa, T.L. Routh, J.T. Lin, J.Y. Lucisano, Function of an implanted tissue glucose sensor for more than 1 year in animals, Science Translational Medicine, 2(2010) 42ra53.

[120] D.S. Bindra, Y. Zhang, G.S. Wilson, R. Sternberg, D.R. Thevenot, D. Moatti, et al., Design and in vitro studies of a needle-type glucose sensor for subcutaneous monitoring, Analytical Chemistry, 63(1991) 1692-6.

[121] A. Heller, B. Feldman, Electrochemical glucose sensors and their applications in diabetes management, Chemical Reviews, 108(2008) 2482-505.

[122] D. Khodagholy, V.F. Curto, K.J. Fraser, M. Gurfinkel, R. Byrne, D. Diamond, et al., Organic electrochemical transistor incorporating an ionogel as a solid state electrolyte for lactate sensing, Journal of Materials Chemistry, 22(2012) 4440-3.

[123] H.E. Koschwanez, F.Y. Yap, B. Klitzman, W.M. Reichert, In vitro and in vivo characterization of porous poly-L-lactic acid coatings for subcutaneously implanted glucose sensors, Journal of Biomedical Materials Research Part A, 87A(2008) 792-807.

[124] S.P. Nichols, N.N. Le, B. Klitzman, M.H. Schoenfisch, Increased In Vivo Glucose Recovery via Nitric Oxide Release, Analytical Chemistry, 83(2011) 1180-4.

[125] A. Koh, Y. Lu, M.H. Schoenfisch, Fabrication of nitric oxide-releasing porous polyurethane membranes-coated needle-type implantable glucose biosensors, Analytical Chemistry, 85(2013) 10488-94.

[126] E.M. Hetrick, H.L. Prichard, B. Klitzman, M.H. Schoenfisch, Reduced foreign body response at nitric oxide-releasing subcutaneous implants, Biomaterials, 28(2007) 4571-80.

[127] D.A. Riccio, K.P. Dobmeier, E.M. Hetrick, B.J. Privett, H.S. Paul, M.H. Schoenfisch, Nitric oxide-releasing S-nitrosothiol-modified xerogels, Biomaterials, 30(2009) 4494-502.

[128] V.F. Curto, S. Scheuermann, R.M. Owens, V. Ranganathan, D.R. MacFarlane, F. Benito-Lopez, et al., Probing the specific ion effects of biocompatible hydrated choline ionic liquids on lactate oxidase biofunctionality in sensor applications, Physical Chemistry Chemical Physics, 16(2014) 1841-9.

[129] M. Naushad, Z.A. Alothman, A.B. Khan, M. Ali, Effect of ionic liquid on activity, stability, and structure of enzymes: A review, International Journal of Biological Macromolecules, 51(2012) 555-60.

[130] C. Wang, W. Zheng, Z. Yue, C.O. Too, G.G. Wallace, Buckled, stretchable polypyrrole electrodes for battery applications, Advanced Materials, 23(2011) 3580-4.

[131] B. Yue, C. Wang, X. Ding, G.G. Wallace, Polypyrrole coated nylon lycra fabric as stretchable electrode for supercapacitor applications, Electrochima Acta, 68(2012) 18-24.

[132] C. Yan, P.S. Lee, Stretchable energy storage and conversion devices, Small, 10(2014) 3443-60.

[133] Y. Zhou, Y. Bayram, F. Du, L. Dai, J.L. Volakis, Polymer-carbon nanotube sheets for conformal load bearing antennas, Antennas and Propagation, IEEE Transactions on, 58(2010) 2169-75.

[134] L. Song, A.C. Myers, J.J. Adams, Y. Zhu, Stretchable and reversibly deformable radio frequency antennas based on silver nanowires, Acs Applied Materials & Interfaces, 6(2014) 4248-53.

[135] J.R. Windmiller, A.J. Bandodkar, G. Valdés-Ramírez, S. Parkhomovsky, A.G. Martinez, J. Wang, Electrochemical sensing based on printable temporary transfer tattoos, Chemical Communications, 48(2012) 6794-6.

[136] Y.J. Heo, S. Takeuchi, Towards smart tattoos: implantable biosensors for continuous glucose monitoring, Advanced Healthcare Materials, 2(2013) 43-56.

[137] Z. Liu, Microelectrodes in an ophthalmic electrochemical sensor, Google Patents2012.

[138]http://www.gmanetwork.com/news/story/360331/scitech/technology/google-s-smart-contact-lenses-may-arrive-sooner-than-you-think., Accessed on: 28 April 2015

[139] http://guardianlv.com/2014/02/apple-iwatch-rumors-persist/, Accessed on: 28 April 2015

[140] http://www.idownloadblog.com/2014/06/21/iwatch-blood-glucose-sensors/. Accessed on: 28 April 2015

Chapter 3.

A Liquid-Junction-Free Reference Electrode Based on a PEDOT Solid-Contact and Ionogel Capping Membrane

Claudio Zuliani*[a], **Giusy Matzeu**[b] and Dermot Diamond*[b]

URL: http://www.sciencedirect.com/science/article/pii/S0039914014001167

ISSN and DOI: 10.1016/j.talanta.2014.02.018

Talanta 125 (2014): 58-64.

*Corresponding author

[a]Clarity Centre for Sensor Web Technologies, National Centre for Sensor Research, Dublin City University, Dublin 9, Ireland

[b]Insight Centre for Data Analytics, Dublin City University, Dublin 9, Ireland.

Aims and Objectives

Chapter 3 describes the design and realisation of novel solid-contact reference electrodes. Screening tests were first carried out to find the best combination in terms of capping membrane (based on ionogels) and solid-contact material to obtain optimum performances. The solid-contact reference electrodes were tested in combination with pH and Na^+ solid-contact ISEs.

Contributions

- Design, conception and optimisation of the experimental trials.
- Analysis of data and writing up of the manuscript.

Abstract

Liquid-junction-free reference electrodes have been prepared on screen-printed substrates using poly-3,4-ethylenedioxythiophene (PEDOT) as solid-contact and novel ionogels as capping membrane. The chemico-physical properties of the PEDOT layer were tuned by changing the electropolymerisation media and electrodeposition technique. PEDOT films electrodeposited potentiostatically or potentiodynamically were found to have a significant impact on the stability of the electrodes during the conditioning step. Optimisation of the capping membrane formulation, e.g., acrylate monomers, Ionic Liquid, cross-linkers and photo-initiators, produced electrodes with properties almost equivalent with a commercial reference electrode. Thus, calibration plots of Na^+ Ion-Selective Electrodes against the optimised Solid-Contact Ionogel Reference Electrodes (SCI-REs) or against a double-liquid-junction Ag/AgCl electrode did not present any significant difference. Such SCI-REs may provide an effective route to the generation of future low-cost components for potentiometric sensing strips.

Keywords

Screen Printing, Poly-3,4-ethylenedioxythiophene (PEDOT), Ion-Selective Electrodes (ISEs), Reference Electrode, Solid-Contact, Ionic Liquid, Ionogel.

3.1 Introduction

In order to realise low-cost potentiometric sensors, a reference electrode compatible with mass production such as screen printing is required [1]. While there has been considerable success in producing devices based on a disposable single/limited use model, a significant challenge remains in the production of devices capable of continuous use over longer periods of time [1-3]. Improving the performance of commercially available reference electrodes compatible with thin and thick film technologies is an issue, which has received relatively little attention [4]. There is a need for all solid state reference electrodes of analytical quality that would retain the performance of a classical reference electrode while offering additional advantages such as maintenance-free use and compatibility with low-cost mass production manufacturing techniques [5].

While minor variations of the salt bridge or junction design [4, 6] may produce some performance improvements, they do not render the design compatible with mass-production and the effectiveness may be relatively short-term. For example, gel-like materials employed in salt bridge electrolytes do commonly suffer from drying and leaching [1, 3]. Mi et al. [7] introduced a novel concept for the preparation of a pseudo-reference using hydrophobic anion-exchanger membranes loaded with the polyanion heparin. Because heparin passively diffuses at a low rate from the ion-exchanger membranes into the sample, the potential drop across the solution/membrane interface is almost sample-independent and well defined [4, 7]. Following this advance, water-immiscible Ionic Liquids, or hydrophobic polymeric membranes doped with Ionic Liquids were employed to overcome some of the typical reference electrode limitations described above [4, 8]. For instance, Kakiuchi et al. [9] introduced ionogels based on the bis(trifluoromethylsulfonyl)imide [NTf_2] Ionic Liquid family as a novel salt-bridge material for reference electrodes. Following this investigation, ionogels based on [NTf_2] ILs [4, 10] were employed as capping membranes in order to prepare disposable solid-contact ionogels reference electrodes (SCI-REs). Since the hydrophobic polymeric membrane contains an Ionic Liquid that is sparingly soluble in water [10, 11], its partition between the two phases creates a local equilibrium distribution thus establishing a potential, E_{PB}, defined by the phase boundary model [10, 11], (see Equation 3.1):

$$E_{PB} = \frac{RT}{z_I F} \ln \frac{k_I a_I}{\gamma_I [I^{z_I}]} \qquad (3.1)$$

where k_I is the phase transfer energy, a_I is the activity of an ion of charge z_I in the sample phase, γ_I and $[I^{z_I}]$ are respectively the activity coefficient and the concentration of the free ion I^{z_I} in the membrane phase; R, T, and F are the gas constant, the absolute temperature, and the Faraday constant, respectively.

The use of ionogels to prepare reference electrodes can be seen as an improvement of the lipophilic salt approach introduced by Mattinen et al. [11, 12] since no solvent is required. However, Cicmil et al. [10] showed that electrodes prepared by drop casting [NTf_2]/PVC ionogels onto a poly(3-octylthiophene-2,5-diyl) (POT) solid-contact layer exhibited changes in potential of up to 20-25 mV and 15-20 mV when the concentration of bathing solutions of KCl and NaCl was increased from 1 to 10 mM, respectively. In addition, Zhang et al. [4] showed that protonation of [NTf_2] within the ionogel phase at pH<4.5 caused trans-membrane fluxes that generated significant changes in the electrode potential. In addition, the role of the solid-contact in SCI-REs has not been explored to any great extent.

In this paper, we present evidence to support the view that the type of IL anion employed during the electropolymerisation of the conducting polymer (CP) layer (i.e., formation of the SC layer) affects the performance of the resulting electrodes, when tested in comparison to a commercial double-junction reference electrode. We also demonstrate that the variation in the potential of the electrodes in contact with Na^+ and K^+ chloride salts solutions can be reduced through careful formulation of the membrane components, e.g., through choice of the IL used in the ionogel capping layer, and the nature of the underlying solid-contact material. Such optimised electrodes are finally shown to perform well as reference electrodes for the potentiometric calibration of NaCl solutions using Na^+ Ion-Selective Electrodes (Na^+ ISEs) and for the measurement of pH in real saliva samples.

3.2 Experimental

3.2.1 Materials

The C2030519P4 carbon ink and the D50706D2 dielectric ink from Gwent Electronic Materials (Pontypool, UK) were used to prepare screen-printed electrodes. 175 µm thick PET sheets from HiFi (Dublin, Ireland) or MacDermid (Oxon, UK) were employed as substrates for screen printing. Potassium and sodium chloride, 3,4-ethylenedioxythiophene (EDOT, 97%), poly(3-octylthiophene-2,5-diyl) regiorandum (POT), high molecular weight poly(vinyl chloride) (PVC), tetrahydrofuran (THF,

≥99.5%), 2-hydroxy-2-methyl-propiophenone (HMPP, >97%), phenylbis(2,4,6-trimethylbenzoyl)phosphine oxide (PBPO, >97%), 2,2-dimethoxy-2-phenylacetophenone (DMPA, >99%), butyl-acrylate (>99%), 1,6-hexanediol diacrylate (HDDA, 80%), and poly(propylene glycol) diacrylate (PPODA, Mn~800) were purchased from Sigma-Aldrich (Dublin, Ireland). When possible, they were of selectophore grade or trace metal standard. N-decyl-methacrylate was obtained from Polysciences (Northampton, UK), 1,4-butanediol diacrylate (BDDA, >99%) from Alfa Aesar (Heysham, UK), chloroform (>99%) and ethanol (EtOH) from Fisher Scientific (Dublin, Ireland). 1-ethyl-3-methylimidazolium [emim][NTf_2], [emim] tris(pentafluoroethyl)trifluorophosphate [FAP], 1-butyl-3-methylimidazolium [bmim][FAP] and 1-hexyl-3-methylimidazolium [hmim][FAP] were obtained from VWR (Dublin, Ireland). All chemicals were used as received. For the preparation of gaskets, 0.8 mm thick adhesive poly foam strips were purchased from Radionics (Dublin, Ireland). Deionised water with resistivity of 18.2 MΩ cm was obtained with a Milli-Q reagent-grade water system and was used to prepare aqueous solutions.

3.2.2 Reference Electrode Preparation

Carbon screen-printed electrodes, see Figure AA.1, were fabricated as described elsewhere [13]. POT and poly(3,4-ethylenedioxythiophene) (PEDOT) were deposited on these electrodes to form the underlying mixed conductivity solid-contact layer. The POT and EDOT solutions were stirred overnight and for ~1 hour, respectively, to facilitate solubilisation. The solid-contact layer was prepared by drop casting a total amount of 15 µL of 2.75 mg/mL POT chloroform solution onto the underlying carbon layer. Alternatively, PEDOT was electrochemically grown on the carbon electrodes from a 0.05 M EDOT solution in [emim][FAP] or [emim][NTf_2] which was stirred at 1000 rpm. During this process, the potential was scanned 25 times between 0 and 1.0 V with a scan rate of 50 mV/s or held at 1.0 V for 900 seconds. Stirring the monomer solution during electropolymerisation produced more homogeneous PEDOT films compared to equivalent electrodeposition without stirring, which tended to produce PEDOT films preferentially at the outer ring of the electro-active disk. At the end of the PEDOT deposition, the electrodes were rinsed with EtOH, followed by H_2O and again with EtOH. The electrodes were finally dried by blowing N_2 over them and stored in a covered petri dish.

For the preparation of the capping membranes, the IL was vortexed for ~1 hour with the acrylate monomer/s, the cross-linker and the photo-initiator. 9 µL of the resulting liquid membrane formulation was drop-cast on the electrodeposited PEDOT layer

within a 3.0 mm diameter well formed by punching a hole in an adhesive foam tape covering layer, which was then fixed around the carbon disk. The acrylate solution was polymerised via a free radical initiated mechanism without flushing N_2, i.e., by 40 minutes irradiation under UV or white light, using the CL-1000 ultraviolet cross-linker UVP source, or the Dolan-Jenner Fiber-lite LMI-6000 lamp, respectively. Table AA.1 in the Appendix A reports details of the membrane formulations screened in this investigation. For all the formulations, the amount of photo-initiator and IL was 0.8% and 6% of the molar content of the acrylate monomer/s used, respectively. (Note: when combining monomers, the molar ratio is referred to the sum of the molar content of the two monomers). Unless differently stated, all the percentages reported for the membrane components are given in respect to the molar content of the acrylate monomer/s. The membrane mixture was freshly prepared, carefully protected from direct sunlight and used within few hours of preparation. If not explicitly stated, the electrodes were conditioned overnight in aqueous 10 mM NaCl. Na^+ SC-ISEs electrodes were prepared in-house. The ISE solid-contact was a PEDOT layer potentiostatically deposited from [emim][NTf_2], as described above for the reference electrodes. The ISE capping membrane, prepared as reported elsewhere [14], was an ionophore doped PVC formulation and was drop-cast on the PEDOT layer.

3.2.3 Instrumentation and Software

The potentiometric measurements were recorded using the EMF-16 voltmeter from Lawson Labs, USA. The potential of the above electrodes was measured against an in-house made silver/silver chloride (saturated KCl) and a double-junction Ag/AgCl (Sigma Aldrich, Ireland) during conditioning and testing, respectively. An Ag and a Pt wire were employed during the EDOT electropolymerisation as pseudo-reference and counter electrodes. CHI900 (CH-Instruments, USA) was used to carry out the electropolymerisation of the conducting polymer on dual screen-printed electrode substrates. A pH meter (SympHony SP70P) from VWR was used to check the pH of aqueous solutions and to validate pH measurements of sublingual saliva samples that were collected using a sterile pipette from volunteers. All the Scanning Electron Microscopy (SEM) images were captured with the Hitachi S3000N in the secondary electron mode, using an accelerating voltage of 5 kV.

3.3 Results and Discussion

POT and PVC doped with ILs have been used previously [10] tested as the solid-contact and capping membrane, respectively, for the preparation of SCI-REs. PVC has been the material of choice for decades in the preparation of Ion-Selective Electrodes (ISEs) and its use in reference electrodes is therefore understandable. However, polyacrylates have attractive qualities for electrodes with ionogel-based capping layers, such as lower levels of ionic contaminants [15] and a lower dielectric constant [16, 17], which reduces ion-exchange behaviour, and may enhance the retention of IL within the layer. The availability of various acrylate monomers, along with diverse cross-linkers and photo-initiators, offers the possibility to create polymers with a wide range of physical and mechanical properties [15]. Besides, non-plasticised polyacrylates matrices are important in biomedical applications because of their biocompatibility and compatibility with thick and thin film microfabrication technologies [5, 6, 8]. Regarding the solid-contact layer, POT re-dissolves during the drop casting of the PVC/IL capping membrane from a THF solution, as experimentally demonstrated in Figure AA.2. Preliminary tests with electrodes prepared with POT (SC) and PVC/IL (capping membrane) layers showed slow polarisation of the potentiometric curves when the measurement was stopped and then re-started after few minutes, without removing the electrodes from the solution (results not shown). This slow polarisation is probably an indication of a water layer building up at the internal interface, i.e., formation of a thin aqueous inner phase beneath the PVC capping membrane [18, 19]. While POT should impede the formation of a water layer at the electrode/polymer interface because of its hydrophobicity, the above re-dissolution into the THF solution produced films that did not fully cover the carbon surface, and this contributed to the slow polarisation curves observed with these electrodes.

For the above reasons, PEDOT electrochemically deposited from IL-media (used as solid-contact) and polyacrylates-based ionogels (as capping membrane materials) were selected for further investigation. Regarding the capping membrane, the [FAP] anion family of ILs was chosen for their low water solubility. For instance, the mole fraction solubilities in water of [hmim][NTf_2] and [hmim][FAP] are 10^{-4} and ~10^{-6} [20-24], respectively. This property raises the possibility of a significantly larger leaching rate of the IL from the membrane in the former case. Leaching may not only impact on the stability of the electrode potential but it may also be hazardous in certain circumstances, e.g., environmental or wearable applications. A range of acrylate formulations containing equal amount of IL ([emim][FAP], 6%), cross-linker (HDDA,

3.0%) and photo-initiator (DMPA, 0.8%) were tested (as listed in Table AA.1). It was found that highly uniform membranes with rubbery (but not tacky) character could be obtained by polymerising a mixture of butylacrylate and N-decylmethacrylate in the molar ratio 9:1. In contrast, polymerisation of butyl-acrylate alone resulted in a more wrinkly gel. In case of N-decylmethacrylate alone or 1:1 mixtures of butylacrylate and N-decylmethacrylate, the resulting polymers tended to be too soft/runny in nature. The level of cross-linker in the co-monomers mixture was also found to have a significant effect on the resulting polymer characteristics. Therefore, an optimisation process was employed starting from a base mixture of butylacrylate and N-decylmethacrylate in the molar ratio 9:1, and varying the composition in a systematic manner. For example, the amount of HDDA was increased from 1.5% through 3.0% to 4.5%, in steps of 1.5%, and the optimal was found to be around 3.0%. The membranes produced using 1.5% and 4.5% of HDDA in the monomers formulation were respectively too sticky or too stiff to be of practical use for our application.

Figure 3.1 (a) shows the results obtained with membranes based on poly(butyl-co-decylmethacrylate) containing various cross-linkers, photo-initiators and types of solid-contact. Several conclusions can be drawn from these results. Firstly, all membranes exhibited moderate cation-exchange behaviour, but they were quite insensitive to variations of the pH of the sample, over the range pH 4-7. This would suggest that [FAP] acted as a cation-exchanger site in the membrane, to a certain extent. The potential of the electrodes immersed in a 0.1 M KCl solution was indeed always higher in comparison to the same electrodes immersed in 0.1 M NaCl solution.

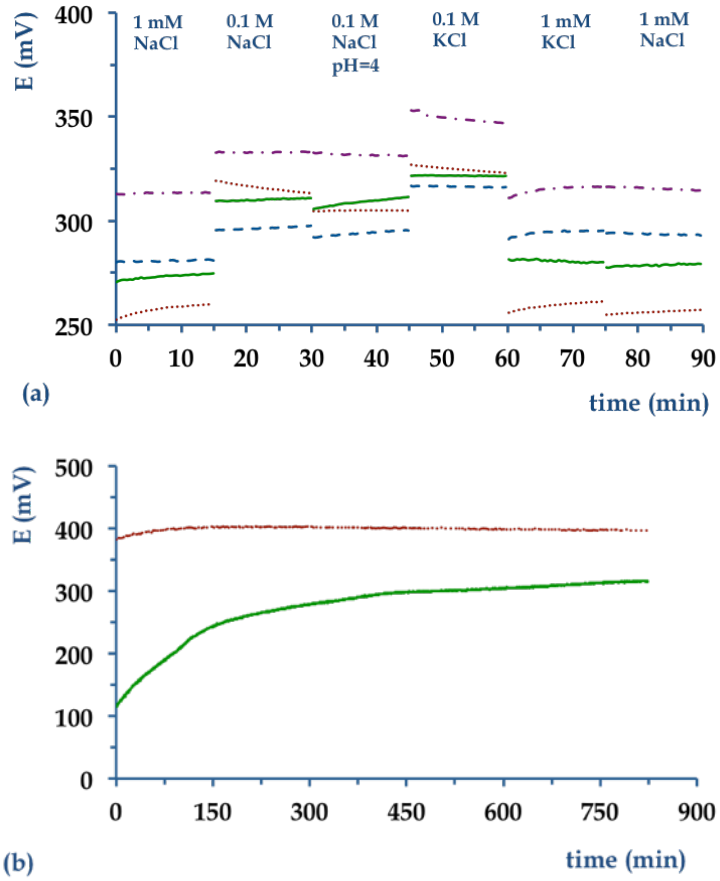

Figure 3. 1: (a) Individual responses of reference electrodes prepared by entrapping [emim][FAP] within a poly(butyl-co-decylmethacrylate) membrane polymerised in situ. Three electrodes have a PEDOT solid-contact layer electrodeposited by CVs from [emim][FAP], and their membranes contained: (blue, – –) 3% HDDA or (red, · · ·) 3% PPODA as cross-linker together with 0.8% of DMPA as photo-initiator, or (green, —) 3% HDDA together with 0.8% of PBPO as photo-initiator. In one case (purple, – · –), the PEDOT solid-contact layer was electrodeposited potentiostatically from [emim][FAP] and the membrane contained: 3% HDDA and 0.8% DMPA. The electrode potential was recorded for 15 minutes in each bathing solution, as labelled in the figure. (b) Conditioning step of reference electrodes prepared by entrapping [emim][FAP] in a poly(butyl-co-decylmethacrylate) membrane while in contact with a 10 mM NaCl solution. The solid-contact consisted of PEDOT deposited from a 50 mM EDOT solution in [emim][FAP] by (red, · · ·) potentiostatic and (green, —) CV polarisation.

Secondly, the figure demonstrates that the use of PBPO instead of DMPA as photo-initiator increased the sensitivity of the electrodes towards Na^+ and K^+. With ionogels formed using PBPO (green, —), the electrode potential increased by ~35 mV and by ~40 mV when the NaCl and KCl concentrations increased from 1 mM to 0.1 M, respectively. For equivalent ionogels formed using DMPA (blue, – –), the electrode potential increased less, i.e., 18.5±1.9 mV and 30.5±8.7 mV (n=4). This difference may

arise from the presence of residual photo-initiator and its by-products in the membrane, as these are known to exhibit ion-exchange behaviour [25]. Thirdly, electrodes with membranes produced using PPODA (red, · · ·) as cross-linker showed larger sensitivity towards Na^+ and K^+ than equivalent membranes produced using HDDA (blue, – –). For example, electrodes based on these membranes showed shifts in potential of the order of ~50 and ~60 mV, respectively, when the Na^+ and K^+ concentrations were raised from 1 mM to 0.1 M. HMPP was discarded as photo-initiator as it was found to produce very stiff and thin membranes that tended to peel away from the underlying layers. HDDA[3.a] and DMPA were therefore selected as cross-linker and photo-initiator, respectively, while PPODA and PBPO were discarded from further investigation.

The redox state of the conducting polymer appears to affect the electrode potential during conditioning, as shown in Figure 3.1 (b). The level of doping in the polymer will be different depending on the deposition technique employed, e.g., PEDOT deposited using cyclic voltammetry should be present in a less oxidised state [26] when compared to the potentiostatically deposited polymer. The latter fact occurs because the potential was reversed back to 0.0 V or held at 1.0 V (corresponding to the onset of the oxidation of the monomer) in case of CV or potentiostatic deposition, respectively. In Figure 3.1 (b), for the CV generated SC layer, the potential of the resulting electrodes increased sharply for the first 2.5 hours during conditioning, at a rate of ca. 0.80-0.90 mV/min, and then levelled off during the final 5 hours, with a typical final drift of 3.5-4.5 mV/h (green, —). However, equivalent electrodes prepared using potentiostatically generated PEDOT SC layer showed significantly different behaviour. After a much smaller increase of ca. 15-20 mV during the initial 1.5 hours, the potential levelled off with a typical drift of -0.01 mV/h during the final 5 hours (red, · · ·).

This finding seems in agreement with the spontaneous oxidation of the PEDOT SC layer accompanied by the relative ion fluxes at the SC/membrane and membrane/sample interfaces to maintain the overall electro-neutrality within the electrode layers (see Figure 3.2).

[3.a] BDDA (characterised by a $-(CH_2)_4-$ chain) produced membranes with almost identical behaviour than the ones obtained using HDDA (with a $-(CH_2)_6-$ chain) (results not shown).

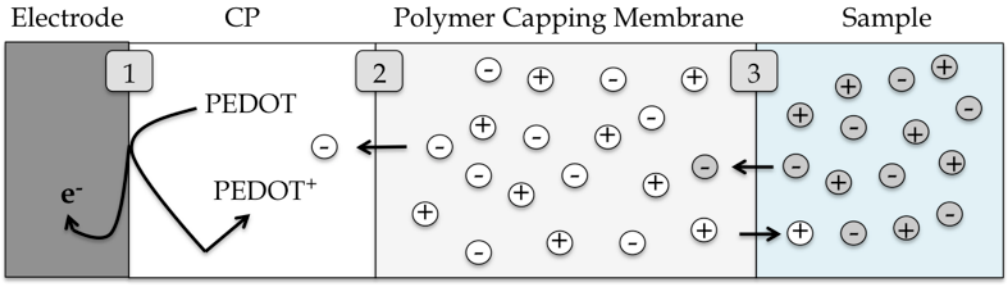

Figure 3. 2: Schematic representation of the ion fluxes at the CP/membrane and membrane/sample interfaces, for a membrane loaded with an IL composed of cations and anions. The ion fluxes are accompanied by the spontaneous oxidation of the PEDOT layer at the CP/electrode interface (1). This charge is compensated by negative ions from the polymer capping membrane exchanging at the CP/membrane interface (2). A similar process happens at the membrane/sample interface (3) through movement of positive ions from the membrane into the boundary layer, or negative ions from the sample into the boundary layer.

Significantly, Michalska and Maksymiuk [27] demonstrated that spontaneous charging/discharging may occur at the SC layer underlying a polymeric ion-selective membrane affecting the response pattern of the sensor. However, it should be also noted that the morphology of the PEDOT layer was significantly different depending on the deposition method, as shown in Figure 3.3 (a) and Figure 3.3 (b). The polymer had web-like structures or a globular film-like appearance when deposited by potentiostatic polarisation or by CV, respectively. In this regard, it is significant that Paczosa-Bator et al. [28] observed that PEDOT films, prepared by dynamic polarisation, doped with triphosphate to bind Mg^{2+} and Ca^{2+}, were smoother and denser that the ones prepared by potentiostatic deposition. In addition, the authors showed that the smoother films resulted in faster potentiometric responses although sensitivities values were similar in both cases. Therefore, further experiments are needed to understand more clearly the impact of the CP redox state on the overall electrode response.

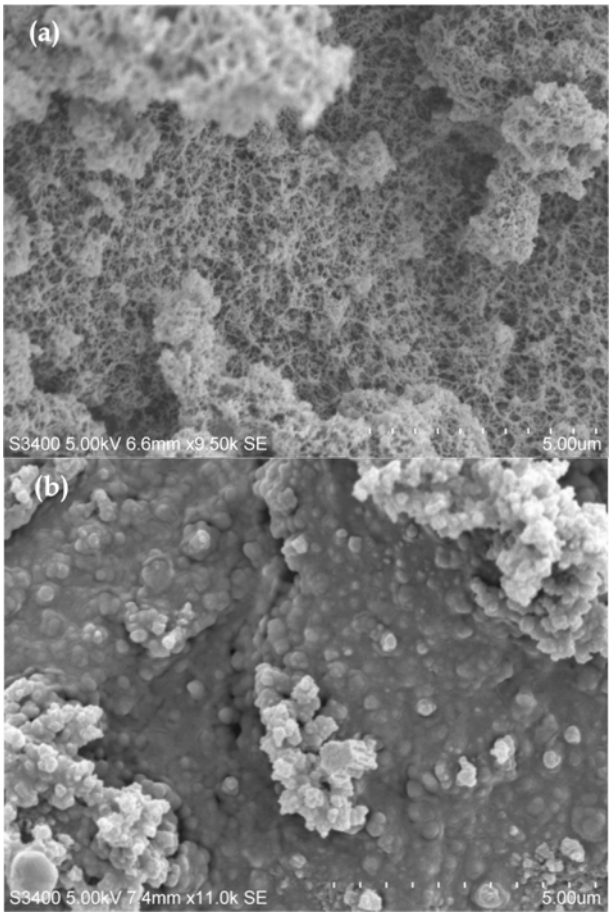

Figure 3. 3: SEM images of PEDOT electrodeposited from [emim][FAP] (a) potentiostatically, at 1.0 V, and (b) by cycling the potential 25 times between 0 and 1.0 V, with scan rate of 50 mV/s.

In order to prepare electrodes with behaviour closer to that of an ideal reference electrode, the above results underline the need to optimise multiple aspects of the device fabrication, such as the media used for the electropolymerisation of the CP and the type of IL present in the membrane. Figure 3.4 demonstrates the effect of the ILs in the membrane formulation when testing electrodes characterised by a potentiostatically grown PEDOT SC-layer. In fact, replacing [emim][FAP] (red, · · ·) with [hmim][FAP] (blue, – –) produced a smaller variation in the potential of the electrodes when these were in contact with different electrolyte solutions. For [hmim][FAP], when NaCl and KCl concentrations were increased from 1 mM to 0.1 M, the electrode potential increased by 5±1 mV and by 15±2 mV (n= 4, excluding the initial 2-3 minutes after swapping solutions), respectively.

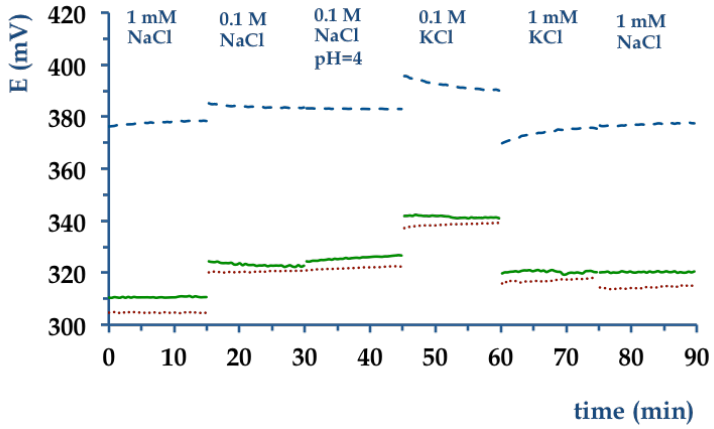

Figure 3. 4: Individual responses of reference electrodes prepared by entrapping (blue, – –) [hmim][FAP], (green, —) [bmim][FAP] or (red, · · ·) [emim][FAP] within a poly(butyl-co-decylmethacrylate) membrane. The solid-contact was a PEDOT layer potentiostatically electrodeposited from [emim][FAP]. The electrode potential was recorded for 15 minutes in each bathing solution.

It is interesting to note that, as shown in Figure AA.3, the choice of IL also impacted on the dynamics of the electrode potential during the conditioning step. During the first 2.5 hours of conditioning, the potential increased in all the three cases, in the order [emim]>[bmim]>[hmim]. Then the potential tended to level off and typical drifts experienced during the last 10 hours of testing were 0.9–1.1 mV/h, 0.2–0.4 mV/h, -(1.5–1.8) mV/h, respectively, for ionogel membranes based on [emim], [bmim] and [hmim]. Thus, it seems that by selecting more hydrophobic IL cations, the initial rise in the potential can be reduced. This observation seems also to be in agreement with Figure 3.2, as the CP layer would be affected to a lesser extent, since bulkier ions will tend to partition less into the aqueous phase and the electrode reaches the "potential at the equilibrium" more rapidly.

Regarding the effect of the CP redox state, it is significant to note that previous reports have highlighted the crucial role of charging/discharging processes of the conducting polymer in correspondence of the limit of detection of SC-ISEs [25]. Less obvious, the media used for the CP electropolymerisation may impact on the doping/de-doping of the CP since this process depends on the anions incorporated in the polymer skeleton backbone [29, 30]. Therefore the polymerisation of EDOT was conducted in [emim][NTf_2] instead than [emim][FAP] and it was found that the electrodeposition proceeded very differently. With [emim][FAP], an orange colour appeared in the IL proximal to the working electrode, while for the equivalent experiment with

[emim][NTf_2], the IL remained transparent. In addition, PEDOT electrodeposited from [emim][NTf_2] by CV resulted in partial coverage of the carbon layer, as shown in the SEM picture in Figure AA.4. Figure AA.5 shows that typically the current and the total charge passed in the oxidative region, and therefore the amount of material deposited, tended to be larger in the CVs recorded in [emim][FAP] than in [emim][NTf_2]. As less material is deposited with [emim][NTf_2], this will lead to thinner layers and may explain the incomplete coverage of the substrate obtained using the same electrochemical deposition technique. Under potentiostically controlled conditions in the same IL, i.e., [emim][NTf_2], a homogenous layer of PEDOT was obtained with cauliflower-like surface nodules, (see Figure AA.6). This different surface topography may arise from the fact that the viscosity and conductivity of [emim][FAP], i.e., 75 cP and 3.6 mS/cm [31], differ significantly from [emim][NTf_2], i.e., 32 cP and 9.1 mS/cm [32]. For instance, the larger viscosity of [emim][FAP] would inhibit monomer diffusion towards the electrode, and therefore the growth of the polymer will be slower in this IL (under diffusion controlled regime) because of the smaller diffusion coefficient, D_i, as given by the Stokes-Einstein equation (see Equation 3.2) [33]:

$$D_i = \frac{k_B T}{6\pi\eta r_i} \qquad (3.2)$$

where k_B, T, η, and r_i are the Boltzmann constant, the absolute temperature, the viscosity of the solution and the radius of the chemical species i, respectively. According to the above equation and the given viscosity values, the diffusion coefficient in [emim][NTf_2] is 2.3 time larger than what would be in [emim][FAP]. In addition, the role of the IL anion acting as a template during the polymerisation cannot be excluded as origin of the morphological difference of the PEDOT layers obtained from the two ILs. For instance, Ahmad et al. [34, 35] showed that 1-ethyl-3-methylimidazolium bis(perfluoroethylsulfonyl)imide assisted the growth of PEDOT in a fibre-type form.

Figure 3.5 (a) and Figure 3.5 (b) show results of immersion tests. They describe the behaviour of electrodes characterised by a PEDOT SC layer (potentiostatically deposited from a [emim][NTf_2] solution) and capping membranes based on [bmim][FAP] and [hmim][FAP], after conditioning in aqueous 10 mM NaCl overnight or for 2 hours, respectively.

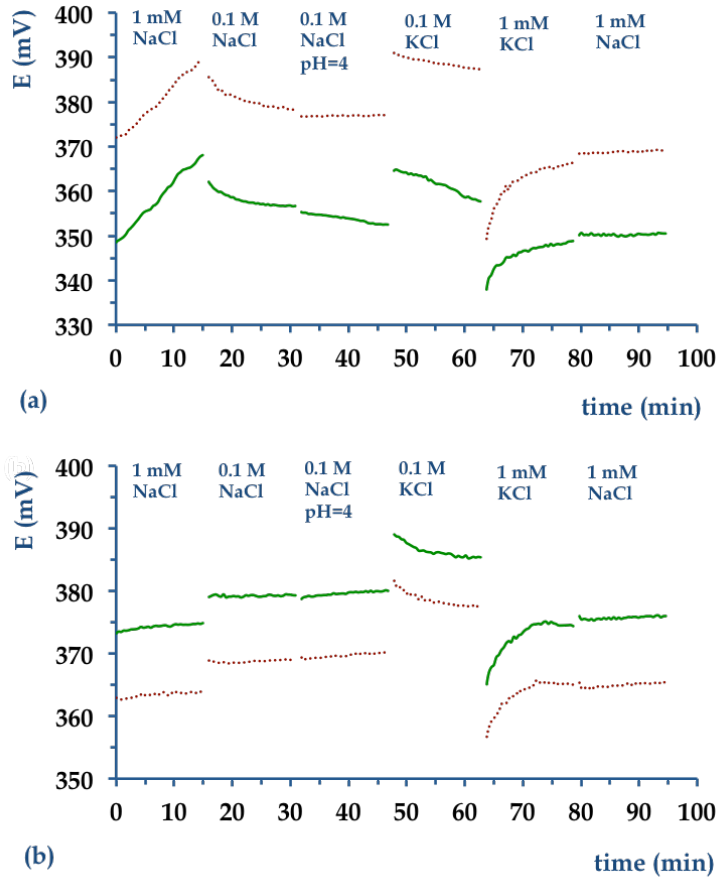

Figure 3. 5: Individual responses of reference electrodes prepared by entrapping (green, —) [hmim][FAP] and (red, · · ·) [bmim][FAP] within a poly(butyl-co-decylmethacrylate) membrane. The solid-contact was a PEDOT layer potentiostatically electrodeposited from [emim][NTf_2]. The electrode potential was recorded for 15 minutes in each bathing solution after (a) overnight and (b) 2 hours conditioning in aqueous 10 mM NaCl.

Figure AA.7 presents the potential profile during the conditioning step and it is interesting to note that for the longer conditioning the electrode potential drifted during the last 10 hours by -(1.0–2.0) mV/h and -(3.0–6.0) mV/h, respectively, for membranes containing [bmim][FAP] and [hmim][FAP]. These values are larger than those observed with electrodes that had the same capping membrane but had the PEDOT SC layer potentiostatically deposited from [emim][FAP], i.e., -(0.2–0.4) mV/h and -(1.5–1.8) mV/h, respectively. More important, the electrodes in Figure 3.5 (a), which were conditioned overnight, showed a steadily increasing response upon initial contact with 1 mM NaCl solution. When the conditioning step was stopped after 2 hours, i.e., at a plateau in the potential response curve and before the start of the drift, for both ionogels, the electrodes showed more stable responses (see Figure 3.5 (b)). When the concentration was increased from 1 mM to 0.1 M, for NaCl and KCl, the

potential increased by 5.5±1.0 mV and 10.5±1.3 mV for [hmim][FAP] and by 4.5±0.6 mV and 14.2±0.3 mV for [bmim][FAP] (n=4, excluding the initial 3-5 minutes after contacting the test solution). Overall, the best performing capping membranes were based on a 9:1 (molar ratio) butylacrylate/decyl-methacrylate mixture containing 0.8% DMPA, 3% HDDA and 6% [hmim][FAP]. Regarding the SC layer, PEDOT films were potentiostatically grown from [emim][FAP] or [emim][NTf_2], and electrodes conditioned overnight or for 2 hours, respectively.

If minimising the offset of the electrode potential in response to sample solutions having different composition is obviously important, at the same time, assuring high batch reproducibility is another key requirement to deliver low-cost reference electrodes. These electrodes should present an inter-electrode offset ideally in the order of few mV at most. This opens the possibility that individual calibration may not be needed, but rather the whole batch can be calibrated by averaging the offset (against a standard reference electrode) of a statistically significant sub-population of the entire batch. It is arguable that batch reproducibility is one of the major limitations affecting this new class of reference electrodes based on ionogels.

Figure 3.6 presents a comparison of 4 electrodes prepared according to the optimised procedure described above. All the electrodes have the same capping membrane (based on a molar ratio 9:1 butylacrylate/decyl-methacrylate mixture containing 0.8% DMPA, 3% HDDA and 6% [hmim][FAP]), the same SC layer (PEDOT film potentiostatically deposited from [emim][NTf_2]) and they were conditioned for 2 hours prior to evaluation. Electrodes based on the PEDOT solid-contact layers, respectively aged for one week and for 6 weeks after its electrodeposition prior depositing the capping membrane, were compared. These results suggest that electrodes belonging to the same batch have very similar trends (within ±5 mV) when tested with solutions of different compositions. More significantly, Figure 3.6 seems to highlight that PEDOT ageing (and perhaps its de-doping) impacts on the offset of the electrodes, but not the electrode-to-electrode behaviour. In other words, although there may be a drift in the offset over time, this may be relatively reproducible between electrodes, and the calibration of one electrode may be used to characterise other electrodes that have been stored in the same manner. However, a larger population study is required to confirm these results and understand the processes underlying this behaviour.

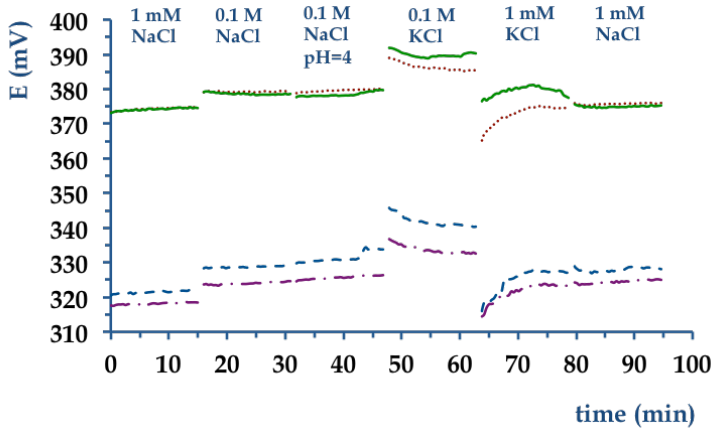

Figure 3. 6: Individual responses of reference electrodes prepared by entrapping [hmim][FAP] within a poly(butyl-co-decylmethacrylate) membrane polymerised in situ. The solid-contact was a PEDOT layer potentiostatically electrodeposited from [emim][NTf_2] which was aged for 1 week (green, —) (red, · · ·) and for 6 weeks (blue, – –) (purple, – · –). The electrode potential was recorded for 15 minutes in each bathing solution.

The best performing SCI-REs were further assessed to evaluate their potential stability in real saliva samples while changing the pH of the sample by adding drop-wise 0.1 M HCl. Figure 3.7 (a) shows that the potential of the SCI-RE was quite stable, i.e., average and standard deviation equal to 273.4 and 4.2 mV, respectively, while the pH of the saliva sample was changed from 7 to 4.1. In addition, the SCI-REs were also assessed as reference electrodes during a potentiometric calibration, using Na^+ SC-ISEs fabricated in-house. Figure 3.7 (b) compares the calibration curves of three different Na^+ SC-ISEs obtained using the optimised SCI-RE, and a conventional double liquid-junction Ag/AgCl. From these calibration curves, the slope was found to be 56.9 mV/loga_{Na^+} and 56.7 mV/loga_{Na^+}, respectively. The small difference in the two slope values means that the two calibration curves overlap almost perfectly when the offset (due to the gap in the potential between the Ag/AgCl and SCI-RE electrodes, ca. 408 mV) is zeroed. These results showed that the combination of a Na^+ SC-ISE and a SCI-RE on the same screen-printed substrate could be used to realise low-cost, disposable potentiometric strips.

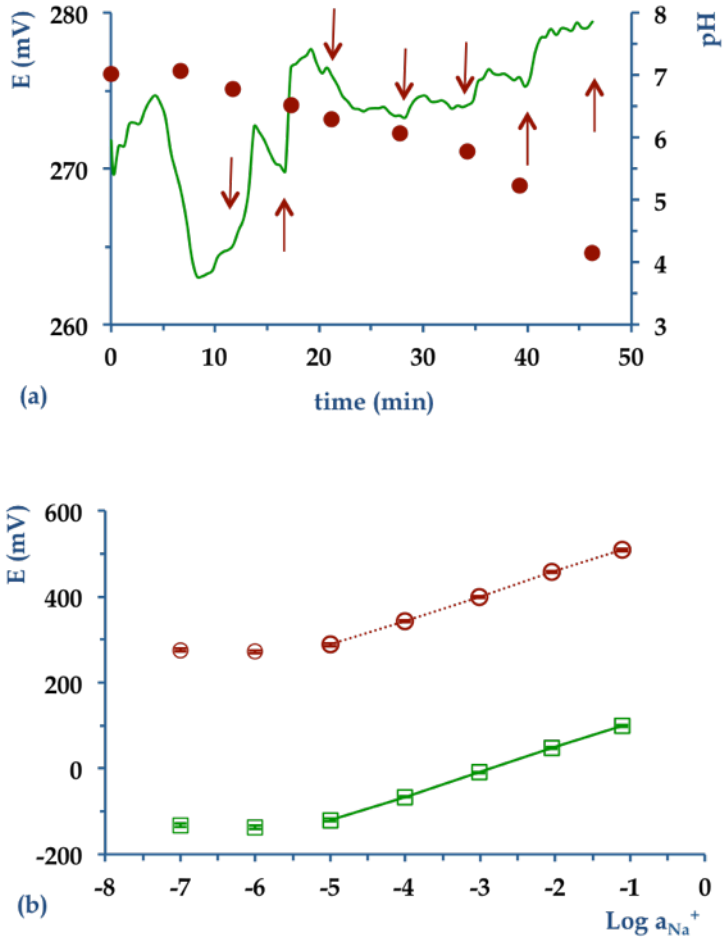

Figure 3. 7: (a) (green, —) Trend of the potential of a SCI-RE against an Ag/AgCl reference electrode while contacting a real saliva sample. The pH of the saliva sample was changed by adding (drop-wise) 0.1 M HCl. (●) Measurements of the pH of a saliva sample (as determined using a pH-meter) after 1 minute stabilisation, following the addition of an aliquot of 0.1 M HCl at the times indicated by the arrows. (b) Average of calibration curves for three Na^+ SC-ISEs against (red, ○) a double liquid-junction Ag/AgCl reference electrode and (green, □) the optimised SCI-RE. Error bars indicate the standard deviation for n=3 electrodes. In both figures the capping membrane was loaded with [hmim][FAP] while the PEDOT SC layer was potentiostatically deposited from (a) [emim] [FAP] or (b) [emim][NTf_2].

The two electrodes have a common SC layer, which is convenient for mass-production since this design offers flexibility in terms of electrode size and form factor. The only difference lies in the final capping membrane. This configuration opens up new potential applications for which glass bodied electrodes or large conventional designs are unsuitable. For example, the use of these for on-body sweat sensing using patch-type configurations will be presented in a future communication.

3.4 Conclusions

This work describes the preparation of disposable reference electrodes based on a PEDOT solid-contact layer and an ionogel capping membrane realised by incorporating ILs within polyacrylate polymerised in situ. The potential of this novel reference electrode monitored against a commercial Ag/AgCl while contacting a real saliva sample seems stable over short times and to pH changes induced by addition of an acid solution. In addition, the reference electrode was employed in combination with Na^+ SC-ISEs for potentiometric calibrations in solutions of increasing sodium concentration. The resulting calibration curves obtained using this novel reference electrode overlap with those obtained using a commercial double-junction Ag/AgCl reference electrode once the offset between the two is zeroed. Future research will address the integration of these electrodes in wearable potentiometric strips for the analysis of accessible body fluids.

3.5 References

[1] A. Michalska, All solid‐state ion selective and all solid‐state reference electrodes, Electroanalysis, 24(2012) 1253-65.

[2] C. Zuliani, D. Diamond, Opportunities and challenges of using ion-selective electrodes in environmental monitoring and wearable sensors, Electrochimica Acta, 84(2012) 29-34.

[3] U. Guth, F. Gerlach, M. Decker, W. Oelßner, W. Vonau, Solid-state reference electrodes for potentiometric sensors, Journal of Solid State Electrochemistry, 13(2009) 27-39.

[4] T. Zhang, C.-Z. Lai, M.A. Fierke, A. Stein, P. Bühlmann, Advantages and limitations of reference electrodes with an ionic liquid junction and three-dimensionally ordered macroporous carbon as solid contact, Analytical Chemistry, 84(2012) 7771-8.

[5] Z. Mousavi, K. Granholm, T. Sokalski, A. Lewenstam, An analytical quality solid-state composite reference electrode, Analyst, 138(2013) 5216-20.

[6] R.E. Dohner, D. Wegmann, W.E. Morf, W. Simon, Reference electrode with free-flowing free-diffusion liquid junction, Analytical Chemistry, 58(1986) 2585-9.

[7] Y. Mi, S. Mathison, E. Bakker, Polyion sensors as liquid junction‐free reference electrodes, Electrochemical and Solid-State Letters, 2(1999) 198-200.

[8] R. Mamińska, A. Dybko, W. Wróblewski, All-solid-state miniaturised planar reference electrodes based on ionic liquids, Sensors and Actuators B: Chemical, 115(2006) 552-7.

[9] T. Kakiuchi, T. Yoshimatsu, N. Nishi, New class of Ag/AgCl electrodes based on hydrophobic ionic liquid saturated with AgCl, Analytical Chemistry, 79(2007) 7187-91.

[10] D. Cicmil, S. Anastasova, A. Kavanagh, D. Diamond, U. Mattinen, J. Bobacka, et al., Ionic Liquid‐Based, Liquid‐junction‐free reference electrode, Electroanalysis, 23(2011) 1881-90.

[11] U. Mattinen, J. Bobacka, A. Lewenstam, Solid‐contact reference electrodes based on lipophilic salts, Electroanalysis, 21(2009) 1955-60.

[12] S. Anastasova, A. Radu, G. Matzeu, C. Zuliani, U. Mattinen, J. Bobacka, et al., Disposable solid-contact ion-selective electrodes for environmental monitoring of lead with ppb limit-of-detection, Electrochimica Acta, 73(2012) 93-7.

[13] C. Zuliani, G. Matzeu, D. Diamond, A potentiometric disposable sensor strip for measuring pH in saliva, Electrochimica Acta, 132(2014) 292-6.

[14] B. Schazmann, D. Morris, C. Slater, S. Beirne, C. Fay, R. Reuveny, et al., A wearable electrochemical sensor for the real-time measurement of sweat sodium concentration, Analytical Methods, 2(2010) 342-8.

[15] Y. Qin, S. Peper, E. Bakker, Plasticizer-free polymer membrane ion-selective electrodes containing a methacrylic copolymer matrix, Electroanalysis, 14(2002) 1375-81.

[16] G. Lisak, E. Grygolowicz-Pawlak, M. Mazurkiewicz, E. Malinowska, T. Sokalski, J. Bobacka, et al., New polyacrylate-based lead (II) ion-selective electrodes, Microchimica Acta, 164(2009) 293-7.

[17] J.-P. Veder, R. De Marco, G. Clarke, R. Chester, A. Nelson, K. Prince, et al., Elimination of undesirable water layers in solid-contact polymeric ion-selective electrodes, Analytical Chemistry, 80(2008) 6731-40.

[18] T. Lindfors, L. Hŏfler, G. Jágerszki, R.E. Gyurcsányi, Hyphenated FT-IR-attenuated total reflection and electrochemical impedance spectroscopy technique to study the water uptake and potential stability of polymeric solid-contact ion-selective electrodes, Analytical Chemistry, 83(2011) 4902-8.

[19] E. Lindner, R.E. Gyurcsányi, Quality control criteria for solid-contact, solvent polymeric membrane ion-selective electrodes, Journal of Solid State Electrochemistry, 13(2009) 51-68.

[20] S. Katsuta, K.-i. Nakamura, Y. Kudo, Y. Takeda, Mechanisms and rules of anion partition into ionic liquids: phenolate ions in ionic liquid/water biphasic systems, The Journal of Physical Chemistry B, 116(2011) 852-9.

[21] M.G. Freire, C.M. Neves, P.J. Carvalho, R.L. Gardas, A.M. Fernandes, I.M. Marrucho, et al., Mutual solubilities of water and hydrophobic ionic liquids, The Journal of Physical Chemistry B, 111(2007) 13082-9.

[22] A. Marciniak, The solubility parameters of ionic liquids, International Journal of Molecular Sciences, 11(2010) 1973-90.

[23] J. Ranke, A. Othman, P. Fan, A. Müller, Explaining ionic liquid water solubility in terms of cation and anion hydrophobicity, International Journal of Molecular Sciences, 10(2009) 1271-89.

[24] R. Gourishetty, A.M. Crabtree, W.M. Sanderson, R.D. Johnson, Anion-selective electrodes based on ionic liquid membranes: effect of ionic liquid anion on observed response, Analytical and Bioanalytical Chemistry, 400(2011) 3025-33.

[25] N. Abramova, A. Bratov, Photocurable polymers for ion selective field effect transistors. 20 years of applications, Sensors, 9(2009) 7097-110.

[26] J. Bobacka, A. Lewenstam, A. Ivaska, Electrochemical impedance spectroscopy of oxidized poly (3, 4-ethylenedioxythiophene) film electrodes in aqueous solutions, Journal of Electroanalytical Chemistry, 489(2000) 17-27.

[27] A. Michalska, K. Maksymiuk, The influence of spontaneous charging/discharging of conducting polymer ion-to-electron transducer on potentiometric responses of all-solid-state calcium-selective electrodes, Journal of Electroanalytical Chemistry, 576(2005) 339-52.

[28] B. Paczosa-Bator, J. Peltonen, J. Bobacka, A. Lewenstam, Influence of morphology and topography on potentiometric response of magnesium and calcium sensitive PEDOT films doped with adenosine triphosphate (ATP), Analytica Chimica Acta, 555(2006) 118-27.

[29] T.F. Otero, J. Arias-Pardilla, Electrochemical devices: artificial muscels, in: A.K. S. Cosnier (Ed.) Electropolymerization, Wiley2011, pp. 241-5.

[30] G.G. Wallace, G.M. Spinks, L.A.P. Kane-Maguire, Assembly of polypyrroles, Conductive Electroactive Polymers: Intelligent Polymer Systems, CRC Press2009, pp. 59-101.

[31] Merck: Ionic Liquids Brochure. Product Information, Accessed on: 05 May 2015

[32] Y. Pan, L.E. Boyd, J.F. Kruplak, W.E. Cleland, J.S. Wilkes, C.L. Hussey, Physical and transport properties of bis (trifluoromethylsulfonyl) imide-based room-temperature ionic liquids: application to the diffusion of tris (2, 2′-bipyridyl) ruthenium (II), Journal of The Electrochemical Society, 158(2011) F1-F9.

[33] J. Koryta, J. Dvořák, L. Kavan, Transport processes in electrolyte systems, Principles of Electrochemistry, Wiley1993, p. 122.

[34] S. Ahmad, M. Deepa, S. Singh, Electrochemical synthesis and surface characterization of poly (3, 4-ethylenedioxythiophene) films grown in an ionic liquid, Langmuir, 23(2007) 11430-3.

[35] S. Ahmad, T. Carstens, R. Berger, H.-J. Butt, F. Endres, Surface polymerization of (3, 4-ethylenedioxythiophene) probed by in situ scanning tunneling microscopy on Au (111) in ionic liquids, Nanoscale, 3(2011) 251-7.

Chapter 4.

A Potentiometric Disposable Sensor Strip for Measuring pH in Saliva

Claudio Zuliani*[a]• and **Giusy Matzeu**[b]•, Dermot Diamond*[b]

URL: http://www.sciencedirect.com/science/article/pii/S0013468614006537

ISSN and DOI: 10.1016/j.electacta.2014.03.140

Electrochimica Acta 132 (2014): 292-296.

•Authors contributed equally to this work

*Corresponding author

[a]Clarity Centre for Sensor Web Technologies, National Centre for Sensor Research, Dublin City University, Dublin 9, Ireland

[b]Insight Centre for Data Analytics, Dublin City University, Dublin 9, Ireland.

Aims and Objectives

Chapter 4 was focused on the optimisation of screen printing protocols to realise sensitive substrates. The design, realisation and optimisation of novel potentiometric strips was first carried out on the bench followed by testing pH variations in saliva.

Contributions

- Design, conception and optimisation of experimental trials.
- Analysis of data and writing up of the manuscript.

Abstract

In this paper, the preparation of a potentiometric strip for pH monitoring in saliva samples is reported. The potentiometric strip consists of a solid-contact pH Ion-Selective Electrode and of a solid-contact ionogel reference electrode prepared on a dual screen-printed substrate. The screen printing protocols, i.e., type of inks and number of deposits, were adjusted to relatively improve the batch reproducibility and the stability of the pH sensor.The pH of real saliva samples was monitored using the optimised potentiometric strip, and results were validated through parallel measurements with a standard laboratory method.

Keywords

Screen Printing, pH Sensor, Reference Electrode, Ionic Liquid, Saliva.

4.1 Introduction

Ion-Selective electrodes (ISEs) have been widely applied to detect many ions in blood [1-3] and saliva [4-8] samples. The ISEs may have a great potential for a wide range of analytical applications, particularly when produced in a solid state form since this can drive down the unit cost. This peculiarity could also enable the sensors to be produced in a variety of form factors which in turn can open new application concepts, such as wearable sensors for real-time monitoring of physiological fluids like sweat or saliva [9]. Solid-contact Ion-Selective electrodes (SC-ISEs) have attracted great attention since the internal reference electrode and the inner filling solution are replaced by a solid material [10]. However, in spite of extensive research in the area, it seems that obtaining SC-ISEs with reproducible standard potentials is still a significant challenge [10] and much research is still focused on the use of standard macroelectrodes rather than low-cost solid state electrodes.

In order to accomplish the potentiometric measurement, a reference electrode compatible with mass production, e.g. planar-type design, screen printing technologies, solid state functional components, is required. The most challenging applications are those that require continuous use over longer periods of time [9, 11, 12]. For instance, Rius-Ruiz et al. [12] developed a potentiometric strip to monitor the potassium content in samples of saliva and soft drinks diluted with buffers. Accessible body fluids such as saliva represent an interesting medium for the realisation of body-sensing, as these fluids also contain important personal physiological information [13-20]. Continuous monitoring of pH in saliva would be extremely beneficial for maintaining healthy mouth conditions, e.g., degradation of tooth enamel [21] and detection of Gastroesophageal Reflux Disease (GERD) [22-24], as well as drug activity, as in some cases this can depend on the pH characterising saliva [17].

In this manuscript, we report on the preparation of a potentiometric strip based on a planar screen-printed substrate for the direct measurement of pH in saliva samples. The strip contains two electrodes, one sensitive to pH and the other one operating as a reference electrode. pH measurements of saliva samples were validated using a commercial glass electrode.

4.2 Experimental

4.2.1 Materials

Silver ink and C10903P14 as carbon ink, both obtained from Gwent Electronic Materials (Pontypool, UK), and Acheson Electrodag 452 SS from Henkel (Irvine, CA, USA) as dielectric were used for the preparation of screen-printed electrodes. C2030519P4 and D50706D2 from Gwent Electronic Materials were used respectively as carbon and dielectric inks in the preparation of silver-free screen-printed electrodes. 175 μm thick PET sheets were obtained from HiFi (Dublin, Ireland) or from MacDermid (Oxon, UK) and they were used without further treatment. Potassium and sodium chloride, 3,4-ethylenedioxythiophene (EDOT, 97%), poly(3-octylthiophene-2,5-diyl) regiorandum (POT), high molecular weight poly(vinyl chloride) (PVC), bis(2-ethylhexyl) sebacate (DOS, ≥97%), tetrahydrofuran (THF, ≥99.5%), 2-nitrophenyl octyl ether (o-NPOE, >99%), 4-nonadecylpyridine selectophore (hydrogen ionophore II), potassium tetrakis(4-chlorophenyl)borate (KTFPB), citric acid, sodium phosphate dibasic, boric acid, nitric acid and standard buffers (pH 4, 5, 6, 7, 8), 2,2-dimethoxy-2-phenylacetophenone (DMPA, >99%), butyl-acrylate (>99%) and 1,6-hexanediol diacrylate (HDDA, 80%) were purchased from Sigma-Aldrich (Dublin, Ireland). When possible, they were of selectophore grade or trace metal standard. N-decyl-methacrylate was obtained from Polysciences (Northampton, UK), chloroform (>99%) and ethanol (EtOH) from Fisher Scientific (Dublin, Ireland). 1-ethyl-3-methylimidazolium [emim] bis(trifluoromethylsulfonyl)imide [NTf_2], and [emim] tris(pentafluoroethyl)trifluorophosphate [FAP] were obtained from VWR (Dublin, Ireland). All chemicals were used as received. 0.8 mm thick adhesive poly foam strips for the preparation of gaskets were from Radionics (Dublin, Ireland). Deionised water with resistivity of 18.2 MΩ cm was obtained with a Milli-Q reagent-grade water system and it was used for making aqueous solutions. The pH of deionised water was ~6.5, measured with a commercial pH electrode.

4.2.2 Methods and Procedures

All screen-printed electrodes (SPEs), with and without silver tracks, were realised using a DEK 248 printer (Weymouth, UK). Single SPEs consisted of a carbon disk having a geometric area of ~ 0.062±0.002 cm^2. For the silver-free SPEs, two layers of the D50706D2 dielectric ink were formed at the speed of 10 cm/s, which represented a good compromise between the quality of the insulation, time and materials used for an additional print. The C2030519P4 carbon ink was printed at 30 cm/s. The squeegee "pressure" value was adjusted to 14 and 10 kg, respectively, for the printing of

D50706D2 and C2030519P4, and the table/screen separation was the closest achievable with the instrument, i.e., ~1-2 mm. Each printed layer was annealed according to the supplier specifications, i.e., silver ink: 5 minutes at 120°C; C10903P14: 15 minutes at 120°C; C2030519P4: 12 minutes at 80°C; D50706D2: 30 minutes at 80°C. In case of multiple prints with the same ink, curing was repeated in between the printing of individual layers. Silver-free dual electrodes were printed according to the procedure followed for the single silver-free screen-printed substrates, where the main differences were the design and the individual geometrical area, i.e., ~ 0.045±0.002 cm^2.

The pH sensitive membrane was prepared as previously reported [25], drop casting a total amount of 24.5 µL of capping membrane according to the following sequence: 1µL, 1.5 µL, 8 additions of 2 µL, 2 additions of 3 µL. In order to improve reproducibility, a new design was developed. The pH ISEs, poly(methyl methacrylate) (PMMA) (125 or 500 µm thick) and pressure-sensitive adhesive (PSA) films (50 µm thick) were cut by means of a CO_2 Laser Micro-machining Light Deck (Optec, Belgium) and laminated onto the SPEs by a thermal roller laminator Titan-110 (GBC Films, USA). By combining the PSA film with the 125 µm and 500 µm PMMA layer, two gaskets with a 2.4 mm diameter and a nominal depth of 175 and 550 µm were prepared. 5.25 µL of a 2.75 mg/mL solution of POT in chloroform (stirred overnight) were drop-cast on top of the carbon layer within the gasket. With the thinner gasket, a total of 8 µL of membrane cocktail solution was drop-cast (two additions of 1 µL and 3 additions of 2 µL), while for the thicker gasket the total amount was 22 µL (1 µL once, 9 additions of 2 µL and 3 µL, once).

The ISEs were conditioned overnight in a solution that was 1 mM each in boric acid, citric acid and sodium phosphate dibasic. The buffer solutions used for the pH sensors calibration were standard buffers (pH 4, 5, 6, 7, 8) or they were made with an opportune amount of citric acid and disodium phosphate, in order to adjust the pH to the desired values during the simulation of saliva. In the last case, the buffer solutions contained 10 mM NaCl and 20 mM KCl as a constant electrolyte background to mimic saliva composition. The Solid-Contact Ionogel Reference Electrodes (SCI-REs) were prepared as reported elsewhere [26], using the silver-free screen-printed substrates. In summary, the solid-contact was a PEDOT layer electrochemically grown on the carbon electrodes from a 0.05 M EDOT solution in [emim][FAP] while the membrane was obtained by entrapping [hmim][FAP] in a poly(butyl-co-decylmethacrylate) phase.

4.2.3 Instrumentation and Software

The potentiometric measurements were recorded using the EMF-16 voltmeter from Lawson Labs, USA. In-house made silver/silver chloride (saturated KCl) or calomel (IJcambria, UK) electrodes were used as references. A CHI600 or 760D potentiostat (CH Instruments, USA) was used to electrodeposit PEDOT. A pH meter (SympHony SP70P) from VWR was used to validate pH measurements of sublingual saliva samples, which were collected using a sterile pipette from volunteers. Photo-polymerisation of the acrylate monomers was obtained using the CL-1000 ultraviolet cross-linker UVP. Thickness and profilometer measurements were recorded using a Dektak 150 Profilometer from Veeco (USA). All the Scanning Electron Microscopy (SEM) images were captured with the Hitachi S3000N in the secondary electron mode.

4.3 Results and Discussion

pH sensors were initially prepared using screen-printed substrates in which a layer of silver ink was deposited between a PET substrate and a carbon upper layer. ISEs with a solid-contact formed by PEDOT electrodeposited from aqueous KCl (Figure AB.1), [emim][NTf_2] or [emim][FAP] (not shown) gave very irreproducible results. POT was preferred as the solid-contact layer for further studies because of the superior reproducibility of the resulting pH sensors. Table 4.1 presents the calibration slopes and offsets obtained with the pH ISEs fabricated using several types of screen-printed substrates. For all the sensors in this table, POT was used as solid-contact layer.

Table 4. 1: Calibration data of pH ISEs prepared using different screen printing protocols. The average slope and offset are reported together with their standard error and % change. The number of sensors for each batch is also specified. Day 0 refers to the electrodes being calibrated after the standard conditioning step. In between the re-calibrations, the sensors were stored in the conditioning solution for a number of days indicated in the table, except in the case labelled as (*) in which the electrodes were kept dry for additional 14 days before the measurement.

Configuration	Calibration (day)	Slope (mV/pH)	Offset (mV)	% Slope Change	% Offset Change
Ag/Carbon/POT	0 (n=4)	-51.9±0.4	519.6±1.0	/	/
Ag/Carbon/POT	4 (n=3)	-54.4±0.6	537.9±12.2	4.8	3.5
Carbon/POT/G22	0 (n=4)	-53.4±0.3	524.0±2.0	/	/
Carbon/POT/G22	6 (n=3)	-55.8±1.1	565.0±7.7	4.5	7.8
Carbon/POT/G22*	19 (n=3)	-55.6±2.4	544.6±10.7	-0.4	-3.6
Carbon/POT/G22	0 (n=4)	-53.5±0.6	537.5±5.3	/	/

When calibrated initially (day 0), pH ISEs prepared from screen-printed substrates containing a silver layer showed a sub-Nerstian slope (slope is 51.9±0.4 mV, n=4) over the range pH 3-8 (see Figure 4.1 (a)). Their response deteriorated when the electrodes were left in the conditioning solution for 3 days (see Figure 4.1 (b)). A decrease in linearity was observed (R^2 decreases to ≤0.96) and also the reproducibility within this batch worsened, as suggested by the larger standard errors for the average values of slope and offset. Under alkaline conditions, a loss of selectivity of the ion-sensitive membrane is apparent, with the sensor response becoming increasingly governed by other ions in the solutions (in accordance with the Nicolsky-Eisenman equation). It is perhaps important to note that the silver track changed its colour to a darker hue (see Figure AB.2) when the sensors were stored in the buffer solution for 3 days. It may also indicate that some oxidation [27] may be happening.

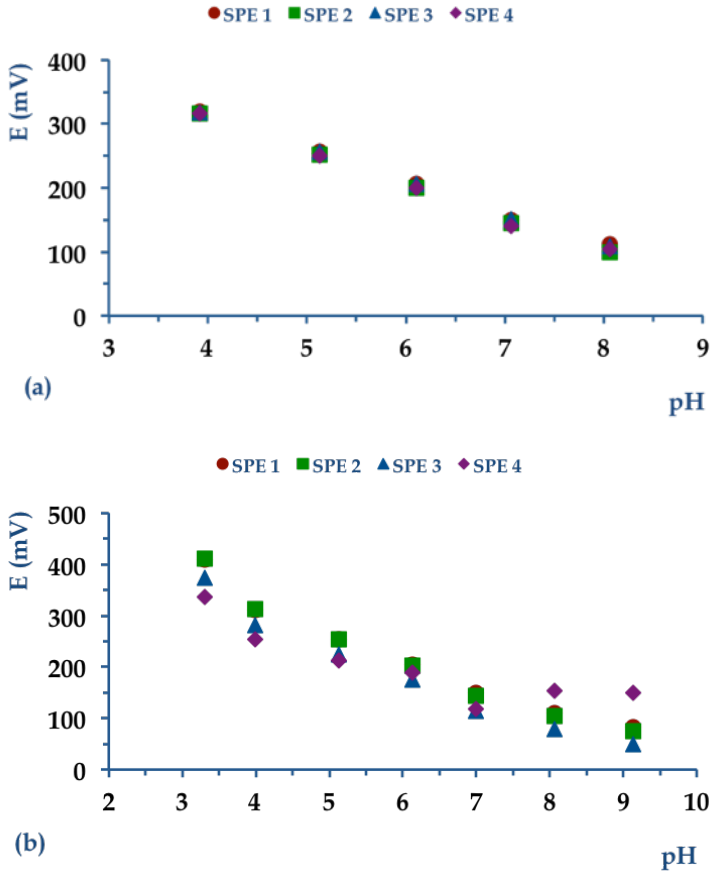

Figure 4. 1: (a) 1st day and (b) 3rd day calibration curves of four pH sensors based on screen-printed electrodes containing a silver layer as contact pad. The electrodes were left in the conditioning solution in between measurements. Data points labels: (●) SPE1, (■) SPE2, (▲) SPE3, and (♦) SPE4.

To avoid any concern, pH sensors were prepared from screen-printed substrates fabricated using a heat curable dielectric and without silver ink. Regarding the preparation of carbon screen-printed electrodes, it should be noted that the height profile of carbon layers formed by 1 carbon print was more uniform (i.e. in terms of average roughness) than those formed by 2 carbon prints characterised by an average roughness of ±5 and ±7 µm, respectively (see Figure AB.3). In addition, the single print film was thinner, with an average thickness of 11.3±0.5 µm, lower than 21.5±1.8 µm recorded for the double print carbon layer. In both cases, SEM images of the carbon prints were similar (see Figure AB.4).

The use of a gasket was found to be beneficial in terms of confining the drop-cast area, both for capping membrane and POT deposition, thus generating layers with more reproducible thicknesses and reproducibility of the sensor response characteristics.

Gaskets of two heights were tested in order to allow drop casting of different amounts of pH sensitive capping PVC membrane, i.e. 8 µL (G8) and 22 µL (G22). The use of G8 gaskets tended to give irreproducible results, which are not discussed further. Table 4.1 shows that sensors prepared using the G22 gasket, one carbon layer and the heat curable dielectric enable good batch reproducibility persisting after 5 days (storing the ISEs in the conditioning solution) or after 14 days (dry storage), with little variations in the slope and offset obtained after calibration. Thus, the pH sensors in the following section were prepared using this optimised configuration.

The pH ISEs were combined with disposable ionogel based liquid-junction-free reference electrodes. These electrodes do not exhibit appreciable changes in potential over the pH range 4-7, and are quite insensitive to potassium and sodium. When the concentrations of K^+ and Na^+ change over two orders of magnitude, i.e., from 1 mM to 0.1 M, the potential of these solid-contact reference electrodes increased by ca. 4-6 mV and 10-15 mV, respectively, against a commercial double-junction reference electrode [26]. In saliva, sodium and potassium levels significantly depend on the area and sampling method, but their concentrations range are always within 1-98 mM and 10-80 mM, respectively [28]. Since the average sodium and potassium concentrations in whole unstimulated saliva are 8±3 mM and 21±4 mM, respectively, the solutions for the pH ISEs calibration were made with similar content of Na^+ and K^+, in order to mimic the saliva composition.

Figure 4.2 shows a typical calibration curve obtained with the pH and Solid-Contact Ionogel Reference Electrode (SCI-REs) combined in a potentiometric strip. The device response was linear over the pH range required for saliva analysis, i.e., ca. 5.0 to 7.5. The values of potential obtained with the same strip for 4 saliva samples are also plotted. Table 4.2 reports other tests done on multiple saliva samples with a batch of 4 potentiometric strips, and the corresponding values found by the pH-meter. The average relative differences between the values recorded using the potentiometric strips and a pH-meter was 0.2±0.2 (n=13).

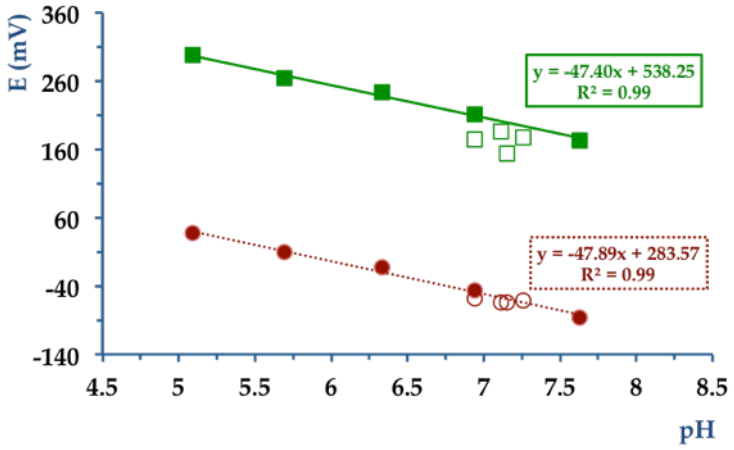

Figure 4. 2: Calibration curve for a pH electrode obtained by plotting its potential bias against (red, · · ·) the SCI-RE or (green, —) against the Ag/AgCl electrode. The potential values obtained with the pH electrode in contact with the calibration solutions and with the saliva samples are reported against the SCI-RE (○) and (●), or against the Ag/AgCl electrode (□) and (■).

Table 4. 2: pH data of saliva samples measured with a commercial glass electrode and the optimised potentiometric strips. 2 saliva samples were at least tested with each platform. In case of 1-point calibration, the potentiometric strips were stored dried for 5 hours and then re-conditioned in a buffer at pH=5.7, with a background of 10 mM of NaCl and 20 mM of KCl, for 40 minutes, before testing the samples.

5-point calibration pH sensor % deviation			**1-point calibration pH sensor % deviation**		
pH	**pH sensor**	**ΔpH**	**pH meter**	**pH sensor**	**ΔpH**
7.1	7.3	-0.2	7.0	7.3	-0.3
7.3	7.2	0.1	7.1	7.4	-0.3
7.2	7.3	-0.1	6.9	6.8	0.1
6.9	7.1	-0.2	7.1	7.2	-0.1
7.1	7.3	-0.2	6.9	6.9	0.0
7.2	7.7	-0.5			
6.9	7.4	-0.5			
7.3	7.8	-0.5			

It is important to note that the signal of the potentiometric strip placed in contact with the saliva sample became stable after 2 minutes, showing an average drift of -0.34

mV/min ±0.08 (standard error, n=17) over the remaining measuring time, i.e., 10-15 minutes. Figure 4.2 also demonstrates that once the saliva was in contact with the potentiometric strip, both the pH and the SC-RE electrodes were affected to a similar extent. Figure 4.2 indeed compares the values of potentials obtained with the pH ISE against the SCI-RE and against an Ag/AgCl reference electrode. These tests were carried out in the calibration solutions and saliva samples. There was no significant difference in the calibration slopes, as expected, and the difference in the offset values depended on the bias between the two reference electrodes. More significantly, it is apparent that the accuracy in measuring the pH in saliva samples was greater when the potentials of the pH electrodes were measured against the SCI-RE rather than the Ag/AgCl RE. This might occur because the potential of both electrodes in the potentiometric strip decreased to a similar extent during the first minute of immersion, and therefore self-compensated the potential drop. A possible explanation of the above behaviour is that the adsorption of saliva components on the two polymer membranes is similar, while it differs for the Vycor® tip employed for the Ag/AgCl electrode.

A common limitation of solid-contact ISEs is the need to re-condition the electrodes after a period of dry-storage. Although this period cannot be universally defined and it is often omitted or not reported in the literature [29], commercial solid-contact ISEs recommend re-conditioning of at least 1 hour before commencing the measurement [30]. Indeed, Table 4.2 shows the pH values of saliva samples obtained with two potentiometric strips, which were re-conditioned for 40 minutes in a buffer solution, after a 5 hour dry-storage period. The average percentage difference between the pH values measured with the glass electrode and the ones extrapolated from the 1-point calibration of the above strips was 0.2±0.1 (n=5). It is noteworthy to highlight that in Table 4.2 some saliva samples were collected before and after consumption of 150 mL of a soft drink and that these samples did not show significant changes in pH. This result probably depends on the buffering properties of saliva [28].

Thus, in order to demonstrate the ability of the potentiometric strips to monitor an extended pH window in real saliva, the pH of a sample was monitored while titrating it with a solution of 0.1 M HCl. Figure 4.3 shows the trace of the potentials recorded with the pH ISE, the SCI-RE and the potentiometric strip. It is noticeable that in Figure 4.3 the pH spontaneously increased from 7.02 to 7.06 in the first 10 minutes, as measured by means of a pH glass electrode. Interestingly, this pH increase agrees with the slight decrease of the potential of the potentiometric strip. Significantly, the stability of the disposable reference electrode of the potentiometric strip was good

since its maximum variation during the titration experiment was ±6 mV. The spiking of HCl solution was performed as indicated by the arrows and the pH of saliva was measured with the pH-meter 2 minutes after this addition. Table 4.3 compares these values with the ones extrapolated from one-point calibration of the potentiometric strip. Indeed, in the latter case, the device offset was determined by reading the potential of the strip in contact with a standard solution at pH=7.5, and taking the average slope (obtained with the batch of sensors reported in Table 4.2) as device sensitivity.

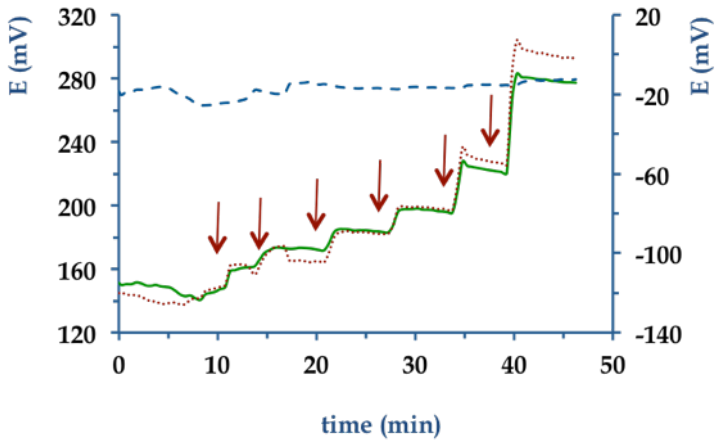

Figure 4. 3: Traces of electrode potential obtained with the (green, —) pH ISE and (blue, – –) SCI-RE against an Ag/AgCl reference electrode immersed into a saliva sample while drop-wise adding a solution of 0.1 M HCl, as indicated by the arrows on the graph. The right y-axis refers to the potential of the potentiometric strip (red, ···) obtained by plotting the pH ISE response against the solid-contact RE.

Table 4.3 demonstrates that the largest bias between the two methods in evaluating the saliva pH in the range 4-7 is smaller than 0.5 units. This small error gives the opportunity for integrating the potentiometric strip into wearable platforms and future work will address this implementation.

Table 4. 3: pH values of a saliva sample measured with a glass electrode and a potentiometric strip during its titration with 0.1 M HCl. In the latter case, the values were obtained by averaging the potential recorded for 3 minutes, after 1.5 minutes from the HCl spiking, and using one-point calibration. The one-point calibration was obtained measuring the device potential once in contact with a solution at pH=7.5, containing 10 mM NaCl and 20 mM KCl and using as device sensitivity the average slope of the potentiometric strips reported in Table 4.2 as device sensitivity.

t/min	pH-meter	pH-Potentiometric strip	ΔpH
10.5	6.5	6.1	0.4
14	6.3	5.9	0.4
20.5	6.1	5.6	0.5
27.5	5.8	5.4	0.4
33.5	5.2	4.9	0.3
39.5	4.1	3.8	0.3

4.4 Conclusions

This work highlights the preparation of a disposable potentiometric strip, which can monitor pH in sublingual saliva samples, in good correlation with data from a commercial pH-meter. It was also demonstrated that the potentiometric strip withstands a short period of dry-storage and that, after a short re-conditioning step, pH measurements of saliva samples obtained employing 1-point calibration were reliable. The small differences in the saliva pH readings given by the pH-meter and the potentiometric strips (with both the calibration methods, i.e., 1- or 5-points) are acceptable for applications targeting the monitoring of in-mouth pH, since the analytical method has to discriminate among saliva samples having wide pH regions: acid (pH 5.0-5.8), moderately acidic (pH 6.0-6.6) and healthy saliva (pH 6.8-7.8). Future work will focus on the integration of the strip into a suitable in-mouth wearable device.

4.5 References

[1] E. Bakker, D. Diamond, A. Lewenstam, E. Pretsch, Ion sensors: current limits and new trends, Analytica Chimica Acta, 393(1999) 11-8.

[2] H. Drake, T. Treasure, Continuous clinical monitoring with ion-selective electrodes: a feasible or desirable objective, Intesive Care Medicine, 12(1986) 104-7.

[3] A. Lewenstam, Clinical analysis of blood gases and electrolytes by ion-selective sensors, in: S. Alegret, A. Merkoçi (Eds.), Comprehensive Analytical Chemistry, Elsevier2007, pp. 5-24.

[4] C. Carey, G. Vogel, Measurement of calcium activity in oral fluids by ion selective electrode: method evaluation and simplified calculation of ion activity products, Journal of Research of the National Institute of Standards and Technology, 105(2000) 267-73.

[5] M. Khairy, R.O. Kadara, D.K. Kampouris, C.E. Banks, In situ bismuth film modified screen printed electrodes for the bio-monitoring of cadmium in oral (saliva) fluid, Analytical Methods, 2(2010) 645-9.

[6] T. Poursaberi, M. Salavati-Niasari, S. Khodabakhsh, L. Hajiagha-Babaei, M. Shamsipur, M. Yousefi, et al., A selective membrane electrode for thiocyanate ion based on a copper-1,8-dimethyl-1,3,6,8,10,13-azacyclotetradecane complex as ionophore, Analytical Letters, 34(2001) 2621-32.

[7] M. Shamsipur, T. Poursaberi, M. Rezapour, M. Ganjali, M. Mousavi, V. Lippolis, et al., $[Cu(L)](NO_3)_2$ (L=4,7-bis(3-aminopropyl)-1-thia-4,7-diazacyclononane) as a suitable ionophore for construction of thiocyanate-selective electrodes and their use in determination of urinary and salivary thiocyanate concentration, Electroanalysis, 16(2004) 1336-42.

[8] O. Kulapina, V. Baraguzina, N. Skoblikova, Ion-selective electrodes for determining cephazolin in biological media, Pharmaceutical Chemistry Journal, 42(2008) 481-4.

[9] M. N. Sawka, L. M. Burke, E. R. Eichner, R. J. Maughan, S .J. Montain, N. S. Stachenfeld, Exercise and fluid replacement, Medicine and Science in Sports and Exercise, 39(2007) 377-90.

[10] J. Bobacka, A. Ivaska, Ion sensors with conducting polymers as ion-to-electron transducers, in: S. Alegret, A. Merkoçi (Eds.), Comprehensive Analytical Chemistry, Elsevier2007, pp. 73-86.

[11] S. Anastasova, A. Radu, G. Matzeu, C. Zuliani, D. Diamond, U. Mattinen, et al., Disposable solid-contact ion-selective electrodes for environmental monitoring of lead with ppb limit-of-detection, Electrochimica Acta, 73(2012) 93-7.

[12] F.X. Rius-Ruiz, G.A. Crespo, D. Bejarano-Nosas, P. Blondeau, J. Riu, F.X. Rius, Potentiometric strip cell based on carbon nanotubes as transducer layer. Towards low-cost decentralized measurements, Analytical Chemistry, 83(2011) 5783-8.

[13] D. Diamond, Internet-scale sensing, Analytical Chemistry, 76(2004) 278A-86A.

[14] E. Papacosta, G.P. Nassis, Saliva as a tool for monitoring steroid, peptide and immune markers in sport and exercise science, Journal of Science and Medicine in Sport, 14(2011) 424-34.

[15] G. Ljungberg, T. Ericson, B. Ekblom, D. Birkhed, Saliva and marathon running, Scandinavian Journal of Medicine and Science in Sports, 7(1997) 214-9.

[16] S.A. Khaustova, M.U. Shkurnikov, A.G. Tonevitsky, Short highly intense exercise causes changes in salivary concentrations of hydrocortisone and secretory IgA, Bulletin of Experimental Biology and Medicine, 149(2010) 635-9.

[17] S. Ghimenti, T. Lomonaco, M. Onor, L. Murgia, A. Paolicchi, R. Fuoco, et al., Measurement of warfarin in the oral fluid of patients undergoing anticoagulant oral therapy, PLOS One, 6(2011) e28182.

[18] A.E. Herr, A.V. Hatch, W.V. Giannobile, D.J. Throckmorton, H.M. Tran, J.S. Brennan, et al., Integrated microfluidic platform for oral diagnostics, in: D. Malamud, R.S. Niedbala (Eds.), Oral-Based Diagnostics2007, pp. 362-74.

[19] C. Yang, E. Brooks, Y. Li, P. Denny, C. Ho, F. Qi, et al., Detection of picomolar levels of interleukin-8 in human saliva by SPR, Lab on a Chip, 5(2005) 1017-23.

[20] K. Yoda, K. Shimazaki, Y. Ueda, Analysis of glycolysis relevant compounds in saliva by microbiosensors, Annals of the New York Academy of Sciences, 864(1998) 600-4.

[21] A. Millward, L. Shaw, E. Harrington, A. Smith, Continuous monitoring of salivary flow rate and pH at the surface of the dentition following consumption of acidic beverages, Caries Research, 31(1997) 44-9.

[22] C.A. Eckley, H.O. Costa, Comparative study of salivary pH and volume in adults with chronic laryngopharyngitis by gastroesophageal reflux disease before and after treatment, Brazilian Journal of Otorhinolaryngology, 72(2006) 55-60.

[23] M. Bouchoucha, F. Callais, P. Renard, O. Ekindjian, P. Cugnenc, J. Barbier, Relationship between acid neutralization capacity of saliva and gastro-oesophageal reflux, Archives of Physiology and Biochemistry, 105(1997) 19-26.

[24] D. Lazarchik, S. Filler, Effects of gastroesophageal reflux on the oral cavity, American Journal of Medicine, 103(1997) 107S-13S.

[25] C. Fay, S. Anastasova, C. Slater, S.T. Buda, R. Shepherd, B. Corcoran, et al., Wireless ion-selective electrode autonomous sensing system, IEEE Sensors Journal 11(2011) 2374-82.

[26] C. Zuliani, G. Matzeu, D. Diamond, A liquid-junction-free reference electrode based on a PEDOT solid-contact and ionogel capping membrane, Talanta, 125(2014) 58-64.

[27] T.J. Smith, K.J. Stevenson, Reference Electrodes, in: C.G. Zoski (Ed.) Handbook of Electrochemistry, Elsevier2007, p. 92.

[28] W.F. Boron, E.L. Boulpaep, Pancreatic and Salivary Glands, Medical Physiology, 2nd Edition ed., Elsevier2012, pp. 927-31.

[29] E. Lindner, R. Gyurcsányi, Quality control criteria for solid-contact, solvent polymeric membrane ion-selective electrodes, Journal of Solid State Electrochemistry, 13(2009) 51-68.

[30] B. Schazmann, D. Morris, C. Slater, S. Beirne, C. Fay, R. Reuveny, et al., A wearable electrochemical sensor for the real-time measurement of sweat sodium concentration, Analytical Methods, 2(2010) 342-8.

Chapter 5.

Solid-Contact Ion-Selective Electrodes (ISEs) based on Ligand Functionalised Gold Nanoparticles

Giusy Matzeu[a]• and Claudio Zuliani[b]•, Dermot Diamond*[a]

URL: http://www.sciencedirect.com/science/article/pii/S0013468615001899

ISSN and DOI: 10.1016/j.electacta.2015.01.143

Electrochimica Acta 132 (2014): 292-296.

•Authors contributed equally to this work

*Corresponding author

[a]Insight Centre for Data Analytics, Dublin City University, Dublin 9, Ireland.

[b]Department of Electrical and Electronic Engineering, Imperial College London, London SW7 2AZ, UK.

Aims and Objectives

Chapter 5 was focused on the synthesis and functionalisation of Gold Nanoparticles with different ligands. They were characterised and tested as solid-contact layer of Pb^{2+} and Na^{+} Ion-Selective Electrodes.

Contributions

- Design, conception and optimisation of experimental trials.

- Analysis of data and writing up of the manuscript.

Abstract

Gold nanoparticles (Au-NPs) functionalised with Lipoic Acid (LAc) or Lipoic Amide (LAm) have been investigated as solid-contact in disposable lead and sodium selective electrodes. In Pb^{2+} and Na^{+} solutions, electrodes incorporating LAm Au-NPs displayed super-Nernstian and Nernstian behaviour whereas electrodes incorporating LAc Au-NPs showed Nernstian and sub-Nernstian responses. During calibration, the response of Solid-Contact Ion-Selective Electrodes (SC-ISEs) was found to depend on the particular ion-analyte/Au-NP ligand pair, suggesting that the ligand decorating the NPs has an important role in regulating the overall electrode response function. Insights into the underlying trans-membrane and the Au-NPs/membrane interface processes have been obtained by means of electrochemical impedance spectroscopy.

Keywords

Solid-Contact, Lipoic Amide, Lipoic Acid, Gold Nanoparticles, Lead and Sodium Ion-Selective Electrodes.

5.1 Introduction

In recent years, research conducted on Ion-Selective Electrodes (ISEs) has been largely focused on replacement of the liquid internal filling solution with a solid interfacial contact layer between the ion-selective outer membrane, and the internal reference electrode surface [1-3]. These so-called Solid-Contact Ion-Selective Electrodes (SC-ISEs) can offer new commercial opportunities [4, 5] since they require little or no maintenance, they are compatible with miniaturised designs, and can potentially be mass-produced as disposable sensors [3]. Conducting polymers (CPs) such as poly-octylthiophene (POT) [6], poly(3,4-ethylenedioxythiophene) (PEDOT) [7], polyaniline [8] and polypyrrole [9] are among the first [10] and most common materials employed as solid-contacts [11]. Recently, other materials such as carbon nanotubes (CNTs) [12] and graphene [13] have also been investigated for this purpose, but in general the opportunity to tailor key properties of this interfacial layer such as hydrophobicity/hydrophilicity have only received minimal attention.

Gold nanoparticles (Au-NPs) represent another promising material for use in solid-contact electrodes. Jaworska et al. [14] compared ISEs wherein the SC was realised using Au-NPs functionalised with aliphatic thiols (butyl and octane thiol chains) or POT. The authors showed that K^+ ISEs incorporating these Au-NPs as the SC demonstrated better stability over time, without affecting performance characteristics such as the Limit of Detection (LOD) when compared to POT. Similarly, Woznica et al. [15] employed dithizone modified Au-NPs as a SC in Cu^{2+} ISEs. When the NP ligand was changed from butanethiol to dithizone, which is known to bind Cu^{2+} selectively, the response of electrodes shifted from Nernstian to super-Nernstian. However, when dithizone functionalised Au-NPs were loaded with copper ions (by conditioning for 15 minutes in 10^{-5} M $CuSO_4$ solution, before the deposition of the Cu^{2+} selective membrane), the calibration slope became Nernstian and was characterised by a lower LOD ($10^{-7.5}$ M) than that obtained using butanethiol (10^{-6} M). This showed clearly that the choice of the ligand bound to the NPs influences the ion fluxes at the membrane/solid-contact interface.

In this manuscript, we compare two solid-contact films prepared from LAm and LAc Au-NPs. In particular, we investigate the impact of the differing physico-chemical properties of the so-functionalised NPs and of their concentration on the sensitivity and dynamic range of the sensors. Electrochemical Impedance Spectroscopy (EIS) [16] has been already used to investigate the mechanisms through which solid-contact films

affect the behaviour of related ISEs [6], and to describe water uptake by acrylate membranes over time [17]. These studies helped to explain the mechanism of ion transport through the membrane and how this is modulated by Au-NPs. Despite these advances, a comprehensive model that takes into account the effects of the specific functional groups used to functionalise the NPs is not yet in place, a problem that we attempt to overcome within this study. As a first step, we focus on two analytes, Pb^{2+} and Na^{+}, which have important applications in the environmental [18], sports science [19] and health fields [20], and examine how Au-NPs decorated with different functional groups can produce SC-ISEs with improved performance characteristics.

5.2 Experimental

5.2.1 Materials

Polyethylene Terephtalate (PET) sheets by HiFi (Dublin, Ireland) or MacDermid (Oxon, UK), with a thickness of 175 μm, were used as a substrate for the screen-printed electrodes, and were employed without any further treatment. C2030519P4 and D50706D2 by Gwent Inc. (Pontypool, UK) were respectively used as carbon ink and dielectric in the preparation of the electrodes. Gold(III) chloride trihydrate ($HAuCl_4 \cdot 3H_2O$, >99.9%), alpha-lipoic amide, alpha-lipoic acid, sodium borohydride, high molecular weight poly(vinyl chloride) (PVC), bis(2-ethylhexyl) sebacate (DOS, ≥97%), tetrahydrofuran (THF, ≥99.5%) of selectophore grade, 2-nitrophenyl octyl ether (o-NPOE, >99%), tert-butylcalix[4]arene-tetrakis(N,N-dimethylthioacetamide) (lead ionophore IV) of selectophore grade, 4-tert-butylcalix[4]arene-tetraacetic acid tetraethyl ester (sodium ionophore X) of selectophore grade, potassium tetrakis(4-chlorophenyl)borate (KClTPB), lead nitrate, sodium chloride, dimethyl sulphoxide (DMSO), tert-butanol, nitric acid, sulfuric acid, toluene were purchased from Sigma-Aldrich (Dublin, Ireland). Methanol (>99%) was from Fisher (Dublin, Ireland) and sodium tetrakis-[3,5-bis(trifluoromethyl)phenyl]borate (NaBARF) was from Strem Chemicals (Cambridge, UK). For the preparation of gaskets, 0.8 mm thick adhesive poly foam strips were purchased from Radionics (Dublin, Ireland).

5.2.2 Preparation of Au-NPs

LAc and LAm Au-NPs were synthesised following a single-phase protocol [21, 22]. 11 mL of an aqueous 31.5 mM $HAuCl_4 \cdot 3H_2O$ solution was mixed with 20 mL of 40 mM LAc (dissolved in methanol) or LAm (dissolved in DMSO) solution. The round bottom flask containing the mixture was refrigerated into an ice bath and N_2 was bubbled

throughout. 9 mL of a 0.45 M sodium borohydride aqueous solution, refrigerated at 4°C, was immediately added to the mixture. The reaction mixture was then left for three hours before the washing steps. The LAc NPs solution was washed in a separation funnel three times with toluene, followed by drop-wise addition of 0.1 M sulphuric acid until the NPs settled. The NPs were re-suspended and washed 5 times in centrifugal tubes with water at a speed of 5000 rpm for 30 minutes. The LAm NPs were washed 5 times with a 1:1 solution of tert-butanol/methanol using centrifugal tubes at a speed of 5000 rpm for 30 minutes and finally dispersed in a methanol solution. Half of the resulting NP suspension was roto-evaporated in order to determine yield and for characterisation purposes.

5.2.3 Preparation of Lead and Sodium ISEs

The screen-printed electrodes were realised using a DEK 248 printer (Weymouth, UK) as reported elsewhere [5]. The NP solution was drop-cast within a 3.0 mm diameter well formed by punching a hole in an adhesive foam tape covering layer. It was then fixed around the carbon disk in order to produce a layer with a theoretical thickness equivalent to a desired number of monolayers of Au-NPs. Assuming hexagonal packing symmetry of the NPs, the theoretical number of nanoparticles needed to form a monolayer, N, was estimated using the expression [23, 24] (see Equation 5.1):

$$N = 0.907 \times \frac{R^2}{r^2} \qquad (5.1)$$

where *R* is the radius of the cross-sectional area of drop-cast and *r* is the radius of the NPs determined by Fe-SEM analysis. PVC-based ion-selective membranes were prepared as previously reported for Pb^{2+} [18] and Na^{+} [25], and a total of 26.25 µL of the PVC ion-selective cocktail in THF was drop-cast on top of the solid-contact by multiple additions, performed with an interval of 15 minutes between each addition, according to the sequence: 1 µL (once), 1.5 µL (3 times), 2.5 µL (3 times), 3 µL (twice), 3.25 µL (once) and 4 µL (once). The Pb^{2+} ISEs were initially conditioned for 2 days in a 10 µM $Pb(NO_3)_2$ solution to exchange all the interfering ions in the membrane for Pb^{2+}, and then conditioned for 1 day in a 1 nM $Pb(NO_3)_2$ solution to completely remove any interfering ion from the membrane, and pre-condition the electrodes for low limit of detection measurements. Both solutions were adjusted to pH 4 with HNO_3 (protocols adapted from Anastasova et al. [26]). The Na^{+} ISEs were instead conditioned in a 10 mM NaCl solution overnight (protocol adapted from Schazmann et al. [25]), in order to optimise the performance in terms of Nernstian sensitivity and accuracy within the dynamic range of interest (10-100 mM).

5.2.4 Instrumentation and Software

During the washing steps, the NP suspensions were centrifuged using a Rotina 420R, from Hettich, UK. NPs were characterised by elemental analysis (Exeter Analytical CE440 CHN Analyser, see Table AC.1), field-emission scanning electron microscopy, Fe-SEM (Hitachi 5500 microscope) (see Figure AC.1), and thermo gravimetric analysis, TGA, (Q50 TA, see Figure AC.2). ImageJ software was used to calculate the average size of the nanoparticles (n>100). The potentiometric measurements were recorded using an EMF 16 channels instrument from Lawson Labs, USA. The cell potential readings were corrected for junction potential effects using the Henderson formalism [27], and ion concentrations were converted to activities via the Debye-Hückel approximation [27]. A silver/silver chloride (saturated KCl) electrode was used as the reference electrode. The EIS measurements were conducted with a CHI760D potentiostat (CH Instruments, USA) using a Pt wire as counter electrode and an Ag/AgCl electrode as reference electrode. The EIS spectra were acquired at the open circuit potential (OCP) while applying an AC-wave with amplitude of 100 mV and scanning frequencies between 10 mHz and 1 MHz. The model describing the EIS experimental data was fitted to the data using the CH760D software.

5.3 Results and Discussion

5.3.1 Au-NPs Characterisation

Figure 5.1 (a) and Figure 5.2 (a) illustrate the structure of the LAm and LAc functional groups, with the head to tail configuration dictated by the sulphur chemi-sorption on the Au-NP surface. The NPs had similar sizes, i.e., 3.2±0.6 nm (n=100) and 3.5±0.6 nm (n=100), for LAm and LAc (see Figure AC.1, Appendix C). The SEM images in Figure 5.1 (b) and Figure 5.2 (b) show that the deposition of an amount of NPs theoretically equivalent to 20 monolayers was not sufficient to fully cover the electrode, due to uneven coverage.

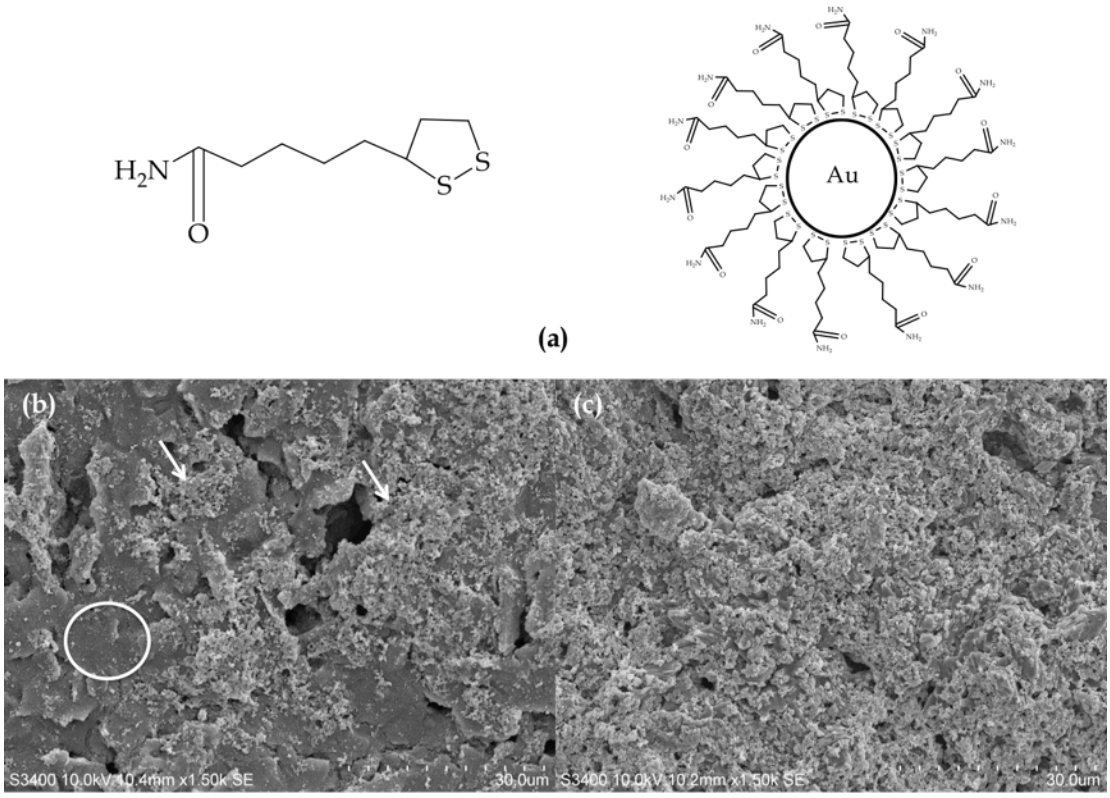

Figure 5. 1: (a) Molecular structure of LAm characterised by a head to tail configuration, after sulphur chemisorption on the Au-NP surface. SEM images of SC realised using LAm Au-NPs (LAm-20 (b) and LAm-100 (c)) drop-cast on top of the carbon layer of screen-printed electrodes. The circles indicate uncovered carbon areas while the arrows point towards the Au-NPs structures. SEM images were obtained at an acceleration voltage of 10 kV.

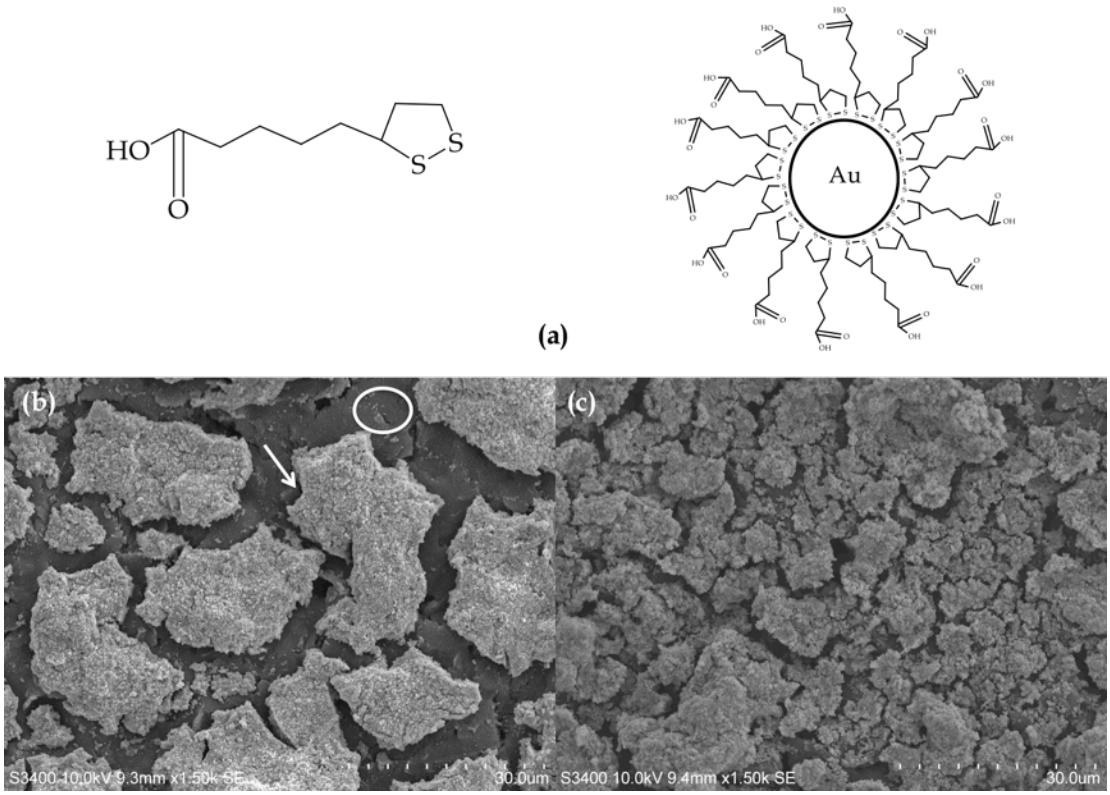

Figure 5. 2: (a) Molecular structure of LAc characterised by a head to tail configuration, after sulphur chemisorption on the Au-NP surface. SEM images of SC realised using LAc Au-NPs (LAc-20 (b) and LAc-200 (c)) drop-cast on top of the carbon layer of screen-printed electrodes. The circle indicates an uncovered carbon area while the arrow points towards the Au-NPs structures. SEM images were obtained at an acceleration voltage of 10 kV.

As the amount of material drop-cast was increased, the degree of coverage was found to depend on the type of ligand involved. Thus, Figure 5.1 (c) and Figure 5.2 (c) suggest that deposition of more than 100 and 200 theoretical monolayers of the LAm and LAc NPs, respectively, was necessary to achieve complete coverage of the electrode area. This is of utmost importance to minimise water pooling effects and ensure the solid-contact layer is continuous with no points of direct contact between the PVC ion-selective outer layer and the internal carbon conductive layer [17, 28, 29]. The SEM images highlight some differences in the resulting structures, with different degrees of aggregation mainly dictated by dissimilar physico-chemical properties of the two functional groups. This also leads to differences in terms of surface roughness (as discussed below), which makes the effective surface area much larger than the geometrical one. Moreover, differences in evaporation rate and surface tension of the two solvents (water for LAc Au-NPs and methanol for LAm NPs) undoubtedly have some influence, as shown in Figure AC.3 (see Appendix C). LAc Au-NPs form

relatively strong intermolecular hydrogen bonds with water, although at pH 7 they are essentially deprotonated to the negative carboxylate form [30], and aggregation will tend to be inhibited by electrostatic repulsion. Moreover, since the carbon layer repels the Au-NPs, they tend to form a drop within which water/water, LAc Au-NP/water and LAc Au-NPs/LAc Au-NP interactions become predominant as the solvent evaporates. This phenomenon leads to the formation of less homogeneous, larger clusters, typically a few hundred micrometers wide (see Figure 5.2). In contrast, LAm hydrogen bonds are less strong [31] and the high affinity for the carbon layer leads to more uniform coverage and, to some extent, retention of nanostructures after evaporation (see Figure 5.1).

5.3.2 Au-NPs used as Solid-Contact for Pb^{2+} ISEs

Pb^{2+} ISEs were prepared using 40, 200 and 2000 theoretical monolayers of LAm Au-NPs corresponding to an incomplete (LAm-40) and complete (LAm-200 and LAm-2000) coverage of the electrode area. Table 5.1 lists the baseline (E^0), calibration slope (S) and limit of detection (LOD) measured over time.

Table 5. 1: Average values of baseline (E^0), sensitivity (S) and LOD (n = 3) and associated standard errors for Pb^{2+} ISEs prepared using LAm-40, LAm-200 and LAm-2000 Au-NPs as the solid-contact. The electrodes were initially conditioned in 10 µM $Pb(NO_3)_2$ followed by exposure to 1 nM $Pb(NO_3)_2$ for 48 and 24 hours, respectively (both solutions at pH 4). For LAm-40 and LAm-200, the 2nd and 3rd calibration took place after storage in 1 nM $Pb(NO_3)_2$, at pH 4, for 24 and 96 hours, respectively. For LAm-2000, the 2nd and 3rd calibration took place after storage in 1 nM $Pb(NO_3)_2$, at pH 4, for 24 and 144 hours, respectively. The symbol "/" indicates the LOD could not be estimated due to associated variations in the response slope.

			LAm Au-NPs		
N° Theoretical Monolayers	**N° Calibration**	**Time (days)**	**E^0 (mV)**	**S (mV/log($a_{Pb^{2+}}$))**	**LOD (-log($a_{Pb^{2+}}$))**
40	1st	1	160.0±41.1	104.9±8.3 ($a_{Pb^{2+}}$ $10^{-6.5}$-$10^{-5.5}$) 26.5±6.3 ($a_{Pb^{2+}}$ $10^{-5.5}$-10^{-4})	/
	2nd	2	232.9±8.8	44.9±0.8	6.99±0.01
	3rd	5	260.8±5.2	37.3±0.2	7.06±0.06
200	1st	1	143.0±36.5	111.9±6.7 ($a_{Pb^{2+}}$ $10^{-6.5}$-$10^{-5.5}$) 28.2±8.6 ($a_{Pb^{2+}}$ $10^{-5.5}$-10^{-4})	/
	2nd	2	218.7±11.0	34.4±1.6	6.82±0.03
	3rd	5	231.9±4.0	36.4±0.5	7.00±0.03
2000	1st	1	176.9±11.5	85.7±7.0 ($a_{Pb^{2+}}$ 10^{-7}-10^{-6}) 41.3±1.4 ($a_{Pb^{2+}}$ 10^{-6}-10^{-4})	/
	2nd	2	220.5±4.0	73.2±1.8	/
	3rd	7	197.5±5.0	47.9±3.8	/

During the initial (day 1) calibration, E^0 values were relatively variable for LAm-40 (standard error of ±41.1 mV) but significantly more reproducible for LAm-2000 (±11.5 mV). At the same time, the slopes exhibited a double trend with high standard error (>± 8.3 mV/log($a_{Pb^{2+}}$)) in all cases, due to high initial variability and super-Nernstian trends. Conditioning the electrodes in 1 nM $Pb(NO_3)_2$ (pH=4) solution during the resting periods induced changes in the second and third calibration manifested through changes in E^0 values and substantial decrease in standard errors (~±5 mV after 5 days). They also exhibited a single super-Nernstian slope, with relatively small electrode-to-electrode variation. Noticeably, electrodes with the largest amount of nanoparticles (LAm-2000, see Figure 5.3) exhibited the highest super-Nernstian slopes for the 1st, 2nd and 3rd calibrations (S≥43 mV/log($a_{Pb^{2+}}$)).

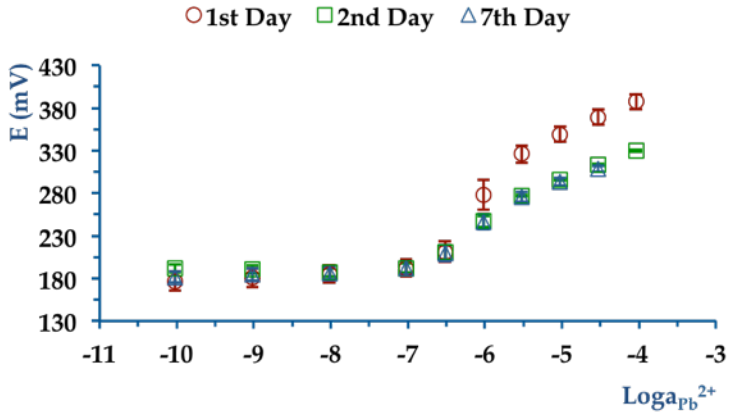

Figure 5. 3: Average calibration curves of a batch (n=3) of LAm-2000 Pb^{2+} ISEs (the error bars represent standard errors): (1st (○), 2nd (□) and 3rd (Δ)). The 1st calibration took place after conditioning the electrodes in 10 μM $Pb(NO_3)_2$ followed by exposure to 1 nM $Pb(NO_3)_2$ at pH 4 for 48 and 24 hours, respectively. The 2nd and 3rd responses were recorded after storage in 1 nM $Pb(NO_3)_2$ at pH 4 for further 72 and 144 hours, respectively. For convenience, the plots were normalised at the response obtained at a Pb^{2+} activity of 10^{-7} M.

The high super-Nernstian trends we observed in several cases (with S>40 mV/log($a_{Pb^{2+}}$)) prevented the estimation of the LOD, as calculated from the intersection of the two extrapolated linear portions of the calibration curve. In all other cases, estimated LODs were in the order of ~10^{-7} M, and were largely independent of the amount of NP material used.

Table 5.2 reports baselines (E^0), calibration slopes (S), and LODs for electrodes incorporating LAc-40 and LAc-200 Au-NPs. E^0 was characterised by poor reproducibility during the first calibration (standard errors of ±21.0 mV and ±37.4 mV for LAc-40 and LAc-200, respectively) that greatly decreased during the second (after 1 day) and third calibration (realised after 5 days), reaching standard errors of ±3.2 mV. Sensitivities were also super-Nernstian during the 5-day period, but closer to the expected ~30 mV/log($a_{Pb^{2+}}$), in contrast to those obtained with LAm Au-NPs based SC-ISEs.

Table 5. 2: Average values of baseline (E^0), sensitivity (S) and LOD (n = 3) and estimated standard errors for Pb^{2+} ISEs prepared using LAc-40 and LAc-200 Au-NPs as the solid-contact. The electrodes were first conditioned in 10 µM followed by exposure to 1 nM $Pb(NO_3)_2$ solution, at pH 4, for 48 and 24 hours, respectively. The 2nd and 3rd calibrations were obtained after storage in 1 nM solution of $Pb(NO_3)_2$, at pH 4, for 24 and 96 hours, respectively.

			LAc Au-NPs		
N° Theoretical Monolayers	**N° Calibration**	**Time (days)**	**E^0 (mV)**	**S (mV/log($a_{Pb^{2+}}$))**	**LOD (-log($a_{Pb^{2+}}$))**
40	1st	1	246.0±21.0	36.7±1.5	7.50±0.02
	2nd	2	237.2±4.2	36.7±0.7	7.38±0.02
	3rd	5	256.9±3.2	38.9±0.5	7.12±0.08
200	1st	1	206.1±37.4	35.6±3.6	7.79±0.06
	2nd	2	240.7±10.9	39.3±0.3	7.40±0.01
	3rd	5	269.8±3.2	38.9±1.1	7.33±0.09

The values were relatively independent of the number of monolayers (see Table 5.2), and comparatively stable, with average values of 37.4±0.7 mV/log($a_{Pb^{2+}}$) and 37.9±1.2 mV/log($a_{Pb^{2+}}$) for LAc-40 and LAc-200, respectively. Regarding the LOD, by increasing the amount of material from LAc-40 to LAc-200, we were able to reach $1.70x10^{-8}$ M (i.e., $10^{-7.79}$ $a_{Pb^{2+}}$), which is approximately one order of magnitude lower than obtained with LAm-200 ($10^{-6.82}$ $a_{Pb^{2+}}$) SC-ISEs. This is an improvement with respect to previously reported values for SC-ISEs based on PEDOT grown in KCl (i.e., $1.17x10^{-7}$ M) [18], but not as low as values obtained using POT drop-cast on screen-printed SC-ISEs (i.e., $1.2x10^{-9}$ M) [26]. The obtained value is lower than thresholds for drinking water set under current legislation, which are 15 ppb; i.e. $7.2x10^{-8}$ M (US-EPA) [32], and 10 ppb; i.e. $4.8x10^{-8}$ M (WFD for EU [33]). It should be noted that the LOD values increased over time, reaching values up to $9.8x10^{-8}$ M (i.e., $10^{-7.03}$ $a_{Pb^{2+}}$) [29, 34]. The results presented above for LAc-200 (characterised by a low drift of 0.02±0.008 mV/min) suggest that these disposable sensors can be used after one-point calibration for screening measurements in the field, particularly in circumstances wherein the Pb^{2+} levels are suspected to be high (i.e. $>10^{-6}$ M). Such low cost sensors could provide a means for consumers to check the status of their supply, or screen for contamination of water bodies in accordance with the growing interest in "citizen science" [35].

In order to investigate the mechanistic reasons underlying the observed differences in the behaviour of the electrodes based on the two functional groups, EIS measurements were acquired at different temporal intervals during the two conditioning steps, i.e., after 2, 7, 21 and 46 hours in a 10 µM $Pb(NO_3)_2$ solution, and after 54 and 72 hours in a

1 nM $Pb(NO_3)_2$ solution. Figure 5.4 (a) and Figure 5.4 (b) show Nyquist plots of the impedance spectra recorded for LAm-2000 and LAc-2000 Pb^{2+} ISEs, respectively. The insets in both figures highlight the high frequency region (1 MHz-0.1 kHz).

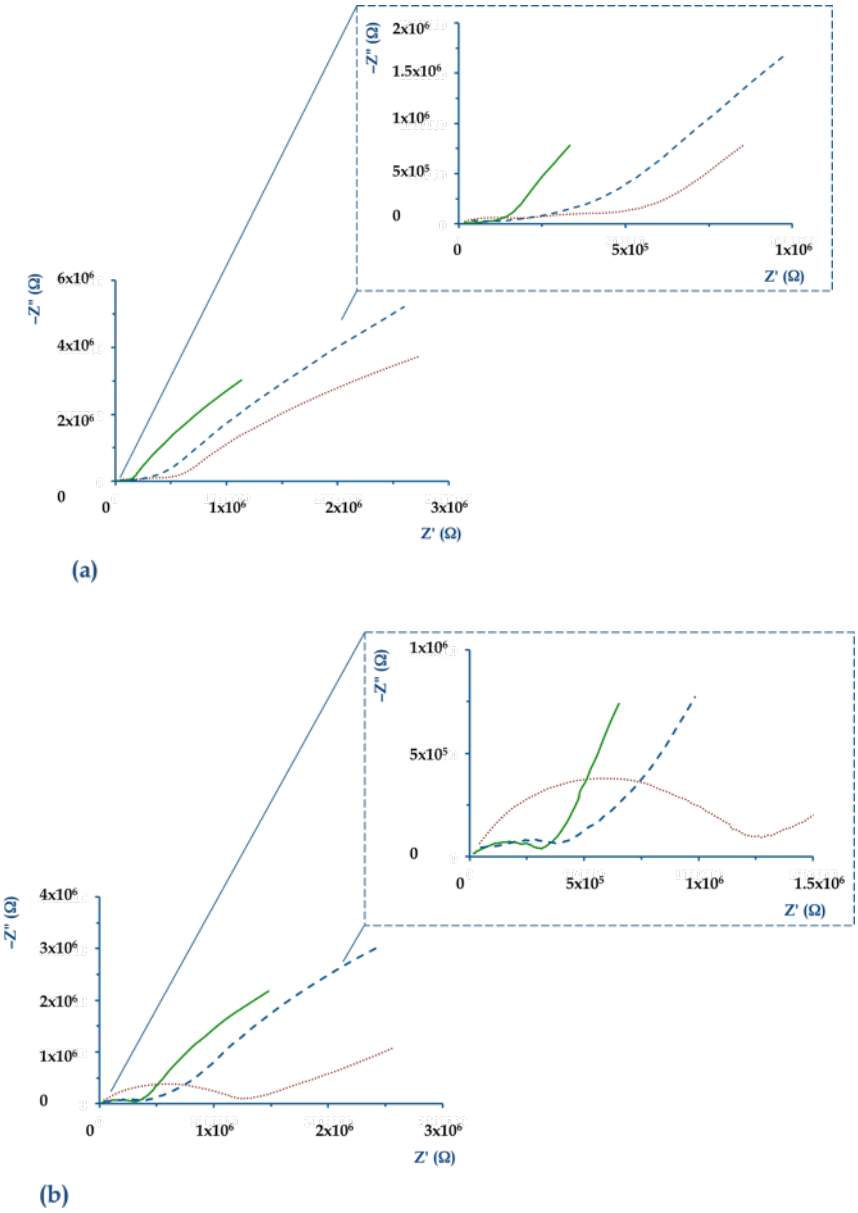

Figure 5. 4: Nyquist plots of LAm-2000 (a) and LAc-2000 (b) Pb^{2+} ISEs. The measurements were taken after 7 (red, · · ·) and 46 (green, –) hours from the start of the 1st conditioning step, in 10 µM $Pb(NO_3)_2$; and after 72 (blue, – –) hours from the start of the whole conditioning process, in 1 nM $Pb(NO_3)_2$. The insets show enlargements of the EIS spectra in the region of frequencies between 1MHz and 1kHz.

Electrodes incorporating LAm-2000 were characterised by two suppressed, partially merged semicircles appearing after 7 hours (overall diameter of ~$5x10^5$ Ω) [36]. The semicircles subsequently became smaller (~$2x10^4$ Ω) after 46 hours and slightly

increased (~1x10^5 Ω,) after 72 hours. In contrast, Figure 5.4 (b) shows a different behaviour for the LAc-2000 Pb^{2+} ISEs. The diameter of the EIS semicircles in the 1 MHz-1 kHz region decreased from 10^6 Ω (after 7 hours) to 10^5 Ω (after 46 hours). After 72 hours, the spectrum exhibited a slightly increased diameter (4x10^5 Ω) together with a distinguishable second semicircle at higher frequencies (1 MHz-10 kHz). At low frequencies (0.1-0.01 Hz), a Warburg impedance related to diffusion phenomena is present for both types of solid-contact (after conditioning in 10 µM $Pb(NO_3)_2$ for 46 hours and 1 nM $Pb(NO_3)_2$ for 72 hours).

Figure 5.5 shows the equivalent circuit model that we used to model the experimental data. The circuit comprises 3 parallel blocks labelled A, B and C, and the bulk solution resistance R_s (see Appendix C, Section AC.1 for more details). Block A represents the solid-contact layer where the charge transfer resistance, R_{sc}, and the double layer capacitance, Q_{sc}, associated with the Au-NPs, are connected in parallel. Block B represents the water uptake occurring over time within the polymeric membrane (see Appendix C, Section AC.1 for more details). Block C describes the diffusion mass transfer with a Warburg element connected to the charge transfer resistance, R_{ct}, and the double layer capacity, Q_{dl}. These last two elements describe the interface between the PVC membrane and the solution [37]. Figure AC.4 shows a good correlation (average relative error ~0.02) between the curves predicted by our best-fit model and the experimental EIS measurements.

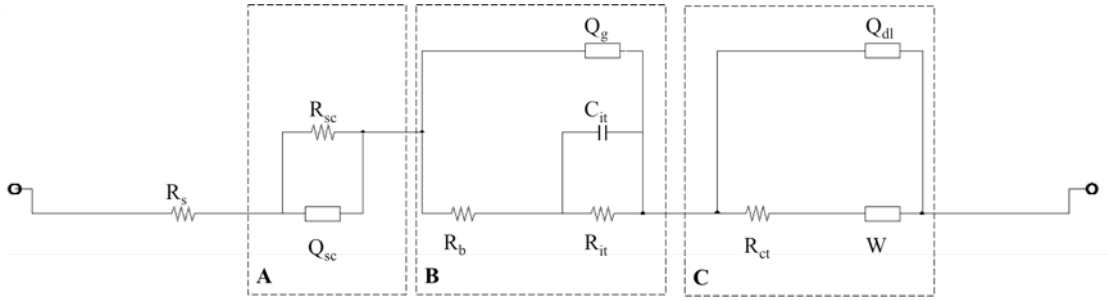

Figure 5. 5: Schematic of the equivalent circuit used to model Pb^{2+} SC-ISEs.

Regardless of the SC employed, R_{ct} increased in the first 7 hours most likely due to water uptake within the polymer [17], and reached similar values for LAc-2000 (0.28 MΩ) and LAm-2000 (0.21 MΩ). It became stable after 21 hours and the PVC membrane/solution interface was characterised by similar time constants at the end of the two conditioning steps (~2.57x10^{-3} s for LAc-2000 and ~2.26x10^{-3} s for LAm-2000).

Table 5.3 lists the most significant model parameters fitted during the final conditioning step (after 54 and 72 hours). Between these times, the charge transfer resistance R_{sc} of the SC changed from 0.61 MΩ to 0.14 MΩ for electrodes incorporating LAc, while it increased from 0.07 MΩ to 0.13 MΩ for electrodes incorporating LAm Au-NPs. Q_{sc} decreased from $7.47x10^{-8}$ to $1.86x10^{-8}$ $\Omega^{-1}s$ and from $3.37x10^{-8}$ to $1.78x10^{-8}$ $\Omega^{-1}s$, for LAc and LAm Au-NPs in the SC electrodes, respectively. Although the initial values of R_{sc} and Q_{sc} are different, these parameters converged in the latter stages of the two conditioning steps, independently of the type of Au-NPs employed as the electrode SC, suggesting that their electronic properties are very similar when the NPs layer is hydrated. These results are not that surprising, as the NPs have the same alkyl chain and terminal groups that are similar in nature (carboxylic vs. amide). Previous studies on Au-NPs monolayers showed that R_{sc} and Q_{sc} are mainly influenced when ligand chain length and terminal groups differ significantly (e.g., switching from carboxylic to ferrocene) in their influence on the overall 3D organisation and chemical nature of the monolayer [38].

Table 5. 3: R_{sc}, Q_{sc} and W values obtained by fitting the experimental data (recorded after 54 and 72 hours from the beginning of the first conditioning step) to the equivalent circuit shown in Figure 5.5 (for LAm-2000 and LAc-2000).

	LAc Au-NPs			**LAm Au-NPs**		
time (hours)	**R_{SC} (MΩ)**	**Q_{SC} ($\Omega^{-1}s$)**	**W ($\Omega^{-1}s^{0.5}$)**	**R_{SC} (MΩ)**	**Q_{SC} ($\Omega^{-1}s$)**	**W ($\Omega^{-1}s^{0.5}$)**
54	0.61	$7.47x10^{-8}$	$5.39x10^{-7}$	0.07	$3.37x10^{-8}$	$3.08x10^{-7}$
72	0.14	$1.86x10^{-8}$	$4.25x10^{-7}$	0.13	$1.78x10^{-8}$	$1.17x10^{-6}$

However, the differing terminal groups of the two ligands do significantly affect the Warburg impedance parameter (W), which is associated with mass transfer behaviour. These results are also consistent with the observed differences in the sensitivity of the ISEs, since this parameter also depends on diffusion and mass transfer. The LAc sensors were characterised by decreasing W over time ($5.39x10^{-7}$ $\Omega^{-1}s^{0.5}$ and $4.25x10^{-7}$ $\Omega^{-1}s^{0.5}$ after 54 and 72 hours, respectively), suggesting that the kinetics of water uptake and mass transfer of Pb^{2+} might slow down towards the end of the conditioning steps. On the other hand, for LAm, the value of W changed significantly over time, increasing from $3.10x10^{-7}$ $\Omega^{-1}s^{0.5}$ to $1.17x10^{-6}$ $\Omega^{-1}s^{0.5}$, an order of magnitude higher than that

recorded under the same conditions for LAc, possibly due to increased inhibition of mass transfer arising from the more hydrophobic nature of LAm, compared to LAc [39, 40].

Moreover, differences in characteristics (i.e. constant super-Nernstian slope for LAm-2000 Pb^{2+} ISEs) are almost certainly due to what happens at the membrane/SC interface [41]. Detailed calculations (see Appendix C, Section AC.2) suggest that the membrane is fully saturated after two conditioning steps, and the diffusion layer occupies its entire thickness [42]. This process may be slow since LAm is not a particularly good ligand [40] as it is uncharged and has no obvious binding site for Pb^{2+} from a chemical perspective. This assumption is corroborated by the high time constant characterising the parallel elements R_{it} (orders of hundred of GΩ) and C_{it} (2.58×10^{-6} Ω^{-1}s) at the end of the conditioning steps (Block B, see Figure 5.5). This suggests for a slow phenomenon that might also be connected to the longer timescale variations characterising the behaviour of LAm Pb^{2+} ISEs. Thus, the super-Nernstian responses can likely be ascribed to Pb^{2+} loading and flux towards the solid-contact, which still appear to be present after 6 days for LAm-2000 Pb^{2+} ISEs (see Figure 5.3).

In contrast, the transfer of Pb^{2+} ions from the ion-selective membrane into the solid-contact layer appears to be faster for LAc NPs, which is characterised by a time constant of ~49 s (R_{it} 7.34 MΩ and C_{it} 6.7×10^{-6} Ω^{-1}s). The duration of this process dictates the time required for the potentiometric response and the nearly Nernstian behaviour become established. The overall results confirm that differences in hydrophobicity/hydrophilicity will influence these trans-membrane fluxes, as already reported by Sokalski et al. [43].

5.3.3 Au-NPs used as Solid-Contact for Na^+ ISEs

The above results suggest that the ligand that decorates the Au-NPs allows specific tuning of the SC-ISE response characteristics according to the ion of interest. Na^+ ISEs find applications in areas like sweat and blood monitoring, where good intra-batch reproducibility and accuracy over a short dynamic range (10^{-2} to 10^{-1} M of Na^+) are required. Figure 5.6 (a) and Figure 5.6 (b) show calibration curves for Na^+ ISEs incorporating SCs based on LAc-2000 and LAm-2000, respectively. The calibration curves of the 4 sensors in Figure 5.6 (a) employing a LAc-NP SC-layer showed sub-Nernstian slopes of 33.23±2.5 mV/log(a_{Na^+}), within the activity range 10^{-5}-$10^{-2.5}$. These sensors also exhibited poor reproducibility in the dynamic range, especially at high Na^+ activities (10^{-2}-10^{-1}). In contrast, the Na^+ ISEs employing LAm Au-NPs as the SC

(see Figure 5.6 (b)) had baselines of -179.9±26.8 mV, and slopes of 50.6±0.3 mV/log(a_{Na^+}), n = 4, within the activity range 10^{-5}-10^{-1}. These disposable sensors showed also good intra-batch reproducibility (small standard errors for slope) and could feasibly be used after a one-point calibration, to correct for inter-electrode differences in E^0, which were ascribed to inconsistencies in the thickness of the solid-contact layer during manual deposition. Automation of the fabrication procedure removes much of the inter-electrode E^0 variations, and opens the way to mass fabrication of very reproducible electrodes. This is exploited in industry, particularly during high volume manufacturing of disposable chemical sensors and biosensors, in which statistical samples are taken from electrode batches and the calibration parameters obtained from these, if deemed to meet manufacturing standards, are applied to all electrodes within the batch.

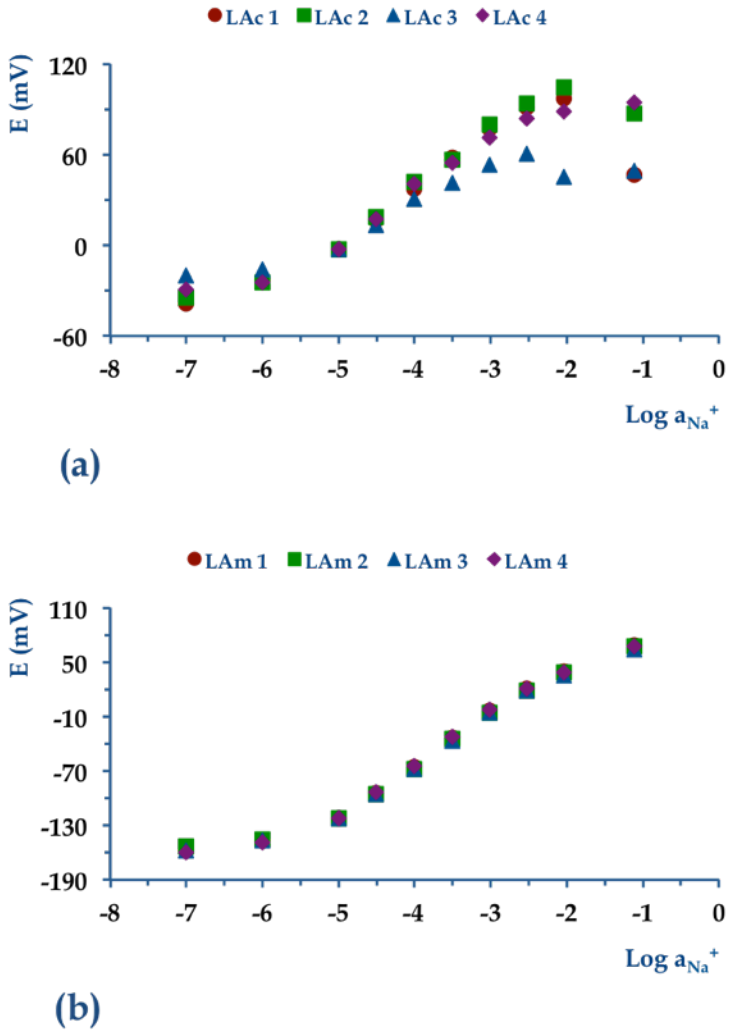

Figure 5. 6: Calibration curves of LAc-2000 (a) and LAm-2000 (b) (●, ■, ▲, ♦), n=4. In both cases, the electrodes were conditioned overnight in 10 mM NaCl before the calibration was performed. For convenience, the plots were normalised to responses at a Na^+ activity of 10^{-5}.

The LOD (ca. 10^{-5} a_{Na^+}) was similar for both electrode types. The differences in calibration curve slopes and dynamic ranges can be attributed to the physico-chemical properties of the two functional groups used to functionalise the NPs, since the Na^+-sensitive capping membrane was the same in both cases. This is exactly analogous to the Pb^{2+} SC-ISEs discussed above.

For example, it is reasonable to expect that the LAc-functionalised NPs exist predominantly in the protonated form in the SC as the pH is acidic (around 6) under the conditions employed in the experiment [30]. As the concentration of Na^+ ions at the PVC IS-membrane/SC interface increases, it is plausible that, in the presence of water, there will be increasing exchange with H^+ ions originating from the LAc carboxylate groups[5.a], that can exchange back into the PVC membrane to maintain overall charge neutrality, effectively lowering the measured slope of the electrode.

In summary, the response characteristics of the ISEs seems to be controlled not only by the IS-membrane, but also by the type of functionalised NPs employed in the SC layer. Therefore, when preparing such electrodes, the effect of various substituent groups on the overall electrode response must be characterised carefully. Given the wide variety of groups available, and the relative simplicity of the functionalisation chemistry [44], this opens another mechanism for tuning the overall electrode response behaviour. Through this, it should be possible to generate libraries of functionalised NPs for preparing SC-ISEs with improved characteristics over equivalent electrodes that depend solely on the chemistry of the PVC capping layer.

5.4 Conclusions

The use of functionalised Au-NPs as solid-contact layer in ISEs opens the possibility of versatile tailoring of the properties of ISEs such as sensitivity, limit of detection, water uptake and batch-reproducibility. This study highlights the importance of matching the functionalising group of Au-NPs to the target ion, with particular attention on the role played by the SC in the development of low-cost solid-state ISEs compatible with high volume production fabrication technologies. Such low-cost, solid state sensors, particularly when coupled with relatively low limits of detection and simple analytical

[5.a] We estimate the concentration of –COOH groups in the SC layer to be ~0.95 M [36] using data from the elemental analysis [23] for a SC of 2000 theoretical monolayers.

procedures, could open up hitherto inaccessible applications in environmental (e.g. Pb^{2+}) or personal health (e.g. Na^{+}) monitoring (e.g. wearable sensor) applications.

5.5 References

[1] E. Bakker, P. Bühlmann, E. Pretsch, Carrier-based ion-selective electrodes and bulk optodes. 1. General characteristics, Chemical Reviews, 97(1997) 3083-132.

[2] E. Bakker, E. Pretsch, P. Bühlmann, Selectivity of potentiometric ion sensors, Analytical Chemistry, 72(2000) 1127-33.

[3] A. Michalska, All solid‐state ion selective and all solid‐state reference electrodes, Electroanalysis, 24(2012) 1253-65.

[4] D. Diamond, Internet-Scale Sensing, Analytical Chemistry, 76(2004) 278 A-86 A.

[5] C. Zuliani, G. Matzeu, D. Diamond, A potentiometric disposable sensor strip for measuring pH in saliva, Electrochimica Acta, 132(2014) 292-6.

[6] J. Bobacka, M. McCarrick, A. Lewenstam, A. Ivaska, All solid-state poly (vinyl chloride) membrane ion-selective electrodes with poly (3-octylthiophene) solid internal contact, Analyst, 119(1994) 1985-91.

[7] M. Vázquez, J. Bobacka, A. Ivaska, A. Lewenstam, Influence of oxygen and carbon dioxide on the electrochemical stability of poly (3, 4-ethylenedioxythiophene) used as ion-to-electron transducer in all-solid-state ion-selective electrodes, Sensors and Actuators B: Chemical, 82(2002) 7-13.

[8] T. Lindfors, A. Ivaska, Stability of the inner polyaniline solid contact layer in all-solid-state K^+-selective electrodes based on plasticized poly (vinyl chloride), Analytical Chemistry, 76(2004) 4387-94.

[9] J. Sutter, E. Pretsch, Response behavior of poly (vinyl chloride) and polyurethane-based Ca^{2+}-selective membrane electrodes with polypyrrole-and poly (3-octylthiophene)-mediated internal solid contact, Electroanalysis, 18(2006) 19-25.

[10] A. Cadogan, Z. Gao, A. Lewenstam, A. Ivaska, D. Diamond, All-solid-state sodium-selective electrode based on a calixarene ionophore in a poly (vinyl chloride) membrane with a polypyrrole solid contact, Analytical Chemistry, 64(1992) 2496-501.

[11] J. Bobacka, Conducting polymer-based solid-state ion-selective electrodes, Electroanalysis, 18(2006) 7-18.

[12] G.A. Crespo, S. Macho, J. Bobacka, F.X. Rius, Transduction mechanism of carbon nanotubes in solid-contact ion-selective electrodes, Analytical Chemistry, 81(2009) 676-81.

[13] E. Jaworska, W. Lewandowski, J. Mieczkowski, K. Maksymiuk, A. Michalska, Simple and disposable potentiometric sensors based on graphene or multi-walled carbon nanotubes–carbon–plastic potentiometric sensors, Analyst, 138(2013) 2363-71.

[14] E. Jaworska, M. Wójcik, A. Kisiel, J. Mieczkowski, A. Michalska, Gold nanoparticles solid contact for ion-selective electrodes of highly stable potential readings, Talanta, 85(2011) 1986-9.

[15] E. Woznica, M.M. Wojcik, J. Mieczkowski, K. Maksymiuk, A. Michalska, Dithizone modified gold nanoparticles films as solid contact for Cu^{2+} ion-selective electrodes, Electroanalysis, 25(2013) 141-6.

[16] B. Pejcic, R. De Marco, Impedance spectroscopy: over 35 years of electrochemical sensor optimization, Electrochimica Acta, 51(2006) 6217-29.

[17] J.-P. Veder, R. De Marco, G. Clarke, R. Chester, A. Nelson, K. Prince, et al., Elimination of undesirable water layers in solid-contact polymeric ion-selective electrodes, Analytical Chemistry, 80(2008) 6731-40.

[18] G. Matzeu, C. Zuliani, D. Diamond, Recent progress in disposable ion-selective sensors for environmental applications, Advances in Science and Technology, 77(2013) 65-70.

[19] C. Zuliani, D. Diamond, Opportunities and challenges of using ion-selective electrodes in environmental monitoring and wearable sensors, Electrochimica Acta, 84(2012) 29-34.

[20] P.B. Davis, U. Yasothan, P. Kirkpatrick, Ivacaftor, Nature Reviews Drug Discovery, 11(2012) 349-50.

[21] H. Zhou, F. Du, X. Li, B. Zhang, W. Li, B. Yan, Characterization of organic molecules attached to gold nanoparticle surface using high resolution magic angle spinning 1H NMR, The Journal of Physical Chemistry C, 112(2008) 19360-6.

[22] P.S. Jensen, Q. Chi, F.B. Grumsen, J.M. Abad, A. Horsewell, D.J. Schiffrin, et al., Gold nanoparticle assisted assembly of a heme protein for enhancement of long-range interfacial electron transfer, The Journal of Physical Chemistry C, 111(2007) 6124-32.

[23] W. Hou, M. Dasog, R.W. Scott, Probing the relative stability of thiolate-and dithiolate-protected Au monolayer-protected clusters, Langmuir, 25(2009) 12954-61.

[24] R.H. Terrill, T.A. Postlethwaite, C.-h. Chen, C.-D. Poon, A. Terzis, A. Chen, et al., Monolayers in three dimensions: NMR, SAXS, thermal, and electron hopping studies of alkanethiol stabilized gold clusters, Journal of the American Chemical Society, 117(1995) 12537-48.

[25] B. Schazmann, D. Morris, C. Slater, S. Beirne, C. Fay, R. Reuveny, et al., A wearable electrochemical sensor for the real-time measurement of sweat sodium concentration, Analytical Methods, 2(2010) 342-8.

[26] S. Anastasova, A. Radu, G. Matzeu, C. Zuliani, U. Mattinen, J. Bobacka, et al., Disposable solid-contact ion-selective electrodes for environmental monitoring of lead with ppb limit-of-detection, Electrochimica Acta, 73(2012) 93-7.

[27] E. Lindner, B.D. Pendley, A tutorial on the application of ion-selective electrode potentiometry: an analytical method with unique qualities, unexplored opportunities and potential pitfalls; Tutorial, Analytica Chimica Acta, 762(2013) 1-13.

[28] R. De Marco, J.P. Veder, G. Clarke, A. Nelson, K. Prince, E. Pretsch, et al., Evidence of a water layer in solid-contact polymeric ion sensors, Physical Chemistry Chemical Physics, 10(2008) 73-6.

[29] E. Lindner, R.E. Gyurcsányi, Quality control criteria for solid-contact, solvent polymeric membrane ion-selective electrodes, Journal of Solid State Electrochemistry, 13(2009) 51-68.

[30] Y. Wang, A.E. Kaifer, Interfacial molecular recognition binding of ferrocenecarboxylate to β-aminocyclodextrin hosts electrostatically immobilized on a thioctic acid monolayer, The Journal of Physical Chemistry B, 102(1998) 9922-7.

[31] P. Gilli, L. Pretto, V. Bertolasi, G. Gilli, Predicting hydrogen-bond strengths from acid−base molecular properties. The pKa slide rule: toward the solution of a long-lasting problem, Accounts of Chemical Research, 42(2008) 33-44.

[32] http://water.epa.gov/drink/contaminants/basicinformation/lead.cfm, Accessed on: 28 April 2015

[33]http://ec.europa.eu/health/scientific_committees/environmental_risks/docs/scher_o_128.pdf, Accessed on: 28 April 2015

[34] G. Lisak, J. Bobacka, A. Lewenstam, Recovery of nanomolar detection limit of solid-contact lead (II)-selective electrodes by electrode conditioning, Journal of Solid State Electrochemistry, 16(2012) 2983-91.

[35] http://www.irishtimes.com/news/environment/hundreds-of-householders-told-not-to-drink-lead-water-1.1884166, Accessed on: 28 April 2015

[36] S. Krause, Impedance methods, in: P. Unwin (Ed.) Encyclopedia of Electrochemistry, Wiley-vch2003, pp. 196-229.

[37] A. Radu, S. Anastasova-Ivanova, B. Paczosa-Bator, M. Danielewski, J. Bobacka, A. Lewenstam, et al., Diagnostic of functionality of polymer membrane–based ion selective electrodes by impedance spectroscopy, Analytical Methods, 2(2010) 1490-8.

[38] A.C. Templeton, W.P. Wuelfing, R.W. Murray, Monolayer-protected cluster molecules, Accounts of Chemical Research, 33(2000) 27-36.

[39] http://www.drugbank.ca/drugs/DB00166, Accessed on: 28 April 2015

[40] http://www.ecmdb.ca/compounds/ECMDB00962, Accessed on: 28 April 2015

[41] T. Sokalski, T. Zwickl, E. Bakker, E. Pretsch, Lowering the detection limit of solvent polymeric ion-selective electrodes. 1. Modeling the influence of steady-state ion fluxes, Analytical Chemistry, 71(1999) 1204-9.

[42] A. Michalska, K. Maksymiuk, The influence of spontaneous charging/discharging of conducting polymer ion-to-electron transducer on potentiometric responses of all-solid-state calcium-selective electrodes, Journal of Electroanalytical Chemistry, 576(2005) 339-52.

[43] T. Sokalski, A. Ceresa, T. Zwickl, E. Pretsch, Large improvement of the lower detection limit of ion-selective polymer membrane electrodes, Journal of the American Chemical Society, 119(1997) 11347-8.

[44] R. Sardar, A.M. Funston, P. Mulvaney, R.W. Murray, Gold nanoparticles: past, present, and future, Langmuir, 25(2009) 13840-51.

Chapter 6.

An integrated sensing and wireless communications platform for sensing sodium in sweat

Giusy Matzeu[a], Conor O'Quigley[a], Eoghan McNamara[a], Claudio Zuliani[b], Cormac Fay[a], Thomas Glennon[a] and Dermot Diamond*[a]

Submitted to Analytical Methods

*Corresponding author

[a]Insight Centre for Data Analytics, Dublin City University, Dublin 9, Ireland.

[b]Department of Electrical and Electronic Engineering, Imperial College London, London SW7 2AZ, UK.

Aims and Objectives

After screening tests to identify the best material that can be used as solid-contact, all plastic potentiometric strips were realised to monitor Na^+ variations. They were then integrated in microfluidic devices ad hoc developed and optimised. The PotMicroChips were then connected to a miniaturised electronic platform integrated within a 3D printed encasing in a wearable configuration that allowed real-time monitoring of Na^+ levels in sweat.

Contributions

- Design, conception and optimisation of experimental trials.

- Analysis of data and writing up of the manuscript.

Abstract

Being able to non-invasively monitor sodium levels in sweat is of outmost importance. Sodium is one of the preferred markers to diagnose and track the progression of Cystic Fibrosis, and the knowledge of sodium levels could potentially enable personalised hydration strategies for athletes under effort or militaries in unfavourable environmental conditions. Here we present our approach to the realisation of disposable potentiometric strips that allow measuring sodium in sweat samples. Our platform consisted of a Solid-Contact Ion-Selective Electrode (SC-ISE) for Na^+ detection and of a liquid-junction-free Reference Electrode (RE), combined together on a dual screen-printed substrate. Poly-3,4-ethylenedioxythiophene (PEDOT) based films were tested as solid-contact, showing a significant impact on sensor characteristics such as sensitivity (i.e. differing from sub-Nernstian to Nernstian), dynamic range (10^{-5}-$10^{-2.5}$ or 10^{-5}-10^{-1} a_{Na^+}), and especially within-batch reproducibility. The SC-ISE/RE combination was integrated onto a microfluidic chip that was tested and optimised via on-bench trials. The Potentiometric Microfluidic Chip (PotMicroChip) was then connected to a wireless electronic platform (Mote) to realise a wearable device whose performance was assessed during real-time stationary cycling sessions.

Keywords

Screen-printed Potentiometric Platforms, Solid-Contact Ion-Selective Electrodes, Microfluidics, Sweat, Wearable Devices

6.1 Introduction

Though Solid-Contact Ion-Selective Electrodes (SC-ISEs) have been used for many years as sensors for blood electrolyte analysis, their mode of operation makes them suitable for "single shot" devices that can be discarded after a single measurement is made. In recent years, driven by several improvements in SC-ISEs overall performance, interest has increasingly been focused on their integration within wearable applications. For this purpose, SC-ISEs should guarantee reliable continuous monitoring for extended periods of time. The stability of the sensors, that is the ability to maintain unaltered calibration parameters, is fundamental as it allows for accurate estimations of ion concentrations when analysing the overall cell potential. Stability has therefore understandably been the focus of several research activities over the past 10-15 years [1-4]. Many studies have targeted the solid-contact material, since this layer controls the stability of the potentiometric signal and affects the dynamic range of the ISE [1, 4-8]. Carbon nanostructured materials like three dimensional ordered mesoporous carbon structures (3DOM) [9] and colloidal imprinted mesoporous carbon (CIM) [10], together with carbon cloth [11], carbon nanotubes [12-14] and graphene [15] have received special attention. Their hydrophobicity seems to improve the adhesion of the membrane and limits water uptake and aqueous layer formation at the inner SC/electrode interface.

Furthermore, conducting polymers (CPs) have been suggested to produce effective solid-contacts [4]. Particular attention was devoted to poly(3-octylthiophene) (POT) [16-18] thanks to its hydrophobicity. However, manual drop casting and the possibility of re-dissolution during capping membrane deposition [19] are significant drawbacks, as these factors can lead to poor reproducibility. Electropolymerisation seems to be an attractive method to generate more reproducible SC layers, as the films can be grown on a variety of substrates under highly controlled conditions. The use of Ionic Liquids (ILs) as electropolymerisation media, rather than aqueous or organic electrolyte solutions, may offer interesting ways to impart particular properties to the CP film in terms of conductivity, electrochemical stability and mechanical features [20]. For instance, the hydrophobicity of the CP layer and the possibility of a water layer building-up at this interface might be regulated through the choice of the IL. This approach has been minimally addressed in the literature, perhaps because the polymer growth is hampered by certain ILs. For instance, Danielsson et al. [21] observed that electrodeposition of poly-3,4-ethylenedioxythiophene (PEDOT) films was largely

hindered in butyl-3-methyl-imidazolium [bmim] diethylene glycol monomethyl ethersulfate [$MDEGSO_4$] but occurred in [bmim] octyl sulfate [$OctSO_4$]. This is indeed the layer that should affect most of the batch reproducibility while the membrane drop casting would have almost no significant influence on the overall performance of the sensor.

If optimisation studies are of fundamental importance when realising working electrodes, reliable solid-contact miniaturised reference electrodes are the other component of the galvanic cell that needs to be optimised (e.g. when aiming at the implementation of wearable applications). There have been some reports on the combination of SC-ISEs with solid-contact reference electrodes to realise low-cost potentiometric combination sensor 'strips' for monitoring K^+ [13, 22] and pH [23] levels in biological samples such as saliva. However, the completion of functionalised fabrics (e.g. to estimate pH, K^+, and NH_4^+, just tested on the bench) [24] or sensitised tattoo transferred on skin (e.g. to detect ammonium, pH, Na^+ and lactate) [25] represent important achievements in the integration of chemical sensors into wearable designs (e.g. allowing for non-invasive monitoring).

The approach here presented for real-time detection of Na^+ in sweat is different. First, optimisation studies of the solid-contact material for Na^+ ISEs showed that conducting polymers based on PEDOT affect the response characteristics, i.e., sensitivity, dynamic range, and within-batch reproducibility of sensors. PEDOT grown in 1-ethyl-3-methylimidazolium bis(trifluoromethanesulfonyl)imide [emim][NTf_2] seemed to offer the best compromise. All plastic potentiometric strips were then realised with a dual electrode configuration based on solid-contact working and reference electrodes. Furthermore, they were integrated into a microfluidic chip, able to drive the fluid and allow for interaction between the sample and the sensitive area, thanks to a special configuration that behaves as a passive pump. After on bench trials, this Potentiometric Microfluidic Chip (PotMicroChip) was connected to a Macroduct® (slightly modified to fulfil the constraints of the platform here presented) used to harvest sweat samples. The connection to the wireless electronic platform (Mote) finally enabled the implementation of a wearable device able to monitor in real-time sodium variations of volunteers undergoing stationary cycling sessions.

6.2 Experimental

6.2.1 Materials

C2030519P4 and D50706D2 from Gwent Inc. (Pontypool, UK) were used respectively as carbon and dielectric ink in the preparation of the screen-printed electrodes. 175 μm thick PET sheets by HiFi (Dublin, Ireland) were used without further treatment. 80 μm pressure-sensitive adhesive (PSA-AR9808) by Adhesives Research (Ireland), 500 and 1500 μm poly(methylmethacrilate) (PMMA) from GoodFellow (UK) were used for the realisation of the microfluidic chip layers. A nozzle (BDML210-9 from Value-Plastic, USA) was used as connector (i.e. preliminary design) between the microfluidic chip and the peristaltic pump or modified Macroduct® (Accuscience, Dublin). Highly absorbent material (Sponge Cloths from Dunnes Stores, Dublin, Ireland), cotton (Verbandwatten from Van Heek Medical, Lasser, Holland) and cotton threads removed from medical bandages (W.O.W. Bandage BP, 5 cm x 5 cm) were used to realise the passive pump system inserted in the microfluidic chip. Potassium and sodium chloride, hydrochloric acid, potassium ferricyanide (III) (99%), iron (III) chloride hexahydrate, 3,4-ethylenedioxythiophene (EDOT, 97%), high molecular weight poly(vinyl chloride) (PVC), tetrahydrofuran (THF, ≥99.5%), 4-tert-butylcalix[4]arene-tetraacetic acid tetraethyl ester (sodium ionophore X), potassium tetrakis(4-chlorophenyl)borate (KTFPB), bis(2-ethylhexyl) sebacate, 2,2-dimethoxy-2-phenylacetophenone (DMPA, >99%), butyl-acrylate (>99%) and 1,6-hexanediol diacrylate (HDDA, 80%) were purchased from Sigma-Aldrich (Dublin, Ireland). When possible, they were of selectophore grade. N-decyl-methacrylate was obtained from Polysciences (Northampton, UK). 1-ethyl-3-methylimidazolium bis(trifluoromethanesulfonyl)imide [emim][NTf_2], [emim] tris(pentafluoroethyl)trifluorophosphate [FAP] and 1-hexyl-3-methylimidazolium [hmim] [FAP] were obtained from VWR (Dublin, Ireland). All the chemicals were used without any further purification. Adhesive poly-foam strips (employed for the preparation of gaskets) were obtained from Radionics (Ireland). FFC-FPC Molex connectors (gold contacts, 14 ways from Farnell, Ireland) were used to plug the potentiometric strip. Deionised water with resistivity of 18.2 MΩ cm obtained with a Milli-Q reagent-grade water system was used for making all aqueous solutions.

6.2.2 Na^+ ISEs

All screen-printed electrodes (SPEs) were realised using a DEK 248 printer, as previously reported [23], in a combined configuration on PET substrates (see Figure 6.1 (a)). To prepare the conducting polymer SC film, EDOT solutions were first vortexed

for ~1 hour to facilitate solubilisation. PEDOT was deposited electrochemically directly on the carbon electrodes from a 0.05 M EDOT solution in pure [emim][FAP], or [emim][NTf_2], or in aqueous 0.1 M KCl. Deposition was accomplished using cyclic voltammetry by scanning the potential 25 times from 0 to 1.0 V vs Ag wire with a scan rate of 50 mV/s. Alternatively, potentiostatic depositions were achieved applying a constant potential of 1.0 V vs. Ag wire (EDOT in IL solutions) or vs. Ag/AgCl reference electrode (EDOT in KCl solution) for 900 seconds. A PEDOT/Prussian Blue (PB) composite was also tested as solid-contact material. The composite deposition was carried out following the procedure previously reported by Lupu et al. [22]. A total of 26.25 µL Na^+ selective membrane material dissolved in THF [26] was drop-cast on top of the solid-contact PEDOT layer in the following sequence: 1 µL (once); 1.5 µL (3 times); 2.5 µL (3 times); 3 µL (twice); 3.25 µL (once) and 4 µL (once). When realising the PotMicroChip, because of the larger diameter of the gasket (3.6 mm), a total of 65 µL of Na^+ selective membrane were drop-cast in the following sequence: 4 µL (11 times); 3 µL (5 times) and 2 µL (3 times). After each addition, the Na^+ selective membrane solution was allowed to dry for 20 minutes before the next addition. All the resulting Na^+ SC-ISEs were conditioned overnight in a 10 mM NaCl solution prior their calibration with NaCl solutions of increasing concentrations. The SCI-REs were prepared as elsewhere reported [19].

6.2.3 Microfluidic Chip Realisation

The microfluidic chip was made up of 7 layers, as shown in Figure 6.1 (b), with the PSA and PMMA layers cut via a CO_2 laser ablation system. The first PET layer contained the screen-printed electrodes, where 80 µm thick PSA (2nd layer), followed by 500 µm thick PMMA (3rd layer) were rolled on top. The RE membrane was photopolymerised following the procedure described by Zuliani et al. [19], followed by the drop casting of the Na^+ membrane on the other electrode (as described in Section 6.2.2). 80 µm thick PSA was then put on top (4th layer), creating a µchannel between the two electrodes (see Figure 6.1 (b)), followed by a 1.5 mm thick layer of PMMA (5th layer) rolled on top. The highly absorbent material (that underwent through a washing step with deionised water to remove any surfactant or ionic impurities, and was then dried at 65°C) was punched with the specular configuration of the 5th layer, to cover the electrodes and fill the channel. A PSA layer was transferred on top (6th layer, see Figure 6.1 (b)) and an additional PMMA layer of 1.5 mm (7th layer) was rolled on top to enclose the system.

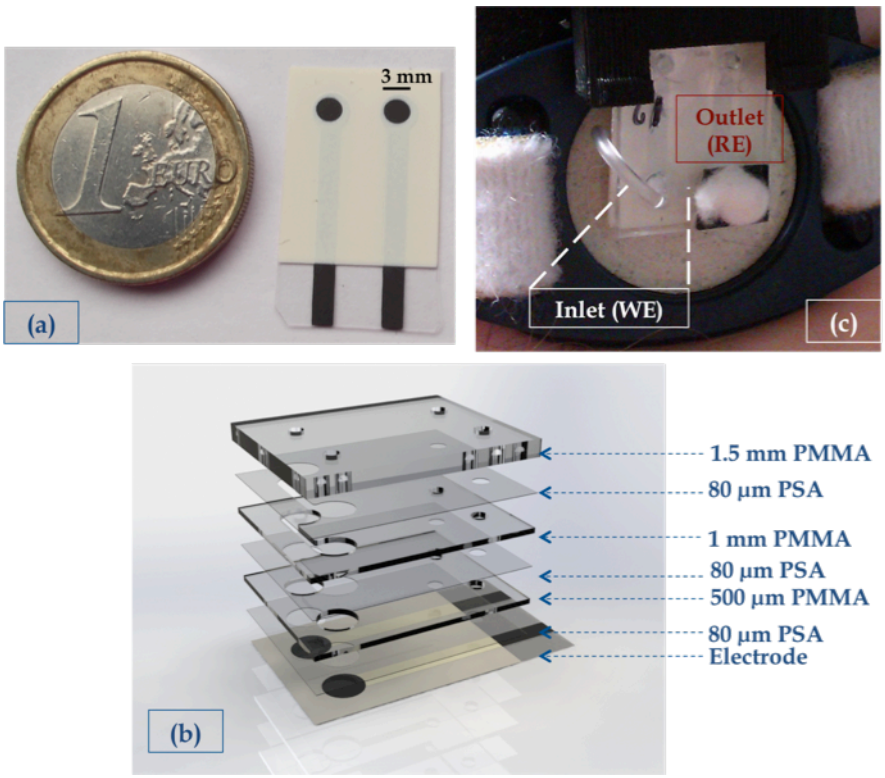

Figure 6. 1: (a) Dual screen-printed electrodes on a PET substrate and (b) different layers employed to build up the microfluidics collecting system. (c) Enlargement of the PotMicroChip showing the inlet (on top of the working electrode) and the outlet (on top of the reference electrode) characterised by a reservoir containing a highly absorbent material.

The 7th layer was characterised by 2 holes through which a cotton thread was inserted (after being washed and dried like the highly absorbent material) to assist fluid movement into the microfluidic chip. The hole located in correspondence of the working electrode was the inlet of the system, connected to the Macroduct® (see Figure 6.1 (c)). The other was the outlet, and was covered by a punched poly-foam strip that worked as a reservoir filled with highly absorbent material (cotton bud, see Figure 6.1 (c)). This section was the ending part of the passive pump, which soaked up the sample delivered by the microfluidic chip. After removal, it can be employed to quantify and compare the Na^+ levels obtained via standard analytical techniques with the ones measured using PotMicroChips.

6.2.4 Real-time Cycling Sessions

Healthy active male athletes participated in indoor cycling sweat trials (average room temperature of 22°C) using a cycle ergometer (Monark Exercise, Sweden) at an intensity load high enough to induce sweating, which was selected by the volunteer. A

PotMicroChip was positioned on the upper left arm (the sampling area was first cleaned with alcohol swabs and deionised water) by means of Velcro® straps. The external forearm was selected as the primary sampling location since it provided a relatively flat surface to secure the collecting device (see Figure 6.2).

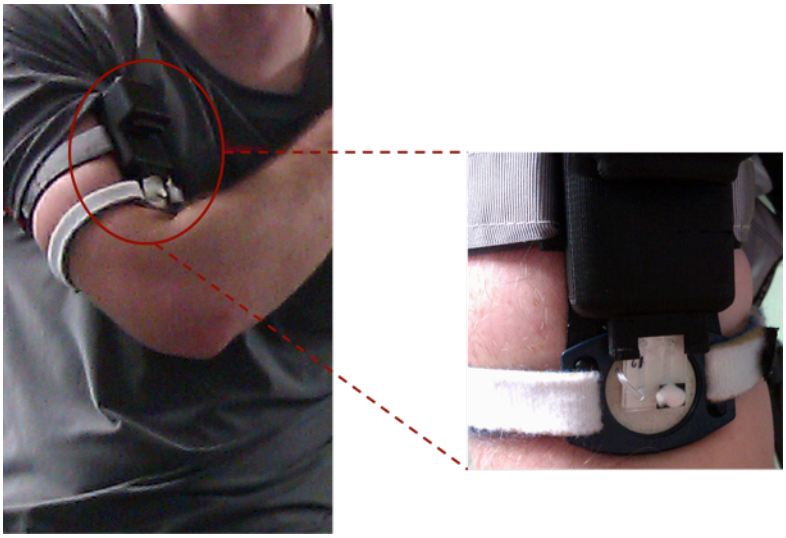

Figure 6. 2: PotMicroChip connected to the Mote and positioned on the upper arm via Velcro® straps and enlargement of the sensing microfluidic area as it is during stationary cycling sessions.

Trials were stopped when the athlete was no longer capable of maintaining the set intensity load.

6.2.5 Instrumentation and Software

The potentiometric measurements were recorded using an EMF-16 channels system from Lawson Labs (USA), along with an in-house made silver/silver chloride (saturated KCl) or double-junction Ag/AgCl reference electrode (Sigma Aldrich, Dublin), for conditioning and testing, respectively. Electropolymerisation was achieved using a CHI760D potentiostat (CH-instruments, USA). Photo-polymerisation of the acrylate monomers (i.e. for the realisation of reference electrodes) was obtained using the CL-1000 ultraviolet cross-linker UVP. The CO_2 laser ablation system was an Epilog Zing Laser Engraver (Epilog, USA) whereas the thermal roller laminator (Titan-110) was from GBC Films (USA). A peristaltic pump (Ismatec Reglo ICC from IDEX Wertheim, Germany) was used at a constant flow rate (0.2 mL/min) to test PotMicroChips on the bench. The wirelesss electronic platform (Mote) was developed by the Tyndall National Institute, Cork, Ireland, as previously described by O'Flynn et

al. [27]. The Mote stack consisted of 3 layers: a lithium polymer rechargeable 950 mAh battery, a ZigBee transceiver and a customised ISE interfacing layer. The mote measured the differential input analogue voltage (potentiometric bias) with a variable gain through high-input impedance and converted it to a digital signal through the ADC component. The digital signal was then wirelessly transmitted to a base-station (see [27] for more details). A PotMicroChip was connected to the Mote (and encapsulated in a 3D printed encasing) via a simple push-in socket (Molex FFC-FPC) and was calibrated in 2 sessions (using 10^{-5} M, 10^{-3} M and 10^{-1} M NaCl solutions) both before and after real-time measurements. Following real-time measurements, the sweat Na^+ levels were interpolated from calibration curves recorded after real-time cycling sessions.

6.3 Results and Discussion

6.3.1 Solid-Contact Na^+ ISEs

As a first assessment of the device performance, we evaluated the impact of the solid-contact materials on the resulting Na^+ SC-ISEs electrodes in terms of sensitivity, dynamic range and sensor batch reproducibility (see Table 6.1). The overall behaviour of sensors having a PEDOT solid-contact layer (electrodeposited from aqueous KCl) was linear (R^2>0.98) within the Na^+ activity range between 10^{-5} and 10^{-1}, with an average slope and offset of 55.5 mV/loga_{Na^+} and 474.8 mV (n=3), respectively. The standard deviations of slope and offset extrapolated from the averaged calibration curve were quite large, i.e., 4.9 mV/loga_{Na^+} and 23.1 mV, respectively. Improving the within-batch reproducibility of the Na^+ SC-ISE is a key step to obtain sensors that can be employed without further calibration. For instance, highly reproducible sensors would be ideal for use in the field of sport sciences (e.g. for body fluid analysis) because of the limited time available to screen exercising athletes, and of the advantages benefit of real-time monitoring using disposable sensors. It seems, therefore, that PEDOT electrodeposited from KCl aqueous solution (see Table 6.1) was not suitable to prepare sensors with these properties.

PEDOT/PB [22] is an organic/inorganic composite material with potentially superior performances due to the well-defined potential of the PB redox couple. Sensors provided with the PEDOT/PB film as SC-layer showed that the calibration trends are linear (R^2>0.98) within the 10^{-5}-10^{-1} Na^+ activity range. By averaging the calibration curves, the slope and offset values were found to be equal to 53.4±3.0 mV/loga_{Na^+} and

524.1±14.4 mV (n=4), respectively (see Table 6.1). Although the standard deviations were smaller than the ones obtained with a PEDOT SC-layer grown from aqueous KCl, they were yet too large compared to the desired levels of reproducibility. These differences dictate the requirement for at least one point calibration before use and the need for further screening of other types of materials to be used as solid-contacts.

Table 6. 1: Dynamic range, slope and offset listed to describe the performance of Na^+ ISEs realised using different materials as solid-contact: Pedot grown in aqueous KCl (PedotKCl); the organic/inorganic composite of Pedot and Prussian Blue (PedotPB); Pedot grown in an Ionic Liquid media such as [emim][FAP] or [emim][NTf_2].

Solid Contact	Dynamic Range (M)	Slope (mV/loga_{Na^+})	Offset (mV)
Pedot(KCl) (n=3)	10^{-5}-10^{-1}	55.5±4.9	474.8±23.1
Pedot(PB) (n=4)	10^{-5}-10^{-1}	53.4±3.0	524.1±14.4
Pedot[emim][FAP] (n=3)	10^{-5}-$10^{-2.5}$	40.6±2.4	235.2±12.4
Pedot[emim][NTf_2] (n=4)	10^{-5}-10^{-1}	53.1±0.8	525.5±3.6

ILs employed as media for the SC-layer electropolymerisation might provide new means to tailor the physico-chemical properties of this layer [20]. For instance, ILs have a low-water content and therefore provide a water-free environment during the CP electrodeposition. In addition, since water can percolate through the membrane during the sensor operation time, the incorporation of the IL within the SC-layer may hinder the formation of a water-layer at the SC/membrane interface in relation to the IL hydrophobicity. By electrodepositing PEDOT from ILs, we speculated that the water uptake within the sensors would be reduced and that perhaps this factor may help improving the sensor batch reproducibility. [emim][FAP] and [emim][NTf_2] were selected for this purpose since these ILs have very different physico-chemical properties (e.g. viscosity and conductivity). PEDOT films electrodeposited using these two ILs showed very different morphologies (as previously discussed in Chapter 3 [19]).

Na^+ SC-ISEs prepared with a PEDOT SC-layer potentiodynamically deposited from [emim][FAP] were characterised by a markedly sub-Nernstian average calibration slope (40.6±2.4 mV/loga_{Na^+}, n=3) and the linear dynamic range was between 10^{-5} and $10^{-2.5}$. Figure 6.3 presents the calibration curve obtained with sensors having a PEDOT SC-layer potentiostatically electrodeposited from [emim][NTf_2]. The trends are linear

(R^2>0.99) within the Na^+ activity range 10^{-5}-10^{-1} and the average values of the slope and offset are 53.1±0.8 mV/$loga_{Na^+}$ and 525.5±3.6 mV, respectively (n=4) (see Table 6.1). For instance, a significant decrease in the standard deviation values of the slope and offset was recorded. The improved batch reproducibility likely arose from the type of solid-contact layer employed since the Na^+ ion-selective membrane was the same in all cases. Additionally, the ISEs were characterised by a drift of -0.04±0.01 mV/min, measured over 4 hours.

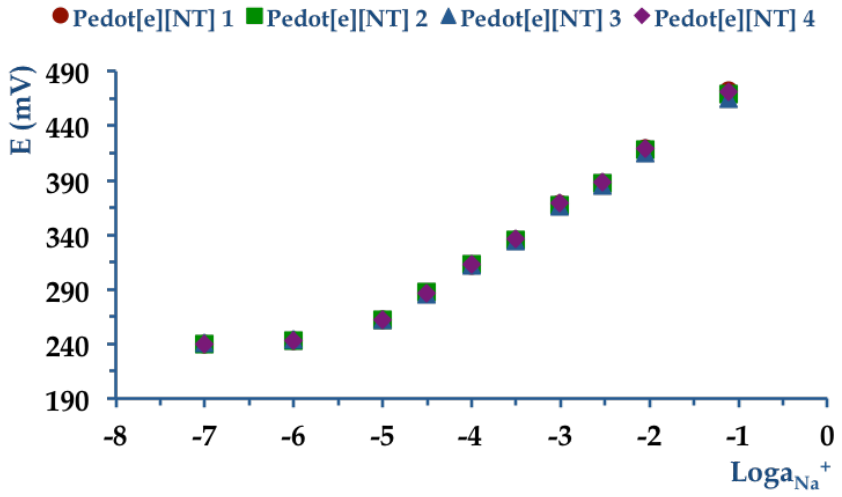

Figure 6. 3: Calibration curves of Na^+ ISEs with a solid-contact made of Pedot potentiostatically grown in [emim][NTf_2] (●, ■, ▲, ♦), n=4. The electrodes were conditioned overnight in 10 mM NaCl before the calibration was performed. For convenience, the plots were normalised to responses at a Na^+ activity of 10^{-5} M.

Thus, [emim][NTf_2] seemed to confer better properties to the solid-contact when compared to KCl or potassium ferricyanide (used for the PEDOT/PB composite preparation). Most likely, this result was achieved not only by avoiding the presence of water during the CP polymerisation process, but also, perhaps, by hampering or slowing down the CP de-doping process. Furthermore, the insertion/expulsion of ions during the redox activity change of the CP depends on the bulkiness and physico-chemical nature of these ions [20, 28]. It is noteworthy that Bobacka et al. [29] observed that anions entrapped in the PEDOT backbone affected the drift of the potential in K^+ SC-ISEs. In addition, Michalska et al. [30, 31] reported that spontaneous charging/discharging may occur at the CP layer underlying that a PVC based ion-selective membrane in turn affects the response pattern of the sensor.

The optimised Na^+ ISEs were combined with a Solid-Contact Ionogel Reference Electrode (SCI-RE) to realise a disposable potentiometric strip. In this strip, the SC layers were deposited at once on both electrodes and the SC-ISE and SCI-RE differed only for the capping membrane.

6.3.2 Realisation and Testing of PotMicroChips

Following the optimisation of the potentiometric platform, we worked to build a system able to deliver the sample to the electrodes. The microfluidic device adopted during the first trials is shown in Figure AD.1 (a) within the Appendix D. The inlet of the platform was connected via nozzle to a benchtop peristaltic pump whereas the electrodes were inserted in the Molex FFC-FPC, which was electrically connected to the Mote (see Figure AD.1 (b) for the experimental set up in the Appendix D). The difference of potential was wirelessly measured for a 3 points calibration (i.e. concentrations of 10^{-5}, 10^{-3} and 10^{-1} M NaCl) (see Figure AD.1 (c)), at a constant flow rate (0.2 mL/min). The calibration slope was subnernstian (43.9 mV/loga_{Na^+}) but suitable for real-time monitoring. However, after the device was connected to the modified Macroduct® via the sampling nozzle and positioned on the upper arm of a volunteer (see Figure AD.2 (a)), we observed that sweat was not able to get to the microfluidic chip. The system was not able to sample the sweat, and this failure was likely due to the high surface tension generated at the interface between the Macroduct® tubing and the nozzle. The recorded signal showed a characteristic flat line with spikes accounting for spurious noise (see Figure AD.2 (b)).

These trials underlined the need for a system endowed at least with a passive pump, able to overcome the surface tension barriers to sample movement at the various interfaces. We thus adopted a strategy where a highly absorbent material was put in contact with the electrodes within the μchannel. Additionally, a cotton thread going from the inlet to the outlet, as already implemented in previous studies [32, 33], was used to assist fluid movement through the system through enhanced capillary forces and hydrophilicity (see Figure 6.4 (a)). A reservoir was finally positioned on top of the outlet, containing a hydrophilic cotton bud, which was the final element of the whole passive pump. The cotton bud provides a high capability for continuous transfer of water through the system, which in turn allows continuous real-time monitoring during cycling sessions, that might be coupled with subsequent validation measurements via standard analytical techniques to verify the Na^+ levels measured by the potentiometric platform (i.e. the bud can be removed and the amount of sweat and concentration of sodium measured using reference analytical techniques to give an

overall picture of the sweat sodium level). This configuration was first examined on the bench (see Figure 6.4 (a)), to assess its efficacy. It was then tested during real-time sessions using exercise bicycles that proved the feasibility of the microfluidic passive design (see Figure 6.4 (b)), as shown by the blue colour characterising the cotton thread and the cotton bud positioned at the outlet. Figure 6.4 (b) shows that the fluid is able to travel along the system, from the inlet to the outlet.

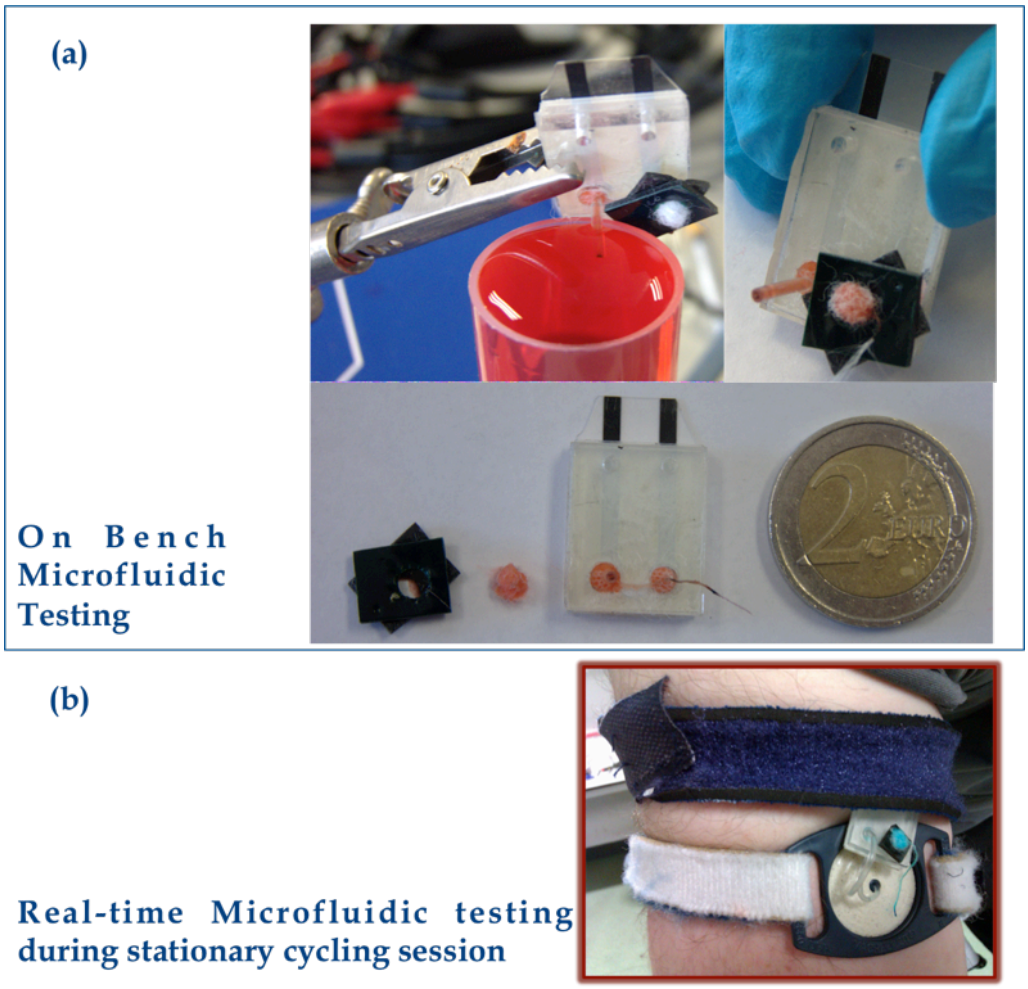

Figure 6. 4: PotMicroChip featured by a passive pump system integrated within the microfluidic channel and used to drive the fluid. (a) PotMicroChip tested on the bench (red solution passively harvested). (b) PotMicroChip tested during real-time stationary cycling sessions (i.e. blue dye that characterises sweat when harvested via an off-the-shelf Macroduct®).

It was then possible to test the performance of the fully integrated PotMicroChips platforms (i.e. potentiometric sensor, microfluidics and wireless electronics). The electrodes were conditioned in 10^{-2} M NaCl and then the microfluidic unit was mounted on top, and the system closed with the last PMMA layer. PotMicroChips

were first tested on the bench (i.e. in NaCl solutions of 10^{-5}, 10^{-3} and 10^{-1} M) in a concentration range consistent with real sweat samples (i.e. 10-60 mM and 65-90 mM for normal subjects and patients affected by Cystic Fibrosis, respectively). Figure 6.5 shows the average calibration of the PotMicroChips (n=3), characterised by a slight sub-nernstian behaviour (50.23±7.7 mV/loga_{Na^+}) in the range 10^{-3}-10^{-1} M.

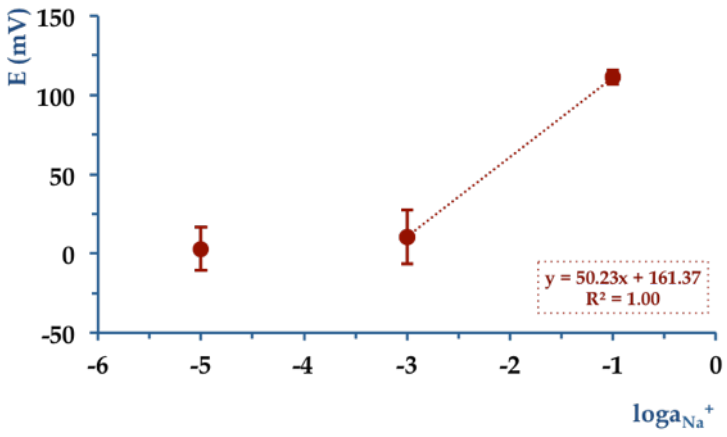

Figure 6. 5: Example of the average of an on-bench calibration of 3 PotMicroChips. The error bars represent the standard deviation.

Before their use to monitor sweat samples in real-time, the chips were flushed with deionised water to remove any ionic background. A PotMicroChip was then connected to the modified Macroduct®. The length of the tubing was shortened of 22.7 mm to allow for the connection with the top PMMA layer of the microfluidics and minimise the dead volume of the platform (i.e. decreased from 110.8 µL to 4.6 µL). The wearable device was finally positioned on the upper arm of volunteers. Figure 6.6 (a) shows real-time potential variations of PotMicroChips during cycling sessions and Figure 6.6 (b) the corresponding sodium levels (i.e. computed from calibration). The potential variations in Figure 6.6 (a) were characterised by a baseline value that described the environment in contact with the electrodes before the collected sample entered the µchannel (as indicated by the arrows). Both potentials were then featured by a rapid increase that occurred at different times, i.e., after nearly 20 minutes (see Figure 6.6 (a), left) and 8 minutes (see Figure 6.6 (a), right)), indicating that perspiration started at different stages in the two subjects (as suggested by previous studies [34]). The signal then reached a steady state within about 2 minutes (see Figure 6.6 (a), left) and 5 minutes (see Figure 6.6 (a), right), which more or less endured until the end of the trial.

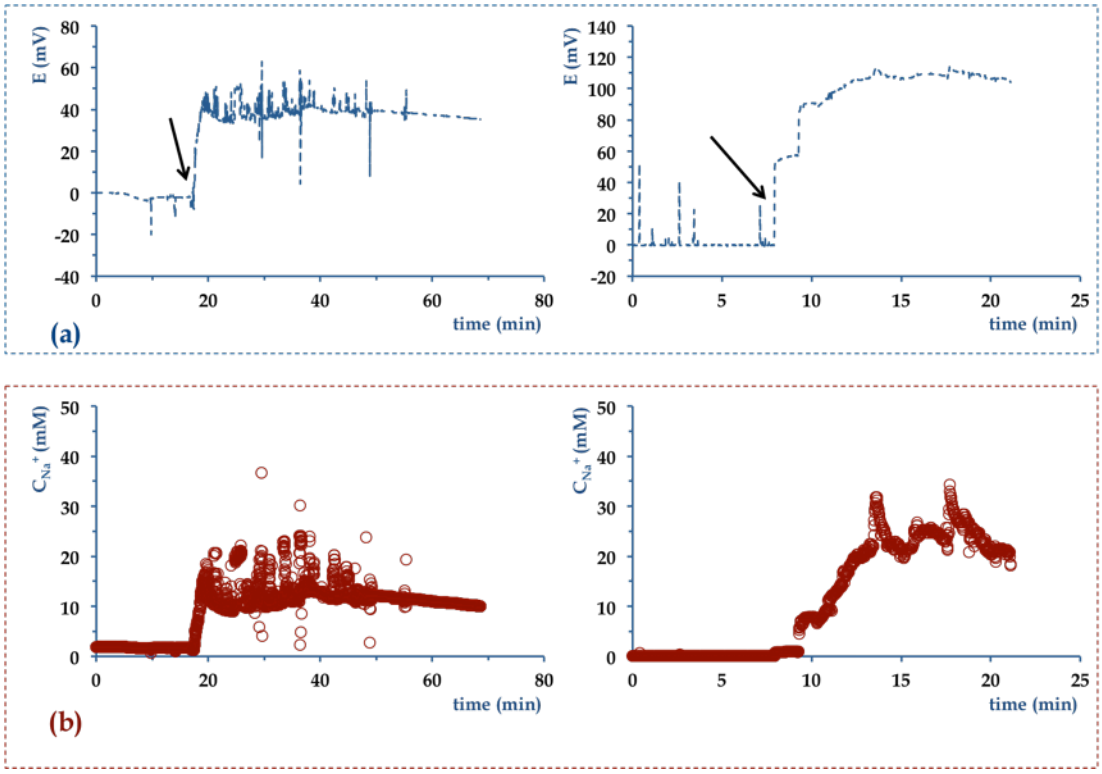

Figure 6. 6: Example of signal recorded in real-time during a stationary cycling session with the wearable device used to monitor Na^+ levels of two different volunteers. (a) shows real-time variations of potential vs time (e.g. the arrows indicate when sweat enters the PotMicroChip). (b) shows real-time changes of Na^+ concentrations vs time. The device was positioned as shown in Figure 6.2.

Figure 6.6 (b) shows real-time variations of Na^+ concentrations. When sweat started to be harvested by PotMicroChips, Na^+ levels increased for 2 minutes (see Figure 6.6 (b), left) and 5 minutes (Figure 6.6 (b), right). Thanks to previous work done by Buono et al. [35], we can speculate that enhancements in Na^+ levels might be related to contemporary augmented sweat rates, until a steady state was attained by both parameters. Na^+ levels then levelled off and reached average values of 10.3±0.2 mM (see Figure 6.6 (b), left) and 24.2±2.7 mM (see Figure 6.6 (b), right) (both of them within the normal physiologic range). Despite similarities on the overall trends, some differences can be noticed, e.g. in terms of time length, absolute values of Na^+ concentrations, etc. (see Figure 6.6). This was expected because diverse athletes (e.g. featured by different genetics, hydration, diet, heat acclimation, etc.) underwent through stationary cycling sessions. Additionally, different workloads were chosen during the trial, according to the fitness level of the volunteer.

Signals were however characterised by some spikes that represent spurious noise, maybe due to sudden vibrations of the wearer. The Mote was endowed with a 3D printed casing able to keep its position reasonably stable and fixed on the body, and minimising vibration of the internal circuitry.

All the trials were performed following the protocol here described (e.g. the average interpolated sodium concentration at the end of cycling sessions was 18.2±8.9 mM, (n=4)) and unique "over time sodium profiles" were recorded for each athlete. We were able to track the all trial, starting from the point of sweat harvested by PotMicroChips, and the subsequent changes in Na^+ levels.

This was possible thanks to the new wearable device here presented that allows monitoring wirelessly and in real-time variations of Na^+ in sweat samples. Due to the configuration that we implemented, issues related to biofouling are minimal, but the small amount of sample that can be collected with localised approaches is so far the main obstacle encountered. On-body continuous evaluation of sodium in sweat has potential applications in the field of sport sciences [2] or in the clinical practice to diagnose and treat cystic fibrosis (CF) patients [36, 37] or during acclimation studies [35].

In the future, PotMicroChip should be validated through wider trials where the detected Na^+ levels are compared with measurements obtained via standard analytical techniques (e.g. Atomic Absorption Spectroscopy or Ion Chromatography), or commercial sodium meters (e.g. AquaTwin®) [38] to bypass tedious sampling and post-treatment protocols. More insights of the physiological phenomena occurring during exercise sessions will be additionally obtained when Na^+ monitoring will be associated to the examination of sweat rate variations.

6.4 Conclusions

The performances of Na^+ ISEs were optimised after analysis of different solid-contact materials based on PEDOT grown in media of different ionic background. The solid-contact potentiometric strips were integrated with microfluidic chips (PotMicroChip) endowed with a passive pump system for the delivery of sweat samples. The system was encased together with a miniaturised electronic platform for wireless transmission and tested to monitor in real-time Na^+ levels in sweat of volunteers undergoing stationary cycling sessions. The work here presented paves the way for the realisation of novel PotMicroChips characterised by different configurations (e.g. miniaturised,

with a different arrangement of the electrodes, able to reduce movement artefacts, etc.) that will allow for their connection to a redesigned electronic platform. Future adaptations will involve moving the sampling location to the wrist for a novel watch-like device with reduced dimensions (see Chapter 8, section 8.2.1).

6.5 References

[1] J. Bobacka, A. Ivaska, Ion sensors with conducting polymers as ion-to-electron transducers, in: S. Alegret, A. Merkoçi (Eds.), Electrochemical Sensor Analysis, Elsevier 2007, pp. 72-81.

[2] C. Zuliani, D. Diamond, Opportunities and challenges of using ion-selective electrodes in environmental monitoring and wearable sensors, Electrochimica Acta, 84(2012) 29-34.

[3] S. Anastasova, A. Radu, G. Matzeu, C. Zuliani, U. Mattinen, J. Bobacka, et al., Disposable solid-contact ion-selective electrodes for environmental monitoring of lead with ppb limit-of-detection, Electrochimica Acta, 73(2012) 93-7.

[4] E. Lindner, R.E. Gyurcsányi, Quality control criteria for solid-contact, solvent polymeric membrane ion-selective electrodes, Journal of Solid State Electrochemistry, 13(2009) 51-68.

[5] J. Bobacka, A. Ivaska, A. Lewenstam, Potentiometric ion sensors, Chemical Reviews, 108(2008) 329-51.

[6] J. Bobacka, A. Ivaska, Chemical Sensors Based on Conducting Polymers, in: A.K. Cosnier (Ed.) Electropolymerisation Concepts, materials and Applications, Wiley-VCH, Weinheim, 2010, p. 173.

[7] T. Lindfors, L. Höfler, G. Jágerszki, R.E. Gyurcsányi, Hyphenated FT-IR-attenuated total reflection and electrochemical impedance spectroscopy technique to study the water uptake and potential stability of polymeric solid-contact ion-selective electrodes, Analytical Chemistry, 83(2011) 4902-8.

[8] J.-P. Veder, R. De Marco, G. Clarke, S.P. Jiang, K. Prince, E. Pretsch, et al., Water uptake in the hydrophilic poly (3, 4-ethylenedioxythiophene): poly (styrene sulfonate) solid-contact of all-solid-state polymeric ion-selective electrodes, Analyst, 136(2011) 3252-8.

[9] C.-Z. Lai, M.A. Fierke, A. Stein, P. Bühlmann, Ion-Selective Electrodes with Three-Dimensionally Ordered Macroporous Carbon as the Solid Contact, Analytical Chemistry, 79(2007) 4621-6.

[10] J. Hu, X.U. Zou, A. Stein, P. Bühlmann, Ion-Selective Electrodes with colloid-imprinted mesoporous carbon as solid contact, Analytical Chemistry, 86(2014) 7111-8.

[11] U. Mattinen, S. Rabiej, A. Lewenstam, J. Bobacka, Impedance study of the ion-to-electron transduction process for carbon cloth as solid-contact material in potentiometric ion sensors, Electrochimica Acta, 56(2011) 10683-7.

[12] T. Kakiuchi, T. Yoshimatsu, N. Nishi, New class of Ag/AgCl electrodes based on hydrophobic ionic liquid saturated with AgCl, Analytical Chemistry, 79(2007) 7187-91.

[13] F.X. Rius-Ruiz, G.A. Crespo, D. Bejarano-Nosas, P. Blondeau, J. Riu, F.X. Rius, Potentiometric strip cell based on carbon nanotubes as transducer layer: toward low-cost decentralized measurements, Analytical Chemistry, 83(2011) 8810-5.

[14] U. Guth, F. Gerlach, M. Decker, W. Oelßner, W. Vonau, Solid-state reference electrodes for potentiometric sensors, Journal of Solid State Electrochemistry, 13(2009) 27-39.

[15] R. Hernandez, J. Riu, J. Bobacka, C. Valles, P. Jimenez, A.M. Benito, et al., Reduced graphene oxide films as solid transducers in potentiometric all-solid-state ion-selective electrodes, The Journal of Physical Chemistry C, 116(2012) 22570-8.

[16] K.Y. Chumbimuni-Torres, N. Rubinova, A. Radu, L.T. Kubota, E. Bakker, Solid contact potentiometric sensors for trace level measurements, Analytical Chemistry, 78(2006) 1318-22.

[17] A. Radu, D. Diamond, Ion-selective electrodes in trace level analysis of heavy metals: Potentiometry for the XXI century, in: S. Alegret, A. Merkoçi (Eds.), Electrochemical Sensor Analysis, Elsevier, 2007 2007, pp. 25-7.

[18] J.-P. Veder, R. De Marco, G. Clarke, R. Chester, A. Nelson, K. Prince, et al., Elimination of undesirable water layers in solid-contact polymeric ion-selective electrodes, Analytical Chemistry, 80(2008) 6731-40.

[19] C. Zuliani, G. Matzeu, D. Diamond, A liquid-junction-free reference electrode based on a PEDOT solid-contact and ionogel capping membrane, Talanta, 125(2014) 58-64.

[20] P. Hapiot, C. Lagrost, Electrochemical reactivity in room-temperature ionic liquids, Chemical Reviews, 108(2008) 2238-64.

[21] P. Danielsson, J. Bobacka, A. Ivaska, Electrochemical synthesis and characterization of poly(3,4-ethylenedioxythiophene) in ionic liquids with bulky organic anions, Journal of Solid State Electrochemistry, 8(2004) 809-17.

[22] S. Lupu, B. Lakard, J.-Y. Hihn, J. Dejeu, P. Rougeot, S. Lallemand, Morphological characterization and analytical application of poly (3, 4-ethylenedioxythiophene)–Prussian blue composite films electrodeposited in situ on platinum electrode chips, Thin Solid Films, 519(2011) 7754-62.

[23] C. Zuliani, G. Matzeu, D. Diamond, A potentiometric disposable sensor strip for measuring pH in saliva, Electrochimica Acta, 132(2014) 292-6.

[24] T. Guinovart, M. Parrilla, G.A. Crespo, F.X. Rius, F.J. Andrade, Potentiometric sensors using cotton yarns, carbon nanotubes and polymeric membranes, Analyst, 138(2013) 5208-15.

[25] A.J. Bandodkar, W. Jia, J. Wang, Tattoo-based wearable electrochemical devices: a review, Electroanalysis, 27(2015) 562-72.

[26] B. Schazmann, D. Morris, C. Slater, S. Beirne, C. Fay, R. Reuveny, et al., A wearable electrochemical sensor for the real-time measurement of sweat sodium concentration, Analytical Methods, 2(2010) 342-8.

[27] B. O'Flynn, S. Bellis, K. Delaney, J. Barton, S.C. O'Mathuna, A.M. Barroso, et al., The development of a novel minaturized modular platform for wireless sensor networks, Information Processing in Sensor Networks, 2005 IPSN 2005 Fourth International Symposium on, IEEE2005, pp. 370-5.

[28] G.G. Wallace, G.M. Spinks, L.A.P. Kane-Maguire, Assembly of polypyrroles, Conductive Electroactive Polymers: Intelligent Polymer Systems, CRC Press2009, pp. 59-101.

[29] J. Bobacka, Potential stability of all-solid-state ion-selective electrodes using conducting polymers as ion-to-electron transducers, Analytical Chemistry, 71(1999) 4932-7.

[30] A. Michalska, M. Wojciechowski, E. Bulska, K. Maksymiuk, Experimental study on stability of different solid contact arrangements of ion-selective electrodes, Talanta, 82(2010) 151-7.

[31] A. Michalska, K. Maksymiuk, The influence of spontaneous charging/discharging of conducting polymer ion-to-electron transducer on potentiometric responses of all-solid-state calcium-selective electrodes, Journal of Electroanalytical Chemistry, 576(2005) 339-52.

[32] V.F. Curto, S. Coyle, R. Byrne, N. Angelov, D. Diamond, F. Benito-Lopez, Concept and development of an autonomous wearable micro-fluidic platform for real time pH sweat analysis, Sensors and Actuators B: Chemical, 175(2012) 263-70.

[33] P.K. Yuen, Fluid control in microfluidic devices using a fluid conveyance extension and an absorbent microfluidic flow modulator, Lab on a Chip, 13(2013) 1737-42.

[34] A.J. Bandodkar, D. Molinnus, O. Mirza, T. Guinovart, J.R. Windmiller, G. Valdés-Ramírez, et al., Epidermal tattoo potentiometric sodium sensors with wireless signal transduction for continuous non-invasive sweat monitoring, Biosensors and Bioelectronics, 54(2014) 603-9.

[35] M.J. Buono, K.D. Ball, F.W. Kolkhorst, Sodium ion concentration vs. sweat rate relationship in humans, Journal of Applied Physiology, 103(2007) 990-4.

[36] A. Lynch, D. Diamond, M. Leader, Point-of-need diagnosis of cystic fibrosis using a potentiometric ion-selective electrode array, Analyst, 125(2000) 2264-7.

[37] B.J. Rosenstein, G.R. Cutting, The diagnosis of cystic fibrosis: a consensus statement, The Journal of Pediatrics, 132(1998) 589-95.

[38] http://www.horiba.com/uploads/media/concept_catalog_en_04.pdf, Accessed on: 28 April 2015

Chapter 7.

A Wearable Device for Monitoring Sweat Rates via Image Analysis

Giusy Matzeu[a] and Cormac Fay[a], Alix Vaillant[a], Shirley Coyle[a]* and Dermot Diamond[a]

Submitted to IEEE Transactions on Biomedical Engineering

*Corresponding author

[a]Insight Centre for Data Analytics, Dublin City University, Dublin 9, Ireland.

Aims and Objectives

Chapter 7 is focused on the use of a wearable device (Macroduct®) that after image analysis allows sweat rates of an athlete undergoing stationary cycling sessions to be estimated.

Contributions

- Design, conception and optimisation of experimental trials.
- Analysis of data and writing up of the manuscript.

Abstract

A feasibility study on a new technique capable of monitoring localised sweat rate is explored in this paper. Wearable devices commonly used in clinical practice for sweat sampling (i.e. Macroducts®) were positioned on the body of an athlete whose sweat rate was then monitored during cycling sessions. The position at which the sweat fills the Macroduct® was indicated by a contrasting marker and captured via a series of

time-stamped photos or a video recording of the device during an exercise period. Given that the time of each captured image/frame is known (either through time stamp on photos or the constant frame rate of the video capture), it was therefore possible to estimate the sweat flow rate through a simple calibration model. The importance of gathering such valuable information is described, together with the results from a number of exercise trials to investigate the viability of this approach.

Keywords

Image Analysis, Sweat Rate, Wearable Technology, Exercise Physiology, Hydration.

7.1 Introduction

Wearable technology is entering a phase of rapid growth, and people are becoming familiar with and accepting new devices and smart garments on the market e.g. MiCoach by Adidas and Smartwatches by Google, Apple and Samsung. A recent report states that the dominant application area of wearable technologies will remain the healthcare sector merging medical, fitness and wellnes [1]. This is favourable for improved healthcare delivery given current demographics, with the world's population growth rate rising at a fast pace. Wearable technologies may reduce the demand on the healthcare system by remote harvesting of health information and transmission of data to medical/health experts [2]. In light of this, the implementation of home-based personalised treatments or fitness programs monitored through wearable devices [3] has been at the core of many research programs within Universities and IT companies during the past 5 years [4].

The current clinical standard for generating information related to the health status of an individual typically requires the employment of highly trained medical personnel and the use of sophisticated instrumentation. For bio/chemical information the sensing model has historically centralised around invasive procedures, i.e. blood collection and laboratory analysis. This is inherently expensive and therefore scalability becomes an issue with increasing demand. Consequently, interest is rapidly growing in the area of non-invasive monitoring techniques, e.g. gathering information through analysis of biological fluids such as breath, saliva, sweat, etc. [5].

Sweat is known to contain important information corresponding to the status of an individual's health [6]. For example, its production is related to the stimuli behind body thermoregulation [7]. Moreover, its composition includes water, biomarkers (e.g. glucose, lactate and urea), and electrolytes (e.g. sodium, potassium, calcium, magnesium, zinc, copper, iron, chromium, nickel, lead, etc.) [6]. Studies appearing in this area have focused on the quantification of chemical analytes [8], (e.g. pH [9, 10], Na^+ [11], lactate [12], etc.) and their correlation with other markers such as sweat rate [13]. This physical parameter is of interest mainly because it can alert athletes of dehydration status, a situation that can negatively impact on their performance [14, 15].

Monitoring of sweat rate variations over time has the capacity to aid in the development of personalised rehydration strategies, which take into account factors

such as age, gender, fitness level, etc., coupled with information related to quantifiable environmental conditions (e.g. ambient temperature, humidity levels, etc.) and exercise intensity [7]. Moreover, the capability to monitor sweat rate can greatly impact on the performance of bio/chemical sensors [13]. However, a gold analytical standard technique capable of accurately estimating sweat rate variations over time is still undefined. The well-known "whole body wash down method" is recognised as the best approach to quantify various analytes [16]. However, the difficulty with this approach is its cumbersome nature for successful execution, i.e. it involves strictly controlled lab conditions such as pre- and post-washing of subjects that cycle in an environment enclosed by "plastic bags". The sweat is manually harvested in containers and analysed at a later stage [17].

Recently, Gonzalez et al. reported a method for estimating and predicting the amount of fluid lost by the whole body via specific models, which were developed in extreme experimental conditions (i.e. acclimation studies). The empirical model takes into account the individual's metabolic rate, type of clothing, environmental conditions, etc., and provides a prediction of sweat rates during extended exercise sessions (from 2 to 8 hours) as per Equation 7.1 [15]:

$$\text{Sweat Rate } \left(\frac{g}{m^2 h}\right) = 147 + 1.527E_{req} - 0.87E_{max} \quad (7.1)$$

Where E_{req} represents the evaporative heat loss, and E_{max} is the maximum evaporative power of the environment. E_{req} and E_{max} are obtained from the individual heat balance equation using heat and mass transfer coefficients (as explained in detail by Gonzalez et al. [15]).

In contrast to estimations of the total body sweat loss, we are interested in monitoring the sweat flow rate at a specific location [14], using wearable technology. To our knowledge, the only study in the literature that describes a wearable device capable of monitoring sweat rate is based on the integration of humidity capacitive sensors on fabric. Although the approach is novel, this device is limited for use under restricted and controlled laboratory conditions. Additionally, it is affected by movement artefacts, which must be minimised because they can lead to false positives/negatives [18]. When considering localised areas of interest, the choice of sampling area is very important as it has been reported that sweat rate is significantly dependent on the sampling location [19, 20].

Localised sweat sampling has been reported in a number of studies using absorbent patches positioned in specific locations (e.g. forearm, thigh, back, and calf) that were

removed at the end of a trial [8, 14, 16, 19] or at specific time intervals [20]. The rates were determined gravimetrically by weighting syringes that aspirated the collected sweat from patches [19] or after weighting the entire patches [20]. Despite the simplicity of this approach, such patches can have an hydromeiosis effect, i.e. they can affect sweat rates by causing sweat pools on skin surfaces, or by suppressing the evaporation of the fluid at the collection sites, and increasing local skin temperatures [8]. One solution that can address these issues may be through the use of Macroducts®. These devices are typically employed in clinical practice to collect sweat samples after pilocarpine iontophoresis stimulation for cystic fibrosis diagnosis [21, 22]. These have the scope to eliminate the drawbacks related to the use of the aforementioned patches as they prevent leakage and sample contamination [23]. Through their use, sweat is immediately removed from the skin, which avoids pooling on the surface and hydromeiosis. Additionally, they can be used outside of constrained laboratory conditions and therefore can be employed in many other environments [24]. Macroducts® also overcome inconveniences encountered when sweat rates are determined via capacitance hygrometry or indirectly via weight lost, in that they can allow parameters to be tracked dynamically over time, rather than provide a single measurement that applies to the entire experiment.

In addition to their intended off-the-shelf use (sweat collection), these appealing features suggest that their use can be expanded to monitor local sweat rate variations over time. This paper describes a new technique capable of estimating localised sweat rates during exercise periods. It is based on a visual analysis method for the monitoring of a Macroduct® as it fills with sweat during a cycling session. The system is initially characterised and calibrated with precision bench top instrumentation before beginning sweat trials. Upon sweat production, the Macroduct® (in its off-the-shelf use) begins to fill, which is visually indicated by a blue coloured dye emanating in a spiral pattern from its centre towards the outer radius. A simple protocol is also reported to prepare the Macroducts® for image analysis of sweat rate.

7.2 Experimental

7.2.1 Materials

Deionised water with resistivity of 18.2 MΩ cm was obtained via a Milli-Q reagent-grade water purification system, and used for the preparation of aqueous solutions. A black food dye from Goodall's (Dublin, Ireland) was employed as the colouring agent

of aqueous solutions during calibration and the regeneration of Macroducts®. The Macroducts® were purchased from Accuscience (Dublin, Ireland). A 3D Digital Microscope VHX-5000 from Keyence (USA) was used to capture images of Macroducts®. A Panasonic FZ38 Lumix Camera and a Samsung Galaxy S4 phone-camera were used to capture videos and/or pictures during calibrations and exercise sessions.

7.2.2 Preparation of Macroducts® for Sweat Rate Analysis

Macroduct® Sweat Collectors are disposable devices characterised by a coiled tubing kept in position by a round plastic frame (see Figure 7.1 (a)) whose underneath presents a concave surface with an orifice (see Figure 7.1 (b)). After being secured in position via straps inserted in the loop holes (see Figure 7.1 (b) and Figure 7.4), the Macroduct® is in contact with the skin and is able to collect the sweat produced by the glands in the subcutaneous layer. The produced fluid develops a hydraulic pressure that drives it towards the external epidermis layer. The same hydraulic pressure passively and automatically drives the sweat into the air-free interface between the skin and the concave surface of the Macroduct®, pushing it into the orifice, inlet of the harvesting system (see Figure 7.1 (b)) [25].

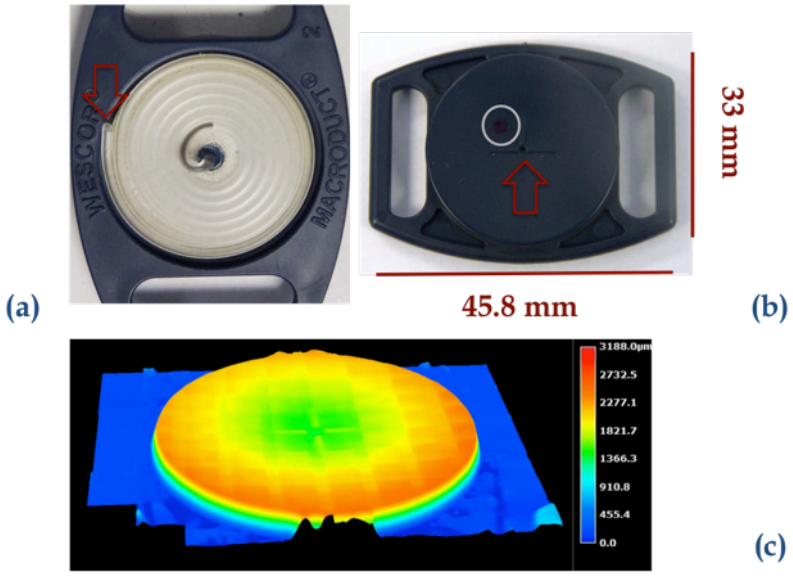

Figure 7. 1: (a) Macroduct® containing 3 µL of the black aqueous solution at its centre, which was used to prime the device prior to use. The arrow indicates the distal end of the channel into which the cleaning solution was entered. (b) An image of the reverse side of an off-the-shelf Macroduct® showing the inlet to the tubing (red arrow), the dye localised around the inlet (grey circle) and the dimensions of the device. (c) An image (obtained using a 3D microscope) that shows the exposed surface for sweat collection (green area).

Sweat emerging on the epidermis layer turns blue when it gets in contact with the water soluble blue dye applied on the surface of the reverse side of the device (see Figure 7.1 (b)) [25]. Consequently, when Macroducts® in their off-the-shelf form are employed, sweat collected is visually indicated by a blue dye travelling from its centre outward following a spiral pattern (see Figure 7.2).

(a) 12 min (b) 37 min

Figure 7. 2: Photos of a Macroduct® visualising the amount of sweat collected during a cycling session by means of a blue coloured dye; (a) t=12 min, (b) t=37 min. The red markers represent the front end of the dye within the tubing. The arrows indicate the direction of the fluid moving within the Macroduct®.

Macroducts® are indeed designed as single use sweat collection devices for Cystic Fibrosis diagnosis with an incorporated blue dye to show clinicians that sweat is being collected. In order to choose a suitable colour dye for image analysis a method has been investigated for their preparation using the following protocol.

The Macroduct® channel was first washed using deionised water via a 1 mL syringe (BD, Fisher Scientific, Ireland) equipped with a 23G flat needle (Nordson EFD International Inc, UK), and inserted as indicated by the arrow in Figure 7.1 (a). A total of 5 flushes were found to be sufficient for cleansing the Macroduct®. It was also necessary to carefully wash the area directly in contact with the skin (especially at the inlet zone, which allows for the collection of sweat and contains the dye in the off-the-shelf form) (see Figure 7.1 (b)). To dry the sampling tubing, the excess water was removed by flushing with nitrogen, after which the Macroduct® was placed in a convection oven at a temperature of 65 °C for at least 4 hours to remove any remaining water.

The device was then ready to be used after priming, which involved attaching an Eppendorf tip to the corresponding Eppendorf dispenser and then injecting an amount

of liquid (3 µL of the black aqueous dye) at the sweat inlet (backside of the Macroduct®, see Figure 7.1 (b)).

When positioned on a chosen location on the body to collect sweat, it was possible to see the fluid moving over time, i.e. a coloured front appeared which moved through the channel preceding the harvested sweat (see Figure 7.4). The black coloured dye was found to give excellent contrast during monitoring and post-processing of the sampling images.

7.2.3 Calibration of the System

The aforementioned black coloured solution was used to calibrate the Macroduct® during bench tests before progressing towards sweat trials. A precision 22 syringe pump from Harvard Apparatus (Cambridge, USA) was employed to fill the system with the coloured solution under a constant and precise flow rate (set at 70 µL/min). A peristaltic pump (Ismatec Reglo ICC from IDEX Wertheim, Germany) was also tested to investigate the occurrences of small backflows. The conditions of the test were similar to the syringe pump, i.e. using the same coloured solution and setting a flow rate to 50 µL/min. During filling, the camera (Panasonic FZ38 Lumix) was placed at a distance of 20 cm (for maximum resolution) perpendicularly to the surface of the Macroduct®, held by a retort stand, and captured a video until the channel was full. This took place in well-illuminated conditions to supply a sufficient contrast of the black dye to its background for visual analysis (Figure 7.1 (a)).

Image analysis techniques were implemented to evaluate flow rates after image or video recording. Frames were extracted at precise time intervals, allowing for the observed sweat volumes to be converted to flow rates. Volume estimation was achieved using the mask shown in Figure 7.3 (a). The mask was centred on the Macroduct® and oriented as shown in Figure 7.3 (b). Every labelled bar represented by numbers denotes the intersection between the coiled tubing and the Cartesian plane (x- and y-axes), and arranged in a clockwise manner starting from the centre (in relation to the point where sweat enters the unit and guided by the strap supports). Every labelled bar represented by letters denotes the intersection between the coiled tubing and the diagonal at 45° in each quadrant, arranged in a clockwise manner as per the intersections with the x- and y- axis.

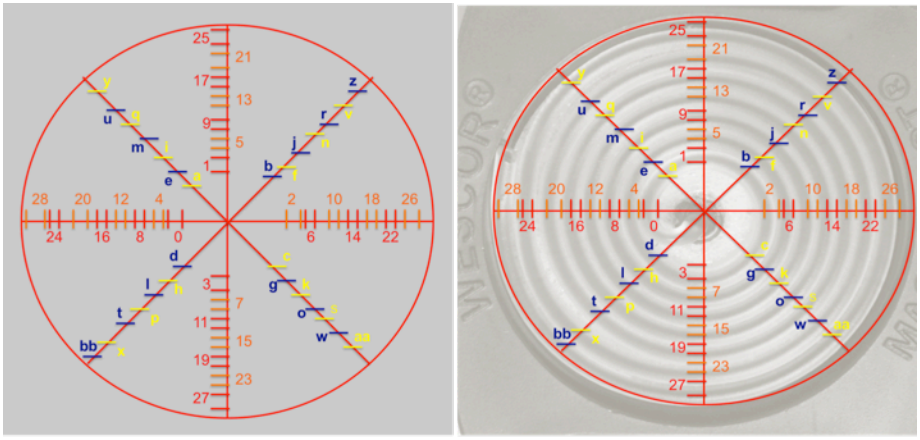

Figure 7. 3: (a) Mask used to estimate sweat volumes. Red, orange, yellow and blue labels represent channel intersections and aid in differentiating adjacent channels for visual contrast. (b) Mask applied to a captured video frame/image of a filled Macroduct®.

Frames within the captured video were cycled through and those that coincided with the point of each mask intersect were extracted. The volume within the tube at each intersection (x- and y- axis, for more details see Table AE.1 in the Appendix E) was calculated using the flow rate of the pump, the frame rate of the captured video, and the frame number or time stamp of the extracted frame (see Table 7.1).

Table 7. 1: Volumes harvested by the Macroduct® in correspondence with every mask intersection. The corresponding location (-x, +x, -y, +y) or intersect is indicated via coloured text; orange or red with shading. Please note that calibration points labelled from a to bb are omitted for compactness (see Table AE.1 in the Appendix E for the complete table of calibration points).

-x	V (µL)	+y	V (µL)	+x	V (µL)	-y	V (µL)
0	0	1	2.3	2	3.5	3	5.8
4	8.2	5	10.5	6	12.8	7	16.3
8	18.7	9	21	10	24.5	11	28
12	31.5	13	35	14	38.5	15	43.2
16	46.7	17	51.3	18	56	19	60.7
20	65.3	21	70	22	74.7	23	80.5
24	86.3	25	92.2	26	98	27	103.8
28	110.8						

The volume contained in every section of the tubing (described by the mask in Figure 7.3 (a)) was also mathematically estimated by measuring the length of each section, the internal diameter (0.67 mm), and the inlet surface area (0.36 mm^2) of the tubing. The rationale behind this was for validation of the pumping approach. In addition to this, the device was filled with precise volumes of solution, i.e. those coinciding with every intersection of the mask in Figure 7.3 (a) and these volumes were quantified gravimetrically on an analytical balance for further validation.

7.2.4 Real-time Cycling Sessions

A healthy active male athlete participated in six indoor cycling sweat trials (average room temperature of 22°C) following an approved, recognised procedure. He used a cycle ergometer (Monark Exercise, Sweden) at an intensity (e.g. self-selected) high enough to induce sweat. A Macroduct® was positioned on the upper left arm and on the lower back (investigated during one trial) by means of Velcro® straps. The external forearm was selected as the primary sampling location. It provided a relatively flat surface to secure the collecting device and it also facilitated video and image capturing (see Figure 7.4).

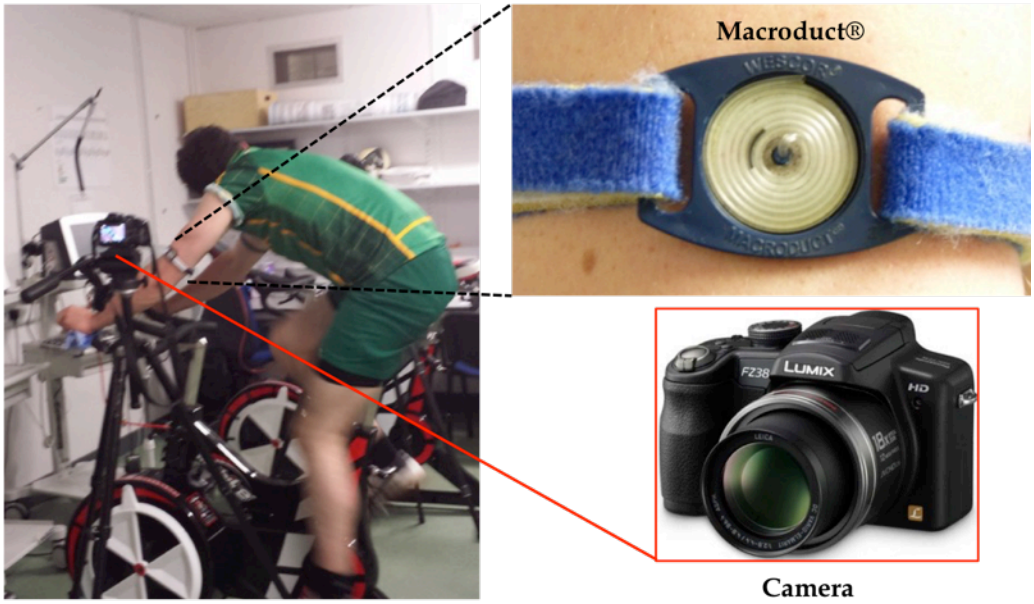

Figure 7. 4: Experimental setup characterised by an athlete cycling under controlled laboratory conditions (left). The enlargements represent a captured image/view of the Macroduct® (top right) and the camera (bottom right) used during an exercise session.

Video and/or image capturing commenced when the volunteer began to cycle. Trials were stopped when the Macroducts® were filled (see Figure AE.1) or at the point

when the athlete was no longer capable of maintaining the set intensity load (average of exercise period was 35 minutes, see Table 7.2 for more details). During the trials the placement of the Macroduct® was monitored to ensure that the optimal contact with the sampling area was maintained.

The collected video/photos were post-processed after cycling sessions. Frames (extracted from the captured video) or photographs taken at precise time intervals were cropped, resized and rotated as shown in Figure 7.3 (b). The mask was then applied to the Macroduct® and the intersection between the fluid and the mask was located and then correlated to the calibration table (see Table 7.1 and Table AE.1) for volume estimation. These steps were repeated when analysing each key frame/image, which allowed for the measurement of fluid in the channels at discrete time periods during a cycling session. We found that linear trends well represented ($R^2 \geq 0.97$) volume variations against time. The average sweat rate (μL/min) was then estimated as the angular coefficient of the best-fit line.

To allow for comparison with previous studies, sweat rates were also expressed in g/(m^{2}h). Since sweat is a water-based solution, the relation 1 μL=1 mg is valid. The underside of the Macroduct® (placed in contact with the skin during trials) was examined using a visual profilometer, i.e., a 3D microscope. This instrument allowed for estimating the exposed surface, represented by the green area in Figure 7.1 (c), characterised by an area of ca. 122.7 mm^2. This area approximates the small concave dome in the lower part of the Macroduct®, which behaves in a similar manner to a small cavity, and therefore it shows that it is not in contact with the area of skin from where sweat is harvested.

7.3 Results and Discussion

7.3.1 Macroduct® Preparation

Figure 7.5 presents images (captured during a sweat trial) of a Macroduct® prepared with the black dye. It can be seen that once sweat collection began, it forced the dye along the channel in a manner analogous to the original blue indicator.

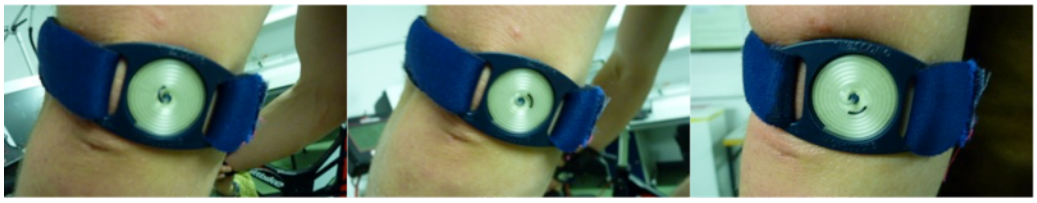

(a) (b) (c)

Figure 7. 5: Captured images of the regenerated Macroduct® during a sweat trial.

Compared to the original dye, the black food colouring agent is higher in contrast for visual inspection (see Figure 7.6). This is likely to reduce the complexity and increase the robustness of this method for furthering the development towards a fully autonomous implementation on portable devices.

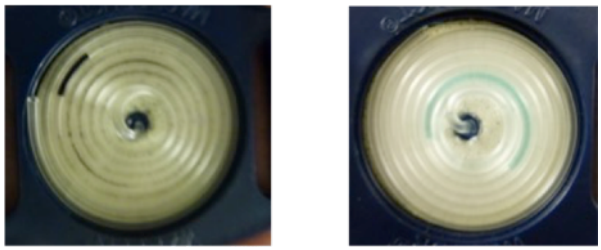

(a) (b)

Figure 7. 6: Differences between a Macroduct® primed with a black colouring agent (a) and the original dye (b).

As can be seen from Figure 7.6 (b), the original blue dye faded as the device filled with sweat. The intended use of the Macroduct® is for this dye to be observed by eye, however, for automated computer image analysis, the dilution effect makes image analysis difficult over time. In its regenerated mode, the black food dye maintained a constant concentration and colour over time as it did not mix with the sweat sample (see Figure 7.6 (a)), making eventual post-trial analytical measurements more feasible. The reason for this may be due to the method of introducing the dye into the Macroduct®. In its off-the-shelf form, the dye is located on the backside of the Macroduct® (see Figure 7.1 (b)) and during sweating the dye first mixes and then enters the Macroduct®. Additionally, it has been observed that during low sweat production trials the dye marks the skin. However, this does not occur with the approach presented here. The Macroduct® is partially prefilled (as described earlier in Section 7.2.2), which also introduced a small air barrier between the dye and the sweat

(this volume was accounted for during image analysis). This barrier did not allow for dilution of the dye and the technique used for regeneration seems to be reproducible and does not affect the sweat rate monitored over time.

7.3.2 Macroduct® Calibration

Figure 7.7 presents two calibration plots of the Macroduct® using the two techniques described earlier, i.e. via a mathematical estimation (using the tubing dimensions) and the syringe pump method (using the known flow rate), which are plotted with respect to gravimetric measurements. It can be seen that both techniques are characterised by a high correlation coefficient ($R^2 \geq 0.9997$) and a low angular coefficient difference (≤ 0.045) relative to the ideal value of 1 (accounting for the accuracy of the method). This yields high confidence in the calibration model and subsequent estimation of the flow rates. The percentage difference between the volumes estimated using the two techniques was characterised by an average of <=4.9%.

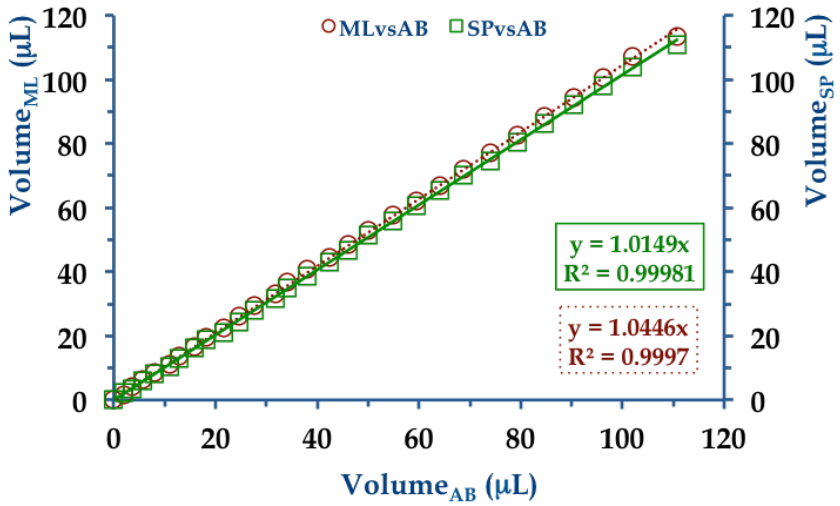

Figure 7. 7: Correlation between volumes obtained after weighing the Macroduct® with an analytical balance vs data obtained following mathematical estimation (○, red · · ·) or calibration with a syringe pump (□, green —).

A comparison between calibrations obtained using a syringe and a peristaltic pump was also performed. The latter was employed to investigate potential issues that may occur in a real-time sweat flow rate experiment, i.e. back flow and non-linear flow rate that may affect trial data. Figure 7.8 (a) presents calibration plots using both pumps as the volume crosses the same intercept. It can be seen that the data associated with the peristaltic pump approach are slightly different than those determined via the syringe

pump. This is prominent when considering the first 3 labels on the mask (average difference between the two volumes 74%). However, the overall differences between the volumes calculated using the two techniques were within 9.5%. Additionally, when analysing the correlation between the two pumping systems, they seem to be in excellent agreement, as confirmed by the high correlation coefficient (R^2=0.998) and the accuracy associated with the estimated volumes was still maintained (slope <1.02, see Figure 7.8 (b)).

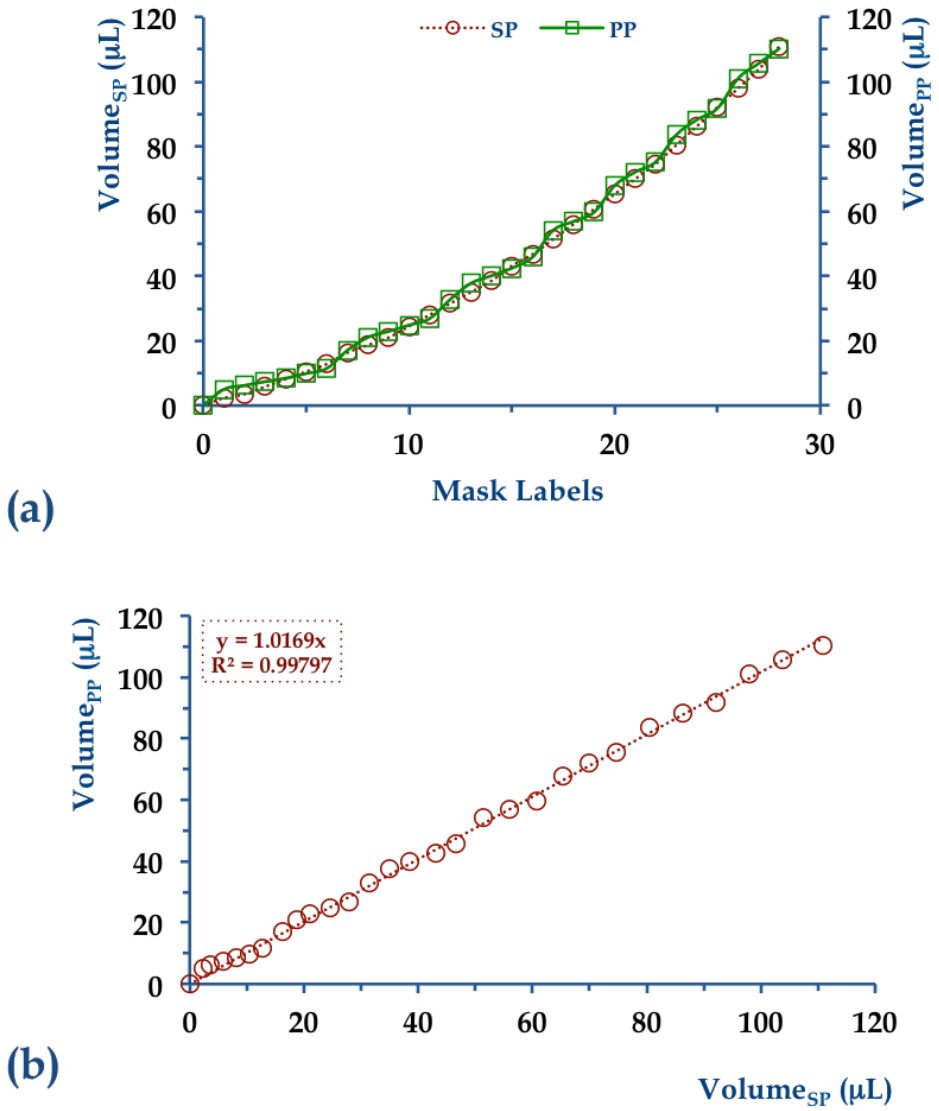

Figure 7. 8: (a) Comparison between the volumes (contained in each labelled section) after calibrating the Macroduct® with the syringe (○, red · · ·) and the peristaltic pump (□, green —). (b) Correlation between calibration data obtained with the syringe pump and those obtained using the peristaltic pump (○, red · · ·).

7.3.3 Real-time Sweat Trials

Preliminary tests were carried out to prove the feasibility of the technique for on-body sweat trials. Videos were recorded of a Macroduct® positioned on the upper left arm of an athlete who was cycling on an exercise bicycle (see Figure 7.4) and the sweat volume at specific times estimated by extracting frames at which the dye coincided with the mask labels. Figure 7.9 presents data collected during a trial lasting 30 minutes. Sweating began after 10 minutes of cycling and sweat volume production over time was characterised by two linear trends ($y=2.26x-20.91$, $R^2=0.98$ and $y=1.51x+1.22$, $R^2=0.99$ from 10 minutes to 20 minutes and from 20 minutes up to the end of the cycling session, respectively). Sweat rate was characterised by an average value of ~2.26 µL/min (~1105 g/(m²h)) during the first 20 minutes. The average sweat rate then decreased down to 1.51 µL/min (~738 g/(m²h)) during the following 10 minutes (a value that was maintained until the end of the cycling session). This is a good example of a trial demonstrating that information related to localised sweat rates can be extracted using the approach proposed in this study.

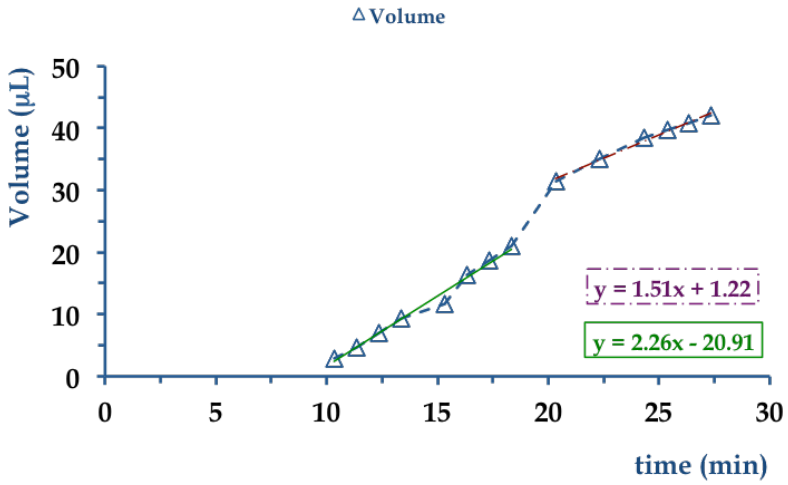

Figure 7. 9: Real-time cycling session lasting 30 minutes, characterised by a Macroduct® positioned on the upper left arm that began to be filled after 10 minutes.

In previous studies by Salvo et al. [18, 26], sweat rate variations were indirectly determined employing a different technique, based on the use of textile capacitive humidity sensors [18, 26]. The trials lasted for 25-30 minutes and they were characterised by an initial peak recorded after nearly 15 minutes (priming time for this system). A maximum was reached after a constant increase in sweat rate due to thermoregulation, followed by a steady state until the end of the trial. When the

exercise session stopped, sweat rates decreased during the recovery time, and constantly monitored for additional ten minutes while the athlete was getting some rest. Similar to our study, Salvo et al. observed that sweat rates seem to reach a steady state at advanced stages in the exercise session. There were differences in experimental design such as sampling location and skin surface area. This prevented a full comparison from taking place, especially in terms of recorded absolute values.

Six tests were carried out with the Macroduct® positioned on the upper left arm. During a subsequent cycling session, it was decided to locate an additional Macroduct® at the lower back. The rationale was two-fold, i.e. to investigate this approach on a location other than the forearm and also to explore variations in sweat rates at two sampling locations on the human body during the same exercise event (see Figure 7.10).

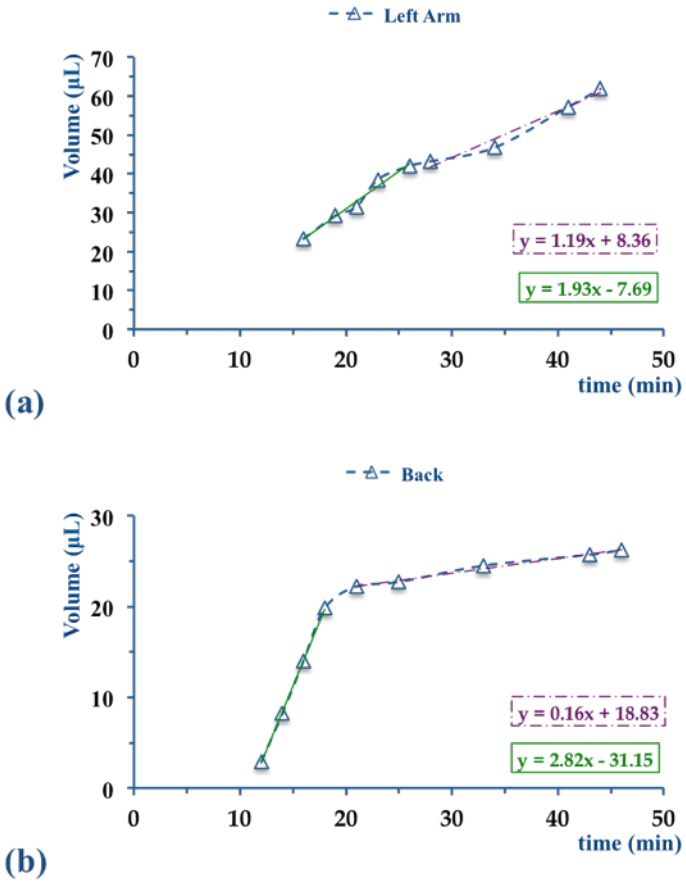

Figure 7. 10: Volume variations recorded over time during a cycling session lasting ca. 50 minutes, measured using two Macroducts® positioned on the upper left arm (a) and on the lower back (b). (a) The Macroduct® placed on the arm began to be filled after 15 minutes. (b) The Macroduct® placed on the back began to be filled after 12 minutes.

When the Macroduct® was positioned on the upper arm (see Figure 7.10 (a)), volume variations were described by two linear trends: $y=1.93x-7.69$, $R^2=0.98$ (during the first 25 minutes); $y=1.19x+8.36$, $R^2=0.97$ (from 25 minutes until the end of the cycling session). During the first 25 minutes, the trial was characterised by an average sweat rate of 1.93 µL/min (~944 g/(m²h)), which decreased down to an average value of 1.19 µL/min (~582 g/(m²h)), and was maintained until the end of the cycling session. Figure 7.10 (a) shows similar patterns to Figure 7.9, although the average sweat rates were different in magnitude. Volume variations were monitored in correspondence with the back, which also can be described by two linear trends: $y=2.82x-31.15$, $R^2=0.99$ (during the first 20 minutes); $y=0.16x+18.83$, $R^2=0.98$ (from 20 minutes until the end of the cycling session). During the first 20 minutes, the trial was characterised by a high average sweat rate of 2.82 µL/min (~1379 g/(m²h)), which decreased down to an average value of 0.16 µL/min (~78 g/(m²h)) until the end of the cycling session.

The reasons behind these differences are not clear. From the literature it has been reported that areas of the body sweat at different rates [19, 20]. In this single trial the upper arm location was featured by lower sweat rates (i.e. 1.93 µL/min (~944 g/(m²h), in the first 25 minutes) than the lower back (i.e. 2.82 µL/min (~1379 g/(m²h), in the first 20 minutes). From an absorbent patch study, Havenith et al. [20] stated that the spine area of the back is characterised by the highest sweat rates while the upper arm has the lowest ones, as obtained in this trial. However, the situation was inverted after ~20 minutes, the average sweat rate estimated for the upper arm was higher than the one estimated at the lower back. We can assume that the athlete stopped sweating in correspondence with the lower back. He began producing less sweat at a lower rate, and the Macroduct® was able to harvest only 3.5 µL in the last 27 minutes (i.e. 0.16 µL/min (~78 g/(m²h)). These results underline that further investigation is needed to see the relationship between regional variations in sweat rate measured using the Macroducts®.

Table 7.2 presents summary information of 6 trials in total, which gives detailed information such as the location on body, length of the exercise trial (i.e. trial period), the method used to collect the information (frames extracted from a video or photo shooting), the total volume and the average sweat rates.

Table 7. 2: Summary of six trials highlighting experimental conditions and results thereof. Average Sweat Rate 1 represents the slope of the first linear trend describing the sweat volume production over the time range indicated between brackets. Average Sweat Rate 2 represents the slope of the second linear trend describing the sweat volume production over the time range indicated between brackets.

Trial	Body Location	Trial Period (min)	Capturing Method	Total Volume (µL)	Average Sweat Rate 1 (µL/min)	Average Sweat Rate 2 (µL/min)
1	Left Arm	18	Video	35	3.26 (7-18 min)	-
2	Left Arm	28	Video	43	2.26 (10-20 min)	1.51 (20-28 min)
3	Left Arm	30	Photos	2.5	-	-
4	Left Arm	30	Photos	110.8	4.89 (9-30 min)	-
5	Left Arm	32	Photos	18.7	0.39 (12-20 min)	0.77 (20-32 min)
6	Back	47	Photos	26.2	2.82 (12-20 min)	0.16 (20-47 min)
	Left Arm	45	Photos	61.8	1.93 (15-25 min)	1.19 (25-45 min)

There were issues during sampling along Trial 3. Almost no sweat was collected by the Macroduct®, although the experiment was carried out in identical experimental conditions. Trial 1 and 4 were described by one value characterising the average sweat rate recorded during the cycling session. The volumes produced over time were described by a single linear trend line, which slopes were however completely different in terms of absolute values. Over time volumes variations in Trial 2, 5 and 6 were described by two different linear trends. The first one describes the first 20 or 25 minutes; the second one describes the volume variations from 20 or 25 minutes until the end of the cycling sessions.

It can be seen from Table 7.2 that the results between each trial differ somewhat in terms of absolute values, both for maximum volume collected and average sweat rates, even though the conditions were kept relatively constant, where possible. They were carried out at similar times of the day, using the same athlete, the room temperature set to 22 °C, and the same exercise machine was used. This might also possibly be

attributed to the freedom given to the athlete in self-selecting his workload during the stationary cycling sessions. Other factors that need to be investigated in future studies are the athlete's physiology before the trial, e.g. hydration level by measuring urine specific gravity, resting heart rate, breathing rate, etc., and also environmental conditions such as humidity.

This approach is novel and differs from sweat rate analysis studies reported in the literature to date. Previous works were carried out employing techniques such as indirect determination via humidity sensors [18, 26] or gravimetrically weighting patches [19, 20].

As suggested by former studies, a more complete physiological understanding of sweat rate variations during exercise sessions might be obtained using the technique described here by simultaneously monitoring four locations (i.e. to correlate local with whole body sweat rates [19]). Relating differences in localised sweat production is a natural extension of this study, which has demonstrated that the image analysis approach is a feasible method of sweat rate estimation. Furthermore, the approach can be easily extended to monitor sweat rate variations dynamically at more than one location on the body. Therefore, this sensing method has considerable potential to aid in the development of a deeper understanding of the processes involved in sweat loss and rehydration.

7.3.4 Future Work

The aim of this study was to demonstrate the use of a wearable, low-cost method for the detection of sweat rates using image analysis.

A key aspect that must be further investigated lies in captured image quality, which can be affected by a number of variables including resolution due to the employed camera and distance from the Macroduct®; non-ideal alignment, which may be accounted for by image warping; lighting conditions, and finally movement artefacts. All of which must be addressed when developing an autonomous app for portable devices such as smartphones. This will also be of fundamental importance while designing the new wearable configuration of the whole device (i.e. Macroduct® and camera integrated together). The photo-shooting device will be programmed to take and transmit the image to a smart phone app that will process and estimate sweat rates in real-time.

Further validation of this proposed approach will need to take place. A clinical study with a number of volunteers (male and female) exercising under strictly controlled conditions (before and after the test, assuring more reproducible pre-exercise hydration status) is in preparation.

One application of this may lie in the area of monitoring people with Cystic Fibrosis, one symptom of which is reduced sweat rate. This might also allow for the understanding of correlation between sweat rates and chemical analytes (e.g. sodium levels for CF patients, workers tested during acclimation studies [13], athletes under effort, etc.). After removal of the biological fluid from the Macroduct®, sweat samples can be further analysed via standard analytical methods or novel on-bench sensors. For example, the sweat rate correlation with lactate might give valuable information on switches between aerobic and anaerobic processes [12]. Additionally, it will be possible to relate how hydration affects sweat rates and then to implement personalised hydration strategies.

Parallel measurements between any chemical target and the sweat flow rate are a necessity for determining total losses. This will be investigated in forthcoming studies by integrating real-time chemical sensors within the device presented in this study.

7.4 Conclusions

The ability to estimate sweat rate variations over time via a low-cost wearable device is intuitively appealing and has been demonstrated using Macroducts®. They are already employed in clinical practice to harvest sweat samples, and they have already been accepted as a valid means for sweat collection. An extension of Macroduct® use for sweat rate estimation using pervasive technology can lead to the production of valuable information.

The overall trials proved the power and strength of the proposed method in this study. In the near future, an application for smartphones will be developed, allowing for real-time estimation of sweat rates and therefore leading to the implementation of personalised hydration strategies of athletes during training regimes.

7.5 References

[1] Wearable technology 2014-2024: Technologies, markets, forecasts, Accessed on: 24 April 2015

[2] Y. Hao, R. Foster, Wireless body sensor networks for health-monitoring applications, Physiological Measurement, 29(2008) R27.

[3] A.J. Bandodkar, J. Wang, Non-invasive wearable electrochemical sensors: a review, Trends in Biotechnology, (2014).

[4] J. Heikenfeld, Let them see you sweat, Spectrum, IEEE, 51(2014) 46-63.

[5] G. Matzeu, L. Florea, D. Diamond, Advances in wearable chemical sensor design for monitoring biological fluids, Sensors and Actuators B: Chemical, 211(2015) 403-18.

[6] C.J. Harvey, R.F. LeBouf, A.B. Stefaniak, Formulation and stability of a novel artificial human sweat under conditions of storage and use, Toxicology in Vitro, 24(2010) 1790-6.

[7] D. Gagnon, O. Jay, G.P. Kenny, The evaporative requirement for heat balance determines whole-body sweat rate during exercise under conditions permitting full evaporation, The Journal of Physiology, 591(2013) 2925-35.

[8] A. Mena-Bravo, M.D. Luque de Castro, Sweat: A sample with limited present applications and promising future in metabolomics, Journal of Pharmaceutical and Biomedical Analysis, 90(2014) 139-47.

[9] V.F. Curto, C. Fay, S. Coyle, R. Byrne, C. O'Toole, C. Barry, et al., Real-time sweat pH monitoring based on a wearable chemical barcode micro-fluidic platform incorporating ionic liquids, Sensors and Actuators B: Chemical, 171(2012) 1327-34.

[10] S. Coyle, K.-T. Lau, N. Moyna, D. O'Gorman, D. Diamond, F. Di Francesco, et al., BIOTEX—Biosensing textiles for personalised healthcare management, Information Technology in Biomedicine, IEEE Transactions on, 14(2010) 364-70.

[11] A.J. Bandodkar, D. Molinnus, O. Mirza, T. Guinovart, J.R. Windmiller, G. Valdés-Ramírez, et al., Epidermal tattoo potentiometric sodium sensors with wireless signal transduction for continuous non-invasive sweat monitoring, Biosensors and Bioelectronics, 54(2014) 603-9.

[12] W. Jia, A.J. Bandodkar, G. Valdes-Ramirez, J.R. Windmiller, Z. Yang, J. Ramirez, et al., Electrochemical tattoo biosensors for real-time noninvasive lactate monitoring in human perspiration, Analytical Chemistry, 85(2013) 6553-60.

[13] M.J. Buono, K.D. Ball, F.W. Kolkhorst, Sodium ion concentration vs. sweat rate relationship in humans, Journal of Applied Physiology, 103(2007) 990-4.

[14] R. Maughan, S. Shirreffs, Dehydration and rehydration in competative sport, Scandinavian Journal of Medicine & Science in Sports, 20(2010) 40-7.

[15] R.R. Gonzalez, S.N. Cheuvront, S.J. Montain, D.A. Goodman, L.A. Blanchard, L.G. Berglund, et al., Expanded prediction equations of human sweat loss and water needs, Journal of Applied Physiology, 107(2009) 379-88.

[16] L.B. Baker, J.R. Stofan, A.A. Hamilton, C.A. Horswill, Comparison of regional patch collection vs. whole body washdown for measuring sweat sodium and potassium loss during exercise, Journal of Applied Physiology, 107(2009) 887-95.

[17] S. Shirreffs, R. Maughan, Whole body sweat collection in humans: an improved method with preliminary data on electrolyte content, Journal of Applied Physiology, 82(1997) 336-41.

[18] P. Salvo, F. Di Francesco, D. Costanzo, C. Ferrari, M.G. Trivella, D. De Rossi, A wearable sensor for measuring sweat rate, Sensors Journal, IEEE, 10(2010) 1557-8.

[19] M.J. Patterson, S.D.R. Galloway, M.A. Nimmo, Variations in regional sweat composition in normal human males, Experimental Physiology, 85(2000) 869-75.

[20] G. Havenith, A. Fogarty, R. Bartlett, C.J. Smith, V. Ventenat, Male and female upper body sweat distribution during running measured with technical absorbents, European Journal of Applied Physiology, 104(2008) 245-55.

[21] C. Taylor, J. Hardcastle, K. Southern, Physiological measurements confirming the diagnosis of cystic fibrosis: the sweat test and measurements of transepithelial potential difference, Paediatric Respiratory Reviews, 10(2009) 220-6.

[22] A. Green, J. Kirk, Guidelines for the performance of the sweat test for the diagnosis of cystic fibrosis, Annals of Clinical Biochemistry, 44(2007) 25-34.

[23] M.R. Ely, R.W. Kenefick, S.N. Cheuvront, T.D. Chinevere, C.P. Lacher, H.C. Lukaski, et al., Surface contamination artificially elevates initial sweat mineral concentrations, Journal of Applied Physiology, 110(2011) 1534-40.

[24] M. Ely, B. Ely, T. Chinevere, C. Lacher, H. Lukaski, S. Cheuvront, Evaluation of the Megaduct sweat collector for mineral analysis, Physiological Measurement, 33(2012) 385.

[25] http://www.wescor.com/translations/Translations/M2551-7A-EN.pdf, Accessed on: 20 July 2015

[26] S. Coyle, D. Morris, K.-T. Lau, D. Diamond, F. Di Francesco, N. Taccini, et al., Textile sensors to measure sweat pH and sweat-rate during exercise, Pervasive Computing Technologies for Healthcare, 2009 PervasiveHealth 2009 3rd International Conference on, IEEE2009, pp. 1-6.

Chapter 8.

Conclusions and Future Work

8.1 Summary and Conclusions

The improvement in performance of chemical sensors observed during the last ten years (as visible in different devices available on the market) [1] is largely the result of several research efforts focused on the development of applications for environmental or biological monitoring [2].

Non-invasive detection of biological fluids is indeed driving investments from many IT companies such as Apple (e.g. Apple i-Watch) [3], Google and Novartis (e.g. glucose monitoring in tears via contact lenses) [4], and Intel (e.g. their "Make it Wearable" challenge) [5]. Breath, saliva, sweat and tears contain important information on the state of health of a person and new solutions have been recently implemented for their employment in non-invasive monitoring [6]. This has been made possible by using miniaturised devices employing "lab on a chip" approaches for wearable applications (see Chapter 2). Additionally, stimulus responsive tools like enhanced patches that embed monitoring and drug delivery functionalities onto the same unit have also been increasingly under the spotlight for the last 5 years [7].

Novel solutions for the development of detection and transduction modules have been based on colorimetric or electrochemical techniques such as amperometry, coulometry and potentiometry. This thesis was mainly directed towards the realisation of all plastic, screen-printed electrodes used in solid-contact potentiometric electrochemical sensors for different types of applications. As already described in Chapter 1, this is based on detecting the difference of potential between an Ion-Selective Electrode (the working electrode) and a Reference Electrode. In Chapter 3, we described our approach to develop a solid-contact Reference Electrode. This was the preliminary step for the development of fully miniaturised, low-cost potentiometric platforms endowed with working electrodes that are tuned according to the analyte of interest. pH strips based on fully screen-printed dual designs were developed and used to successfully monitor pH variations in saliva, as described in Chapter 4.

The good performance of the pH potentiometric strips stimulated our interest on exploring other aspects related to the implementation of solid-contact ISEs through varying the analyte of interest, and improving the sensitivity, reproducibility and linear range of the sensors. We explored the use of functionalised Au-NPs decorated with two different ligands, and verified their suitability for incorporation into solid-contacts of low-cost solid state ISEs compatible with requirements for high volume

production. Special attention was paid to the realisation of Pb^{2+} and Na^{+} ISEs because of their potential applications in environmental (i.e. Pb^{2+}) or personal health monitoring (i.e. Na^{+}), as described in detail in Chapter 5.

We also investigated the integration of Na^{+} ISEs in all plastic potentiometric strips, and optimised their performance using PEDOT grown in the Ionic Liquid [emim][NTF_2] as solid-contact material. The potentiometric strips were then integrated into microfluidic chips (PotMicroChip) and connected to a miniaturised electronic platform (Wireless Mote). During real-time stationary cycling sessions, the integrated devices were tested to monitor variations of Na^{+} levels in sweat, as shown in Chapter 6.

Sweat is promising for non-invasive monitoring of bio-markers. However, it must be taken into account that concentrations of various analytes in sweat differ from the ones in the blood system and depend on hydration levels. It might also be difficult to avoid contamination during sampling. Sweat seems to be additionally suitable for non-invasive monitoring of physical condition. For instance, information on the physiological mechanisms related to body thermoregulation and analyte production is related to the estimation of sweat rate variations over time. Such measurements were achieved via a low-cost wearable device based on the use of Macroducts®, sweat sampling units positioned on the arm of a subject via home-made straps. The processing of video recordings and photo shootings of the device acquired during physical exercise sessions allowed sweat rate variations to be tracked over time, as described in Chapter 7.

The work here presented can be considered as a starting point for the development of integrated wearable platforms that are able to monitor, communicate, and store parameters of chemical nature related to the status of health of an individual. We expect that potentiometric sensors will be employed in combination with other approaches (e.g. based on colorimetric detection) to deploy systems for pervasive sensing.

8.2 Future Applications

8.2.1 pH and Na^{+} Wearable Designs

The research presented in this thesis can potentially be adapted for applications in the field of wearable sensors, spanning from monitoring of physical parameters to the more challenging integration of chemical devices [8]. Figure 8.1 (a) shows the principal

research trends in the realisation of progressively smaller and comfortable devices for non-invasive monitoring of different parameters of biological interest.

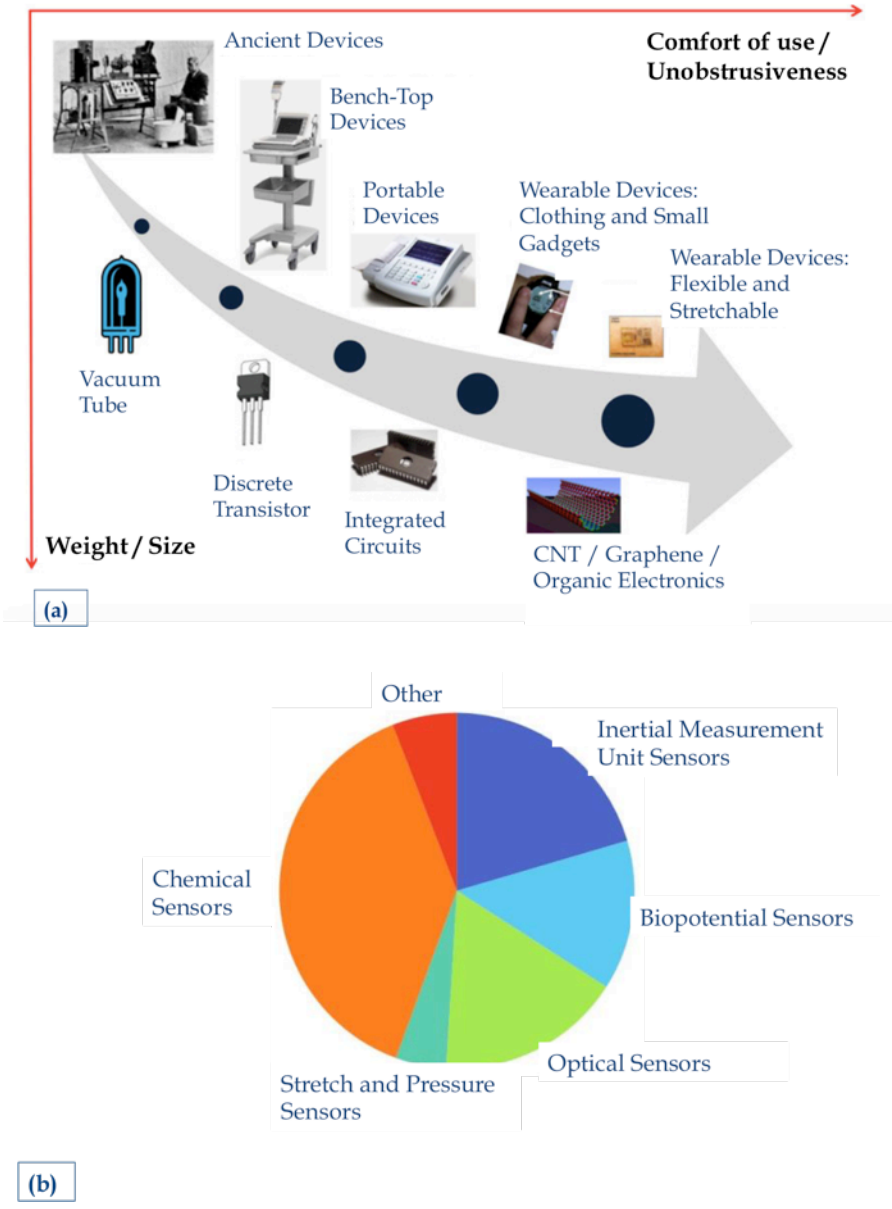

Figure 8. 1: (a) Over time trends in the design of wearable sensors with special attention given to reduced sizes featured by parallel improvements in terms of wearability (image adapted from [8]). (b) Market predictions on the role played by wearable sensors in 2020 (image adapted from [9]).

Recently published market predictions show that 3 billion of wearable sensors will be available in 2025 (e.g. with an increase of 32% for what concerns chemical sensors, see Figure 8.1 (b)) [9]. The sensors presented in this thesis are potentially suitable to be combined into wearable devices, after some rearrangement in design. For example, in the future, our attention will be focused on the integration of pH potentiometric

sensors (presented in Chapter 4) into an instrumented gum shield. The screen-printed dual electrode configuration linking a pH ISE with a SCI-RE will be connected to a WIXEL wireless communications platform to transfer the sensor measurements to a remote logging station (see Figure 8.2 (a)). This wearable and minimally-invasive chemical-sensing device will allow for continuous monitoring of pH in patients affected by Gastroesophageal Reflux. The prototype design is shown in Figure 8.2 (see (b) and (c)), along with the components (i.e. potentiometric strip and electronic platform). So far, all the modules have been tested separately (see Figure 8.2 (a)) and full integration will be soon performed.

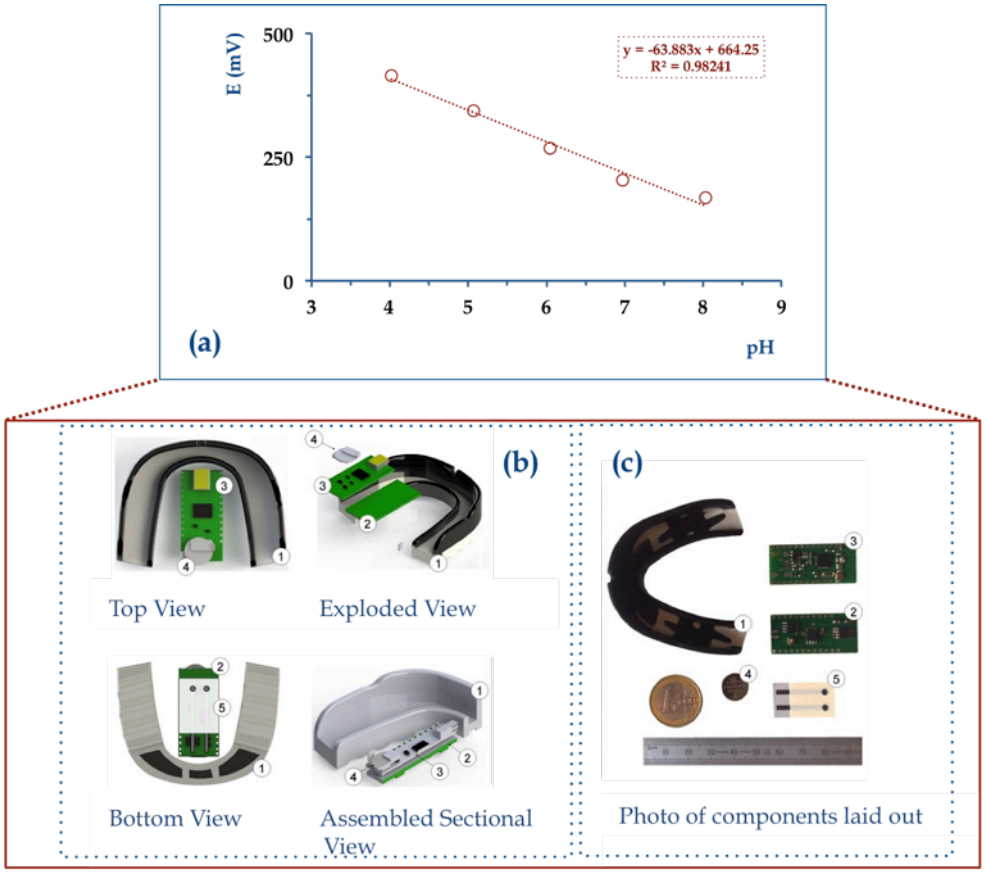

Figure 8. 2: (a) Calibration plot of the pH electrode obtained with the wireless sensing platform shown in (b) (CAD drawings) or (c) (photograph of the different components). (1) Commercial gum shield, (2) conditioning circuitry, (3) wireless Wixel, (4) battery and (5) dual electrodes (pH and reference electrodes).

The dual screen-printed electrodes are also suitable to monitor on-body sodium levels in sweat, and they have already been integrated into a wearable configuration, as described in Chapter 6. Further miniaturisation is needed to realise more comfortable devices and this will require several modifications of our initial design (see Figure 8.3

(a)). First of all, the size of the screen-printed electrodes will have to be reduced and the microfluidic circuit redesigned (see Figure 8.3 (b)). The wireless miniaturised electronics will be developed in collaboration with Shimmer® and the all components will be integrated in a watch-like configuration, that can be worn on the wrist (see Figure 8.3 (b)). This will allow for real-time monitoring of Na^+ variations. Clinical trials will be carried out to prove the efficacy of this system that could significantly improve monitoring the health condition of people affected by chronic diseases like Cystic Fibrosis. The work will be carried out in collaboration with Prof. Gordon Wallace's group at IPRI, University of Wollongong [10].

Figure 8. 3: (a) First generation design of the wearable system used to monitor Na^+ variations, with all the components constituting the device. (b) Second generation miniaturised design with a watch-like configuration where all the different components are disclosed, characterised by new shapes and sizes: (1) 3D-printed encasing with a watch-like design; (2) 3D-printed electronic circuit board; (3) battery sizes; (4) sweat collector and microfluidic design integrated on top of the (5) screen-printed electrodes.

Information on Na^+ variations over time can be very helpful also when monitoring athletes under effort. In coordination with the monitoring of sweat rate variations (work that will be carried out in the future), more insight can be gained on

physiological mechanisms regulating sweat production and body thermoregulation. This last physical parameter is of interest mainly because it can alert athletes of eventual dehydration, a condition that can negatively impact on their performance [11, 12]. This cannot be distinguished using occasional sampling based on adsorbent patches. We were able to carry out sweat rate measurements using a wearable, low-cost device (i.e. Macroduct®) and custom image analysis procedure, as described in Chapter 7. However, integration of the processing functionalities into a smartphone app will ultimately provide real-time estimates of sweat production rate after video recording or images taken at multiple time intervals.

In the future, we plan to perform a study involving a larger number of volunteers (both male and female) exercising under strictly controlled conditions (assessed before and after the test to ensure reproducible hydration conditions) where chemical targets (e.g. sodium and lactate) and sweat flow rates will be measured simultaneously to investigate eventual correlations. We will be able to estimate, e. g., Na^+ concentrations via potentiometric measurements (C_{Na^+}), volume variations of sweat via Macroduct® (V_{sweat}), and then calculate the number of moles of Na^+ lost (i.e. lost $moles_{Na^+} = C_{Na^+} x V_{sweat}$) during an exercise session. This study will provide insights into how hydration affects sweat production, ultimately enabling the implementation of personalised hydration strategies.

8.2.2 On-fabric or Paper based Patches: Two Novel Approaches for the Integration of Potentiometric Sensors.

Functionalised fabrics are another approach for the integration of chemical sensors into wearable configurations [13]. In the near future, potentiometric sensors might also become an active element integrated onto textiles, provided the electrodes are available in compatible formats and made from compatible materials. To contribute to this concept, we first focused on the development of a new Reference Electrode. The approach previously described (see Chapter 3) relied on the use of a polymeric membrane embedding Ionic Liquids, which although interesting, is an impractical design to be transferred on fabrics. Consequently, we explored the use of other materials and implemented a novel fabrication strategy.

Inspired by a methodology already used in Lithium Ion Batteries, we first considered commercial powders (i.e. $LiFePO_4$, carbon and graphite) suspended in a suitable solvent (N-methyl-pyrrolidone), and then mixed with a polymer (i.e. polyviniylidene fluoride (PVdF)) operating as a binding agent to create a slurry [14]. The relative ratios

of the various components were changed and optimised to obtain the most convenient "ink" viscosity according to the technique used for depositing the material. We wanted to attain a compound that could be drop-cast, spray-coated and eventually transferred after stamping on top of screen-printed electrodes with high reproducibility. Preliminary screening trials were performed drop casting the material, followed by two electrochemically pre-conditioning steps in a 1M LiCl solution: a first potentiodynamic step was applied to perform full oxidation and reduction; a second potentiodynamic step was carried out until half oxidation of the material was attained (i.e. for more details see La Mantia et al. [14]). The reference electrodes were then conditioned in 10^{-2} M NaCl for at least 24 hours or until a stable signal was reached.

To guarantee the functioning of the REs, we looked for evidence of sensitivity to variations in the normal composition of the target body fluids (i.e. Na^+ changes in this case). The electrodes were first tested in an ionic background (similar to sweat) [15] with Na^+ levels varying from 10^{-7} to 10^{-1} M NaCl (see Figure 8.4 (a) for more details). Sensitivity to pH was then tested in a buffered solution of citric acid and Na_2HPO_4 (varying pH levels from 4 to 6.5, with increments of 0.4) (see Figure 8.4 (b)). Finally we tested the electrodes in a constant ionic background where K^+ and Na^+ concentrations of 10^{-3} M or 0.1 M were switched over time (for more details see Figure 8.4 (c)).

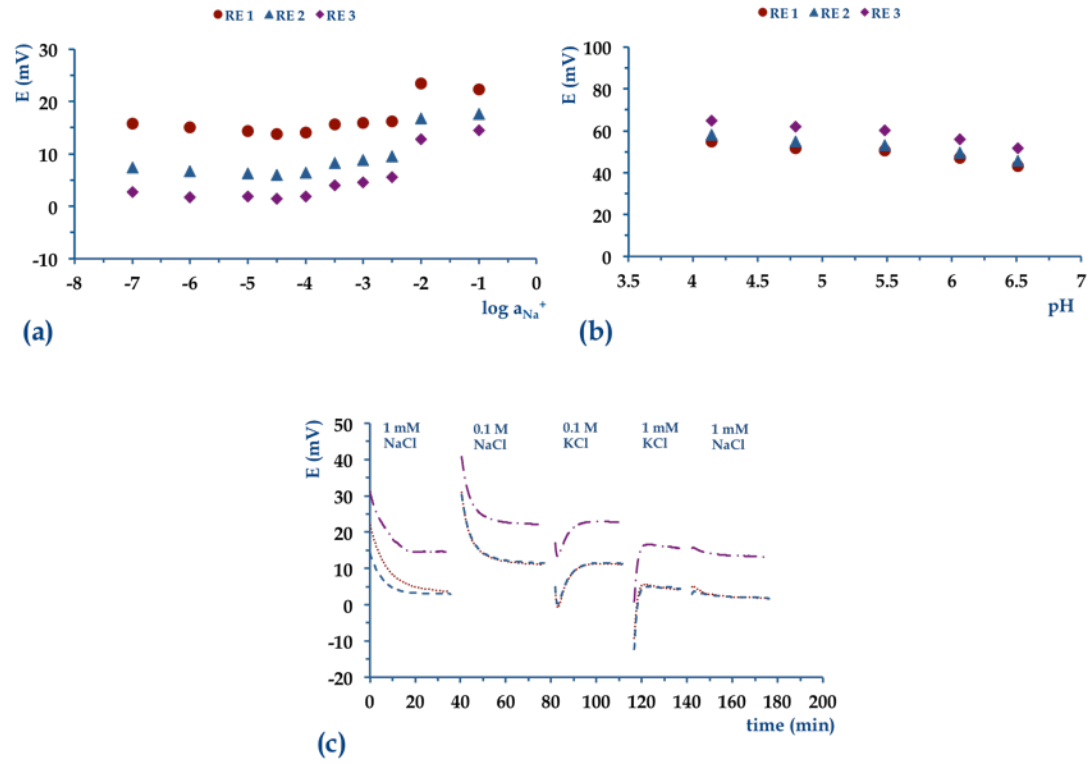

Figure 8. 4: Performances of reference electrodes, realised on screen-printed electrodes using a material based on $LiFePO_4$. (a) Calibration curves of 3 reference electrodes (RE 1 ●, RE 2 ▲, RE 3 ♦) obtained changing Na^+ concentrations (range of 10^{-7}-10^{-1} M) and (b) the pH (range 4-6.5), with a constant ionic background in both cases. (c) Individual responses of electrodes which potential was recorded in the bathing solution indicated by the label on the graph ((RE 1 red, · · ·), (RE 2 blue, – –), (RE 3 purple, – · –)).

The results here presented are really promising, and show a maximum variation of 11.3±3.3 mV (n=3) from the recorded baseline at 10^{-7} M NaCl, which is likely acceptable for monitoring Na^+ changes in sweat over time (see Figure 8.4 (a)). Our electrodes were featured by good reproducibility intra-batch, with an average offset of 7.3 mV±8.4 (n=3) as shown by recordings taken during the first calibration (see Figure 8.4 (a)). This could be further improved avoiding manual drop casting via techniques such as screen printing, spray coating, and stamping. The over time drift was monitored for 2 hours in 0.1 M NaCl solutions and was characterised by an average of -0.05±0.003 mV/min (n=3). The reference electrodes were also relatively insensitive to pH changes in the range 4-6.5, with an average sensitivity of -4.9±0.3 mV/pH (see Figure 8.4 (b)). Additionally, when tested in different bathing solutions, the electrodes showed minor sensitivity towards changes in the ionic strength of the solution, when the concentration of NaCl was increased from 1 mM to 0.1 M (7.8±0.6 mV, n=3) or the

concentration of KCl was decreased from 0.1 M to 1 mM (-6.9±0.1 mV, n=3) (see Figure 8.4 (c)). More trials are however needed to characterise the electrodes both morphologically and electrochemically, a fundamental step to improve the reproducibility of the fabrication procedure and to better understand their working mechanisms. The versatility of the fabrication material makes it suitable also for different systems. Its formulation, in fact, can be first adjusted and used to screen print or inkjet conductive paths (e.g. with different configurations) or even directly transferred onto different substrates such as textiles (e.g. inert or conductive woven fabrics like the ones from Shieldex Inc. [16]). This will allow a full transfer of an approach belonging to the world of batteries, to the one of smart-fabrics. This work was carried out in collaboration with Prof. Wolfgang Schuhmann's group from Ruhr University [17].

Combining and adapting this work with other projects under study in our group we plan to implement working electrodes directly on textiles. For example, spray coating of a water based dispersion of graphene oxide was used to functionalise lycra fabrics, that can in turn be used as solid-contact for working electrodes, whose membrane can be tuned according to the application of interest (e.g. Na^+, K^+, pH monitoring). A fully on-fabric integrated chemical sensor needs to be connected to a battery and to a wireless electronic system to transmit information at a distance. Several opportunities are offered by textile electronics where RFID technologies allow storing and transmitting signals. Electrical circuits can be directly sewn into fabrics thanks to conducting threads.

Fabrics do not represent the only substrate that can be functionalised to realise wearable chemical sensors. Other interesting opportunities are offered by paper-based devices where the sampling and detecting unit can be localised on the same substrate in patch-like configurations, with the electrodes being directly screen-printed on paper and the fluidic channels defined by ink stamping [18-20]. The functionalisation of the paper substrate can be performed according to the application of interest and applied on skin to monitor sweat or implemented in a microneedle configuration used to harvest and monitor various parameters in interstitial fluids [21-24].

8.3 References

[1] D. Diamond, Internet-Scale Sensing, Analytical Chemistry, 76(2004) 278 A-86 A.

[2] D. Diamond, S. Coyle, S. Scarmagnani, J. Hayes, Wireless sensor networks and chemo-/biosensing, Chemical Reviews, 108(2008) 652-79.

[3] http://www.nytimes.com/2014/09/08/technology/can-apple-build-a-cool-and-convenient-iwatch.html?_r=0, Accessed on: 22 April 2015

[4] http://www.wsj.com/articles/novatis-google-to-work-on-smart-contact-lenses-1405417127, Accessed on: 22 April 2015

[5] https://makeit.intel.com, Accessed on: 20 April 2015

[6] A.J. Bandodkar, J. Wang, Non-invasive wearable electrochemical sensors: a review, Trends in Biotechnology, (2014).

[7] G. Matzeu, L. Florea, D. Diamond, Advances in wearable chemical sensor design for monitoring biological fluids, Sensors and Actuators B: Chemical, 211(2015) 403-18.

[8] Y. Zheng, X. Ding, C. Poon, B. Lo, H. Zhang, X. Zhou, et al., Unobtrusive sensing and wearable devices for health informatics, IEEE Transactions on Biomedical Engineering, 61(2014) 1538-54.

[9] Wearable Sensors 2015-2025: Market Forecasts, Technologies, Players http://www.idtechex.com/research/reports/wearable-sensors-2015-2025-market-forecasts-technologies-players-000431.asp, Accessed on: 02 May 2015

[10] http://ipri.uow.edu.au/index.html, Accessed on: 03 May 2015

[11] R. Maughan, S. Shirreffs, Dehydration and rehydration in competative sport, Scandinavian Journal of Medicine and Science in Sports, 20(2010) 40-7.

[12] R.R. Gonzalez, S.N. Cheuvront, S.J. Montain, D.A. Goodman, L.A. Blanchard, L.G. Berglund, et al., Expanded prediction equations of human sweat loss and water needs, Journal of Applied Physiology, 107(2009) 379-88.

[13] J.R. Windmiller, J. Wang, Wearable electrochemical sensors and biosensors: a review, Electroanalysis, 25(2013) 29-46.

[14] F. La Mantia, C. Wessells, H. Deshazer, Y. Cui, Reliable reference electrodes for lithium-ion batteries, Electrochemistry Communications, 31(2013) 141-4.

[15] C. Taylor, J. Hardcastle, K. Southern, Physiological measurements confirming the diagnosis of cystic fibrosis: the sweat test and measurements of transepithelial potential difference, Paediatric Respiratory Reviews, 10(2009) 220-6.

[16] http://www.shieldextrading.net/aboutus.html, Accessed on: 20 April 2015

[17] http://www.ruhr-uni-bochum.de/elan/index.html, Accessed on: 03 May 2015

[18] Z. Nie, F. Deiss, X. Liu, O. Akbulut, G.M. Whitesides, Integration of paper-based microfluidic devices with commercial electrochemical readers, Lab on a Chip, 10(2010) 3163-9.

[19] Z. Nie, C.A. Nijhuis, J. Gong, X. Chen, A. Kumachev, A.W. Martinez, et al., Electrochemical sensing in paper-based microfluidic devices, Lab on a Chip, 10(2010) 477-83.

[20] V.F. Curto, N. Lopez-Ruiz, L.F. Capitan-Vallvey, A.J. Palma, F. Benito-Lopez, D. Diamond, Fast prototyping of paper-based microfluidic devices by contact stamping using indelible ink, RSC Advances, 3(2013) 18811-6.

[21] N.F. Chiu, J.M. Wang, C.W. Liao, C.H. Chen, H.C. Chen, L.J. Yang, et al., An implantable multifunctional needle type biosensor with integrated RF capability, Engineering in Medicine and Biology Society, 2005 IEEE-EMBS 2005 27th Annual International Conference of the, IEEE2006, pp. 1933-6.

[22] X. Huang, C. Leduc, Y. Ravussin, S. Li, E. Davis, B. Song, et al., Continuous monitoring of glucose in subcutaneous tissue using microfabricated differential affinity sensors, Journal of Diabetes Science and Technology, 6(2012) 1436-44.

[23] P.R. Miller, S.A. Skoog, T.L. Edwards, D.M. Lopez, D.R. Wheeler, D.C. Arango, et al., Multiplexed microneedle-based biosensor array for characterization of metabolic acidosis, Talanta, 88(2012) 739-42.

[24] J.R. Windmiller, N. Zhou, M.-C. Chuang, G. Valdes-Ramirez, P. Santhosh, P.R. Miller, et al., Microneedle array-based carbon paste amperometric sensors and biosensors, Analyst, 136(2011) 1846-51.

Appendix A

Figure AA. 1: Picture of a screen-printed carbon electrode.

Table AA. 1: Membrane formulation specifying acrylate monomer/s, cross-linker, photo-initiator, IL and the appearance of the resulting membrane. The percentage values reported for the cross-linker, photo-initiator and IL are given in respect to the molar content of the acrylate monomer/s (monomer or sum of the monomers equal to 3.57 mmoles).

Monomer/s	Cross-linker	Photo-initiator	IL	Appearance
Butylacrylate (512.0 µL)	HDDA 24.0 µL (3.0%)	DMPA 7.3 mg (0.8%)	[emim][FAP] 69.0 µL (6.0%)	Wrinkly
Decylmethacrylate (461.0 µL)	HDDA 12.0 µL (3.0%)	DMPA 3.6 mg (0.8%)	[emim][FAP] 34.5 µL (6.0%)	Runny
Butylacrylate (256.0 µL) Decylmethacrylate (461.0 µL)	HDDA 24.0 µL (3.0 %)	DMPA 7.3 mg (0.8%)	[emim][FAP] 69.0 µL (6.0%)	Runny
Butylacrylate (461.0 µL) Decylmethacrylate (92.3 µL)	HDDA 24.0 µL (3.0%)	DMPA 7.3 mg (0.8%)	[emim][FAP] 69.0 µL (6.0%)	Rubbery
Butylacrylate (461.0 µL) Decylmethacrylate (92.3 µL)	HDDA 12.0 µL (1.5%)	DMPA 7.3 mg (0.8%)	[emim][FAP] 69.0 µL (6.0%)	Rubbery/Soft
Butylacrylate (461.0 µL) Decylmethacrylate (92.3 µL)	HDDA 36.0 µL (4.5%)	DMPA 7.3 mg (0.8%)	[emim][FAP] 69.0 µL (6.0%)	Rubbery/Stiff
Butylacrylate (461.0 µL) Decylmethacrylate (92.3 µL)	BDDA 19.6 µL (3.0%)	DMPA 7.3 mg (0.8%)	[emim][FAP] 69.0 µL (6.0%)	Rubbery
Butylacrylate (461.0 µL) Decylmethacrylate (92.3 µL)	HDDA 24.0 µL (3.0%)	PBPO 12.0 mg (0.8%)	[emim][FAP] 69.0 µL (6.0%)	Rubbery
Butylacrylate (461.0 µL) Decylmethacrylate (92.3 µL)	PPODA 91.2 µL (3.0%)	DMPA 7.3 mg (0.8%)	[emim][FAP] 69.0 µL (6.0%)	Rubbery
Butylacrylate (461.0 µL) Decylmethacrylate (92.3 µL)	HDDA 24 µL (3.0%)	HMPP 12.0 mg (0.8%)	[emim][FAP] 69.0 µL (6.0%)	Very Stiff
Butylacrylate (461.0 µL) Decylmethacrylate (92.3 µL)	HDDA 24.0 µL (3.0%)	DMPA 7.3 mg (0.8%)	[bmim][FAP] 76.5 µL (6.0%)	Rubbery
Butylacrylate (461.0 µL) Decylmethacrylate (92.3 µL)	HDDA 24.0 µL (3.0%)	DMPA 7.3 mg (0.8%)	[hmim][FAP] 83.6 µL (6.0%)	Rubbery

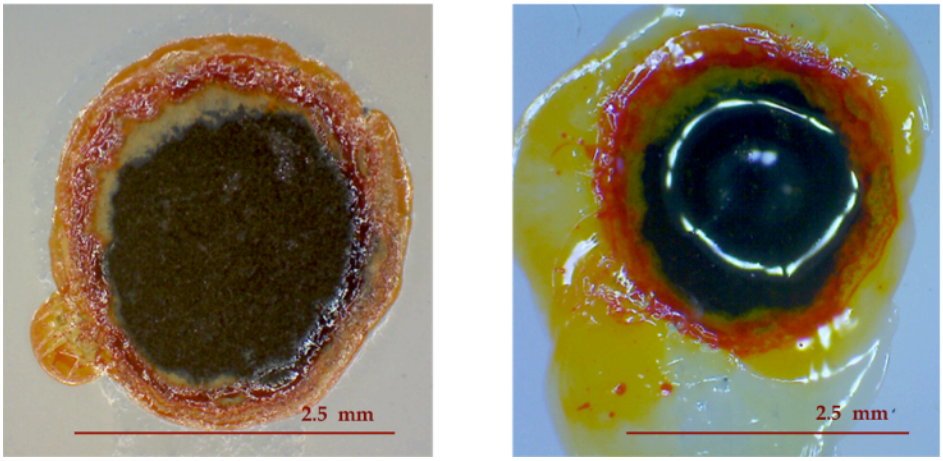

Figure AA. 2: Photograph of the sensitive carbon area covered by POT (left) and after drop casting a PVC/IL mixture solubilised in THF (right).

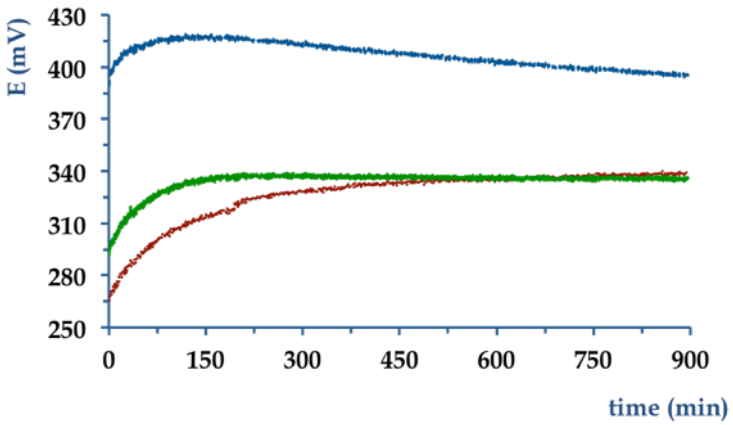

Figure AA. 3: Conditioning step of reference electrodes prepared by entrapping (blue, – –) [hmim][FAP], (green, —) [bmim][FAP] or (red, · · ·) [emim][FAP] within a poly(butyl-co-decylmethacrylate) membrane. The conditioning solution was 10 mM NaCl while the solid-contact was a PEDOT layer potentiostatically electrodeposited from [emim][FAP].

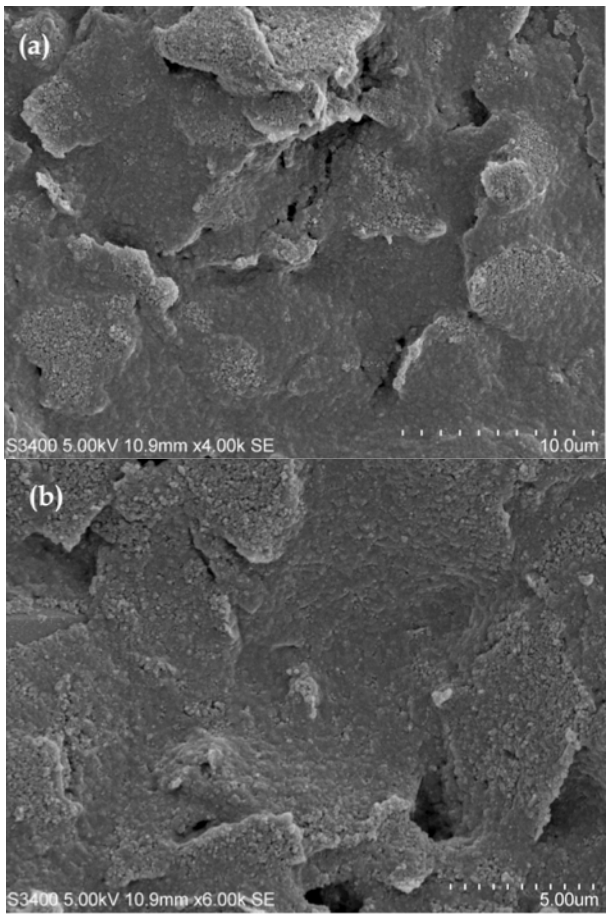

Figure AA. 4: SEM images of PEDOT electrodeposited from [emim][NTf_2] by cycling the potential between 0 and 1.0 V vs Ag wire, for 25 times, with a scan rate equal to 50 mV/s.

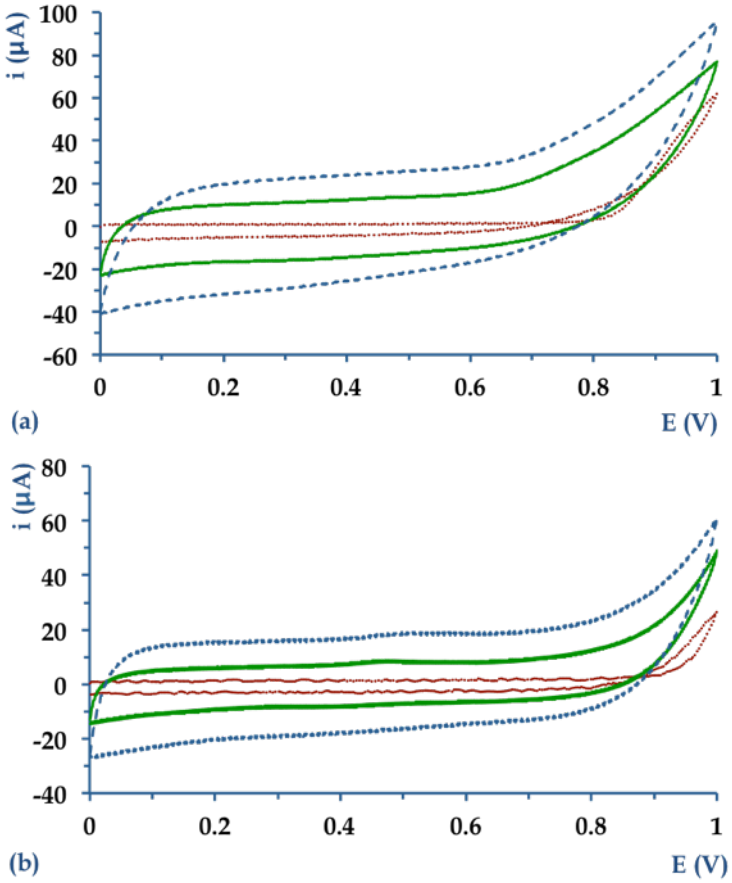

Figure AA. 5: Electrodeposition of EDOT from a 50 mM solution in (a) [emim][FAP] and (b) [emim][NTf_2]. The traces show the (red, · · ·) 1st, (green, —) 10th and the (blue, – –) 25th polymerisation cycles.

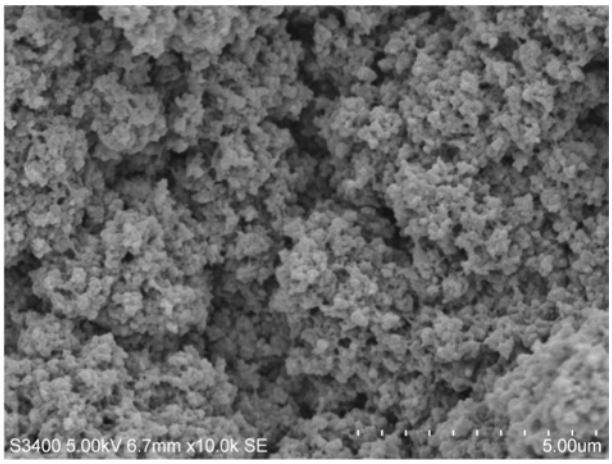

Figure AA. 6: SEM image of PEDOT electrodeposited from [emim][NTf_2] by applying a constant potential of 1.0 V vs Ag wire for 900 seconds.

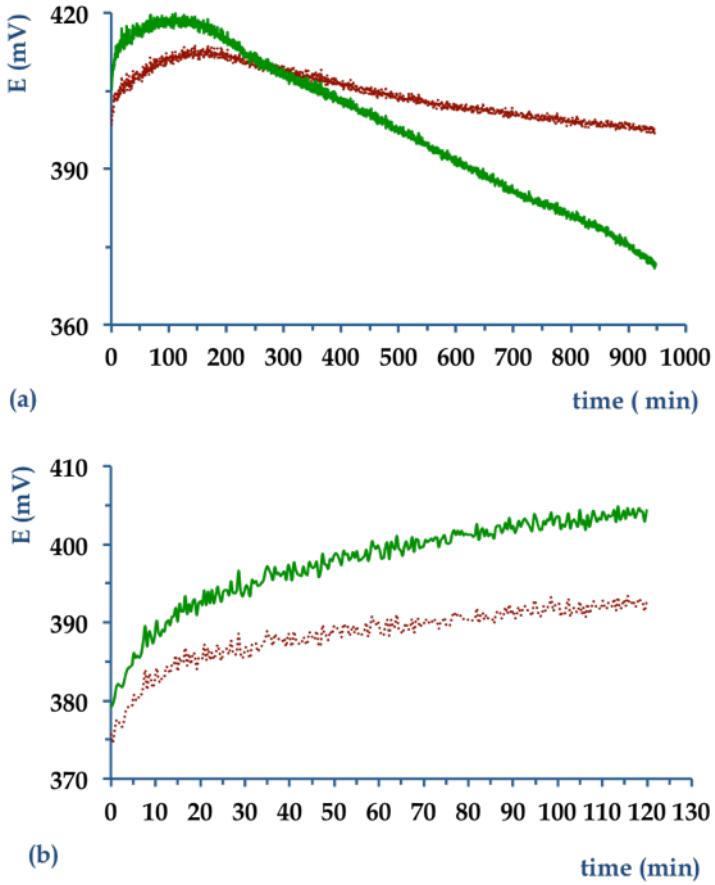

Figure AA. 7: Conditioning step of reference electrodes prepared by entrapping (green, —) [hmim][FAP] and (red, · · ·) [bmim][FAP] within a poly(butyl-co-decylmethacrylate) membrane. The solid-contact was a PEDOT layer potentiostatically deposited from [emim][NTf_2]. The electrodes were conditioned in aqueous 10 mM NaCl (a) overnight and (b) for 2 hours.

Appendix B

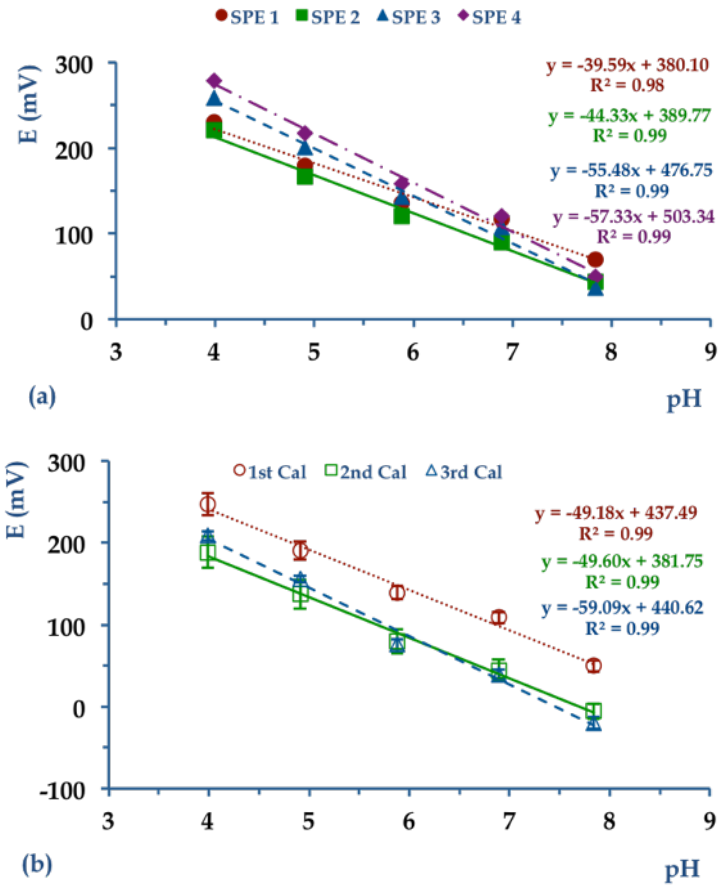

Figure AB. 1: (a) First day calibrations of individual pH sensors prepared using an electrochemically grown layer of PEDOT from an aqueous KCl solution. Data points labels: (●) SPE 1, (■) SPE 2, (▲) SPE 3, and (♦) SPE 4. Linear fit labels: (red, · · ·) SPE 1, (green, —) SPE 2, (blue, – –) SPE 3, and (purple, – · –) SPE 4. (b) Average and relative standard error (n=4) of the same sensors related to the 1st (○), 2nd (□) and 3rd (Δ) calibration. Linear fit labels: (red, · · ·) 1st calibration, (green, —) 2nd calibration, (blue, – –) 3rd calibration.

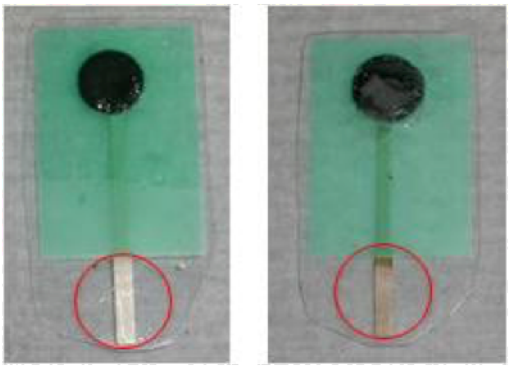

Figure AB. 2: Photograph of pH sensors just after membrane drop casting, before dipping into the conditioning solution (left) and 3 days after being left in that solution (right). The change of colour of the silver contact pad is apparent, as indicated by the circles.

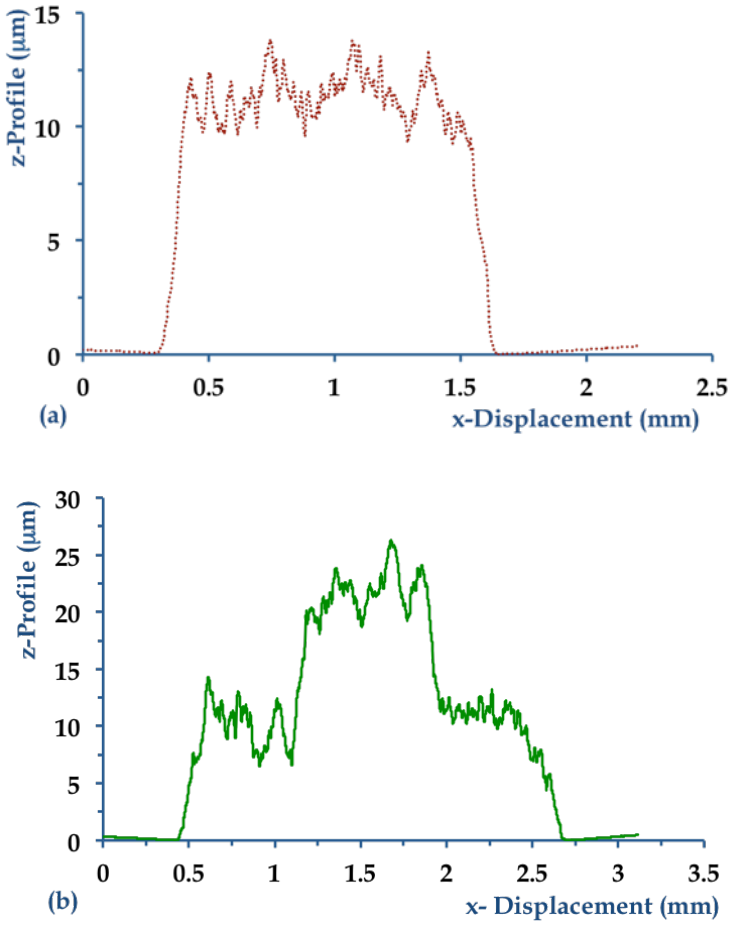

Figure AB. 3: Z-profiles of the conductive track of screen-printed electrodes formed by (a) 1 and (b) 2 printed carbon layers. Profiles are the average of 6 scans.

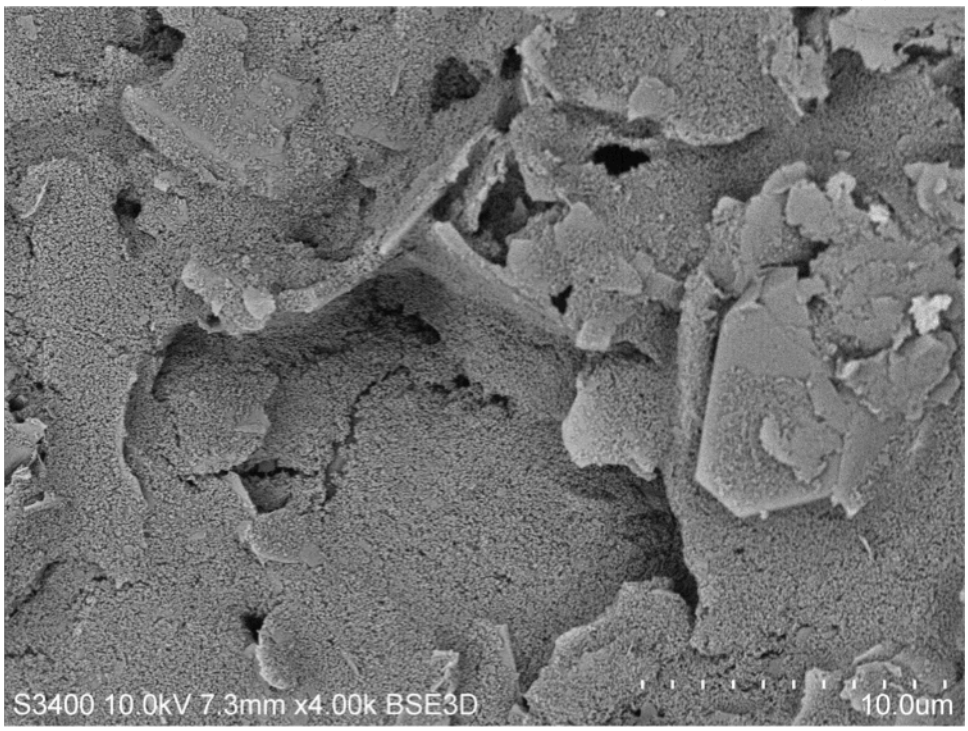

Figure AB. 4: Scanning Electron Microscopy image of a screen-printed substrate in which 2 layers of carbon were printed. Image taken in backscattered mode, applying an accelerating voltage of 10 kV.

Appendix C

Table AC. 1: Elemental analysis of the LAc and LAm Au-NPs expressed in terms of % weight.

Chemical Element	LAc Au-NPs (%wt)	LAm Au-NPs (%wt)
C	13.42	13.65
H	1.22	1.69
N	0	1.51
Au	66.90	68.77
S	8.52	9.89
Total	90.06	95.51

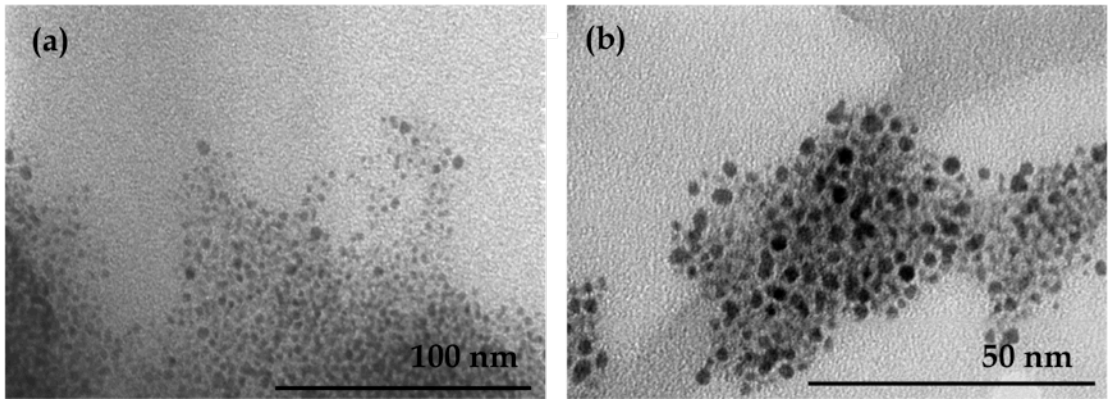

Figure AC. 1: FeSEM images of LAc (a) and LAm Au-NPs (b). 30 kV was chosen as accelerating voltage for the imaging.

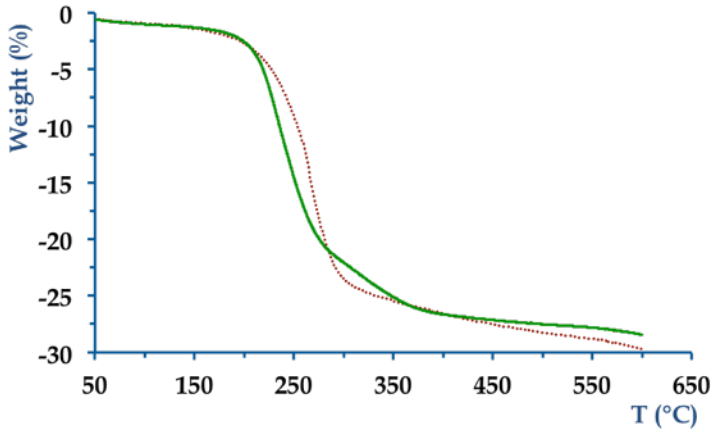

Figure AC. 2: Thermogravimetric analysis of LAm Au-NPs (green, —), characterised by the release of the disulphur alkyl chain (nearly 27% of weight loss) at ~200 °C. LAc Au-NPs (red, · · ·) characterised by the release of the disulphur alkyl chain (nearly 25% of weight loss) at ~200 °C.

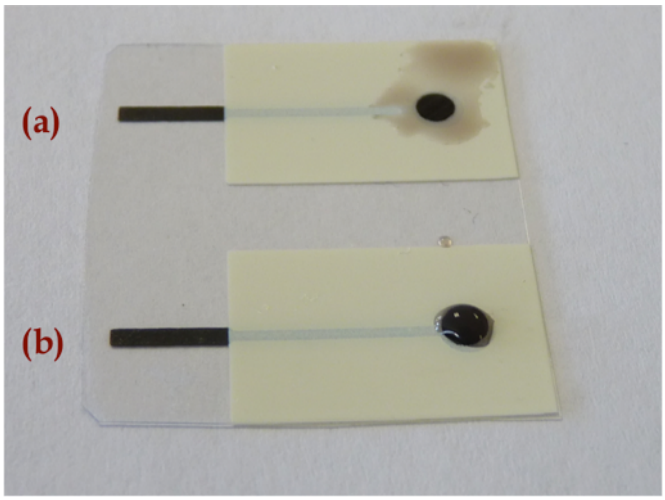

Figure AC. 3: The image shows the different surface tensions of LAc Au-NPs (b) and LAm Au-NPs (a) suspension towards the screen-printed carbon layer.

Section AC.1: Modelling Electrochemical Impedance.

The electric circuit model is characterised by the presence of resistors and capacitors together with constant phase elements in order to take into account the inhomogeneities characterising the materials present in a real system [1]. The Warburg Impedance is describing mass transfer phenomena due to diffusion. Block B (see Figure 5.5, Chapter 5) models the water uptake and its evolution over time occurring within the polymer membrane, as previously described by Armstrong et al. [2] for poly(ethylmethacrylate) layers, that can be also used while employing, as in our case,

PVC membranes [3]. In this block, R_b and Q_g (see Figure 5.5, Chapter 5) are the bulk resistance coupled to the geometric capacitance of the polymer layer, the last one represented by a constant phase element. In addition, R_{it} and C_{it} (see Figure 5.5, Chapter 5) represent the charge transfer resistance and the double layer capacitance at the interface between the percolated water through the membrane and the solid-contact, respectively [4], defining eventual interactions between the ions percolating through the membrane and the Au-NPs [2].

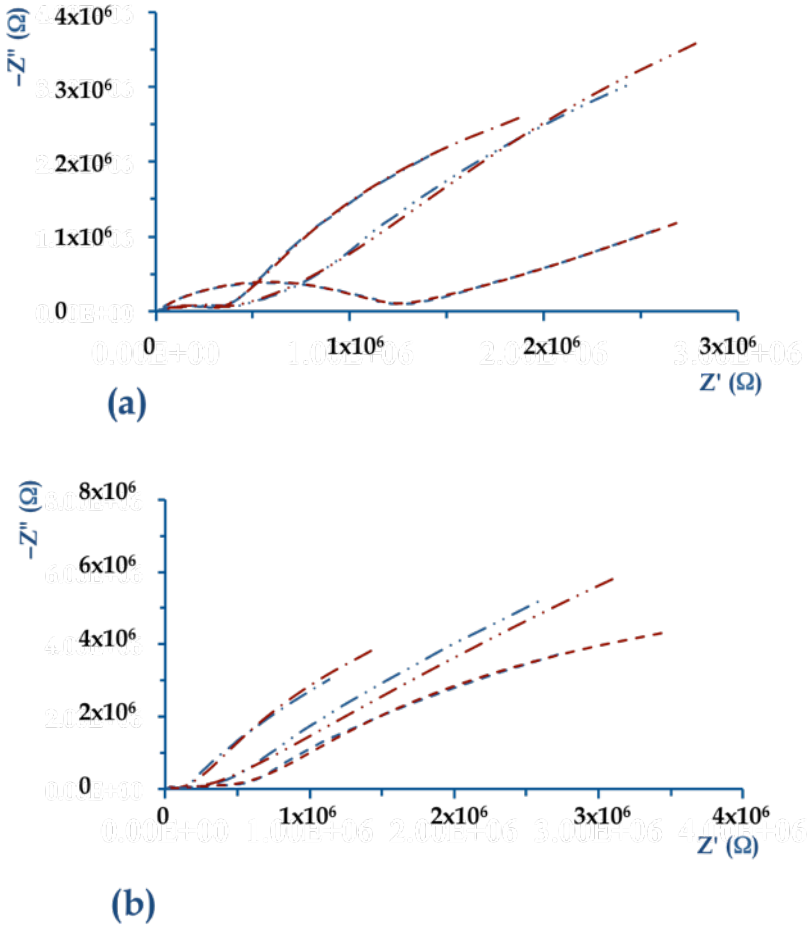

Figure SIC. 1: Nyquist plots of Pb^{2+} ISEs employing Au-NPs functionalised with LAc (a) or LAm (b). The measurements show the experimental (blue) and fitted data (red) after 7 (– –) and 46 (– · –) hours in pH 4 10 µM $Pb(NO_3)_2$, since the beginning of the 1st conditioning step and after an additional 26 (– · · –) hours in pH 4 10 nM $Pb(NO_3)_2$, since the start of the 2nd conditioning step.

Section AC.2: Flux Behaviour in IS-Membranes.

The constant presence of super-Nernstian slopes over time suggests the presence of inward (towards the membrane) ion fluxes [5]. Some calculations allow clarifying which between the two layers (polymeric membrane or solid-contact) might dictate the described behaviour. In fact, the conditioning time required to saturate the membrane can be indirectly estimated. The local current I at the interface solution/membrane, related to the inward flux of Pb^{2+}, i.e., from the solution towards the membrane, can be evaluated as a function of concentration [6] (see Equation SIC.1):

$$c(0,t) = c^0 + \frac{2I}{nFA}\sqrt{\frac{t}{D\pi}} \qquad \text{(SIC.1)}$$

where $c(0,t)$ is the concentration at the interface membrane/solution, c^0 is the concentration at which the calibration slope changes from a Nernstian to super-Nernstian linear trend in the calibration curve (10^{-6} M in this case), n is the cationic charge, F is the Faraday constant, A is the surface exposed to the flux, t is the experimental time, and D is the diffusion coefficient of lead in water. Assuming that $c(0,t)=0$, negligible if compared to the bulk concentration in solution [5], the following values are $n=2$, $A=0.10\ cm^2$, $t=300\ s$ and $D=9.45x10^{-6}\ cm^2/s$ [7], and $I=3.16\ nA$. On the other hand, the steady-state current of Pb^{2+} across the membrane after its saturation can be expressed as [6] (see Equation SIC.2):

$$I = \frac{nFAD_m c_m}{\delta} \qquad \text{(SIC.2)}$$

where D_m represents the Pb^{2+} diffusion coefficient in the PVC membrane, c_m is the concentration of the ion-ionophore complex near the interface membrane-solution, and δ is the thickness of the membrane. Assuming that c_m is half of the lipophilic ion-exchanger ($c_m = 0.190x10^{-3}\ M$), $\delta = 270\ \mu m$ as measured using a caliper, $D_m \sim 10^{-8}\ cm^2/s$ [8], $I=4.24\ nA$, and thus almost identical to the estimate from Equation SIC.1. This result suggests that the membrane is saturated by Pb^{2+} cations and that the diffusion layer occupies its entire thickness [6]. Thus, the super-Nernstian trends observed during the first calibration, and the ones recorded in the following measurements, can likely be ascribed to Pb^{2+} loading and flux towards the SC.

Appendix C References

[1] S. Krause, Impedance methods, in: P. Unwin (Ed.) Encyclopedia of Electrochemistry, Wiley-vch2003, pp. 196-229.

[2] R.D. Armstrong, D. Wright, Polymer protective coatings—the distinction between coating porosity and the wetted metal area, Electrochimica Acta, 38(1993) 1799-801.

[3] S. Krause, Impedance methods, in: P. Unwin (Ed.) Encyclopedia of Electrochemistry, Wiley-vch2003, pp. 212-3.

[4] J.-P. Veder, R. De Marco, G. Clarke, R. Chester, A. Nelson, K. Prince, et al., Elimination of undesirable water layers in solid-contact polymeric ion-selective electrodes, Analytical Chemistry, 80(2008) 6731-40.

[5] T. Sokalski, T. Zwickl, E. Bakker, E. Pretsch, Lowering the detection limit of solvent polymeric ion-selective electrodes. 1. Modeling the influence of steady-state ion fluxes, Analytical Chemistry, 71(1999) 1204-9.

[6] A. Michalska, K. Maksymiuk, The influence of spontaneous charging/discharging of conducting polymer ion-to-electron transducer on potentiometric responses of all-solid-state calcium-selective electrodes, Journal of Electroanalytical Chemistry, 576(2005) 339-52.

[7] H. Sato, M. Yui, H. Yoshikawa, Ionic diffusion coefficients of Cs^{+}, Pb^{2+}, Sm^{3+}, Ni^{2+}, SeO^{2-}_{4} and TcO^{-}_{4} in free water determined from conductivity measurements, Journal of Nuclear Science and Technology, 33(1996) 950-5.

[8] L.Y. Heng, K. Toth, E.A. Hall, Ion-transport and diffusion coefficients of non-plasticised methacrylic–acrylic ion-selective membranes, Talanta, 63(2004) 73-87.

Appendix D

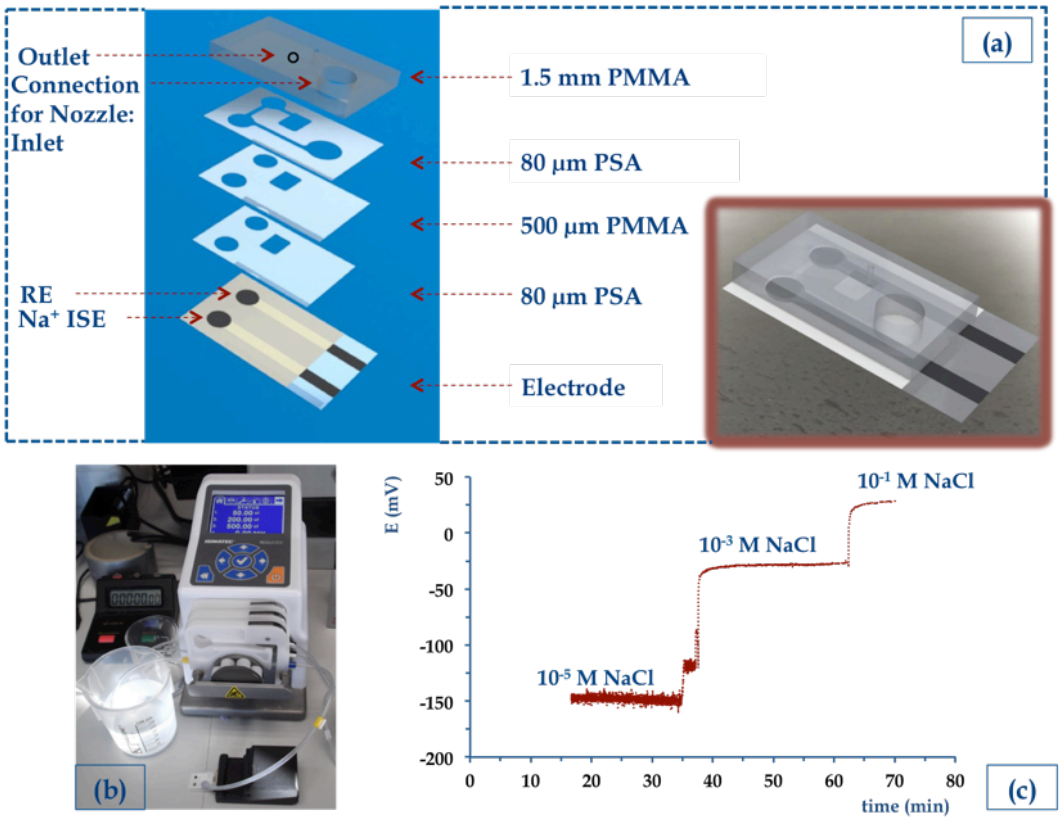

Figure AD. 1: (a) 1st generation of the Microfluidic unit integrated on top of the screen-printed electrodes and (b) the experimental set-up used to carry out the first on-bench tests (i.e. potentiometric strip connected to a peristaltic pump). (c) Example of an over time 3 points calibration curve realised using the set-up in (b).

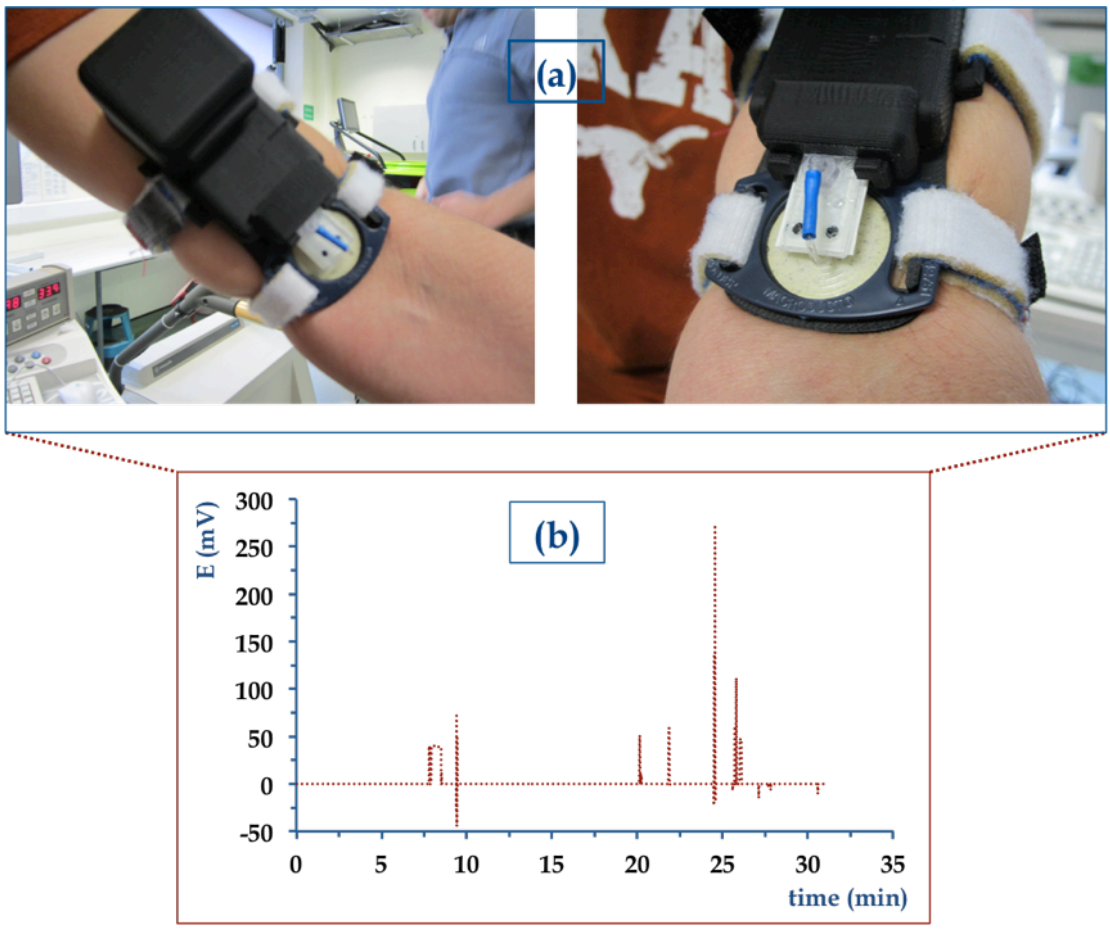

Figure AD. 2: (a) 1st Generation of the wearable PotMicroChip worn on the upper arm and (b) signal recorded in real-time during a stationary cycling session.

Appendix E

Table AE. 1: Volumes harvested by the Macroduct® in correspondence with every mask intersection. The corresponding location (L) or intersect represent the numbers on the +x, -x, +y and –y axes; the letters represent the intersects on the axes at 45° in each quadrant. The table is divided in subsections denoting each quadrant, starting in a clockwise manner from the closest point to the inlet (0).

L	V (µL)	L	V (µL)	L	V (µL)
0	0			1	2.3
		a	1.2		
4	8.2			5	10.5
		e	9.3		
8	18.7			9	21
		i	19.8		
12	31.5			13	35
		m	32.1		
16	46.7			17	51.3
		q	49		
20	65.3			21	70
		u	67.6		
24	86.3			25	92.2
		y	89.2		
28	110.8				

L	V (µL)	L	V (µL)	L	V (µL)
1	2.3			2	3.5
		b	2.9		
5	10.5			6	12.8
		f	11.7		
9	21			10	24.5
		j	22.8		
13	35			14	38.5
		n	36.7		
17	51.3			18	56
		r	53.6		
21	70			22	74.7
		v	72.4		
25	92.2			26	98
		z	95.7		

L	V (µL)	L	V (µL)	L	V (µL)
2	3.5			3	5.8
		c	4.6		
6	12.8			7	16.3
		g	14.5		
10	24.5			11	28
		k	26.3		
14	38.5			15	43.2
		o	40.8		
18	56			19	60.7
		s	58.3		
22	74.7			23	80.5
		w	77.6		
26	98			27	103.8
		aa	100.9		

L	V (µL)	L	V (µL)	L	V (µL)
3	5.8			0	0
		d	7		
7	16.3			4	8.2
		h	17.5		
11	28			8	18.7
		l	29.7		
15	43.2			12	31.5
		p	44.9		
19	60.7			16	46.7
		t	63		
23	80.5			20	65.3
		x	83.4		
27	103.8			24	86.3
		bb	107.3		
				28	110.8

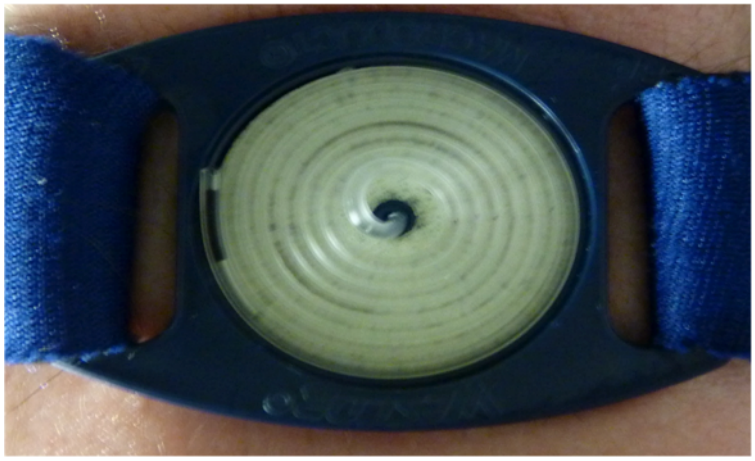

Figure AE. 1: Filled Macroduct® at the end of a cycling session.

T

U